Relativistic Many-Body Studies of Parity Non-Conservation (PNC) in Heavy Atomic Ions

A thesis Submitted For The Degree of

Doctor of Philosophy

in

the Faculty of Science

Bangalore University

by

Geetha K. P.

Indian Institute of Astrophysics

Bangalore 560 034, India

May 2001

Declaration

I hereby declare that this thesis is the result of the investigations carried out by me at the Indian Institute of Astrophysics, Bangalore under the guidance and supervision of Prof. Bhanu Pratap Das. This thesis has not been submitted for the award of any degree, diploma, associateship, fellowship, etc. of any university or institute.

In keeping with the general practice of reporting scientific observations, due acknowledgement has been made whenever the work described is based on the findings of other investigators. Any omission which might have occurred by oversight or error in judgement is regretted.

Geetha K. P.
(Candidate)

Bangalore
May 2001

Certificate

This is to certify that the thesis entitled 'Relativistic Many Body Studies of Parity Non-Conservation (PNC) in Heavy Atomic Ions' submitted to the Bangalore University by Mrs. Geetha K.P. for the award of the degree of Doctor of Philosophy in the faculty of science, is based on the results of the investigations carried out by her under my supervision and guidance, at the Indian Institute of Astrophysics. This thesis has not been submitted for the award of any degree, diploma, associateship, fellowship, etc., of any university or institute.

Prof. Bhanu Pratap Das
(Supervisor)

Bangalore
May 2001

To my parents

Abstract

Parity Non-Conservation (PNC) is caused by weak electron-nucleon interaction, as predicted by electroweak unification theory. In 1974 Bouchiat and Bouchiat pointed that this interaction is strongly enhanced in heavy atoms. Since then PNC has been observed in heavy atoms like Cs, Tl, Pb etc., The accuracy of atomic experiments has reached a level, which in combination with atomic many body theory can be an important probe of physics beyond Standard Model. Latest measurements on cesium has yielded a result of unprecedented accuracy (0.35%) and has lead to the discovery of the nuclear anapole moment. Fortson (N. Fortson, *Phys. Rev. Lett.* **70**, 2383 (1993)) has proposed an experiment to measure PNC in $6s_{1/2} \rightarrow 5d_{3/2}$ using the techniques of laser cooling and ion trapping. In this work, three different many body methods are applied to compute parity non-conserving electric dipole transition amplitude ($E1PNC$) in Ba^+ for the $6s_{1/2} \rightarrow 5d_{3/2}$ transition.

We have computed $E1PNC$ for the above transition which is sensitive to both Nuclear Spin Independent (NSI) and Nuclear Spin Dependent (NSD) interactions using the configuration interaction (CI) method. Preliminary calculations for this transition by Malhotra et al. points to the importance of the many-body effects from the low lying levels. We have improved this result by adding more configuration state functions (CSFs) obtained by the excitations from 5s and 5p core orbitals to various higher virtual orbitals. The NSI $E1PNC$ reduced matrix element with about 2000 relativistic CSFs converged to $0.5264 \times 10^{-12} a_0 Q_W$. It may also be possible to perform a similar PNC experiment on the $6s_{1/2} \rightarrow 5d_{5/2}$ transition in Ba^+ and $7s_{1/2} \rightarrow 6d_{5/2}$ in Ra^+. These transitions are found to have an important advantage; it is only sensitive to NSD effect and is therefore a very direct way of measuring the nuclear anapole moment.

Many-Body Perturbation Theory (MBPT) with one order in Couloumb and one order in PNC has been studied in detail. We categorize the corresponding Goldstone diagrams depending on the physical effects into three classes; *viz.*, Coupled Perturbed Hartree Fock (CPHF), Random Phase Approximation (RPA) and Double Perturbation (CPHF-RPA). Few of the $E1PNC$ pair correlation diagrams are also considered and the results shows that CPHF contributes $\sim 3.8\%$ and RPA contributes $\sim 0.5\%$ to $E1PNC$. The first order calculations shows that CPHF-RPA and pair correlation diagrams contributes $\sim 0.5\%$ and $\sim 8\%$ respectively to $E1PNC$. The total NSI $E1PNC$ contributing from CPHF, RPA, CPHF-RPA and pair correlation effects is found to be $2.18\, iea_0(-Q_W/N) \times 10^{-11}$. Dzuba et al. (V.A. Dzuba, V.V. Flambaum

and J.S.M. Ginges, *Phys. Rev. A* **63** 62101 (2001)) using a mixed parity approach obtained 2.17 $iea_0(-Q_W/N) \times 10^{-11}$.

The formulation of relativistic Coupled Cluster Singles and Doubles (CCSD) applied to atomic systems, with and without the PNC interaction is studied in detail. We have used the CC amplitudes with partial triples, for the calculation of Ionization Potential (IP) and Excitation Energy (EE) for different low lying levels of Ba^+. Orbitals that are part analytical and part numerical have been considered as the Dirac-Fock single particle basis. Accuracies of the IPs and EEs hence obtained are approximately 0.2 and 1% respectively. We find that the inclusion of triple excitations were crucial to achieve this degree of precision. The reliability of computed values of $E1PNC$ using sum over intermediate states have been ensured by applying the same methodology to Ba^+, where experimental quantities like electric dipole, hyperfine constant and lifetime are available. The formulation of mixed parity approach for the computation of $E1PNC$ is discussed in detail. The total contribution to $E1PNC$ by sum over intermediate bound states for 6p,7p,8p(1/2,3/2) states using all order CCSD and DF contribution from bound core and continuum virtuals is 2.35 $iea_0(-Q_W/N) \times 10^{-11}$ respectively. This in comparison with Dzuba et al. (V.A. Dzuba, V.V. Flambaum and J.S.M. Ginges, *Phys. Rev. A* **63** 62101 (2001)) is 2.34 $iea_0(-Q_W/N) \times 10^{-11}$.

Acknowledgment

I consider it as a privilege to express my sincere and deep sense of gratitude to Prof. Bhanu Pratap Das my supervisor, for his innovative ideas behind this thesis and constant motivation given to me. I am really fortunate to have been associated with you.

My heartfelt thanks to Prof. D. Mukherjee, Director of I.A.C.S., Kolkata for his valuable suggestions and time extended to me during the course of this work. I would like to thank R.K. Chaudhuri, I.I.A., for the tremendous amount of help which I have received from him at each and every phase of my research program. Thank you Rajat for patiently teaching me the angular momentum adaptations, the initial steps of computation and the beauty of Coupled Cluster Method. My profound thanks to my graduate and post-graduate teachers especially Prof. S. Ramamurthy of Gandhigram Rural Institute for the constant motivation and concern shown all through out this work. I am grateful to Prof. R. Cowsik, Director of I.I.A., for all the facilities I have availed from I.I.A.

I express my sincere thanks to the authorities of CDAC, Pune especially Dr. Sundarajan, for the super-computing facilities made available to me. I thank all members of BGS, I.I.A. and Dr. Anantharaman, Chairman, Physics Department, Bangalore University, for making the University and administrative formalities smooth. I thank staff of library, computer center and administration for their timely help.

Above all I would like to thank all the members of NAPP group for the valuable ideas, suggestions and time spend for weekly discussions on Fridays. The remarkable co-operation and help extended to me by all my seniors, batch mates and juniors all throughout my research program is remembered with deep sense of gratitude.

Abbreviations and notations

C	Charge conjugation	P	Parity
T	Time-reversal	SCF	Self Consistent Field
V	Vector	A	Axial vector
S	Scalar	P	Pseudo scalar
PNC	Parity Non-Conservation	E1PNC	Electric dipole transition
E	Electric Field		amplitude induced by PNC
CI	Configuration Interaction	CC	Coupled Cluster
MBPT	Many Body Perturbation Theory	IPM	Independent Particle Method
NSI	Nuclear Spin Dependent	NSD	Nuclear Spin Independent
CSF	Configuration State Function(Φ)	ASF	Atomic State Function (Ψ)
D	Dipole	CPHF	Coupled Perturbed Hartree Fock
RPA	Random Phase Approximation	FBSE	Finite Basis Set Expansion
IP	Ionization Potential	EE	Excitation Energy
A	Hyperfine constant	NAM	Nuclear Anapole moment
p	Proton	n	Neutron
Q_W	Weak charge	Z	Atomic number
N	Nucleon number	$\sin^2\theta_W$	Weinberg mixing angle
$E1$	Electric dipole transition	$E2$	Electric Quadrapole transition
	amplitude		amplitude
HF	Hartree-Fock	DF	Dirac-Fock
GRASP	General Relativistic Atomic	RSPT	Rayleigh-Schrödinger
	Structure Program		Perturbation Theory
BWPT	Brillouin-Wigner	CPMET	Coupled Pair Many
	Perturbation Theory		Electron Theory
T	Closed shell CC amplitudes	S	Open shell CC amplitudes
EPC	Even Parity Channel	UCC	Unitary Coupled Cluster

Contents

List of Figures

List of Tables

Chapter 1

Introduction

1.1 Symmetry: An Introduction

Symmetry or invariance of the equations of motion describing a physical system is an important concept in physics. In general, a symmetry of a particular kind exists when a certain operation leaves certain properties unchanged. With each symmetry there is an associated transformation and it obeys certain characteristic group structures. If a particular process remains the same after it is transformed by an operation, then it is said to be invariant under the symmetry associated with that transformation. A remarkable theorem discovered early in this century by the German mathematician Emmy Noether states that

Every conservation principle corresponds to a symmetry in nature.

For example, invariance under rotational symmetry leads to conservation of angular momentum and invariance under translational symmetry leads to conservation of linear momentum. A particular theory in general obeys several conservation laws, wherein the invariance restricts possible forms of the interactions involved. The concept of parity has been of fundamental importance to the development of theories which unify forces observed in nature.

The symmetries exhibited by physical systems can be classified as continuous and discrete. Continuous symmetries are associated with transformations which have the concept of infinitesimal transformation, and a finite transformation can be achieved by applying a sequence of infinitesimal transformations. In discrete symmetries instead, there is no concept of infinitesimal transformations. Instead the transformation

takes the physical system from one state to another. The three important discrete symmetries of interest in physical studies are charge conjugation (C), parity (P) and time-reversal (T). According to the Charge Parity Time-reversal (CPT) theorem [1] all physical systems described in local field theories are invariant under the combined CPT transformations. A physical system/process can violate each of these symmetries individually as long as the combined CPT is conserved.

1.2 Parity as a Symmetry Transformation

The parity operation, as applied to transformation on the co-ordinate system, changes a right-handed (RH) system to a left-handed (LH) system [2]. However, one considers a transformation on the state kets rather than on the co-ordinate system. Given $|\Psi(\vec{r})\rangle$, we consider a space-inverted state, assumed to be obtained by applying a unitary operator P known as the parity operator, which is as follows:

$$|\Psi(\vec{r})\rangle \rightarrow P|\Psi(\vec{r})\rangle = |\Psi(-\vec{r})\rangle. \tag{1.1}$$

Since the space inversion operation is defined as a transformation in which each point of space $\vec{r}$ goes to $-\vec{r}$, we require the expectation value of position operator $\hat{X}$ taken with respect to the space inverted state to be opposite in sign given by

$$\langle\Psi(\vec{r})|P^{\dagger}\hat{X}P|\Psi(\vec{r})\rangle = -\langle\Psi(\vec{r})|\hat{X}|\Psi(\vec{r})\rangle, \tag{1.2}$$

which is possible if $P^{\dagger}\hat{X}P = -\hat{X}$, and $\hat{X}P = -P\hat{X}$, where we have used the fact that P is unitary$[P^{\dagger} = P^{-1}]$. It can be shown that P is also Hermitian with eigenvalues ± 1. A system described by a Hamiltonian H then under the parity transformation takes the form $H_P = PHP^{-1}$. The system is invariant under parity transformation if $H_P = H$ or $PHP^{-1} = H$ and therefore $[H, P] = 0$. As P commutes with H, $\Psi(\vec{r})$ is a simultaneous eigenfunction of P and H. This clearly implies that the condition for parity non-conservation/violation in a physical system is that, it's Hamiltonian does not commute with the parity operator and at the same time the eigenfunctions of H are not simultaneous eigenfunctions of P.

Operators in general have parity transformation properties; they can be even or odd under P. One can categorise these operators with respect to the effect of the parity transformation on them as vector, axial vector, scalar and pseudo scalar. A vector (V) quantity is one that transforms in the same way as $\vec{r}$ under parity, so in general for a vector $\vec{a}$,

$$P : \vec{a} \rightarrow -\vec{a} \tag{1.3}$$

An axial vector (A) is defined by the product of two such vectors, e.g., $\vec{L} = \vec{r} \times \vec{p}$, which transforms under parity like

$$P : \vec{a} \times \vec{b} \rightarrow +\vec{a} \times \vec{b} \tag{1.4}$$

Hence it is also known as pseudo vector. Two other quantities which have definite parity properties are

$$P : \vec{a}.\vec{b} \rightarrow +\vec{a}.\vec{b} \tag{1.5}$$

and

$$P : \vec{a}.(\vec{b} \times \vec{c}) \rightarrow -\vec{a}.(\vec{b} \times \vec{c}) \tag{1.6}$$

where the operator defined in Eq. 1.5 is a Scalar (S) which does not change sign under parity and the one defined in Eq. 1.6 is a Pseudo scalar (P) that changes sign under parity.

1.3 Conservation and Non-Conservation of Parity: Examples

The discussion below draws heavily on a review article on atomic parity Non-Conservation (PNC) by M.A.Bouchiat and C.Bouchiat [3]. PNC does not belong to our everyday experience and there are large domains of physics where the question of parity conservation is never addressed although it concerns one of the most elementary symmetry properties *i.e.*, mirror symmetry - symmetry with respect to a plane. For any object, we can talk about left handed and right handed configurations. All the objects with such handedness are said to be chiral. One example is the chiral molecule. The right and left handed molecules differ by the geometrical arrangement of the atoms inside the molecule. Such molecules share identical physical properties but they differ in properties involving handedness, for instance the rotatory power i.e., rotation of a plane of polarisation of light transmitted through a gas or a solution of these molecules. If we observe a left-handed molecule and measure its optical rotation in a mirror we see a right-handed molecule which has an opposite optical rotation, hence it has the same optical rotation as a right-handed molecule in the real world. The optical rotation of a chiral molecule is a property which preserves mirror symmetry and we say that it is parity conserving. In the context of an atom, we are considering a physical system whose chiral property arises not from the spatial arrangement of the constituents, but from the interactions between the constituents which favour one orientation of the physical space with respect to the other.

In the absence of external field, left and right circularly polarised photons interact identically with unoriented atoms. But the results of careful experiments suggest that the process of emission and absorption of photons by atoms manifests a slight preference for left or right circularly polarised photons or in more general preference to a particular orientation in space. These observed effects are very small. This actually reveals the existence of a new type of interaction which was ignored before 1970's. Until then an atom was regarded as a system governed only by the electro magnetic interaction, which is known to conserve parity.

1.4 Parity Non-Conservation in Physical Systems: Brief Remarks

The first hint of PNC came in 1956 while solving the puzzle that the K meson was observed to decay sometimes into 2 pions and sometimes into 3 pions *i.e.*, into two different final states of opposite parity. It was T.D.Lee and C.N.Yang [4], who proposed that either parity is not conserved in the decay, or the K meson is a parity doublet *i.e.*, a two component state of opposite parities.They noted that there was no experimental evidence then available for parity conservation in transitions which, like the K decay, were induced by weak interactions [5]. They devised new rules to test parity conservation in processes where the initial and final states do not have necessarily well defined parities. Going by their suggestions, the basic principle for such experiments is to compare the rate of a given transition between two states, A and B, with the transition rate between the mirror states, $\tilde{A}$ and $\tilde{B}$. The experimental outcome is conveniently characterised by the difference between these rates divided by their sum, the so-called left-right asymmetry, A_{LR}. The measurement of a non-zero value of A_{LR} constitutes an unambiguous evidence for PNC in the transition. We note that A_{LR} is a pseudo scalar quantity. In 1957, C.S.Wu and her collaborators [6] performed the first successful experiment to observe parity non-conservation in the β-decay. This experiment was performed on ^{60}Co nuclei whose spins $\vec{I}$ were oriented. In β decay of this nuclei it was observed that the probability for an electron to be emitted with a given momentum $\vec{p}$ involves a larger contribution proportional to the scalar product $\vec{I}.\vec{p}$. In simpler terms, the electrons are found to be emitted preferentially in the direction opposite to the orientation of the ^{60}Co nuclei. Since $\vec{I}$ is an angular momentum, i.e., an axial vector, the quantity $\vec{I}.\vec{p}$ is a pseudo scalar and this manifests the PNC. Earlier, in 1950, Purcell and Ramsey [7] had also questioned parity conservation on a fundamental level by pointing out that the possible evidence

of an electric dipole moment of a neutron, although violating parity conservation, remained purely an experimental question.

Until the early 1970s, it was believed that all processes observed involving weak interactions were accompanied by an exchange of electric charge between the interacting particles and hence the modification of their identities. This was thought to be so since β decay, where it was first discovered, is accompanied by a change in the electric charge of the decaying neutron [$n \rightarrow p + e^- + \gamma_e^-$]. These transformations are brought about by the particles which mediate weak interaction; they are called gauge bosons and are analogous to the photons that mediate the electro magnetic interaction. Unlike the photon, the gauge bosons W^+ and W^- that mediate the weak interaction carry a unit of electric charge. It was therefore misunderstood that the weak interaction and its associated PNC were not relevant to physics of the stable atom.

A complete theoretical understanding of weak interactions emerged only in late 1960s. Glashow [8], Weinberg [9] and Salam [10] suggested independently that the weak interaction and the electro magnetic interaction could be understood as different manifestations of a single underlying interaction: the electroweak interaction [11]. This unified electroweak theory was subsequently shown by G.'t Hooft to be amenable to a perturbation treatment in the same way as Quantum Electrodynamics [12]. The calculation of higher order terms lead to the evaluation of the top quark mass even before its direct observation at Fermi Lab. An important prediction of the theory which has given a new dimension to atomic physics was the existence of a new gauge boson, the Z^0 that mediates a new kind of weak interaction. Both the $W^{\pm}$ and Z^0 bosons are results of the unification of electro magnetic and weak forces in Standard Model. The $W^{\pm}$ mediates the charged current interactions such as nuclear β decay, muon decay etc., and the Z^0 mediates a new type of interaction called the neutral weak current interaction. These interactions are schematically represented in Fig. 1.1. Because of this union, the Z^0 is expected to exhibit a chiral behaviour wherein it's coupling to the electron is proportional to the electron helicity (h_e), a pseudo scalar quantity [$h_e = \vec{\sigma}_e.\vec{v}_e$ where $\vec{\sigma}_e$ is the spin of the electron and $\vec{v}_e$ is the velocity] which is odd under space reflection. This contribution turns out to play a dominant role in atoms. By analogy with the nuclear electric charge, one is led to introduce the weak charge of the nucleus Q_W [3]. Unlike the Coulomb potential, the chiral electron-nucleus interaction has a very short range compared to atomic size. As a consequence, the strength of this interaction is proportional to the electron density inside the nucleus. Thus weak charge Q_W plays the role of a fundamental constant of the atomic electroweak chiral interaction. Another PNC mechanism exists, in which

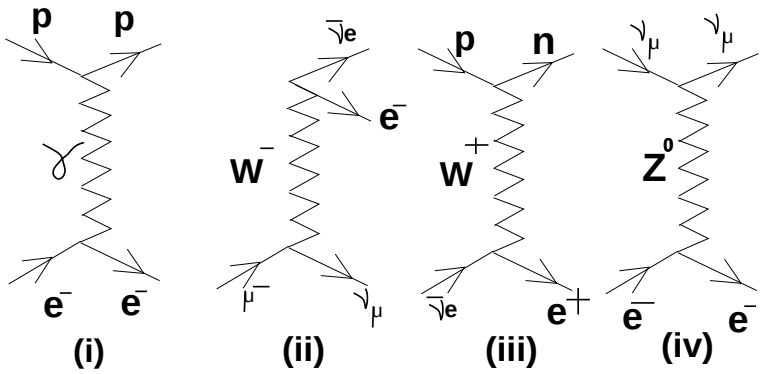

Figure 1.1: Types of Interaction in Electroweak theory: (i) Photon exchange, (ii) W^- exchange, (iii) W^+ exchange and (iv) Z^0 exchange

PNC inside the nucleus is communicated electro magnetically to the atomic electrons. Nuclear PNC here is parameterised in terms of an odd-parity vector moment called anapole moment [13].

From a theoretical view point, weak interaction in an atom leads to atomic eigenstates which no longer have a definite parity, but contain admixtures of states of opposite parity. Atomic Hamiltonian is the sum of kinetic energy parts of the electron, electron-nucleus interaction, electron-electron Coulomb interaction and the parity non-conserving interaction. Theoretical computations are done by treating PNC Hamiltonian as a perturbation. Due to this admixture one looks for electric dipole transition amplitudes induced by PNC interaction (E1PNC) between states having the same nominal parity. This is parameterised in terms of Q_W the weak charge, which in comparison with the experiments is a test of existing value in the Standard Model of Particle Physics [14]. Existence of any discrepancy of the weak charge between the theory and the Standard model could lead to new physics beyond the Standard Model. This will also add significant constraints on models that suggest new types of contact interaction or the possible observation of leptoquarks in the events that were observed a few years ago at the HERA collider [15].

In atomic physics experiments, a small $E1$ transition takes place between states originally of the same parity because PNC admixes the states as described above. E1 amplitude will interfere with an allowed electro magnetic amplitude, giving rise to an observable PNC effect. Experimental techniques related to laser cooling and trapping proposed for Ba^+ ion [16] for doing PNC experiments will be discussed in the next chapter.

1.5 Motivation

Main objective of this thesis is to develop relativistic many-body methods which can be used to calculate reliable values of $E1PNC$ for heavy atomic ions, which can be combined with experimental values to test the validity of the Standard Model. The Standard Model has a steadily growing weight of evidence in its favour [17], so that one often now speaks of "testing the standard model" [18]; but one has to realise that it is only a model. It is a renormalisable gauge theory, and any more complete theory will surely remain of this type; but the way nature actually behaves within this framework has to be established by experiment. Atomic physics experiments are of course much less direct than those at high energies. However, they are sensitive to certain types of physics beyond the Standard Model, and are potentially useful in a field in which it is difficult and expensive to make accurate measurements. There is a factor of about 10^{10} [19] in the square of the momentum transfer between the high energy and atomic PNC experiments. Hence a model of such kind links the results of different experiments with theoretical values which in turn allows one to determine values of the parameters and the consistency of it provides a test of the model. They also place severe constraints on possible alternative models. For example, super string inspired grand-unification models predict the existence of additional light particles and additional neutral currents mediated by another neutral gauge boson Z'. Also it can be shown that the combination of PNC and M_Z^2 gives a check on the Standard Model which is independent of uncertainties introduced by m_t, m_H and $sin^2\theta_W$ [20], where M_Z is the mass of the Z_0 boson, m_t is the mass of the top quark, m_H is the Higgs mass and θ_W is the Weinberg mixing angle.

In the early days of this field, when it was still a very open question as to whether parity was conserved in atoms or not, the experiments and the atomic theory were not reliable enough to give a clear message. In recent years the reliability and precision have improved enormously. The precision needed to make useful contributions has also increased, thereby demanding a better understanding of atomic many-body theories and experimental techniques. A determination of Q_W will therefore depend on the combined accuracy of theory plus experiment which needs to be better than 1% to compete with high energy experimental results. In this thesis we have tried to evaluate electric dipole transition amplitude induced by PNC (E1PNC) in singly ionised barium for which experiments are done at Seattle [16] using three different atomic many-body theories *viz.*, Configuration Interaction (CI), Many-Body Perturbation Theory (MBPT) and the Coupled Cluster Method (CCM).

1.6 Outline of the Chapters

First chapter of this thesis discusses some general aspects of PNC. A brief history of PNC starting from the work by Lee and Yang [4] and an introduction to electroweak theory of particle physics is described. The PNC observable related to atomic physics experiments/theory is then discussed. Towards the end, the motivation for doing the theory work which we have undertaken is mentioned.

In second chapter, "Parity Non-Conservation in Atomic Systems", possible sources for atomic PNC are discussed and the effective form of the Hamiltonian and the corresponding matrix elements are derived. The extraction of Q_W and its implications for physics beyond the Standard Model are then described with the present status of Nuclear Spin Independent PNC in various ions and atoms. Since any prediction beyond the Standard Model of particle physics requires both high precision calculations and techniques, we discuss the experimental techniques related to laser cooling and trapping which are proposed for singly ionised barium.

In third chapter, "Application of the Configuration Interaction method to Parity Non-Conservation in atoms", we start with a brief introduction to Independent Particle Method (IPM). The Configuration Interaction method is then described. It is followed by the evaluation of $E1PNC$ in singly ionised barium for the transition $5p^6 6s_{1/2} \rightarrow 5p^6 5d_{3/2}$ for the Nuclear Spin Independent (NSI) and Nuclear Spin Dependent (NSD) PNC as the continuation work by our group [21]. The basis and the various Configuration State Functions (CSFs) used are described. PNC in atom arises from two sources- neutral weak current and nuclear anapole moment. Although it is not possible to experimentally distinguish between these two effects, it is known from theoretical considerations that the contribution of the latter to PNC in heavy atoms is much larger than that of the former. We have identified a transition which is sensitive only to the NSD effect and thereby leads to an observation of the nuclear anapole moment. The transition from $5p^6 6s_{1/2} \rightarrow 5p^6 5d_{5/2}$ for singly ionised barium and $6p^6 7s_{1/2} \rightarrow 6p^6 6d_{5/2}$ in singly ionised radium are sensitive only to NSD effect and are therefore a direct way of measuring the nuclear anapole moment. Instead of doing intermediate summation of the odd parity states in the above transition we compute them as a linear equation which will be discussed in this chapter.

In fourth chapter, "Many-Body Perturbation Theory applied on PNC in atoms", a very general expression for the effective electric dipole transition amplitude (D_{eff}) operator starting from Bloch equation is derived. From the general expression for E1PNC various orders of expressions like first order (one order in PNC and one order in Dipole(D)), second order (one order in PNC, one order in D and one order

in Coulomb), and third order (one order in PNC, one order in D and two orders of Coulomb) are derived. In the next section, we combine the first and second order diagrams and group them in three categories, *viz.* Coupled Perturbed Hartree Fock (CPHF), RPA (Random Phase Approximation) and CPHF-RPA (Double Perturbation). The MBPT(3) diagrams involving at least one double excitation which are called the pair correlation diagrams are categorised in two classes. For solving these huge number of diagrams, we have defined pairs which are stored in file and later used for the computation of pair diagrams of a certain kind discussed in this chapter. Contributions from above MBPT diagrams are compared with Flambaum and others [22], where the computation is done using the mixed parity approach. The basis generation using finite basis set expansion (FBSE) [23] followed by the new method of generation is discussed. A comparison of the above mentioned new basis with the FBSE is done by computing Ionisation Potential (IP) and Excitation Energy (EE) using Coupled Cluster Method which is described in Chapter 5.

In chapter 5, "Coupled Cluster Method applied to PNC in atoms", we start with a very general introduction to the subject by comparing with previously described methods using physical arguments. The exponential form of the wave function starting from the Dirac Fock reference state is derived. It is then followed by a brief history of Coupled Cluster method starting from the linked cluster theorem. In next section, Coupled Cluster method applied to closed shell system is described. Here we present the equations and also the corresponding terms/diagrams for the single and double cluster amplitudes preceded by the derivation of the linear equation to be computed. Same procedure is then applied to an open shell system and we describe the method of solving it to obtain IPs and EEs for bound orbitals. For closed and open shell system with PNC in the Hamiltonian, one obtains similar linear equations which can be solved to obtain perturbed closed and open shell cluster amplitudes. This is then followed by the formulation for obtaining the typical E1PNC diagrams/terms using these perturbed and unperturbed cluster amplitudes. In next section, we describe the selection rules and the form of the Couloumb matrix elements. Validity of these cluster amplitudes are checked in next section by computing known experimental quantities like electric dipole transition probability, lifetime and hyperfine constant (A) which in turn limit the accuracy of the PNC numbers computed. We have also computed the NSI PNC and dipole matrix elements using unperturbed T and S cluster amplitudes, which has been used for the computation of E1PNC using intermediate summation approach. This method is compared with that of Dzuba et al. [22]. By comparing the IPs and EEs computed using FBSE and new basis described in Chapter 4, we show the advantage of the new basis approach. At the end of this chapter we give a

theoretical formalism for Unitary Coupled Cluster method applied to PNC and the reduction of it to the MBPT diagrams described in Chapter 4.

The last chapter of the thesis, "Conclusions and Future Directions", gives in brief the shortcomings in our theoretical approach applied to PNC and discusses the possible ways in which they can be improved. We summarise here the percentage of accuracy, which we have got for various properties using CCM and extrapolate to our PNC calculations.

Bibliography

[1] W. Pauli, *Neils Bohr and the Development of Physics* (McGraw Hill, New York, 1955).

[2] J. J. Sakurai, *Modern Quantum Mechanics*, (Addison-Wesley Company Inc., Revised Edition, 1994).

[3] M.A. Bouchiat and C. Bouchiat, *Atomic Parity Violation: An Overview*, published in the book Parity Violations in Atoms and Polarised Electron Scattering, Eds. Bernard Frois and Marie-Anne Bouchiat, (World Scientific, 1999).

[4] T.D. Lee and C.N. Yang, *Phys.Rev.* **105**,1671(1956)

[5] D. Griffiths, *Introduction to elementary particles*, (John Wiley and Sons, Singapore, 1987).

[6] C.S. Wu, E. Ambler, R.W. Hayward, D.D. Hoppes and R.P. Hudson, *Phys.Rev.* **105**, 1413 (1957).

[7] E.M. Purcell and N.F. Ramsey, *Phys. Rev.* **78**, 807 (1950).

[8] S.L. Glashow, *Nucl. Phys.* **22**, 579 (1961).

[9] S. Weinberg, *Phys. Rev. Lett.* **19**, 1264 (1967).

[10] A. Salam, *Elementary Particle Theory: Relativistic Groups and Analyticity (8th Nobel Symposium), ed. N. Svartholm*(Stockholm: Almqvist and Wicksell, 1968).

[11] C. Itzykson and J.B. Zuber, *Quantum Field Theory* (Mc-Graw Hill, New York, 1980).

[12] G.'t Hooft, *Nucl. Phys.* **B33**, 173 (1971); and **B35**, 167(1971).

[13] Ya. B. Zeldovich, *Zh., E. T. F.* **33**, 1531 (1957), L.M. Barkov, I.B. Khirplovich and M.S. Zolotorev, *Comments At. Mol. Phys.*, **8**, 79 (1979).

[14] W.J. Marciano and J.L. Rosner, *Phys. Rev. Lett.* **65**, 2963 (1990).

[15] H1 Collaboration, *Report No. DESY-97-024 and No. hep-ex/9702012 Zeus Collaboration, Report No. DESY-97-25 and No. hep-ex/9702015.*

[16] N. Fortson, *Phys. Rev. Lett.* **70**, 2383 (1993).

[17] DELPHII Collaboration, *CERN Preprint PPE-91-95* (1991).

[18] K. Riles, *Contemporary Physics* **39**, (1998).

[19] D.N. Stacey, *Physica Scripta* **T40**, 15 (1992).

[20] E.R. Boston, *Theory of Parity Non-Conservation in Atoms*, Wolfson College, Trinity Term 1990.

[21] S. Malhotra, A.D. Singh and B.P. Das, *Phys. Rev. A* **51** R2665 (1995).

[22] V.A. Dzuba, V.V. Flambaum and J.S.M. Ginges, *Phys. Rev. A* **63** 62101 (2001).

[23] R.K. Chaudhuri, P.K. Panda and B.P. Das, *Phys. Rev. A* **59**, 1187 (1999).

Chapter 2

Parity Non-Conservation in Atomic Systems

2.1 Introduction

In 1958, Zeldovich [1] first discussed the possibility of Parity Non-Conservation (PNC) in atomic physics long before any theory or experiment required the existence of neutral currents. He estimated the rotation of the plane of polarisation of visible light propagating in optically inactive matter to be 10^{-13} rad/m and concluded that such an effect will be difficult to be observed in atomic experiments. A similar much more detailed investigation was performed later by Michel [2]in 1965. The predicted effects were also not very encouraging. So, it was concluded that PNC effects in atoms would be far too small to observe, although the effect would be enhanced by the near degeneracy of states of the same quantum number, $\vec{J}$ and $\vec{S}$ but of opposite parity P. The first evidence for neutral weak interaction was in neutrino physics by the Gargamelle collaboration in CERN [3] and it was then confirmed by the two Fermi-lab experiments [4]. Since neutrinos were particles belonging to single state of helicity, it was not possible to perform two-mirror-experiments to compare the results and to check whether symmetry is conserved in neutral weak current interactions. It was concluded that the test about parity non-conservation in weak neutral currents must be done with electrons. The first experiment which demonstrated that the Z^0 exchange is parity non-conserving was performed at SLAC in 1979 [5]. This provided the first empirical evidence for a chiral electron-quark interaction. In 1974, Bouchiat and Bouchiat [6] took a vital step towards the detection of PNC in atoms by pointing

out that the effect is proportional to Z^3, and could therefore be observed in heavy atoms. They also showed how a measurement of the PNC effect could lead to a measurement of $sin^2\theta_W$ in the low momentum transfer region not previously probed by the high energy physics experiments. This lead to different PNC experiments in heavy atoms in the hope that its measurement might play a role in choosing between different models of the neutral weak current interactions. In next section, we talk about possible sources of PNC in atoms and derive their respective matrix elements.

2.2 Possible Sources of Parity Non-Conservation in Atoms

There are two possible sources of PNC in atoms:
(i) The neutral weak current interaction between the nucleus and the electrons mediated by the intermediate vector boson Z^0.
(ii) The electro magnetic interaction between the nuclear anapole moment (NAM) and the electrons of the atoms. This will be discussed in detail towards the end of this chapter.

2.2.1 PNC Hamiltonian Arising from Neutral Weak Current Interaction

Any interaction can be written as the interaction of currents which can be constructed using the bilinear covariants [7]. The PNC interaction Hamiltonian can be written as

$$H_{\rm PNC} = \sum_N \frac{G_F}{2\sqrt{2}} 2 J^n_\mu J^\mu_e, \tag{2.1}$$

where G_F is the Fermi coupling constant ($G_F = 2.22 \times 10^{-14}$ a.u.) which gives a measure of the 'weakness' of the interaction, N is the sum over nucleons (protons and neutrons), J^n_μ and J^e_μ are the nucleon and electron currents respectively. Since neutral weak currents are mediated by Z^0 bosons, which are massive, the interaction is point-like on the atomic scale. Thus, two particles can only exchange Z^0, if their wave functions overlap in the nuclear region. Expressions for the electron-nucleon interaction are given by many authors [8, 9, 10, 11]. Here we discuss the non-relativistic limit of the PNC interaction Hamiltonian. Since the interaction is parity non-conserving, and occurs between the nucleus and the electrons, it could have two forms.They are:

(i) $V^n.A^e$ *i.e.*, Vector nucleus . Axial vector electron

(ii)$V^e.A^n$ *i.e.*, Vector electron . Axial vector nucleus.

The bilinear covariant form for vector and axial vector are given by

$$V = \bar{\Psi}\gamma_\mu\Psi$$

and

$$A = \bar{\Psi}\gamma_\mu\gamma_5\Psi,$$

where $\bar{\Psi} = \Psi^+\gamma_0$ and γ_μ, γ_0 and γ_5 are the Dirac matrices. An axial vector is one which doesn't change sign under parity and a vector is one which changes sign under parity. Therefore a quantity like $V{\cdot}A$ changes sign under parity. Substituting the vector and axial vector form in the Eq. 2.1, we get

$$H_{\rm PNC} = \frac{G_F}{2\sqrt{2}} \int\int \sum_{i=p,n} 2[C_{1i}V_n.A_e + C_{2i}V_e.A_n]\delta(r_i - r_e)d\tau_e d\tau_i \tag{2.2}$$

where i can be either proton (p) or neutron (n) and C_{1i}, C_{2i} are the appropriate electron-nucleon coupling coefficients. The interaction takes place within the nucleus and hence the point-like nature gives rise to the delta function.

Thus the total Hamiltonian can be split up into two parts. One is the Nuclear Spin Independent (NSI) term and the other is the nuclear spin dependent (NSD) term. First part of the Eq. 2.2 leads to the nuclear spin independent Hamiltonian which takes the form

$$H^{\rm NSI}_{\rm PNC} = \frac{G_F}{2\sqrt{2}} \int\int \sum_{i=p,n} 2[C_{1i}\bar{\Psi}_N\gamma_\mu\Psi_N.\bar{\Psi}_e\gamma_\mu\gamma_5\Psi_e]\delta(r_i - r_e)d\tau_e d\tau_i. \tag{2.3}$$

Substituting for $\bar{\Psi}$ we get

$$H^{\rm NSI}_{\rm PNC} = \frac{G_F}{2\sqrt{2}} \int\int \sum_{i=p,n} 2[C_{1i}\Psi^+_N\gamma_0\gamma_\mu\Psi_N.\Psi^+_e\gamma_0\gamma_\mu\gamma_5\Psi_e]\delta(r_i - r_e)d\tau_e d\tau_i. \tag{2.4}$$

Considering only the diagonal terms($\mu = 0$) and neglecting the off-diagonal terms the Hamiltonian reduces to

$$H^{\rm NSI}_{\rm PNC} = \frac{G_F}{2\sqrt{2}} \int \Psi^+_e\gamma_5\Psi_e \sum_{i=p,n} 2C_{1i}\Psi^+_i\Psi_i\delta(r_i - r_e)d\tau_e d\tau_i. \tag{2.5}$$

Summation over i gives terms like $\sum \Psi^+_p\Psi_p$ and $\sum \Psi^+_n\Psi_n$. These summations over the nuclear wave functions yield the number densities of protons and neutrons, which, in simple nuclear models are proportional to the nuclear density [9] given by

$$\sum \Psi^+_p\Psi_p = Z\rho_N(r),$$
$$\sum \Psi^+_n\Psi_n = N\rho_N(r),$$

where Z and N denote the number of protons and neutrons respectively and $\rho_N(r)$ is the nucleon number density normalised so that

$$\int \rho_N(r) 4\pi r^2 dr = 1. \tag{2.6}$$

Writing the terms separately for contribution from protons and neutrons, we get

$$\begin{aligned} H_{\rm PNC}^{\rm NSI} &= \frac{G_F}{2\sqrt{2}} \int\int \Psi_e^+ \gamma_5 \Psi_e 2 \Big[C_{1p} \sum_p \Psi_p^+ \Psi_p \delta(r_p - r_e) d\tau_e d\tau_p \\ &+ C_{1n} \sum_n \Psi_n^+ \Psi_n \delta(r_n - r_e) d\tau_e d\tau_n \Big], \end{aligned} \tag{2.7}$$

which over the nuclear integration gives

$$H_{\rm PNC}^{\rm NSI} = \frac{G_F}{2\sqrt{2}} \int \Psi_e^+ \gamma_5 \Psi_e 2 [C_{1p} Z + C_{1n} n] \rho_N(r) d\tau_e, \tag{2.8}$$

where we define $2(C_{1p}Z + C_{1n}n) = Q_W$ and Q_W is called the weak charge of the nucleus. Using the first quantisation procedure, we can rewrite the above equation as

$$H_{\rm PNC}^{\rm NSI} = \frac{G_F}{2\sqrt{2}} Q_W \gamma_5 \rho_N(r). \tag{2.9}$$

Since the parity operator is represented as β it can be shown that $[\beta, \gamma_5] \neq 0$ and hence $H_{\rm PNC}^{\rm NSI}$ is a parity non-conserving Hamiltonian.

Second part of the Eq. 2.2 leads to the nuclear spin dependent Hamiltonian given by

$$H_{\rm PNC}^{\rm NSD} = \frac{G_F}{2\sqrt{2}} \int\int \sum_{i=p,n} 2 C_{2i} V_e . A_n \delta(r_i - r_e) d\tau_i d\tau_e \tag{2.10}$$

which on substitution for vector and axial vector and explicitly writing for different components leads to

$$\begin{aligned} H_{\rm PNC}^{\rm NSD} &= \frac{G_F}{2\sqrt{2}} \int\int \sum_{i=p,n} 2 C_{2i} \Big[\bar{\Psi}_e \gamma_0 \bar{\Psi}_e \bar{\Psi}_i \gamma_0 \gamma_5 \Psi_i \\ &+ \bar{\Psi}_e \gamma_r \Psi_e \bar{\Psi}_i \gamma_0 \gamma_r \gamma_5 \Psi_i \Big] \delta(r_i - r_e) d\tau_i d\tau_e. \end{aligned} \tag{2.11}$$

Substituting for $\bar{\Psi}$ and using the properties of Dirac matrices the above equation reduces to

$$\begin{aligned} H_{\rm PNC}^{\rm NSD} &= \frac{G_F}{2\sqrt{2}} \int\int \sum_{i=p,n} 2 C_{2i} \Big[\bar{\Psi}_e \bar{\Psi}_e \bar{\Psi}_i \gamma_5 \bar{\Psi}_i \\ &+ \Psi_e^+ \alpha_r \Psi_e \Psi_i^+ \alpha_r \gamma_5 \Psi_i \Big] \delta(r_i - r_e) d\tau_i d\tau_e. \end{aligned} \tag{2.12}$$

Since γ_5 is a diagonal operator, the contribution scales as v/c and can be neglected from the above equation which reduces to

$$H_{\rm PNC}^{\rm NSD} = \frac{G_F}{2\sqrt{2}} \int\int \sum_{i=p,n} 2C_{2i} \Psi_e^+ \alpha_r \Psi_e \Psi_i^+ \sigma \Psi_i \delta(r_i - r_e) d\tau_i d\tau_e, \tag{2.13}$$

where we have used the identity $\alpha_r \gamma_5 = \sigma$. Integral over the nuclear wave functions produces a quantity proportional to the spin of the nucleus $\vec{I}$ and the nuclear density $\rho_N(r)$. A constant of proportionality is defined such that

$$\sum_{i=p,n} 2C_{2i} \sigma_i \delta(r_i - r_e) = R_W \rho_N(r) = \frac{R_W}{I} \rho_N(r), \tag{2.14}$$

where R_W is called the 'weak magnetic moment' of the nucleus, just as Q_W is the 'weak charge'. This gives a final form for the NSD PNC contribution to the Hamiltonian given by

$$H_{PNC}^{\rm NSD} = \frac{G_F}{2\sqrt{2}I} R_W \alpha_e . \vec{I} \rho_N(r). \tag{2.15}$$

2.2.1.1 NSI and NSD PNC Matrix Elements

Before computing the matrix elements of the NSI and NSD PNC Hamiltonian, we introduce the relativistic notation of the two component single-particle orbitals. A relativistic orbital $|n\kappa m\rangle$ is an eigenfunction of the angular momentum operators $\hat{j}^2$ and $\hat{j}_z$ with

$$\hat{j}^2 |n\kappa m\rangle = j(j+1)|n\kappa m\rangle,$$
$$\hat{j}_z |n\kappa m\rangle = m|n\kappa m\rangle,$$

and the parity operator $\hat{P}$ which acts on the orbital to give

$$\hat{P}|n\kappa m\rangle = (-1)^l |n\kappa m\rangle, \tag{2.16}$$

where n is the principal quantum number, l is the azimuthal quantum number and κ is the relativistic angular quantum number given by

$$\kappa = -\left(j + \frac{1}{2}\right) a, \tag{2.17}$$

where $a = +1$ when $l = j - \frac{1}{2}$ and

$a = -1$ when $l = j + \frac{1}{2}$.

Each of these orbitals with the same (n, κ) but differing m quantum number are assumed to have the same radial form. Using the conventions of [12], an explicit representation of the single-particle orbitals is given by

$$\langle r|n\kappa m\rangle = \frac{1}{r} \begin{Bmatrix} P_{n\kappa}(r) & \chi_{\kappa,m}(\theta,\phi) \\ iQ_{n\kappa}(r) & \chi_{-\kappa,m}(\theta,\phi) \end{Bmatrix}, \tag{2.18}$$

where $P_{n\kappa}(r)$ and $Q_{n\kappa}(r)$ are the large and small component radial wave functions respectively. $\chi_{\kappa,m}(\theta,\phi)$ are the spinor spherical harmonics given by

$$\chi_{\kappa,m}(\theta,\phi) = \sum_{\sigma=\pm\frac{1}{2}} \langle lm-\sigma\frac{1}{2}\sigma|l\frac{1}{2}jm\rangle Y_l^{m-\sigma}(\theta,\phi)\phi^\sigma. \tag{2.19}$$

Here, $\langle lm-\sigma\frac{1}{2}\sigma|l\frac{1}{2}jm\rangle$ is a Clebsch-Gordan coefficient, $Y_l^{m-\sigma}$ is a spherical harmonic and ϕ^σ is a spinor basis function. Using above definitions, one can compute the matrix elements of the NSI and NSD PNC Hamiltonian at single-particle level.

Using Wigner Eckart theorem [13], the single-particle matrix element can be written as

$$\langle\phi_a|H_{\rm PNC}^{\rm NSI}|\phi_b\rangle = (-1)^{(j_a-m_a)}\begin{pmatrix} j_a & 0 & j_b \\ m_a & 0 & m_b\end{pmatrix}\langle\phi_a||H_{\rm PNC}^{\rm NSI}||\phi_b\rangle. \tag{2.20}$$

While computing the matrix element only the z component is considered. Substituting for the Hamiltonian and the orbitals, the actual matrix element takes the form

$$\langle\phi_a|H_{\rm PNC}^{\rm NSI}|\phi_b\rangle = \int \begin{pmatrix} P_a\chi^+_{\kappa_a m_a} & -iQ_a\chi^+_{-\kappa_a m_a}\end{pmatrix}\begin{pmatrix} 0 & -I \\ -I & 0\end{pmatrix}\begin{pmatrix} P_b\chi_{\kappa_b m_b} \\ iQ_b\chi_{-\kappa_b m_b}\end{pmatrix}\rho_N(r)Q_W dr d\Omega, \tag{2.21}$$

where $d\Omega$ denotes the integration over the angular coordinates. One can show that the angular factors obey the selection rule given by

$$\int \chi^+_{\kappa_a m_a}\chi_{-\kappa_b m_b}d\Omega = \delta_{\kappa_a,-\kappa_b}\delta_{m_a,m_b}. \tag{2.22}$$

The selection rule $\kappa_a = -\kappa_b$ implies that $j_a = j_b$ but of opposite symmetry. Substituting these we get the matrix element of NSI PNC Hamiltonian as

$$\langle\phi_a|H_{\rm PNC}^{\rm NSI}|\phi_b\rangle = i\int(P_bQ_a - Q_bP_a)\rho_N(r)Q_W dr. \tag{2.23}$$

Reduced matrix elements can be got by using Eq.2.20.

Single-particle matrix elements for NSD PNC can be written as

$$\langle\phi_a|H_{\rm PNC}^{\rm NSD}|\phi_b\rangle = (-1)^{(j_a-m_a)}\begin{pmatrix} j_a & 1 & j_b \\ m_a & 0 & m_b\end{pmatrix}\langle\phi_a||H_{\rm PNC}^{\rm NSD}||\phi_b\rangle. \tag{2.24}$$

Here the rank of the NSD PNC is 1, whereas for NSI PNC the rank is 0. As in the case of NSI PNC, only the z component is considered while computing the matrix element. Substituting for the Hamiltonian and the orbitals, the actual matrix element takes the form

$$\langle\phi_a|H_{\rm PNC}^{\rm NSD}|\phi_b\rangle = \int \begin{pmatrix} P_a\chi^+_{\kappa_a m_a} & -iQ_a\chi^+_{-\kappa_a m_a}\end{pmatrix}\begin{pmatrix} 0 & \sigma_z \\ \sigma_z & 0\end{pmatrix}\begin{pmatrix} P_b\chi_{\kappa_b m_b} \\ iQ_b\chi_{-\kappa_b m_b}\end{pmatrix}\rho_N(r)\mu_W dr d\Omega, \tag{2.25}$$

where $d\Omega$ denotes the integration over the angular co-ordinates. On further reduction, the matrix element of NSD PNC Hamiltonian takes the form

$$\langle\phi_a|H_{\rm PNC}^{\rm NSD}|\phi_b\rangle = \int (P_b Q_a - \frac{1}{3} Q_b P_a)\rho_N(r)\mu_W dr. \tag{2.26}$$

To get the reduced matrix element we need to divide the above matrix element by a phase factor and the 3j-symbol [13] available as a table. The radial integration for the NSI and NSD PNC has limits from 0 to ∞, though the value of it will be zero outside the nuclear region, where $\rho_N(r)$ is zero. A fairly accurate model of the nuclear density which agrees quite well with the experimental results is the Fermi-nucleus. In the this model, the nuclear density is given by

$$\rho_N(r) = \frac{\rho_0}{1 + e^{\frac{(r-b)}{a}}}, \tag{2.27}$$

where ρ_0 is a constant, b is the half density radius as $\rho_N(r) = \rho_0/2$ and a is related to the skin thickness t as $t/a = 4ln3$.

2.2.2 Properties of $H_{\rm PNC}$

(i)$H_{\rm PNC}^{\rm NSI,NSD}$ matrix elements are non-zero only for electron wave functions with finite value at the nucleus; thus $H_{\rm PNC}^{\rm NSI,NSD}$ connects only $s_{1/2}$ and $p_{1/2}$ orbitals having different parity.

(ii) While defining weak charge Q_W and weak moment R_W for heavy atoms we sum over all the nucleons coherently. Hence Q_W is proportional to Z. However, R_W comes from the sum over nucleon spin. These cancel in pairs over the nucleus, leaving just the unpaired spins. Thus, there is no Z enhancement for R_W and the NSD effects are a factor Z^{-1} smaller than the NSI ones.

(iii)Making a Foldy-Wouthuyson transformation [14] to the lowest order, we can write for a point-like nucleus and non-relativistic electron: [15]

$$H_{\rm PNC}^{\rm NSI} = \frac{G_F Q_W}{2\sqrt{2}} \frac{1}{2mc} [\sigma_e.p_e, \delta(r)]_+, \tag{2.28}$$

and

$$H_{\rm PNC}^{\rm NSD} = \frac{G_F R_W}{2\sqrt{2}I} \frac{1}{2mc} [\sigma_e.p_e, \sigma_e.I^N \delta(r)]_+, \tag{2.29}$$

where the + sign indicates an anticommutator. From the above form, it is easy to derive the well known result, pointed out by Bouchiat and Bouchiat [6], that matrix elements of $H_{\rm PNC}^{\rm NSI}$ for heavy atoms are proportional to Z^3. This factor arises from

(i) $Q_W \propto N$ and $N \propto 3Z/2$ for heavy atoms.

(ii) The matrix element is proportional to the density of the electronic wave functions at the origin, $|\Psi(0)|^2$, which is proportional to Z for heavy atoms.

(iii) $\sigma.p \propto$ velocity of the electron at the origin which is proportional to Z.

2.2.3 PNC Hamiltonian arising from NAM.

The parity non-conserving weak interaction between the nucleons can lead to NAM [16, 17] which in turn can interact with the atomic electrons via the electro magnetic interaction. The possible existence of an anapole moment was first predicted by Zeldovich in 1958 [18]. In order to understand the physical concepts underlying this unusual moment, we consider a current distribution with density $\vec{j}(\vec{r})$. The total magnetic field due to this current distribution is

$$\vec{B} = \vec{B_l} + \vec{B_{nl}}, \tag{2.30}$$

where B_l and B_{nl} are the magnetic fields inside and outside the current distribution respectively. The local vector potential $\vec{A_l}$ related to $\vec{B_l}$ by the following relations

$$\vec{B_l} = \vec{\nabla} \times \vec{A_l}. \tag{2.31}$$

The electro magnetic interaction energy of an external current distribution with $\vec{A_l}$ is given by

$$W = \frac{1}{c} \int \vec{j'}(\vec{r}).\vec{A_l} d\tau. \tag{2.32}$$

Density of the external current distribution can be expanded as

$$\vec{j'}(\vec{r}) = \vec{j'}(0) + (\vec{r}.\vec{\nabla})\vec{j'}(0) + ... \tag{2.33}$$

Considering just the first term *i.e.*, assuming that the extent of the external current distribution is small and that $\vec{j'}$ is essentially uniform, we get

$$W = -\frac{1}{c}\vec{j'}(0) \int \vec{A_l} d\tau = -\frac{1}{c}\vec{j'}(0).\vec{a} \tag{2.34}$$

where $\vec{a} = \int \vec{A_l} d\tau$ is known as the anapole moment of the current distribution. Note that $\vec{A_l} = \vec{a}\delta(\vec{r})$. The anapole moment is clearly a vector and is therefore odd under parity. A multipole expansion of $\vec{A_l}$ yields [19]

$$\vec{a} = -\frac{\pi}{c} \int r^2 \vec{j}(\vec{r}) d\tau. \tag{2.35}$$

One could consider the anapole moment being associated with a toroidal current distribution.

2.2.3.1 Nuclear Anapole Moment

General features of the anapole moment of the nucleus have been discussed by Flambaum and Khriplovich [20]. They use the shell model and assume a nucleus-nucleus parity non-conserving interaction of the type

$$H_{\rm PNC}^{ana} = \frac{G_F g}{2\sqrt{2}m}(\vec{\sigma}.\vec{p} + \vec{p}.\vec{\sigma})\rho_N(r), \tag{2.36}$$

where $\vec{\sigma}$ and $\vec{p}$ are the spin and momentum operators of valence nucleon, m is the mass of the proton and others as described previously. The dimensionless constant g characterises the parity odd interaction of the valence nucleon with the nucleon core. It is estimated that $g_p \approx 4$ for an external proton and $g_n \leq 1$ for a neutron.

Treating $H_{\rm PNC}^{ana}$ as a first-order perturbation, it can be shown that the NAM arises only from the spin part of the current density and it can be expressed as [19]

$$\vec{a_N} = \frac{G_F}{2\sqrt{2}}\frac{1}{e}\frac{2\chi K_a}{(I+1)}\frac{\vec{I}}{I}, \tag{2.37}$$

where

$$\chi = (I + 1/2)(-1)^{I+1/2-l}, \tag{2.38}$$

and

$$K_a = \frac{9}{10}(24\alpha^2\mu g A^{2/3}). \tag{2.39}$$

Here l is the orbital angular momentum of the valence electron. The contribution of the core excitations to the NAM has been found to be small [21]. Note that the quantity K_a contains information about g, the parity non-conserving nucleon-meson coupling constants. Indeed an accurate determination of K_a can lead to accurate values of g. The NAM therefore can be a valuable source of information about nuclear parity non-conservation.

2.2.3.2 Interaction of the NAM with Atomic Electrons

A peculiar feature of the NAM is that it cannot be probed by real photons. It can be observed in processes where virtual photons are exchanged with some interacting particle, such as an atomic electron. Therefore in order to detect the NAM one has to perform an experiment on an atom. The Hamiltonian describing the electro magnetic interaction of the NAM with an atomic electron

$$H_{an} = -\frac{1}{c}\vec{j_e}.\vec{A_N}, \tag{2.40}$$

where $\vec{j_e}$ is the electron current density and $\vec{A}_N$ is the nuclear vector potential and

$$\vec{j_e} = -ec\vec{\alpha}. \tag{2.41}$$

Here, $\vec{\alpha}$ represents three Dirac matrices. Using an earlier result, we write

$$\vec{A}_N = \vec{a}_N \delta(\vec{r}). \tag{2.42}$$

One can therefore write

$$H_{\rm PNC}^{ana} = \frac{G_F}{2\sqrt{2}} K_a \frac{2\chi}{(I+1)} \vec{\alpha}.\frac{\vec{I}}{I}\delta(\vec{r}). \tag{2.43}$$

We define

$$S_W = K_a \frac{2\chi}{(I+1)}. \tag{2.44}$$

Hence the PNC Hamiltonian arising due to anapole moment takes the form

$$H_{\rm PNC}^{ana} = \frac{G_F}{2\sqrt{2}} S_W \vec{\alpha}.\frac{\vec{I}}{I}\delta(\vec{r}). \tag{2.45}$$

It is interesting to note that $H_{\rm PNC}^{ana}$ has the same form as $H_{\rm PNC}^{\rm NSD}$ arising from neutral weak current interaction so that they both lead to the same observable effects. However, in the case of heavy atoms, the contributions of $H_{\rm PNC}^{ana}$ is larger than the $H_{\rm PNC}^{\rm NSD}$ arising from neutral weak current interactions [16]. The reason can be attributed to the scaling of anapole moment Hamiltonian as $A^{2/3}$. The total NSD parity non-conserving interaction which arises from the NAM and the neutral current can be written as

$$H_{\rm PNC}^{\rm NSD} = \frac{G_F}{2\sqrt{2}} \mu_W \vec{\alpha}.\frac{\vec{I}}{I}\delta(\vec{r}), \tag{2.46}$$

where

$$\mu_W = R_W + S_W. \tag{2.47}$$

However, an atomic parity non-conservation experiment cannot distinguish between these two interactions. Together the two interactions can be separated from the nuclear spin independent interaction by measuring the difference in the parity non-conserving observable corresponding to two different transitions between hyperfine states [19]. More detailed study on anapole moment is given by Boston [15]. The present status and the future prospects are given in the paper by Das et al. [22].

2.3 Parity Non-Conserving Electric Dipole Transition Amplitude $E1PNC$

Accurate calculations of $E1PNC$ are essential if we have to connect experimental results to electro-weak theory. In this section, we discuss in brief how this quantity in

combination with PNC experiments can yield important information about physics beyond the Standard Model. As the NSI PNC term is proportional to Z^3, most experiments and theory to date have concentrated on heavy atoms.

The atomic Hamiltonian of the system will contain in addition the PNC Hamiltonian $H_{\rm PNC}$ and hence the eigenfunctions will become states of mixed parity given by

$$|\tilde{\Psi}_i\rangle = |\Psi_i^{(0)}\rangle + |\Psi_i^{(1)}\rangle, \tag{2.48}$$

where $|\Psi_i^{(1)}\rangle$ is given by perturbation theory in terms of the zeroth-order unperturbed eigenfunctions as

$$|\Psi_i^{(1)}\rangle = \sum_{j\neq i} \frac{\langle\Psi_j^{(0)}|H_{\rm PNC}|\Psi_j^{(0)}\rangle}{(E_i^0 - E_j^0)}. \tag{2.49}$$

The perturbed wave function $|\Psi_i^{(1)}\rangle$ and the unperturbed wave function $|\Psi_i^{(0)}\rangle$ are of opposite parity. For example, an $s_{1/2}$ function will contain admixtures which have $p_{1/2}$ angular characteristics and vice versa. These PNC ad mixtures allow non-zero E1 matrix elements between states originally of the same parity given by

$$\begin{aligned} E1PNC &= \langle\tilde{\Psi}_f|D|\tilde{\Psi}_i\rangle \qquad (2.50)\\ &= \langle\Psi_f^{(0)}|D|\Psi_i^{(1)}\rangle + \langle\Psi_f^{(1)}|D|\Psi_i^{(0)}\rangle, \end{aligned}$$

where the other terms disappear because they have same parity. The general PNC matrix element can now be written in terms of parity eigenstates as

$$E1PNC = \sum_{I\neq i} \frac{\langle\Psi_f^{(0)}|D|\Psi_I^{(0)}\rangle\langle\Psi_I^{(0)}|H_{\rm PNC}|\Psi_i^{(0)}\rangle}{E_i - E_I} \tag{2.51}$$

$$+ \sum_{I\neq f} \frac{\langle\Psi_f^{(0)}|H_{\rm PNC}|\Psi_I^{(0)}\rangle\langle\Psi_f^{(0)}|H_{\rm PNC}|\Psi_i^{(0)}\rangle}{E_f - E_I}. \tag{2.52}$$

A variety of *ab initio* and semi-empirical methods have been employed to calculate this quantity [23]. Many-Body Perturbation Theory (MBPT) is the most widely used method for such calculations. Apart from the parity non-conserving interaction, the residual interaction (difference of the two-electron Couloumb interaction and the one-electron Hartree-Fock potential) is also treated as a perturbation. In this approach, the wave function is computed order-by-order. Using Coupled Cluster (CC) method one can compute the wave function to all orders for particular types of excitations (singles, doubles etc.,). For atoms with strongly interacting configuration, it would be appropriate to use a hybrid approach consisting of the Configuration Interaction (CI) and MBPT or CC approaches. Examples of such atoms are bismuth and ytterbium.

Quantity that is measured in experiment depends on the interference of $E1PNC$ and an allowed electro magnetic transition amplitude [24]. Experiments that have

been successful so far are based on fluorescence and optical rotation [25, 26]. In the former case the interference is between $E1PNC$ and a Stark-induced electric dipole transition amplitude. In the latter it is between $E1PNC$ and an allowed magnetic dipole transition amplitude.

By combining the results of atomic parity non-conservation experiments and calculations, it is possible to extract Q_W and quantities characterising the NSD interaction. The extraction of Q_W has important implications for physics beyond the Standard Model. One can express the deviation of this quantity from its Standard Model value as

$$\Delta Q_W = Q_W - Q_W^{SM}, \tag{2.53}$$

where the Standard Model value of Q_W is given by

$$Q_W = Z(1 - 4sin^2\theta) - N. \tag{2.54}$$

Here, Z is the atomic number, N is the number of neutrons and $\sin^2\theta_W$ is the Weinberg mixing angle. The present value of $\sin^2\theta_W$ estimated from the relative rates of the charged and neutral weak current interactions is 0.23 [27]. One can deduce the atomic physics value of $\sin^2\theta_W$, by knowing the theoretical and experimental $E1PNC$ matrix element and simply equating them to get Q_W. One can check the experimental values of $E1PNC$ by taking the present value of $\sin^2\theta_W$ thereby deducing Q_W and using this in the theoretical matrix element. After the inclusion of radiative corrections

$$Q_W^{SM} = (0.9793 - 3.8968sin^2\theta_W)Z - 0.9793N. \tag{2.55}$$

It is possible to parameterise Q_W and hence ΔQ_W in terms of the isospin conserving and breaking parameters, S and T [28] given by

$$Q_W = (0.9857 \pm 0.0004)\rho(-N + Z[1 - 4.012 \pm -0.010)\bar{x}]), \tag{2.56}$$

where

$$\rho = 1 + 0.00782T$$

and

$$\bar{x} = 0.2323 + 0.00365S - 0.00261T.$$

If $S \sim 1$ as predicted by certain model [29], then Q_W clearly must be determined to at least an accuracy of one percent. It may be shown that Q_W is sensitive to new physics where weak isospin is conserved [30]. In other words the combined accuracy of atomic PNC experiment and the theory has to be at least a percent to test physics beyond the Standard Model. Other related implications to particle physics are given in the paper by Sandars [31] and the references therein. The uncertainty arising

from atomic calculations can be circumvented by measuring the fractional difference of Q_W, but that could lead to nuclear structure uncertainties [32]. The value of K_a defined earlier can give quantitative information about the nuclear anapole moment. The present status of PNC experiments and theory is given below.

2.4 Present Status of NSI PNC in Atoms/Ions

The present status of NSI atomic parity non-conservation is summarised in the Table 2.1: It is clear that one can only use the results for caesium at this stage to make

Table 2.1: Present status of NSI PNC in various atoms/ions.

Atom	Transition	Accuracy of Experiment	Accuracy of Theory
Caesium	$5\mathrm{p}^6 6s_{\frac{1}{2}} \rightarrow 5p^6 7s_{\frac{1}{2}}$	0.35%	$\sim$ 1%
Thallium	$6\mathrm{s}^2 6p_{\frac{1}{2}} \rightarrow 6s^2 6p_{\frac{3}{2}}$	$\sim$ 1%	$\sim$ 3%
Thallium	$6\mathrm{s}^2 6p_{\frac{1}{2}} \rightarrow 6s^2 7p_{\frac{1}{2}}$	$\sim$ 15%	$\sim$ 5%
Lead	$6\mathrm{p}^2, J=0 \rightarrow 6p^2, J=1$	$\sim$ 1%	$\sim$ 10-15%
Bismuth	$6\mathrm{p}^3, J=\frac{3}{2} \rightarrow 6p^3, J=\frac{3}{2}$	$\sim$ 2%	$\sim$ 10%
Bismuth	$6\mathrm{p}^{\ 3}, J=\frac{3}{2} \rightarrow 6p^3, J=\frac{5}{2}$	$\sim$ 2%	$\sim$ 10%
Barium +	$5\mathrm{p}^6 6s_{\frac{1}{2}} \rightarrow 5p^6 5d_{\frac{3}{2}}$		$\sim$ 10%
Ytterbium	$6\mathrm{s}^{\ 2} \rightarrow 6s5d, J=1$		$\sim$ 15%
Francium	$6\mathrm{p}^6 7s_{\frac{1}{2}} \rightarrow 6p^6 8s_{\frac{1}{2}}$		$\sim$ 1%

predictions about physics beyond the Standard Model. Using the results of the latest experiment and theory for that atom, we find that

$$Q_W = (-72.41 \pm 0.25 \pm 0.80). \tag{2.57}$$

If we assume that there can be physics beyond the Standard Model, *i.e.* $\Delta Q_W \neq 0$, then we deduce the following limit

$$S + 0.006T = (-1.3 \pm 0.3 \pm 1.1). \tag{2.58}$$

Recently Bennett and Wieman [33] have measured certain spectroscopic properties of caesium relevant to PNC, and have arrived at the conclusion that for Cs^{133}

$$Q_W = (= 72.06 \pm 0.28 \pm 0.3). \tag{2.59}$$

This differs from the prediction of the Standard Model by 2.5σ. For all the quantities which have been extracted above, the first and second errors correspond to experimental and theoretical errors respectively. The latter must clearly be improved in order to make definitive predictions about physics beyond the Standard Model. In the next section, the proposed experiment on Ba^+ ion using laser cooling and trapping is discussed.

2.5 PNC in Laser Cooled Ion

The last two decades have witnessed remarkable advances in trapping and laser cooling of ions and atoms [34]. Application of strong electro magnetic fields has made the trapping of ions possible [35]. Trapped ions can be cooled in various ways [36]. Here we discuss how some of the techniques of trapping and laser cooling can be applied to the study of symmetry violations in atomic systems. A novel approach to the measurement of atomic parity non-conservation exploiting some of these advances was proposed by Fortson in 1993 [37]. The accuracy of this approach would most likely be sufficient to test the Standard Model.

An experiment to observe parity non-conservation in Ba^+ is currently under way at the University of Washington, Seattle. Ba^+ has been trapped by a potential well 50 eV depth created by RF fields of frequency 25 MHz and cooled to an orbital radius $< 0.1\ \mu m$ by Dehmelt and co-workers [38]. This ensures that the wavelength of the $6s_{1/2} \rightarrow 5d_{3/2}$ transition which has been proposed for observing parity non-conservation ($\lambda = 2.05\ \mu m$) is much larger than the radius of the ion after it has been trapped and cooled. This requirement known as the Lamb-Dicke condition is necessary to overcome the first-order Doppler shift. Physical quantity that has been proposed to be measured in the afore mentioned experiment is a parity non-conserving light shift (AC Stark Shift) arising from the interference of the parity non-conserving electric dipole transition amplitude ($E1PNC$) and the electric quadrupole transition amplitude (E2).

Electric field of the laser inducing the parity non-conserving transition is given by

$$\vec{E}(\vec{r},t) = \frac{1}{2}[\vec{E}(\vec{r})e^{-i\omega t} + C.C.] \tag{2.60}$$

where ω is the frequency of laser and C.C refers to complex conjugate. Parity non-conserving and electric quadrupole Rabi frequencies are

$$\Omega^{\rm PNC}_{m'm} = -\frac{1}{2\hbar}\sum_i (E1PNC_{m'm})_i E_i(0) \tag{2.61}$$

and

$$\Omega^{quad}_{m'm} = -\frac{1}{2\hbar}\sum_{ij}(E2_{m'm})_{ij}\frac{\partial E_i}{\partial x_j}\mid_0, \tag{2.62}$$

where m and m$'$ are the magnetic quantum numbers of initial and final states respectively. $\mathrm{E}_i(0)$ and $\frac{\partial E_i}{\partial x_j}\mid_0$ are the components of the electric field of laser and its gradient at the position of the ion.

The parity non-conserving effects are related to

$$\begin{aligned} \mid \Omega_{m'm} \mid^2 &= \mid \Omega^{quad}_{m'm} + \Omega^{\mathrm{PNC}}_{m'm} \mid^2 \\ &= \mid \Omega^{quad}_{m'm} \mid^2 + 2Re(\Omega^{\mathrm{PNC}*}_{m'm}\Omega^{quad}_{m'm}). \end{aligned} \tag{2.63}$$

Light shift of the m^{th} sub level of initial state is given by [39].

$$\hbar\triangle\omega_m = \hbar[\frac{(\omega_0-\omega)}{2} - \Omega_m], \tag{2.64}$$

where $\Omega_m = \Sigma_{m'} \mid \Omega_{m'm} \mid^2$ and ω_0 is the resonant frequency. Since contribution to the light shift comes from the parity non-conserving electric dipole and electric quadrupole transitions, we get

$$\hbar\triangle\omega_m = \hbar\triangle\omega^{\mathrm{PNC}}_m + \hbar\triangle\omega^{quad}_m, \tag{2.65}$$

where

$$\triangle\omega^{\mathrm{PNC}}_m \approx -Re^{\Sigma}_{m'}(\Omega^{\mathrm{PNC}*}_{m'm}\Omega^{quad}_{m'm})/\Omega^{quad}_m, \tag{2.66}$$

and

$$\triangle\omega^{quad}_m \approx \frac{(\omega_0-\omega)}{2} - \Omega^{quad}_m. \tag{2.67}$$

Here, $(\Omega^{quad}_m)^2 = \sum_{m'} \mid \Omega^{quad}_{m'm} \mid^2 \triangle\omega^{\mathrm{PNC}}_m$ changes sign when the sign of m changes, from $+\frac{1}{2}$ to $-\frac{1}{2}$, but $\triangle\omega^{quad}_m$ does not. This is exploited to measure the difference of the light shift for the magnetic quantum numbers $m = \frac{1}{2}$ and $m = -\frac{1}{2}$

$$\triangle\omega_{m=\frac{1}{2}} - \triangle\omega_{m=-\frac{1}{2}} = \triangle\omega^{\mathrm{PNC}}_{m=\frac{1}{2}} - \triangle\omega^{\mathrm{PNC}}_{m=-\frac{1}{2}}. \tag{2.68}$$

For the $6s_{1/2} \rightarrow 5d_{3/2}$ transition in Ba^+, this difference is approximately 1.2 Hz for an electric field equal to about $2 \times 10^4 V/cm$. Statistical accuracy of this kind of a PNC experiment is given by

$$\frac{E^{\mathrm{PNC}}_1}{\partial E^{\mathrm{PNC}}_1} = \frac{E^{\mathrm{PNC}}_1 E}{\hbar} f\sqrt{N\tau t}, \tag{2.69}$$

where f is the efficiency factor, τ is the coherence time determined by the decay of the final state, t is the total time available for the measurement and $N = 1$ is the

number of ions. For $f = 0.2$, E_1^{PNC} can, in principle, be measured to 1 part in a 1000 in about a day. It is clear from the above expression that competitive accuracy of the single ion experiment is due to the possibility of applying a large electric field to the ion and the long coherence time associated with the decay of the final state (the lifetime of the $5d_{3/2} = 79.8$ sec) [40].

Bibliography

[1] Y.B. Zeldovich, *Sov. Phys.*, JETP, **9**, 682 (1959).

[2] F. Curtis-Michel, *Phys. Rev. B* **138**, 408 (1965).

[3] F.J. Hasert et al. *Phys. Lett.* **46**, 138 (1973).

[4] G. Arnison et al. *Phys. Lett.* **122B**, 476 (1983); *Phys. Lett.* **126B**, 398 (1983), UA1 Collaboration; G. Banner et al. *Phys. Lett.* **122B**, 476 (1983), UA2 Collaboration.

[5] C.Y. Prescott et al. *Phys. Lett.* **77B**, 347 (1978) and **84B**, 524 (1979).

[6] M.A. Bouchiat and C. Bouchiat, *Phys. Lett.* **B48**, 111 (1974), M.A. Bouchiat and C. Bouchiat, *J. Phys.* (France) **35**, 899 (1974).

[7] I.J.R. Aitchison, *Relativistic Quantum Mechanics*, Macmillan.

[8] E.N. Fortson and L. Wilets, *Adv. Atom. Mol. Phys.* **16**, 319 (1980).

[9] G. Feinberg and M.Y. Chen, *Phys. Rev.*, **D10**, 3789 (1974).

[10] R.W. Dunford, R.R. Lewis and W.L. Williams, *Phys. Rev.* **A18**, 2421 (1978).

[11] W.J. Marciano, W.J.A. Sirlin, *Phys. Rev.* **D27**, 552 (1983).

[12] I.P. Grant, *Adv. Phys.* **19**, 747 (1970).

[13] I. Lindgren, J. Morrison, *Atomic Many-Body Theory*, Springer-Verlag, New York (1981).

[14] J.D. Bjorken and S.D. Drell, McGraw Hill, International Edition (1995).

[15] E.R. Boston, *D. Phil Thesis*, University of Oxford (1990).

[16] V.V. Flambaum and I.B. Khriplovich, *ZH. Esp. Teor. Fiz.* **79**, 1656 (1980) [*Sov. Phys.* JETP **52**, 835 (1980)].

[17] C. Bouchiat, *Z. Phys.* **C49**, 91 (1991).

[18] Y.B. Zeldovich, *Sov.Phys* **JETP 6**, 1184 (1958).

[19] I.B. Khriplovich, *Comments, At. Mol. Phys.* **23**, 189 (1989).

[20] V.V. Flambaum, I.B. Khriplovich and O.P. Sushkov, *Phys. Lett. B* **146**, 367 (1984).

[21] V.V. Flambaum, I.B. Khriplovich and O.P. Sushkov, *Phys. Lett. B* **162**, 213 (1985).

[22] B.P. Das, A.D. Singh, K.P. Geetha, *Proceedings of the DAE Nuclear Physics Symposium*, eds. V.M. Datar and A.B. Santra, **404**, 2 (1997).

[23] S.A. Blundell et al. *Theor. Chim. Acta* **80**, 257 (1991).

[24] D.N. Stacey, *Physica Scripta* **T40**, 15 (1992).

[25] C.S. Wood, S.C. Bennett, D. Cho, B.P. Masterson, J.L. Roberts, C.E. Tanner and C.E. Wieman, *Science* **275**, 1759 (1997).

[26] P. Vetter et al. *Phys. Rev. Lett.* **74**, 2658 (1995).

[27] G. Rajasekaran, M.G.K. Menon, V.S. Narasimham, P.V. Ramanamurthy, B.V. Sreekantan, K. Hinotani, S. Miyake, D.R. Creed, J. Osborne, J. Pattison and A. Wolfendale, *Phys. Lett.* **18**, 196 (1965).

[28] V.A. Dzuba, V.V. Flambaum, P.G. Silvestrov and O.P. Sushkov, *J. Phys. B* **20**, 3297 (1987).

[29] M. Peskin and T. Takeuchi, *Phys. Rev. Lett.* **65**, 964 (1990).

[30] W. Marciano and Rosner, *J. Phys. Rev. Lett.* **65**, 2963 (1990).

[31] P.G.H. Sandars, *Physica Scripta* **T46**, 16 (1993).

[32] S.J. Pollock, E. Fortson and L. Wilets, *Phys. Rev. C.* **46**, 2587 (1992).

[33] S.C. Bennett and C.E. Wieman, *Phys. Rev. Lett.* **82**, 2484 (1999); **82**, 4153 (E) (1999); **83**, 889 (E) (1999). Revised Edition (1994).

[34] C.E. Wieman, D.E. Pritchard and D.J. Wineland, *Rev. Mod. Phys.* **71**, S253 (1999).

[35] P.K. Ghosh, *Ion traps*, Clarendon, Oxford (1995).

[36] D.J. Wineland and W.M. Itano, *Phys. Today* **40**, 34 (1987).

[37] N. Fortson, *Phys. Rev. Lett.* **70**, 2383 (1993).

[38] G. Janik, W. Nagourney and H. Dehmelt, *J. Opt. Soc. Am. B* **2**, 1251 (1985).

[39] C. Cohen-Tannoudji and S. Reynaud, *Phys. Rev. B* **10**, 345 (1977).

[40] N. Yu, W. Nagourney, and H. Dehmelt, *Phys.Rev.Lett.* **78**, 4898 (1997).

Chapter 3

Configuration Interaction Method Applied to Parity Non-Conservation in Atoms

---

3.1 Introduction

Liquids and solids, atoms and molecules, and nuclei all these clearly are interacting many-body systems. Even a nucleon may be regarded as a many-particle system not just because it is now known to consist of three quarks interacting via gluons, but because of the possibility in quantum field theory of virtual excitation of many particles from vacuum. So one defines many-body physics as a branch of theoretical physics that studies new phenomena or "emergent properties" that arise from the interactions among "elementary" constituents of a many-particle system. This provides the means and the methods for carrying out precise calculations of characteristic properties of these systems as compared with experimental results to verify the hypotheses about the nature of the constituents and their interactions. In the beginning of this chapter we give a brief overview of independent-particle model for the wave function of a many-body system, then describe the Configuration Interaction (CI) method and it's applications to PNC in atoms.

3.2 Independent Particle Model

The Independent Particle Model (IPM) has played a central role in electronic structure calculations ever since its introduction for the treatment of many-electron atoms by Slater in 1929 [1]. The term IPM refers to the formalism in which a many-particle wave function is based on a product of single-particle functions. Each single-particle function is often called a spin-orbital. Each of these single-particle orbitals is determined by methods that consider the effect of all the other single-particle orbitals, so that the "independence" is formal rather than physical. Hartree-Fock (HF) model is the most widely used method in deriving the single-particle orbitals for atoms. It is an approximation which yields a very good starting point from which we apply a variety of techniques for improving electronic-structure description.

We discuss a system containing N electrons characterised by a Hamiltonian of the form,

$$H = H_0 + V_{es}, \tag{3.1}$$

where H_0 and V_{es} are the single and two electron operators. In the HF approximation, it is given by

$$H_0 = \sum_i -\frac{1}{2}\nabla_i^2 + \frac{Z}{r_i} + u_i(r_i) \tag{3.2}$$

and

$$V_{es} = -\sum_i u_i(r_i) + \sum_{i<j}\frac{1}{r_{ij}}. \tag{3.3}$$

The exact two-body interaction between the electrons is approximated in the Hamiltonian H_0 by an average one-electron interaction. V_{es} causes departures from the single-particle description and is treated as a perturbation. In order to satisfy Pauli's exclusion principle, the wave function of a many-electron system must be antisymmetric with respect to the interchange of electrons. Hence the many-electron IPM wave function using the single-particle orbitals is written as a determinant given by

$$\Phi = \sqrt{(1/N!)}\begin{vmatrix} \phi_1(1) & \phi_1(2) & \phi_1(3)... & \phi_1(N) \\ \phi_2(1) & \phi_2(2) & \phi_2(3)... & \phi_2(N) \\ ..... & ..... & ..... & \\ \phi_N(1) & \phi_N(2) & \phi_N(3)... & \phi_N(N) \end{vmatrix}.$$

We determine single-particle orbitals ϕ by the criterion that the expectation value of the Hamiltonian, $\langle\Phi|H|\Phi\rangle$, is minimum subject to the constraint that ϕ's are orthonormal. This leads to the HF equation given by

$$H_0|\phi_i\rangle = \epsilon_i|\phi_i\rangle, \tag{3.4}$$

where

$$u_i(r)|\phi_i(r)\rangle = \sum_j \langle\phi_j(r')|v(r,r')|\phi_j(r)\rangle|\phi_i(r)\rangle - \sum_j \langle\phi_j(r')|v(r,r')|\phi_j(r)\rangle|\phi_i(r)\rangle. \quad (3.5)$$

This interaction consists of two parts of which first is the Couloumb part which is simply the electrostatic interaction of the i^{th} electron with the charge density of all other electrons. This is normally called the direct part and the remaining is called the exchange part, which has no classical analog and is due to the antisymmetry requirement on many-electron wave function. It should be noted that Eq. 3.4. does not define a typical linear eigenvalue problem, because the potential $u_i(r)$ contains the eigenfunctions ϕ. Hence an iterative solution is needed with an input set of ϕ's which is used to define the potential and based on it a new set of ϕ's is obtained. This procedure is repeated till self-consistency is reached and it is for this reason that the HF method is also known as the self-consistent field (SCF) method.

Even though each ϕ is determined from an equation that includes interaction with all other electrons, the function Φ cannot be an exact solution to the many-electron Schrödinger equation. It is deficient in that it ignores the fact, that the probability distribution of each electron as a function of positions of all other electrons, and not merely dependent upon their distributions as a whole. In other words, the true probability of electron i being in any particular volume element must correlate with the probabilities that other electrons are individually in particular volume elements. It is customary to refer to this deficiency of the HF wave function as lack of electron correlation.

The IPM often yields qualitatively correct results for quantities such as total energy. However, there are many physically important properties for which the IPM is inadequate. In this chapter, we introduce the CI approach in order to go beyond the IPM in the computation of parity non-conserving electric dipole transition amplitude.

3.3 Overview of CI Method

The CI method is more appropriately referred to as the method of superposition of configurations. This involves the expansion of the many-electron wave function as a linear combination of determinantal functions, with the coefficient of various determinants found by the application of variation principle. Given an orthonormal set of single-particle functions (ϕ_i), the most general fully antisymmetric CI wave functions generally referred as Configuration State Functions (CSFs) can be constructed as a linear combination of determinants. These determinants are made of ϕ_is identified

by total angular momentum J, total magnetic quantum number M and the γ which is an additional quantum number required to define the CSF uniquely. The atomic state function (ASF) can then be obtained as a linear combination of these CSFs. An ASF is defined by same J and M as the CSFs but with a different additional quantum number Γ, and is given by

$$|\Psi(\Gamma_i JM)\rangle = \sum_j C_{ij}|\Phi(\gamma_j JM)\rangle. \tag{3.6}$$

ASFs are eigenfunctions of the atomic Hamiltonian and satisfy the Schrödinger equation

$$H|\Psi(\Gamma_i JM)\rangle = E_i|\Psi(\Gamma_i JM)\rangle, \tag{3.7}$$

where E_i is the energy eigenvalue of the ASF. While computing matrix elements of operators it is summed over M and effectively it is the quantum numbers Γ and J that identify an ASF. H commutes with parity operator P defined earlier in Chapter 2, hence CSFs and ASFs are parity eigenstates.

The possible determinants in a CSF include the reference HF $|\Phi_0\rangle$, the singly excited determinants $|\Phi_a^r\rangle$ (which differ from $|\Phi_0\rangle$ in having the orbital ϕ_a replaced by ϕ_r), the doubly excited determinant $|\Phi_{ab}^{rs}\rangle$, etc., including N-tuply excited determinants. Using these many-electron wave functions as basis, the exact many-electron wave function can be written as

$$|\Psi_0\rangle = c_0|\Phi_0\rangle + \left(\frac{1}{1!}\right)^2 \sum_{ar} c_a^r|\Phi_a^r\rangle + \sum_{abrs}\left(\frac{1}{2!}\right)^2 c_{ab}^{rs}|\Phi_{ab}^{rs}\rangle + ... \tag{3.8}$$

Considering the above as the trial wave function, the problem of finding the optimum coefficients $c's$ can be reduced to that of a matrix diagonalisation. The matrix representation of the Hamiltonian operator in the basis $|\Phi_i\rangle$ is an $N \times N$ matrix $\mathbf{H}$ with elements given by

$$(H)_{ij} = \langle\Phi_i|H|\Phi_j\rangle. \tag{3.9}$$

Since the Hamiltonian is Hermitian and the basis are real, $\mathbf{H}$ is symmetric, *ie.*, $H_{ij} = H_{ji}$. The trial function is normalised, so that

$$\langle\Psi_0|\Psi_0\rangle = \sum_{ij} c_i c_j\langle\Phi_i|\Phi_j\rangle = \sum_i c_i^2 = 1. \tag{3.10}$$

The expectation value

$$\langle\Psi_0|H|\Psi_0\rangle = \sum_{ij} c_i\langle\Phi_i|H|\Phi_j\rangle c_j = \sum_{ij} c_i c_j H_{ij}, \tag{3.11}$$

is a function of the expansion coefficients. We find the parameters $c's$ for which $\langle\Psi_0|H|\Psi_0\rangle$ is a minimum given by

$$\frac{\partial}{\partial c_k}\langle\Phi|H|\Phi\rangle = 0, k = 1, 2, ...N. \tag{3.12}$$

This leads to

$$\sum_j H_{ij}c_j - Ec_i = 0. \tag{3.13}$$

By introducing a column vector $\mathbf{c}$ with elements c_i, this set of equations can be written in matrix notation as

$$H\mathbf{c} = E\mathbf{c}, \tag{3.14}$$

which is the standard eigenvalue problem for the matrix $\mathbf{H}$. Since $\mathbf{H}$ is symmetric, the above equation can be solved to yield N orthonormal eigenvectors c_i and corresponding eigenvalues E_i, which for convenience are arranged so that $E_0 \leq E_1 \leq ... \leq E_{N-1}$. This is called full CI matrix, and the method is referred to as full CI. The lowest eigenvalue will be an upper bound to the ground state energy of the system. Eq. 3.8 can be conveniently rewritten as

$$|\Psi_0\rangle = c_0|\Phi_0\rangle + c_S|S\rangle + c_D|D\rangle + c_Q|Q\rangle + ..., \tag{3.15}$$

where $|S\rangle$ represents the terms involving single excitations, $|D\rangle$ represents the double excitations, and so on. The criteria for choosing the configurations for the computation are summerised below:

(i) There is no coupling between the HF ground state and singly excited state *i.e.*, $\langle\Phi_0|H|S\rangle = 0$. This is the consequence of Brillouin's theorem [2].

(ii) There is no coupling between the HF ground state, triples and quadruples. This is the consequence of Slater Condon Rule [2] due to which elements between states which differ by the quantum numbers of two orbitals are zero.

(iii) Single excitations do not mix directly with HF ground state, but they can be expected to have a very small effect because they mix indirectly with doubles which in turn interact with HF state.

(iv) Since double excitation mix directly, they play an important role in determining the correlation energy. It turns out that quadruple excitations are more important than the triple or single excitations [2].

In next section we discuss how we compute $E1PNC$ using the CI method.

3.4 Expression for $E1PNC$

If H_0 is the unperturbed atomic Hamiltonian and $|\Psi_0\rangle$ is the atomic state function, then

$$H_0|\Psi_0\rangle = E_0|\Psi_0\rangle. \tag{3.16}$$

Treating the NSI/NSD parity non-conserving interaction as a first order perturbation results in changing a state of definite parity to a state of mixed parity

$$|\Psi_i^0\rangle \rightarrow |\Psi_i^0\rangle + |\Psi_i^1\rangle, \tag{3.17}$$

$$|\Psi_f^0\rangle \rightarrow |\Psi_f^0\rangle + |\Psi_f^1\rangle. \tag{3.18}$$

Using first order perturbation theory, the perturbed wave function can be written as

$$|\Psi_{i,f}^1\rangle = \sum_I \frac{|\Psi_I\rangle\langle\Psi_I|H_{\rm PNC}^{\rm NSI/NSD}|\Psi_{i,f}\rangle}{E_{i,f}^0 - E_I^0}. \tag{3.19}$$

The electric dipole transition amplitude corresponding to the mixed parity initial and final states is given by

$$E1PNC^{\rm NSI/NSD} = \sum_I \frac{\langle\Psi_f^0|D|\Psi_I^0\rangle\langle\Psi_I^0|H_{\rm PNC}^{\rm NSI/NSD}|\Psi_i^0\rangle}{E_i^0 - E_I^0} + \sum_I \frac{\langle\Psi_f^0|H_{\rm PNC}^{\rm NSI/NSD}|\Psi_I^0\rangle\langle\Psi_I^0|D|\Psi_i^0\rangle}{E_f^0 - E_I^0}. \tag{3.20}$$

3.4.1 CI Wave functions

The form of $H_{\rm PNC}^{\rm NSI/NSD}$ Hamiltonian is given in Chapter 2. The parity of Ψ_I is opposite to that of Ψ_i and Ψ_f as $H_{\rm PNC}$ and D are odd under parity. The atomic states Ψ_i, Ψ_f and Ψ_I can be expressed as a linear combination of configuration state functions (CSF's) of the same angular momentum and parity, which are built out of an appropriate set of single-particle orbitals. This in terms of CSFs with appropriate CI coefficients takes the form

$$E1PNC^{\rm NSI/NSD} = \sum_{Iabcd} C_{ia}C_{Ib}C_{Ic}C_{fd}\frac{\langle\Phi_a|D|\Phi_b\rangle\langle\Phi_c|H_{\rm PNC}^{\rm NSI/NSD}|\Phi_d\rangle}{E_i - E_I} + c.c. \tag{3.21}$$

The diagonalisation of the atomic Hamiltonian in the space spanned by all the configurations yields its eigenvalues and eigenvectors, which are respectively the energies and the configuration mixing coefficients of the atomic states. This approach requires two diagonalisations, one each in the two opposite parity CSF sub-spaces. When the

number of CSF's are large the diagonalisation approach is less desirable in terms of computational efficiency and memory requirement. This approach was improved in terms of the computational efficiency using perturbed CI method which is described below.

3.4.2 Perturbed CI Wave functions

Electric dipole transition amplitude between states of mixed parity is given by Eq. 3.20. In this method, we define the states of mixed parity as

$$\begin{aligned} |\Psi_i\rangle &\rightarrow |\Psi_i^{(0)}\rangle + |\Psi_i^D\rangle \\ &= \sum_{k=1}^{neven} C_{ik}^{+}|\Phi_k^{+}\rangle + \sum_{m=1}^{nodd} C_{im}^{-}|\Phi_m^{-}\rangle \end{aligned} \tag{3.22}$$

and

$$\begin{aligned} |\Psi_i\rangle &\rightarrow |\Psi_i^{(0)}\rangle + |\Psi_i^{\mathrm{PNC}}\rangle \\ &= \sum_{k=1}^{neven} C_{ik}^{+}|\Phi_k^{+}\rangle + \sum_{n=1}^{nodd} C_{in}^{-}|\Phi_n^{-}\rangle, \end{aligned} \tag{3.23}$$

where we have used the notation of + for even and − for odd parities. The perturbed wave functions are defined as

$$|\Psi_i^{D-}\rangle = \sum_I \frac{|\Psi_I^{-}\rangle\langle\Psi_I^{-}|D|\Psi_i^{+}\rangle}{E_f - E_I} \tag{3.24}$$

and

$$|\Psi_i^{\mathrm{PNC}-}\rangle = \sum_I \frac{|\Psi_I^{-}\rangle\langle\Psi_I^{-}|H_{\mathrm{PNC}}|\Psi_i^{+}\rangle}{E_i - E_I}. \tag{3.25}$$

Using the above definitions, $E1PNC$ takes the form

$$E1PNC = \langle\Psi_f^{+}|D|\Psi_i^{\mathrm{PNC}-}\rangle + \langle\Psi_f^{+}|H_{\mathrm{PNC}}|\Psi_i^{D-}\rangle. \tag{3.26}$$

In terms of $C's$ we get

$$E1PNC = \sum_{km} C_{fk}^{+}C_{im}^{-}\langle\Phi_k^{+}|D|\Phi_m^{-}\rangle + \sum_{kn} C_{fk}^{+}C_{in}^{-}\langle\Phi_k^{+}|H_{\mathrm{PNC}}|\Phi_n^{-}\rangle. \tag{3.27}$$

$|\Psi_f\rangle$ satisfies the Schrödinger equation, hence by diagonalising the Hamiltonian the coefficient C_{fk}^{+} can be obtained. The odd parity coefficients can be obtained by the following way:

(i) To find out C_{in}^{-}

Operating Eq. 3.24 by $(E_f - H_0)$, we get

$$(E_f - H_0)|\Psi_i^{D-}\rangle = \sum_I |\Psi_I^-\rangle\langle\Psi_I^-|D|\Psi_i^+\rangle. \tag{3.28}$$

By making use of the completeness theorem given by

$$\sum_I^{odd} |\Psi_I\rangle\langle\Psi_I| = 1 - \sum_J^{even} |\Psi_J\rangle\langle\Psi_J|, \tag{3.29}$$

the above equation reduces to a linear equation of the form

$$(H_0 - E_f)|\Psi_i^{D-}\rangle = -D|\Psi_i^+\rangle. \tag{3.30}$$

In matrix notation, the above linear equation using the coefficients can be rewritten as

$$(\mathbf{H_0^{--}} - \mathbf{E_f I})\mathbf{C_i^-} = -\mathbf{D^{-+}}\mathbf{C_i^+}. \tag{3.31}$$

(ii) To find out C_{im}^{-}

Operating Eq. 3.25 by $(E_i - H_0)$ we get

$$(E_i - H_0)|\Psi_i^{\rm PNC-}\rangle = \sum_I |\Psi_{I-}\rangle\langle\Psi_{I-}|H_{\rm PNC}|\Psi_{i+}\rangle. \tag{3.32}$$

Using the completeness theorem as before, we get

$$(H_0 - E_i)|\Psi_i^{\rm PNC-}\rangle = -H_{\rm PNC}|\Psi_{i+}\rangle. \tag{3.33}$$

In matrix notation, the above linear equation using the coefficients reduces to

$$(\mathbf{H_0^{--}} - \mathbf{E_i I})\mathbf{C_i^-} = -\mathbf{H_{PNC}^{-+}}\mathbf{C_i^+}. \tag{3.34}$$

Solving these matrix equations gives the required coefficients for the opposite parity CSFs given by $\mathbf{C_i^-}$. The $E1PNC$ can then be computed using the perturbed CI method given by Eq. 3.27. The advantage of the above method over the previous one is due to the formalism in which one needs to do the diagonalisation only in the even parity states. The odd parity states are got by solving the linear equation which is less processor intensive.

3.5 Reduced Matrix Elements of $E1PNC^{\rm NSI}$ and $E1PNC^{\rm NSD}$

The reduced matrix element of $E1PNC^{\rm NSI}$ is of the form

$$E1^{\rm NSI}_{red} = \frac{G_F Q_W}{2\sqrt{2}}(-1)^{I+J_i+J_f+1}\left\{\begin{array}{ccc} J_f & F_f & I \\ F_i & J_i & 1 \end{array}\right\}[F_i,F_f]^{1/2}\widetilde{T}^k(f,i) \tag{3.35}$$

where

$$\begin{aligned}\widetilde{T}^k(f,i) = \sum_I [J_i]^{-\frac{1}{2}}\frac{\langle\Psi_f||D||\Psi_I\rangle\langle\Psi_I||H^{\rm NSI}_{\rm PNC}||\Psi_i\rangle}{E_i-E_I} \\ +[J_f]^{-\frac{1}{2}}\frac{\langle\Psi_f||H^{\rm NSI}_{\rm PNC}||\Psi_I\rangle\langle\Psi_I||D||\Psi_i\rangle}{E_f-E_I}.\end{aligned} \tag{3.36}$$

The reduced matrix element of $E1PNC^{\rm NSD}$ is of the form

$$E1^{\rm NSD}_{red} = \frac{G_F \mu_W}{2\sqrt{2}}\frac{(-1)}{\sqrt{3}}[k,F_i,F_f,1]^{\frac{1}{2}}\frac{\langle I||\widehat{I}||I\rangle}{I}\left\{\begin{array}{ccc} I & I & 1 \\ J_i & J_f & k \\ F_i & F_f & 1 \end{array}\right\}\widetilde{T}^k(f,i) \tag{3.37}$$

where

$$\begin{aligned}\widetilde{T}^k(f,i) = \sum_I (-1)^{k+J_i+J_f}[k]^{\frac{1}{2}}\left\{\begin{array}{ccc} 1 & 1 & k \\ J_i & J_f & J_I \end{array}\right\}\frac{\langle\Psi_f||D||\Psi_I\rangle\langle\Psi_I||H^{\rm NSD}_{\rm PNC}||\Psi_i\rangle}{E_i-E_I} \\ +(-1)^k\frac{\langle\Psi_f||H^{\rm NSD}_{\rm PNC}||\Psi_I\rangle\langle\Psi_I||D||\Psi_i\rangle}{E_f-E_I}.\end{aligned} \tag{3.38}$$

Here, $|\Psi\rangle$ refers to atomic state functions. The detailed derivation of the above expression has been carried out by Singh [3].

3.6 Computation of $E1PNC$: $|5p^6 6s\rangle_{1/2} \rightarrow |5p^6 5d\rangle_{3/2}$ Transition in Ba^+

The observable which we are interested in, is the electric dipole transition amplitude ($E1PNC$) induced by NSI/NSD PNC Hamiltonian between states of same nominal parity. The ion which we are interested in is a 55 electron system. In singly ionised barium, one looks for such transition between $|5p^6 6s\rangle_{1/2}$ and $|5p^6 5d\rangle_{3/2}$. This is forbidden according to spectroscopic selection rules, but becomes allowed due to the

mixing of opposite parity states which in turn leads to

$$E1PNC = \sum_I \frac{\langle \Psi_f | D | \Psi_I \rangle \langle \Psi_I | H_{\rm PNC}^{\rm NSI/NSD} | \Psi_i \rangle}{(E_i - E_I)} + \sum_I \frac{\langle \Psi_f | H_{\rm PNC}^{\rm NSI/NSD} | \Psi_I \rangle \langle \Psi_I | D | \Psi_i \rangle}{(E_f - E_I)}, \tag{3.39}$$

where $|\Psi_I\rangle$ are CSFs of odd parity. Before going into the actual computation of the above quantity we first describe the basis and the generation of CSF's using the same.

3.6.1 Basis

For any problem in atomic many-body theory, basis plays an important role in the computation of atomic properties. The single-particle orbitals used in such theory can be of any form, but they should satisfy the completeness condition. If ϕ denotes the single-particle orbitals, the completeness condition can be expressed as

$$\sum_i |\phi_i\rangle\langle\phi_i| = 1. \tag{3.40}$$

These conditions are satisfied by a set of orbitals generated using the single-particle Hamiltonian like the Hartree-Fock potential. Also a set of orbitals generated using the V^{N-1} [4] potential satisfy this condition. Since the property which we are interested in has a Z^3 dependence [5], heavy atoms/ions are considered and hence relativistic theory is employed. We have made use of Dirac-Fock (DF) V^{N-1} potential for our calculations. The Dirac-Couloumb Hamiltonian of an atom is given by

$$H = \sum_i (c\alpha_i.p_i + (\beta - 1)c^2 - \frac{Z}{r_i}) + \sum_{i>j} \frac{1}{r_{ij}}. \tag{3.41}$$

Defining U_{DF} as the independent central field DF potential, the atomic Hamiltonian takes the form

$$H = \sum_i (t_i + U_{DF}) + V_{es} = H_0 + V_{es}, \tag{3.42}$$

where

$$V_{es} = \sum_{i>j} \frac{1}{r_{ij}} - U_{DF}$$

and

$$t_i = c\alpha_i.p_i + (\beta_i - 1)^2 - \frac{Z}{r_i}.$$

The completeness criterion of the orbital space is determined by the convergence of the property like $E1PNC$ which we are interested in.

Ground state configuration of singly ionised barium is given by $|1s^2 2s^2 ..5p^6 6s^1\rangle$. Hence one starts the generation of occupied orbitals with singly ionised barium denoted as Ba^+, using the direct and exchange potentials that are due to $N-1$ occupied

Table 3.1: Single-particle orbital energies of Ba^+ generated with the starting potential as Ba^+ using GRASP DF code.

Orbital	Energy(au)	Orbital	Energy(au)	Orbital	Energy(au)
1s	−1384.03387	6p⋆	−0.26165	3d⋆	−30.49721
2s	−222.77665	7p⋆	−0.13803	4d⋆	−4.11229
3s	−48.85071	8p⋆	−0.08600	5d⋆	−0.31451
4s	−10.45578	9p⋆	−0.05883	6d⋆	−0.15214
5s	−1.79929	10p⋆	−0.04281	7d⋆	−0.09250
6s	−0.34517	2p	−195.20960	8d⋆	−0.06242
7s	−0.16836	3p	−40.36659	9d⋆	−0.04500
8s	−0.06693	4p	−7.71210	3d	−29.91125
9s	−0.04777	5p	−1.06860	4d	−4.01134
10s	−0.03582	6p	−0.25522	5d	−0.31232
2p ⋆	−209.28741	7p	−0.13554	6d	−0.15134
3p ⋆	−43.15589	8p	−0.084761	7d	−0.09211
4p ⋆	−8.29803	9p	−0.05813	8d	−0.06220
5p ⋆	−1.15264	10p	−0.04237	9d	−0.04487

electrons. The other virtual orbitals are then obtained by replacing the valence orbital $6s$ with the i^{th} virtual orbital, keeping the core orbitals frozen. We make use of the GRASP multi-configuration Dirac-Fock code [6] to generate the numerical core and virtual orbitals used in our calculation. Since the above mentioned code generates only bound orbitals, for the present calculation using CI we haven't included the effects of the continuum. We have used both bound and continuum orbitals for other methods like Many-Body Perturbation Theory (MBPT) and Coupled Cluster (CC), where we have generated the basis using finite basis set expansion method (FBSE) [7]. These calculations are described in subsequent chapters.

The numerical single-particle energies of the bound orbitals are given in Table 3.1. Here the single-particle orbital with $j = l - s$ is denoted with a suffix $\star$ and $j = l + s$ without the $\star$. Completeness of the bound orbitals is checked with respect to the addition of CSF's generated by physical considerations applicable to the property of our interest.

3.6.2 CSFs Considered

The configurations are generated by considering single and double excitations from the occupied orbitals to the bound virtual orbitals in all possible ways such that it gives the required angular momentum. The ground state reference for Ba^+ is $|5p^6 6s\rangle$. In the present calculation which is the continuation of the work by Malhotra et al. [8], we treat $1s2s....5s,\ 2p\star 3p\star ...5p\star, 2p, 3p, ...5p, 3d\star 4d\star, 3d4d$ as the $(N-1)$ occupied electrons and the outermost orbital $6s$ is considered as the valence orbital. The virtual orbitals for each symmetry are $7s, 8s, 9s, 10s,\ 6p\star, 7p\star, 8p\star, 9p\star, 10p\star$, $6p, 7p, 8p, 9p, 10p,\ 5d\star, 6d\star, 7d\star, 8d\star, 9d\star$ and $5d, 6d, 7d, 8d, 9d$. Writing each atomic state as a sum of CSFs, we incorporate contributions to Ψ_i, Ψ_I and Ψ_f from different configurations. Here we generate different CSF's from a given set of occupied and valence orbitals taking into consideration certain types of correlation effects. CSFs generated hence are summerised in the Table 3.2.

3.6.3 Results and Discussion

It is reasonable to expect that the major contribution to the above transition in Ba^+ would come from configurations built from the core as well as $6s, 5d$ and $6p$ orbitals [8]. This is verified by comparing the lowest order result with the odd intermediate configuration $|5p^6 6p\rangle$, and adding the configuration $|5p^6 7p\rangle$ which changes the result by only 3%. In this work we have tried to increase the configurations by considering excitations from the core $5s$ and $5p$ to various high lying virtual orbitals. The contribution to $E1PNC$ with NSI Hamiltonian is tabulated in Table 3.3. The values are given in units of $iea_0 \times Q_W 10^{-12}$. Addition of $|5p^5 6s5d\rangle$ is negligible and the reason for this can be attributed to the strong cancellation between core polarisation contributions arising from $|5p_{1/2}5p^4_{3/2}6s5d_{3/2}\rangle$ and $|5p^2_{1/2}5p^3_{3/2}6s5d_{3/2}\rangle$ configurations. Addition of the configuration $|5p^5 5d6p\rangle$ has more important effect compared to the configurations $|5p^5 6s5d\rangle$. The contribution using CI calculation done with 179 configurations [8] for NSI is $0.518 \times 10^{-12} iea_0 Q_W$. Examining the final result given in the Table 3.3. and comparing with the previous calculations by Malhotra et al. [8], which is repeated again here (till the 7th run in Table 3.3.), the total correlation from the high lying levels is about 1.6% which is worthwhile to get better accuracy. One can determine the contribution due to addition of each shell (*i.e.*, an increase in principal quantum number) in the virtual orbitals for the five symmetries which we have taken for the present calculation. All the comparisons are performed with respect to the result obtained by Malhotra et al. [8] using the low lying bound orbitals. The contribution from $7s,\ 8s,\ 7p,\ 8p,\ 6d$ and $7d$ virtuals calculated by considering all possible

Table 3.2: Generation of Configuration.

No.	Type of CSF	Limits of Principal quantum number	Angular momentum	Parity of the CSF
1	$\|5p^6ks\rangle$	k=6,7,8,9,10	$\frac{1}{2}$	even
2	$\|5p^6kd\rangle$	k=5,6,7,8,9	$\frac{3}{2}$	even
3	$\|5p^6kp\rangle$	k=6,7,8,9,10	$\frac{1}{2}, \frac{3}{2}$	odd
4	$\|5p^5ksk'p\rangle$	k=6,7,8,9,10		
		k'=6, 7, 8, 9, 10	$\frac{1}{2}, \frac{3}{2}$	even
5	$\|5p^5kpk'd\rangle$	k=6,7,8,9,10		
		k'=5,6,7,8,9	$\frac{1}{2}, \frac{3}{2}$	even
6	$\|5p^5ksk'd\rangle$	k=6,7,8,9,10		
		k'=5,6,7,8,9	$\frac{1}{2}, \frac{3}{2}$	odd
7	$\|5p^5ksk's\rangle$	k=6,7,8,9,10		
		k'=6,7,8,9,10	$\frac{1}{2}, \frac{3}{2}$	odd
8	$\|5p^5kpk'p\rangle$	k=6,7,8,9,10		
		k'=6,7,8,9,10	$\frac{1}{2}, \frac{3}{2}$	odd
9	$\|5p^5kdk'd\rangle$	k=5,6,7,8,9		
		k'=5,6,7,8,9	$\frac{1}{2}, \frac{3}{2}$	odd
10	$\|5s^15p^6ks^2\rangle$	k=6,7,8,9,10	$\frac{1}{2}$	even
11	$\|5s^15p^6kp^2\rangle$	k=6,7,8,9,10	$\frac{1}{2}, \frac{3}{2}$	even
12	$\|5s^15p^6kd^2\rangle$	k=5,6,7,8,9	$\frac{1}{2}, \frac{3}{2}$	even

CSFs generated by the single and double excitations from $5p$ and $6s$ is about 1.1%. The addition of CSFs generated by taking one electron from $5s$ reduces it by 0.2%. This makes the contribution from $n \leq 8$ for s and p and $n \leq 7$ for d symmetry to be about 0.9%. Similarly the addition of CSF's generated from excitations of the core $5p$ to $n = 9$ for s and p and $n = 8$ for d symmetry is about 0.46% comparing with the previous calculation. Addition of CSF's from the core $5s$ to the above mentioned virtuals has no effect on total contribution. Contribution from the shell n=10 for s and p and $n = 9$ for d symmetry increases by about 0.3%. CSFs generated from excitations of the core $5s$ have negligible effect as in the previous case. Percentage of contribution from various shells are shown schematically by plotting the contribution from each shell with respect to the principal quantum numbers of the various shells. This provides a check of convergence with respect to the finite basis used. As

Table 3.3: CI results for the reduced matrix elements of the NSI $E1PNC$ $(5p^6 6s\rangle_{1/2} \rightarrow |5p^6 5d\rangle_{3/2})$ in Ba^+ in units of $iea_0 Q_W \times 10^{-12}$.

No.	Configurations	E1PNC (NSI)	No.	Configurations	E1PNC (NSI)
1	$\|5p^6 6s\rangle_{1/2}, \|5p^6 5d\rangle_{3/2}$, $\|5p^6 6p\rangle_{1/2,3/2}$	0.58363	34	pre + $\|5p^5 8s 5d\rangle_{1/2,3/2}$	0.5316
2	pre + $\|5p^5 6s 5d\rangle_{1/2,3/2}$	0.5839	35	pre + $\|5p^5 8s 6d\rangle_{1/2,3/2}$	0.5316
3	pre + $\|5p^5 6s 6p\rangle_{1/2,3/2}$	0.5783	36	pre + $\|5p^5 8s 6p\rangle_{1/2,3/2}$	0.5322
4	pre + $\|5p^5 5d 6p\rangle_{1/2,3/2}$	0.5045	37	pre + $\|5p^5 8s 7p\rangle_{1/2,3/2}$	0.5322
5	pre + $\|5p^5 6s^2\rangle_{1/2,3/2}$	0.5284	38	pre + $\|5p^5 6s 8s\rangle_{1/2,3/2}$	0.5319
6	pre + $\|5p^5 5d^2\rangle_{1/2,3/2}$	0.5177	39	pre + $\|5p^5 8s\rangle_{1/2}$, $\|5p^6 7d\rangle_{3/2}$	0.5324
7	pre + $\|5p^5 6p^2\rangle_{1/2,3/2}$	0.5185	40	pre + $\|5p^5 8p\rangle_{1/2,3/2}$	0.5358
8	pre + $\|5p^6 7s\rangle_{1/2}, \|5p^6 6d\rangle_{3/2}$	0.522	41	pre + $\|5p^5 8s 8p\rangle_{1/2,3/2}$	0.5358
9	pre + $\|5p^6 7p\rangle_{1/2,3/2}$	0.535	42	pre + $\|5p^5 6p 7d\rangle_{1/2,3/2}$	0.5343
10	pre + $\|5p^5 6s 6d\rangle_{1/2,3/2}$	0.5384	43	pre + $\|5p^5 7p 5d\rangle_{1/2,3/2}$	0.5239
11	pre + $\|5p^5 6s 7p\rangle_{1/2,3/2}$	0.5379	44	pre + $\|5p^5 7p 7d\rangle_{1/2,3/2}$	0.5237
12	pre + $\|5p^5 7s 5d\rangle_{1/2,3/2}$	0.5330	45	pre + $\|5p^5 8p 7d\rangle_{1/2,3/2}$	0.5236
13	pre + $\|5p^5 7s 6d\rangle_{1/2,3/2}$	0.5333	46	pre + $\|5p^5 8s 7d\rangle_{1/2,3/2}$	0.5236
14	pre + $\|5p^5 7s 6p\rangle_{1/2,3/2}$	0.5356	47	pre + $\|5p^5 7s 8s\rangle_{1/2,3/2}$	0.5236
15	pre + $\|5p^5 7s 7p\rangle_{1/2,3/2}$	0.5354	48	pre + $\|5p^5 8s^2\rangle_{1/2,3/2}$	0.5236
16	pre + $\|5p^5 6s 7s\rangle_{1/2,3/2}$	0.5369	49	pre + $\|5p^5 8p^2\rangle_{1/2,3/2}$	0.5236
17	pre + $\|5p^5 6p 7p\rangle_{1/2,3/2}$	0.5368	50	pre + $\|5p^5 7d^2\rangle_{1/2,3/2}$	0.5237
18	pre + $\|5p^5 6p 6d\rangle_{1/2,3/2}$	0.5325	51	pre + $\|5s^1 5p^6 6s^2\rangle_{1/2,3/2}$	0.5235
19	pre + $\|5p^5 7p 6d\rangle_{1/2,3/2}$	0.5319	52	pre + $\|5s^1 5p^6 6s^2\rangle_{1/2}$, $\|5s^1 5p^6 7s^2\rangle_{1/2}$,	0.5235
20	pre + $\|5p^5 7s^2\rangle_{1/2,3/2}$	0.5319	53	pre + $\|5s^1 5p^6 8s^2\rangle_{1/2}$, $\|5s^1 5p^6 6p^2\rangle_{1/2}$	0.5248
21	pre + $\|5p^5 6d^2\rangle_{1/2,3/2}$	0.5319	54	pre + $\|5s^1 5p^6 7p^2\rangle_{1/2}$, $\|5s^1 5p^6 8p^2\rangle_{1/2}$	0.5248
22	pre + $\|5p^5 7p^2\rangle_{1/2,3/2}$	0.5320	55	pre + $\|5s^1 5p^6 5d^2\rangle_{1/2,3/2}$	0.5269
23	pre + $\|5p^5 5d 6d\rangle_{1/2,3/2}$	0.5320	56	pre + $\|5s^1 5p^6 6d^2\rangle_{1/2,3/2}$	0.5269
24	pre + $\|5p^5 6s 7d\rangle_{1/2,3/2}$	0.5337	57	pre + $\|5s^1 5p^6 7d^2\rangle_{1/2,3/2}$	0.5268
25	pre + $\|5p^5 7s 7d\rangle_{1/2,3/2}$	0.5339	58	pre + $\|5s^1 5p^6 6p^2\rangle_{3/2}$, $\|5s^1 5p^6 7p^2\rangle_{3/2}$	0.5226
26	pre + $\|5p^5 5d 7d\rangle_{1/2,3/2}$	0.5345	59	pre + $\|5s^1 5p^6 8p^2\rangle_{3/2}$, $\|5p^6 9s\rangle_{1/2}$	0.5228
27	pre + $\|5p^5 6d 7d\rangle_{1/2,3/2}$	0.5346	60	pre + $\|5p^6 8d\rangle_{3/2}$ $\|5p^6 9p\rangle_{1/2}$	0.5251
28	pre + $\|5p^5 6s 8p\rangle_{1/2,3/2}$	0.5344	61	pre + $\|5p^6 9p\rangle_{3/2}$, $\|5p^5 6s 9p\rangle_{1/2}$... from the core $5p$ and $5s$	0.5250
29	pre + $\|5p^5 7s 8p\rangle_{1/2,3/2}$	0.5344	62	pre + $5p^6 10p\rangle_{1/2,3/2}$, $\|5p^6 10s\rangle_{1/2}$... from the core $5p$	0.5264
30	pre + $\|5p^5 6p 8p\rangle_{1/2,3/2}$	0.5343	63	pre + from the core $5s$	0.5264
31	pre + $\|5p^5 7p 8p\rangle_{1/2,3/2}$	0.5343			
32	pre + $\|5p^5 5d 8p\rangle_{1/2,3/2}$	0.5319			
33	pre + $\|5p^5 6d 8p\rangle_{1/2,3/2}$	0.5317			

inferred from the Fig. 3.1, addition of higher shells ($n > 10$ for s, $n > 9$ for p, d) will have substantial contribution to the $E1PNC$. As the next step of calculation, one can consider increasing the configurations arising from excitations, to higher shells and also the addition of continuum orbitals which we haven't included in the present calculation. In the Fig. 3.1, the contribution of $E1PNC$ starting from the lowest order to the complete CI is plotted and the steep fall in the graph shows the addition of $|5p^5 6p 5d\rangle$ which leads to large cancellations. In the present calculation, the total NSI $E1PNC$ reduced matrix element converged to $0.5264 \times 10^{-12} ie a_0 Q_W$ with about 2000 relativistic configurations.

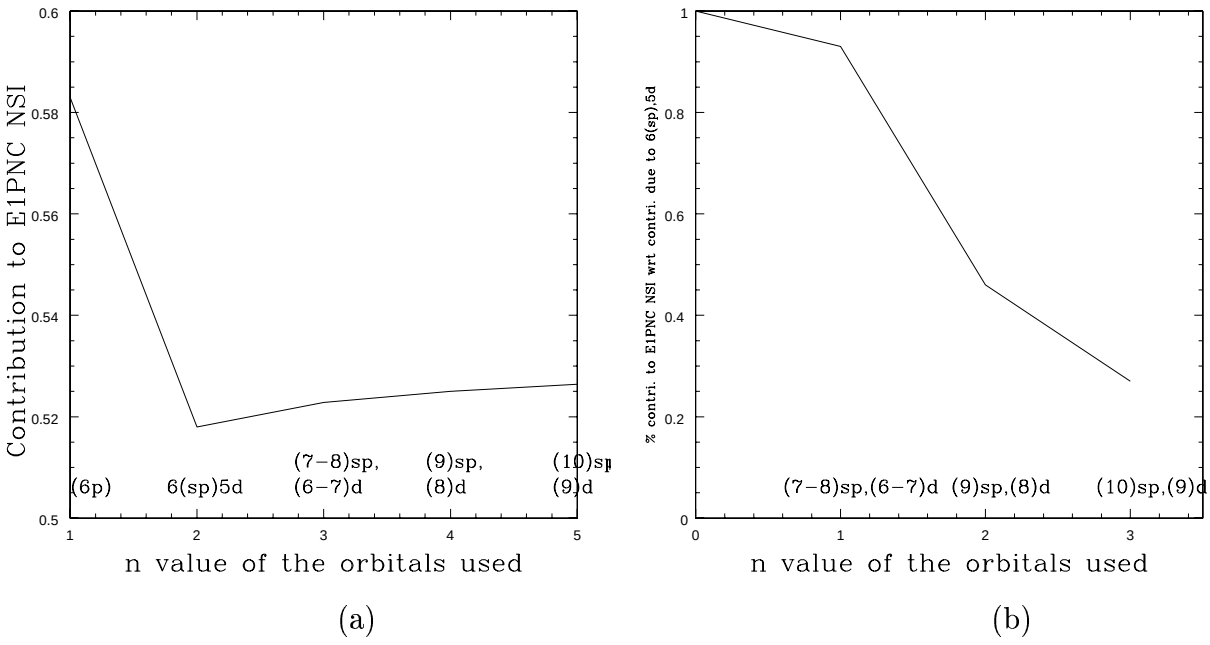

(a) (b)

Figure 3.1: Contribution of $E1PNC$ NSI with the addition of CSFs which are generated by the virtual orbitals represented by n and the symmetry.

The atomic states and hence $E1PNC$ can be expressed in terms of the angular momentum quantum numbers (J, M_J, or F, M_F). The total angular momentum $F = I + J$ and $M_F = M_I + M_J$. Using the similar configurations the contribution to $E1PNC$ (NSI) ($F_i,\ F_f$) is found to be $0.696 \times 10^{-12} ie a_0 Q_W$ for $F_i = 2$ to $F_f = 3$.

For the same transition, $E1PNC$ NSD calculations were done and the results are tabulated in Table 3.4. The value of $E1PNC$ with about 2000 relativistic configurations converged to $0.621 \times 10^{-12} ie a_0 \mu_W$.

Table 3.4: CI results for the reduced matrix elements of the NSD $E1PNC$ $(5p^6 6s\rangle_{1/2} \rightarrow |5p^6 5d\rangle_{3/2})$ in Ba^+ in units of $iea_0\mu_W \times 10^{-12}$.

No.	Configurations	$E1PNC$ (NSD)
1	$\|5p^6 6s\rangle_{1/2}, \|5p^6 5d\rangle_{3/2}, \|5p^6 6p\rangle_{1/2,3/2}$	0.762
2	previous + $\|5p^5 6s 5d\rangle_{1/2,3/2}$	0.786
3	previous + $\|5p^5 6s 6p\rangle_{1/2,3/2}$	0.751
4	previous + $\|5p^5 5d 6p\rangle_{1/2,3/2}$	0.659
5	previous + $\|5p^5 6s^2\rangle_{1/2,3/2}$	0.629
6	previous + $\|5p^5 5d^2\rangle_{1/2,3/2}$	0.614
7	previous + $\|5p^5 6p^2\rangle_{1/2,3/2}$	0.616
8	previous + $\|5p^6 7s\rangle_{1/2}, \|5p^6 6d\rangle_{3/2}$	0.621
9	previous + $\|5p^6 7p\rangle_{1/2,3/2}$	0.638
10	previous + $\|5p^5 6s 6d\rangle_{1/2,3/2}$	0.641
11	previous + $\|5p^5 6s 7p\rangle_{1/2,3/2}$	0.640
12	previous + $\|5p^5 7s 5d\rangle_{1/2,3/2}$	0.639
13	previous + $\|5p^5 7s 6d\rangle_{1/2,3/2}$	0.639
14	previous + $\|5p^5 7s 6p\rangle_{1/2,3/2}$	0.637
15	previous + $\|5p^5 7s 7p\rangle_{1/2,3/2}$	0.636
16	previous + $\|5p^5 6s 7s\rangle_{1/2,3/2}$	0.633
17	previous + $\|5p^5 6p 7p\rangle_{1/2,3/2}$	0.633
18	previous + $\|5p^5 6p 6d\rangle_{1/2,3/2}$	0.629
19	previous + $\|5p^5 7p 6d\rangle_{1/2,3/2}$	0.628
20	previous + $\|5p^5 7s^2\rangle_{1/2,3/2}$	0.628
21	previous + $\|5p^5 6d^2\rangle_{1/2,3/2}$	0.628
22	previous + $\|5p^5 7p^2\rangle_{1/2,3/2}$	0.628
23	previous + $\|5p^5 5d 6d\rangle_{1/2,3/2}$	0.629
24	previous + $\|5p^5 6s 7d\rangle_{1/2,3/2}$	0.630
25	previous + $\|5p^5 7s 7d\rangle_{1/2,3/2}$	0.630
26	previous + $\|5p^5 5d 7d\rangle_{1/2,3/2}$	0.631
27	previous + $\|5p^5 6d 7d\rangle_{1/2,3/2}$	0.631
28	previous + $\|5p^5 6s 8p\rangle_{1/2,3/2}$	0.631
29	previous + all the CSF's got using 7s,8s, 7p,8p,6d and 7d with 5p and 5s as core	0.617
29	previous + all the CSF's got using 9s,9p, and 8d with 5p and 5s as core	0.620
30	previous + all the CSF's got using 10s,10p, and 9d with 5p and 5s as core	0.621

3.7 Computation of $E1PNC$:$|5p^6 6s\rangle_{1/2} \rightarrow |5p^6 5d\rangle_{5/2}$ in Ba^+ and $|6p^6 7s\rangle_{1/2} \rightarrow |6p^6 6d\rangle_{5/2}$ in Ra^+

3.7.1 Introduction

PNC arising from the NSI neutral weak current interaction has been observed in several experiments conducted in atoms during the last two decades [9]. However, the observation of the PNC induced NSD interaction is rather recent. The importance of this work is that, the first definitive measurement of the nuclear anapole moment [10] was carried out for the $6s \rightarrow 7s$ transition in atomic caesium. Experiments of this type based on sophisticated optical techniques in combination with atomic PNC calculations induced by the NSD interactions can provide an unique opportunity for studying hardronic weak interactions which can give rise to nuclear PNC [11]. It is therefore important to consider atomic systems which can be used for carrying out PNC experiments to observe NSD effects.

Fortson has proposed an experiment to measure PNC in the $6s \rightarrow 5d_{3/2}$ transition in Ba^+ using the techniques of laser cooling and trapping [12], which is sensitive to both the NSI and NSD interactions. It may also be possible to do a similar PNC experiment on the $6s \rightarrow 5d_{5/2}$ transition in Ba^+. This transition has an important advantage; it is only sensitive to the NSD effect and is therefore a direct way of measuring the nuclear anapole moment. The reason why the NSI effect is zero is explained at the end of this chapter. In this approach, one does not have to disentangle the NSD effect from its much larger NSI counterpart. Preceeding remarks also apply to the $7s \rightarrow 6d_{5/2}$ transition in Ra^+. Lasers required for these two experiments are available (see Fig. 3.2). Several high precision experiments on laser cooled and trapped Ba^+ have been carried out [13] and a PNC experiment for the $6s \rightarrow 5d_{3/2}$ transition is presently underway [12]. The possibility of performing a similar PNC experiment for the $7s \rightarrow 6d_{5/2}$ transition in Ra^+ is being presently explored [14]. In this section, we calculate the parity non-conserving NSD electric dipole transition amplitudes for the afore mentioned transition in $^{137}Ba^+$ and $^{227}Ra^+$.

3.7.2 Basis

In the present calculation, we treat $1s^2 2s^2 ... 5p^6$ as the $(N-1)$ occupied electrons and the outermost orbital $6s$ is considered as the valence orbital.The virtuals considered for the calculation are $7s, 8s, 6d, 7d, 6p, 7p$ and $8p$. In the case of Ra^+, we treat $1s^2 2s^2 .... 6p^6$ as the $(N-1)$ occupied electrons and the outermost orbital $7s$

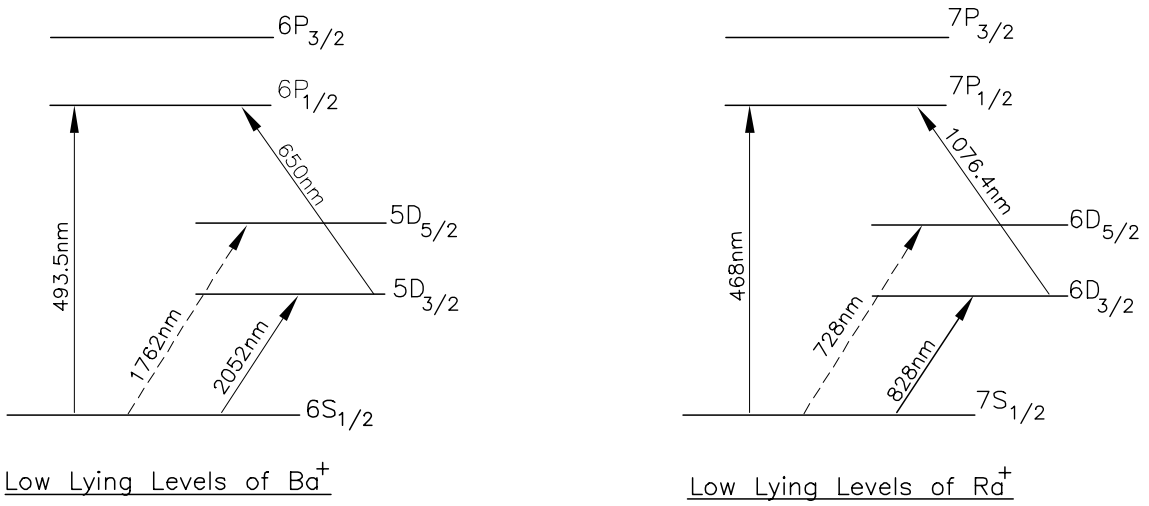

Fig. 1

Figure 3.2: Energy Levels for Ba^+ and Ra^+.

is considered as valence orbital. The virtual orbitals considered for the calculation are $8s$, $9s$, $7d$, $8d$, $7p$, $8p$ and $9p$. The GRASP (General Relativistic Atomic Structure Programe) multi-cofiguration Dirac-Fock code [6] was used to generate virtual V_{N-1} orbitals as in the previous case. The single-particle orbital energies for Ra^+ is tabulated in Table 3.5.

3.7.3 CSFs Considered

We have taken into consideration the core-valence correlation wherein the $5p$ and $6s$ orbitals for Ba^+ are excited to other virtual orbitals. In the case of Ra^+, $6p$ and $7s$ orbitals are excited to other virtual orbitals. We have also considered single excitations from the core and the valence orbitals; such excitations having odd parity are extremely important for PNC. The core-core correlation and excitation of two core orbitals to valence and/or virtual orbitals are not taken into consideration. The generation of CSFs is given in Table 3.6.

3.7.4 Results and Discussion

Contributions from the low lying configurations of Ba^+ *i.e.* the configurations arising out of single and double excitations from $5p$ and $6s$ to $6p$ and $5d$ are tabulated in Table 3.7. The addition of $|5p^6 6p\rangle_{3/2}$ alone as the intermediate CSF does not contribute

Table 3.5: Single-particle orbital energies of Ra^+ generated with the starting potential as Ra^+ using GRASP DF code.

Orbital	Energy(au)	Orbital	Energy(au)	Orbital	Energy(au)
1s	−3846.10603	6p⋆	−1.17231	4d⋆	−23.23720
2s	−712.96883	7p⋆	−0.26044	5d⋆	−3.08801
3s	−179.99787	8p⋆	−0.13736	6d⋆	−0.28743
4s	−45.95157	9p⋆	−0.08563	7d⋆	−0.14439
5s	−10.21918	2p	−572.24565	8d⋆	−0.08883
6s	−1.82345	3p	−141.49562	3d	−116.18028
7s	−0.349068	4p	−33.66010	4d*	−23.23720
8s	−0.10056	5p	−6.58530	5d	−3.08801
9s	−0.04775	6p	−0.93719	6d	−0.28406
2p*	−685.40599	7p	−0.24200	7d	−0.14266
3p*	−167.5469	8p	−0.13019	8d	−0.08795
4p*	−40.38511	9p	−0.08206	4f⋆	−11.27521
5p*	−8.05943	3d⋆	−121.54581	4f	−10.96559

to the parity non-conserving E1 reduced matrix element because of the vanishing PNC matrix elements. But due to the addition of $|5p^5 6s5d\rangle_{3/2}$ the contribution becomes non-zero due to the mixing between these two CSFs. Also from the table it is clear that CSF $|5p^5 6s6p\rangle_{1/2,5/2}$ and $|5p^5 5d6p\rangle_{1/2,5/2}$ make important contributions. By adding excitations from the $5s$ core to the above, the value turns out to be $-0.070\, iea_0\mu_W \times 10^{-12}$. This is tabulated in Table 3.7.

An important reason for the difference between the values for the above two cases for Ba^+ given in Table 3.7 is the non-vanishing PNC and electric dipole matrix elements between the valence-core correlation CSF $|5s5p^6 6p^2\rangle$ and the intermediate CSF $|5s5p^6 6s6p\rangle_{3/2}$. The interplay between other correlation and electric dipole/PNC effects involving configuration with $5d$ orbitals also contribute to this difference.

Contributions from the low lying configurations of Ra^+ *i.e.* the configurations arising out of single and double excitations from $6s$, $6p$ and $7s$ orbitals to $7p$ and $6d$ orbitals are tabulated in Table 3.7. The contributions due to the excitations from the $6s$ core in Ra^+ follows the same trend as in the case of Ba^+. This is also tabulated in Table 3.7. From the calculation using the low lying configurations, it is clear that the mixing of the CSFs $|6p^6 7p\rangle_{3/2}$ and $|6p^5 7s6d\rangle_{3/2}$ leads to a non-zero contribution. From the table it can be seen that ($|6p^5 7s7p\rangle$, $|6p^5 6d7p\rangle$, $|6s6p^6 7p^2\rangle$) $(1/2, 5/2)$ and

Table 3.6: Generation of Configuration for Ba^+ and Ra^+ for NSD PNC.

No.	CSF	Limits of n for Ba^+	Limits of n for Ra^+	Angular Momentum	Parity of the CSF
1	$\|5p^6ks\rangle$	k=6,7,8	k=7,8,9	$\frac{1}{2}$	even
2	$\|5p^6kd\rangle$	k=5,6,7	k=6,7,8	$\frac{5}{2}$	even
3	$\|5p^6kp\rangle$	k=6,7,8	k=7,8,9	$\frac{3}{2}$	odd
4	$\|5p^5ksk'p\rangle$	k=6,7,8	k=7,8,9		
		k'=6,7,8	k'=7,8,9	$\frac{1}{2}, \frac{5}{2}$	even
5	$\|5p^5kpk'd\rangle$	k=6,7,8	k=7,8,9		
		k'=5,6,7	k'=6,7,8	$\frac{1}{2}\frac{5}{2}$	even
6	$\|5p^5ksk'd\rangle$	k=6,7,8	k=7,8,9		
		k'=5,6,7	k'=6,7,8	$\frac{3}{2}$	odd
7	$\|5p^5ksk's\rangle$	k=6,7,8	k=7,8,9		
		k'=6,7,8	k'=7,8,9	$\frac{3}{2}$	odd
8	$\|5p^5kpk'p\rangle$	k=6,7,8	k=7,8,9		
		k'=6,7,8	k'=7,8,9	$\frac{3}{2}$	odd
9	$\|5p^5kdk'd\rangle$	k=5,6,7	k=6,7,8		
		k'=5,6,7	k'=6,7,8	$\frac{3}{2}$	odd
10	$\|5s^15p^6ks^2\rangle$	k=6,7,8	k=7,8,9	$\frac{1}{2}$	even
11	$\|5s^15p^6kp^2\rangle$	k=6,7,8	k=7,8,9	$\frac{1}{2}, \frac{5}{2}$	even
12	$\|5s^15p^6kd^2\rangle$	k=5,6,7	k=6,7,8	$\frac{1}{2}, \frac{5}{2}$	even
13	$\|5s^15p^6ks^1k'p\rangle$	k=6,7,8	k=7,8,9		
		$k' = 6, 7, 8$	$k' = 7, 8, 9$	$\frac{1}{2}, \frac{5}{2}$	even
14	$\|5s^15p^6ks^1k'd\rangle$	k=6,7,8	k=7,8,9		
		$k' = 5, 6, 7$	$k' = 6, 7, 8$	$\frac{1}{2}, \frac{5}{2}$	even
13	$\|5s^15p^6kp^1k'd\rangle$	k=6,7,8	k=7,8,9		
		$k' = 5, 6, 7$	$k' = 6, 7, 8$	$\frac{3}{2}$	odd

Table 3.7: $E1^{\rm NSD}_{red}$ for Ba^+ and Ra^+ in units of $iea_0\mu_W \times 10^{-12}$ Note: I=3/2.

Ion	Configurations	$F_f = 3$ to $F_i = 2$	$F_f = 2$ to $F_i = 2$	$F_f = 2$ to $F_i = 1$	$F_f = 1$ to $F_i = 2$	$F_f = 1$ to $F_i = 1$
	$\|5p^6 6s\rangle_{1/2}, \|5p^6 5d\rangle_{5/2}$,					
	$\|5p^6 6p\rangle_{3/2}, \|5p^5 6s5d\rangle_{3/2}$	-0.080	-0.045	-0.045	-0.013	-0.029
	$+\|5p^5 6s6p\rangle_{1/2}, \|5p^5 6s6p\rangle_{5/2}$	-0.068	-0.038	-0.038	-0.011	-0.025
	$+\|5p^5 5d6p\rangle_{1/2}, \|5p^5 5d6p\rangle_{5/2}$	-0.055	-0.031	-0.031	-0.010	-0.020
Ba^+	$+\|5p^5 6s^2\rangle_{3/2}, \|5p^5 5d^2\rangle_{3/2}$,					
	$\|5p^5 6p^2\rangle_{3/2}$	-0.052	-0.029	-0.029	-0.009	-0.019
	$+\|5s5p^6 6s^2\rangle_{1/2}, \|5s5p^6 5d^2\rangle_{1/2}$					
	$\|5s5p^6 5d^2\rangle_{5/2}$	-0.046	-0.026	-0.026	-0.008	-0.017
	$+\|5s5p^6 6p^2\rangle_{1/2}, \|5s5p^6 6p^2\rangle_{5/2}$,					
	$\|5s5p^6 5d6p\rangle_{3/2}, \|5s5p^6 6s6p\rangle_{3/2}$	-0.070	-0.039	-0.039	-0.011	-0.0255
	$\|6p^6 7s\rangle_{1/2}, \|6p^6 6d\rangle_{5/2}$,					
	$\|6p^6 7p\rangle_{3/2}, \|6p^5 7s6d\rangle_{3/2}$	-0.989	-0.553	-0.553	-0.161	-0.362
	$+\|6p^5 7s7p\rangle_{1/2}, \|6p^5 7s7p\rangle_{5/2}$	-0.57	-0.319	-0.319	-0.093	-0.209
Ra^+	$+\|6p^5 6d7p\rangle_{1/2}, \|6p^5 6d7p\rangle_{5/2}$	-0.45	-0.233	-0.233	-0.070	-0.166
	$+\|6p^5 7s^2\rangle_{3/2}, \|6p^5 6d^2\rangle_{3/2}$,					
	$\|6p^5 7p^2\rangle_{3/2}$	-0.417	-0.233	-0.233	-0.068	-0.153
	$+\|6s6p^6 7s^2\rangle_{1/2}, \|6s6p^6 6d^2\rangle_{1/2}$,					
	$\|6s6p^6 6d^2\rangle_{5/2}$	-0.378	-0.211	-0.211	-0.062	-0.138
	$+\|6s6p^6 7p^2\rangle_{1/2}, \|6s6p^6 7p^2\rangle_{5/2}$,					
	$\|6s6p^6 6d7p\rangle_{3/2}, \|6s6p^6 7s7p\rangle_{3/2}$	-0.615	-0.344	-0.344	-0.100	-0.225

($|6s6p^6 6d7p\rangle$, $|6s6p^6 7s7p\rangle$) (3/2) make important contributions. Contributions from the configurations arising out of single and double excitations from $5s$, $5p$ and $6s$ to $7s$, $8s$, $5d$, $6d$,$7d$, $6p$, $7p$ and $8p$ for Ba^+ and $6s$, $6p$ and $7s$ to $8s$, $9s$, $6d$, $7d$, $8d$, $7p$, $8p$ and $9p$ for Ra^+ are tabulated in Table 3.8. Calculations using the above orbitals leads to 774 relativistic configurations. Comparing with the result in Table 3.7, we find that the dominant contributions come from the low lying configurations.

The final results given in Table 3.8 for the NSD contribution to PNC for the transitions $|5p^6 6s\rangle_{1/2} \rightarrow |5p^6 5d\rangle_{5/2}$ and $|6p^6 7s\rangle_{1/2} \rightarrow |5p^6 6d\rangle_{5/2}$ in Ba^+ and Ra^+ respectively can now be compared with our earlier calculation [8] for NSD contribution for Ba^+, for the transition $|5p^6 6s\rangle_{1/2} \rightarrow |5p^6 5d\rangle_{3/2}$ for the case $F_f = 3$ to $F_i = 2$. The NSD contribution for $s_{1/2} \rightarrow d_{5/2}$ transition in Ba^+ is 8 times smaller than that for the $s_{1/2} \rightarrow d_{3/2}$ transition, but it is worth pursuing experimental studies since it is only sensitive to the NSD effect. For Ra^+, the NSD contribution for $s_{1/2} \rightarrow d_{5/2}$

Table 3.8: $E1^{\rm NSD}_{red}$ for Ba^+ and Ra^+ in units of $iea_0\mu_W \times 10^{-12}$ for the complete calculation.

Ions	$F_f = 3$ to $F_i = 2$	$F_f = 2$ to $F_i = 2$	$F_f = 2$ to $F_i = 1$	$F_f = 1$ to $F_i = 2$	$F_f = 1$to $F_i = 1$
Ba^+	-0.082	-0.046	-0.046	-0.0134	-0.030
Ra^+	-0.635	-0.355	-0.355	-0.104	-0.232

transition is about the same as the NSD contribution in Ba^+ for the $s_{1/2} \rightarrow d_{3/2}$ transition. This makes Ra^+ an attractive choice for a clean measurement of nuclear anapole moment. Comparing the present results with those of the NSD calculation computed for Cs for the transition $|5p^6 6s\rangle_{1/2} \rightarrow |5p^6 7s\rangle_{1/2}$ for $F_f = 4$ to $F_i = 3$ we find that while the NSD contribution in Ba^+ is roughly 10 times smaller, for Ra^+ it is only one and half times smaller [15].

3.7.5 Explanation for Zero NSI Effect in $5p^6 6s_{1/2} \rightarrow 5p^6 5d_{5/2}$

According to Wigner Eckart theorem,

$$\langle \Psi^0_f(j_f, m_f)|O^{k1}_1|\Psi^0_i(j_i, m_i)\rangle = (-1)^{(j_f - m_f)} \begin{Bmatrix} j_f & k1 & j_i \\ -m_f & m_{k1} & m_i \end{Bmatrix} \langle \Psi^0_f(j_f)||O^{k1}_1||\Psi^0_i(j_i)\rangle \quad (3.43)$$

Here O^{k1}_1 is any tensor of rank $k1$ and $|\Psi_f\rangle$ and $|\Psi_i\rangle$ are the initial and final angular momentum states. The third term in the right hand side is referred to as the reduced matrix element. This reduced matrix element is independent of m_f, m_i, m_{k1}. The 3-j symbol and the phase factor contains the geometric contribution and the reduced element contains the physical contribution. Conditions for non-zero 3j symbol are:

$$j_f + j_i \geq k1 \geq |j_f - j_i| \quad (3.44)$$

$$m_f + m_{k1} + m_i = 0 \quad (3.45)$$

The first and second conditions are due to vector addition and magnetic moment conservation. In this case the Dipole operator D, $\mathrm{H}^{\rm NSD}_{\rm PNC}$ are of rank $k = 1$ and $H^{\rm NSI}_{\rm PNC}$ is of rank $k = 0$.

We consider below each case in detail:

Case I: NSI

Initial state $=|5p^6 6s\rangle_{1/2}$
Final state $= |5p^6 5d\rangle_{5/2}$

(i) Intermediate state $= |5p^6 6p\rangle_{1/2}$

$$E1PNC = (-1)^{5/2-1/2}\langle 5d5/2||D^1||kp1/2\rangle \begin{Bmatrix} 5/2 & 1 & 1/2 \\ -1/2 & 0 & 1/2 \end{Bmatrix} (-1)^{1/2-1/2}\langle kp1/2||H^0_{\rm PNC}||6s1/2\rangle \begin{Bmatrix} 1/2 & 0 & 1/2 \\ -1/2 & 0 & 1/2 \end{Bmatrix} + C.C. \tag{3.46}$$

$$\begin{aligned} 5/2+1/2 \geq k \geq |5/2-1/2| \\ \text{so, } k = 2,3 \\ 1/2+1/2 \geq k \geq |1/2-1/2| \\ \text{so, } k = \mathbf{0}, 1 \end{aligned} \tag{3.47}$$

So, the transition is not possible between $s_{1/2}$ and $d_{5/2}$ with intermediate state j values as $1/2$.

(ii) Intermediate state $= |5p^6 6p\rangle_{3/2}$

$$E1PNC = (-1)^{5/2-3/2}\langle 5d5/2||D^1||kp3/2\rangle \begin{Bmatrix} 5/2 & 1 & 3/2 \\ -1/2 & 0 & 1/2 \end{Bmatrix} (-1)^{3/2-1/2}\langle kp3/2||H^0_{\rm PNC}||6s1/2\rangle \begin{Bmatrix} 3/2 & 0 & 1/2 \\ -1/2 & 0 & 1/2 \end{Bmatrix} + C.C. \tag{3.48}$$

$$\begin{aligned} 5/2+3/2 \geq k \geq |5/2-3/2| \\ so, k = \mathbf{1}, 2, 3, 4 \\ 3/2+1/2 \geq k \geq |3/2-1/2| \\ so, k = 1, 2 \end{aligned} \tag{3.49}$$

Table 3.9: Summary of the allowed NSI and NSD transitions in Ba^+ and Ra^+ for $s_{1/2} - d_{5/2}$.

Intermediate state Interactions	$p_{1/2}$ (NSI)	$p_{3/2}$ (NSI)	$p_{1/2}$ (NSD)	$p_{3/2}$ (NSD)
	not allowed	not allowed	not allowed	**allowed**

So, the transition is not possible between $s_{1/2}$ and $d_{5/2}$ with intermediate state j values as $3/2$.

Case II: NSD

Initial state $=|5p^6 6s\rangle_{1/2}$
Final state $= |5p^6 5d\rangle_{5/2}$

(i) Intermediate state $= |5p^6 6p\rangle_{1/2}$

$$E1PNC = (-1)^{5/2-1/2}\langle 5d5/2||D^1||kp1/2\rangle \begin{Bmatrix} 5/2 & 1 & 1/2 \\ -1/2 & 0 & 1/2 \end{Bmatrix}$$
$$(-1)^{1/2-1/2}\langle kp1/2||H^1_{\rm PNC}||6s1/2\rangle \begin{Bmatrix} 1/2 & 1 & 1/2 \\ -1/2 & 0 & 1/2 \end{Bmatrix} + C.C. \tag{3.50}$$

$$\begin{aligned} 5/2 + 1/2 \geq k \geq |5/2 - 1/2| \\ so, k = 2, 3 \\ 1/2 + 1/2 \geq k \geq |1/2 - 1/2| \\ so, k = 0, \mathbf{1} \end{aligned} \tag{3.51}$$

So, the transition is not possible between $s_{1/2}$ and $d_{5/2}$ with intermediate state j values as $1/2$.

(ii) Intermediate state $= |5p^6 6p\rangle_{3/2}$

$$E1PNC = (-1)^{5/2-3/2}\langle 5d5/2||D^1||kp3/2\rangle \begin{Bmatrix} 5/2 & 1 & 3/2 \\ -1/2 & 0 & 1/2 \end{Bmatrix}$$

$$(-1)^{3/2-1/2}\langle kp3/2||H^1_{\rm PNC}||6s1/2\rangle \begin{Bmatrix} 3/2 & 1 & 1/2 \\ -1/2 & 0 & 1/2 \end{Bmatrix} + C.C. \tag{3.52}$$

$$\begin{aligned} 5/2+3/2 \geq k \geq |5/2-3/2| \\ so, k = \mathbf{1}, 2, 3, 4 \\ 3/2+1/2 \geq k \geq |3/2-1/2| \\ so, k = \mathbf{1}, 2 \end{aligned} \tag{3.53}$$

So, the transition is possible between $s_{1/2}$ and $d_{5/2}$ only with intermediate state j values as 3/2. The above result is summerised in the Table 3.9.

Bibliography

[1] F.E. Harris, H.J. Monkhorst and D.L. Freeman, *Algebraic and Diagrammatic Methods in Many-Fermion Theory*, New York, Oxford Univ. Press (1992).

[2] I. Lindgren, J. Morrison, *Atomic Many-Body Theory*, Springer-Verlag, New York (1981).

[3] A.D. Singh, A study of the Electric Dipole Moment of Atoms, Ph.D. Thesis, Bangalore University (1998).

[4] H.P. Kelly, *Phys. Rev.* **131**, 684 (1963).

[5] M.A. Bouchiat and C. Bouchiat, *Phys. Lett.* **B48**, 111 (1974); M.A. Bouchiat and C. Bouchiat., *J. Phys.*, France **35**, 899 (1974).

[6] F.A. Parpia, C.F. Fischer and I.P. Grant (unpublished).

[7] R.K. Chaudhuri, P.K. Panda and B.P. Das, *Phys. Rev. A* **59**, 1187 (1999).

[8] S. Malhotra, A.D. Singh and B.P. Das, *Phys. Rev. A* **51**, R2665 (1995).

[9] D.N. Stacey, *Physica Scrptica* **T40**, 15 (1992); M.A. Bouchiat (unpublished).

[10] C.S. Wood et al. *Science* **275**, 1759 (1997).

[11] W.C. Haxton, *Science* **275**, 1753 (1997).

[12] N. Fortson, *Phys. Rev. Lett.* **70**, 2383 (1993).

[13] N.Y.W. Nagourney and H. Dehmelt, *Phys. Rev. Lett.* **78**, 4898 (1997).

[14] A.D.Singh, K.P. Geetha, B.P. Das and C.S. Unnikrishnan (unpublished).

[15] K.P. Geetha, A.D. Singh, B.P. Das and C.S. Unnikrishnan, *Phys. Rev. A* **58**, R16 (1998).

Chapter 4

Many Body Perturbation Theory applied to Parity Non-Conservation in Atoms

---

4.1 General Considerations

In the previous chapter, we considered the most straight forward and widely used technique for going beyond the independent-particle model for a many-electron system; the Configuration Interaction (CI) expansion. The upper-bound character of the CI method (due to the variational procedure) have made it popular for atomic and molecular calculations. But this method possesses shortcomings that makes it unsuitable for macroscopic systems which suggests a need for alternative approaches. The most well known drawback of the CI method is the lack of size-extensivity (*i.e.*, the failure of the energy to scale properly with the number of particles in the system).

In this chapter, we analyse another approach to the many-electron problem Many-Body Perturbation Theory (MBPT). In this method, different orders of the perturbation are introduced in a systematic way unlike different orders of excitations in the case of CI method. This has an advantage when basis-set expansions are used, since the number of terms in each order of perturbation doesn't change with the increase in the single-particle basis, but has an effect on the amount of time needed for the computation at each order. Whereas in the case of CI method the many-particle basis (corresponding to the possible number of configurations in a CI expansion) increases far more rapidly with the increase in single-particle basis, and for most of

the problems it is impractical to use the complete set of configuration due to the large memory needed to store the matrix for diagonalisation. But in terms of the physics involved, MBPT will only have contributions from terms up to a given order, whereas in CI by the addition of all possible configurations to certain excitations one can include effects to all orders in the sub-space spanned by the configuration state functions. Another important advantage of this method is the size-extensivity through the linked diagram expansion [1, 2].

Perturbation theory however, also has some drawbacks for energy calculations. In its basic structure, the wave function and energy are expanded in terms of a perturbation parameter that should be small enough to yield converged results. In many problems of interest this assumption may not be valid, and converged results are obtained only if certain types of perturbative contributions are summed to infinite order. In some problems, individual low order contributions diverge and infinite order summations are needed to obtain finite results. This behaviour very clearly indicates that order-by-order summation will generally not be a useful way to evaluate perturbation expansions. Nevertheless, the study of perturbation theory is important, partly because it can be applied to a wide range of problems, and partly because it facilitates the comparison with other approaches like the Coupled Cluster Method (CCM), since the latter can easily be reduced to the former by suitable approximations.

4.2 Partitioning of the Hamiltonian

In the perturbative approach the Hamiltonian of the system (H) is split into two parts, a model Hamiltonian (H_0) and a perturbation (V) so that

$$H = H_0 + V,$$

where the zeroth-order part H_0 has known eigenfunctions and eigenvalues given by

$$H_0|\Psi_k^{(0)}\rangle = E_k^{(0)}|\Psi_k^{(0)}\rangle. \tag{4.1}$$

If the perturbation is assumed to be small, the zeroth-order solution $|\Psi_k^{(0)}\rangle$ and $E_k^{(0)}$ approximate the exact solutions $|\Psi_k\rangle$ and E_k to an acceptable accuracy. If the set $\{\Psi_k^{(0)}\}$ is complete, the exact wave function Ψ can be expanded as

$$|\Psi\rangle = \sum_k C_k|\Psi_k^{(0)}\rangle. \tag{4.2}$$

Here, the complete set of zeroth-order eigenfunctions are assumed to be known. The coefficient for the zeroth-order ground state is often chosen to be $C_0 = 1$ which can

be achieved by appropriate renormalisation of $|\Psi\rangle$. By this choice, Eq. 4.2 becomes

$$|\Psi\rangle = |\Psi_0^{(0)}\rangle + \sum_{k\neq 0} C_k |\Psi_k^{(0)}\rangle, \tag{4.3}$$

It follows from Eq. 4.3 that

$$\langle\Psi|\Psi_0^{(0)}\rangle = 1 \tag{4.4}$$

which is termed as intermediate normalisation. If the zeroth-order wave function $|\Psi_0^{(0)}\rangle$ is a good approximation to $|\Psi\rangle$, the coefficients C_k are expected to be small and can be expanded in perturbation series as:

$$C_k = \sum_{\lambda=1}^{\infty} C_k^{(\lambda)}, \tag{4.5}$$

where $C_k^{(\lambda)}$ is the λth-order contribution to C_k. Similarly, the exact energy E can be expanded in a perturbation series as:

$$E_k = E_k^{(0)} + E_k^{(1)} + E_k^{(2)} + ... \tag{4.6}$$

The most well-known perturbation schemes are the Rayleigh-Schrödinger (RS) and the Brillouin-Wigner (BW) expansions [3]. The BW expansion is formally simple, but it contains the unknown energy of the system, which means that the contributions due to the perturbation have to be computed in a self-consistent way. The other disadvantage is that it is not a size consistent expansion. RS expansion, on the other hand, is given in terms of the known eigenvalues of the Hamiltonian H_0, but it has instead a number of additional terms not appearing in the BW case.

The aim of perturbation theory is to derive expressions for $C_k^{(\lambda)}$ and $E^{(\lambda)}$. The expressions for these quantities contain the eigenvalues of H_0 and matrix elements of the perturbation between the eigenfunctions of H_0. Terms that involve products of n such matrix elements are grouped together to constitute the n^{th}-order perturbation theory. If we choose H_0 judiciously, then V would be small and the perturbation expansion would converge quickly. The choice of H_0 in principle is arbitrary, but care should be taken so that it yields convergent (true or asymptotic) series. The most widely used form of H_0 is the Dirac-Fock (DF) operator given by

$$H_0 = \hat{F} = \sum_i^N h_0(i) = \sum_i \epsilon_i a_i^+ a_i, \tag{4.7}$$

where index i runs over the N particles of the system. The basis functions are single determinants constructed out of single-particle orbitals given by

$$|\Phi_a\rangle = det\{\phi_1(1)\phi_2(2)...\phi_N(N)\}, \tag{4.8}$$

with

$$h_0|\phi_i\rangle = \epsilon_i|\phi_i\rangle.$$

From the above it is clear that

$$H_0|\Phi_a\rangle = E_0^a|\Phi_a\rangle \tag{4.9}$$

with

$$E_0^a = \sum_i \epsilon_i,$$

where $|\phi_i\rangle$ and ϵ_i are the single-particle orbital and its energy respectively. This choice of Hamiltonian with the application to N electron system was first done by C. Møller and M.S. Plesset. By this choice, the perturbation operator V describes the electron correlation (physical effects beyond the DF approximation) and the aim of the perturbation calculation is to improve the DF energy towards the exact solution of the Schrödinger equation using the same basis set. This is the so-called Møller-Plesset partitioning [4, 5]. The correlation energy can be calculated perturbatively also in the Epstein-Nesbet partitioning [6] in which the zeroth-order is defined by the diagonal elements of the CI matrix.

In modern perturbation theory the space for the wave functions is separated into two parts; a model space and an orthogonal space (complementary space). The basic idea here is to find an "effective operator" which acts only on limited space called "model space" but generates the same result as do the original operators acting on the entire functional space. The model space represents all functions associated with one or several configurations. The reason for including several configurations in the model space is that it is possible in this way to take into account strongly interacting configurations to all orders and treat the weakly interacting ones by means of a lower order expansion. A larger model space chosen properly is therefore expected to lead to a better first-order approximation but at the expense of the intruder states which disrupts the perturbative convergence at higher orders [7, 8, 9, 10]. Above all the model space should be complete if standard BW or RS perturbation theory is invoked. The proper choice of the model space may therefore be of vital importance for the success of the perturbation calculation.

4.3 Diagrammatic Representation of Perturbations

It is convenient to separate the single-particle orbitals into following three categories:

(a) *core orbitals*, defined as orbitals occupied in all determinants of the model and virtual space,

(b) *valence or open-shell orbitals*, defined as orbitals occupied in some but not all determinants of the model space,

(c) *excited or virtual orbitals*, defined as orbitals not occupied in any determinant of the model space.

In the diagrammatic representation the following convention is used: A core orbital is represented by a vertical line with an arrow pointing downwards and a virtual orbital by a vertical line with an arrow pointing upwards. For valence orbitals we use Sandars' notation with a double arrow, normally pointing upwards. We use vertical time axis instead of horizontal time axis. The one-particle operator of the perturbation is drawn with a horizontal line with a circle and the two-particle with broken lines. The other perturbations like dipole is represented by a horizontal line with a square and PNC interactions by a circle with a cross inside. Each of the vertex has an associated matrix element. The creation operators are associated with outgoing orbital lines and annihilation operators with incoming orbital lines with respect to the interaction vertex. We use standard rules for the evaluation of a Goldstone diagrams [3]. Here, indices *a, b, c, ...* denote core orbitals, *p, q, r, ...* stand for virtual orbitals and v refers to the valence orbitals. Indices *i, j, k, ...* denote general orbitals.

4.4 General Form of the Effective Operator

With PNC Hamiltonian as the perturbation, the total Hamiltonian takes the form

$$H = H_0 + V_{es} + \lambda H_{\rm PNC} \tag{4.10}$$

where V_{es} is the residual electrostatic interaction. Due to the presence of $H_{\rm PNC}$, an atomic state function (ASF) (defined in Chapter 3) becomes a state of mixed parity. For example, if $|\Psi_\alpha\rangle$ and $|\Psi_\beta\rangle$ are states of even parity in the absence of $H_{\rm PNC}$, and in the presence of $H_{\rm PNC}$ it becomes

$$|\tilde{\Psi}_\alpha\rangle = |\Psi_\alpha^{+(0)}\rangle + |\Psi_\alpha^-({\rm corre})\rangle \tag{4.11}$$

$$|\tilde{\Psi}_\beta\rangle = |\Psi_\beta^{+(0)}\rangle + |\Psi_\beta^-({\rm corre})\rangle. \tag{4.12}$$

Here $|\Psi_\alpha^{+(0)}\rangle$ and $|\Psi_\beta^{+(0)}\rangle$ denotes the unperturbed part which is even under parity and $|\Psi_\alpha^-({\rm corre})\rangle$ and $|\Psi_\beta^-({\rm corre})\rangle$ denotes the correction due to the perturbation which is odd under parity and/or *vice versa*. According to the Laporte's rule [11]

$$e\int \Psi_\beta \hat{r} \Psi_\alpha d\tau = 0 \tag{4.13}$$

if Ψ_β and Ψ_α have the same parity. This selection rule, due to Wigner, is of importance in discussing radiative transitions between ASFs where $e.\hat{r}$ is the dipole operator which is denoted further in the chapter as D which is odd under parity. But due to the mixing of parity in the ASFs, one can look for non-zero dipole transition amplitude between states of same parity induced by PNC denoted as $E1PNC$. It is given by

$$E1PNC = \langle\tilde{\Psi}_\beta|D|\tilde{\Psi}_\alpha\rangle \tag{4.14}$$

Here the ASF's considered have a single valence electron outside the closed shell core. For example, Ba^+

$$|\Psi_\alpha\rangle = |1s^2 2s^2 ....5p^6 6s_{1/2}\rangle$$

and

$$|\Psi_\beta\rangle = |1s^2 2s^2 ....5p^6 5d_{3/2}\rangle.$$

Let us consider that we have only one parity (in this case even) in the model space *i.e.*,

$$|\Psi_\alpha^{(0)}\rangle = |\Psi_\alpha^{(0)+}\rangle$$

and

$$|\Psi_\beta^{(0)}\rangle = |\Psi_\beta^{(0)+}\rangle.$$

We can construct a wave operator Ω, acting on the unperturbed states to give the exact state given by

$$\Omega'|\Psi_\alpha^{(0)}\rangle = |\tilde{\Psi}_\alpha\rangle, \tag{4.15}$$

$$\Omega''|\Psi_\beta^{(0)}\rangle = |\tilde{\Psi}_\beta\rangle \tag{4.16}$$

Using the above two equations the physical observable of interest in PNC can be written as

$$E1PNC = \langle\Psi_\beta^{+(0)}|\Omega''^\dagger D\Omega'|\Psi_\alpha^{+(0)}\rangle \tag{4.17}$$

Once Ω is known, $E1PNC$ can be computed. We start with the Bloch equation [12] given by

$$\hat{Q}[\Omega^{(n)}, H_0]\hat{P} = \hat{Q}[V\Omega^{(n-1)} - \sum_{m=1}^{n-1}\Omega^{(m)}\hat{P}V\Omega^{(n-m-1)}]\hat{P}, \tag{4.18}$$

where

$$V = V_{es} + \lambda H_{\rm PNC},$$

$$\hat{P} = \sum_{a\in M}|\Phi_a\rangle\langle\Phi_a|$$

and

$$\hat{Q} = 1 - \hat{P} = \sum_{r\notin M}|\Phi_r\rangle\langle\Phi_r|$$

with M as the dimension of the model space considered. Since the PNC perturbation which we are interested scales as G_F, (Fermi's constant) we consider terms linear in λ, but containing different orders in the Couloumb interaction. We therefore write

$$\Omega' = \Omega'_0 + \lambda\Omega'_{\rm PNC}$$
$$\Omega'' = \Omega''_0 + \lambda\Omega''_{\rm PNC}. \tag{4.19}$$

4.4.1 General Expression for $E1PNC^{(n)}$

Substituting for Ω' and Ω'' in Eq. 4.17, and writing D as an effective operator, we get

$$E1PNC = \langle\Psi^{+(0)}_\beta|D_{\rm eff}|\Psi^{+(0)}_\alpha\rangle \tag{4.20}$$

where

$$\mathbf{D}_{\rm eff} = \sum_{m,n=0}^{\infty}[\Omega''^{(m)}_0 + \lambda\Omega''^{(m)}_{\rm PNC}]^\dagger D \sum_{n=0}^{\infty}[\Omega'^{(n)}_0 + \lambda\Omega'^{(n)}_{\rm PNC}]$$

and m, n are the order of perturbation of Couloumb operator corresponding to the initial and final states. Here $\mathbf{D}_{\rm eff}$ refers to only **connected diagrams**. From the effective operator we have to consider different orders of $D_{\rm eff}$ for each order in MBPT. Hence we write the effective operator to have an effective order as

$$D_{\rm eff} = \sum_{n=0}^{\infty} D^{(n)}_{\rm eff}. \tag{4.21}$$

We know $\Omega^{(0)}_{\rm PNC} = 0$ and $\Omega^{(0)}_0 = 1$ which can be obtained from the general expression by putting $n = 0; m = 0$ which leads to a zero contribution. This clearly tells that we need at least one order in λ in the $D_{\rm eff}$. Hence, for non-zero contribution to $E1PNC$, Eq. 4.21 can be written with new summation given by

$$D_{\rm eff} = \sum_{n=1}^{\infty} D^{(n)}_{\rm eff}, \tag{4.22}$$

where

$$D^{(n)}_{\rm eff} = \sum_{m=0}^{n}[\Omega''^{(m)}_0 + \Omega''^{(m)}_{\rm PNC}]^\dagger D[\Omega'^{(n-m)}_0 + \Omega'^{(n-m)}_{\rm PNC}]. \tag{4.23}$$

Hence $E1PNC$ to any order n is given by

$$E1PNC^{(n)} = \langle\Psi^{+(0)}_\beta|D^{(n)}_{\rm eff}|\Psi^{+(0)}_\alpha\rangle. \tag{4.24}$$

For $E1PNC^{(1)}$ with one order in λ and zero orders in Couloumb interaction, $D^{(1)}_{\rm eff}$ reduces to

$$D^{(1)}_{\rm eff} = DR'V_{es}\hat{P} + DR'H_{\rm PNC}\hat{P} + (R''V_{es}\hat{P})^\dagger D + (R''H_{\rm PNC}\hat{P})^\dagger D \tag{4.25}$$

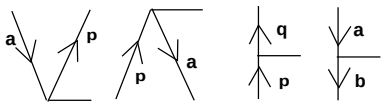

Figure 4.1: Diagrams representing one-body operators (Dipole and PNC).

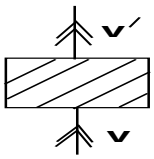

Figure 4.2: Form of the diagram for $E1PNC$.

where R' and R'' are the resolvent operators given by

$$R' = \sum_{\gamma \notin D} \frac{|\Phi_\gamma\rangle\langle\Phi_\gamma|}{E_\alpha - E_0^\gamma}$$
$$R'' = \sum_{\gamma \notin D} \frac{|\Phi_\gamma\rangle\langle\Phi_\gamma|}{E_\beta - E_0^\gamma}. \tag{4.26}$$

4.4.1.1 Evaluation of $E1PNC^{(1)}$ Terms

Taking only the term with one order in λ, $E1PNC^{(1)}$ takes the form using R' and R'' as

$$E1PNC^{(1)} = \sum_{I \notin D} \frac{\langle\Psi_\beta^{+(0)}|D|\Psi_I\rangle\langle\Psi_I|H_{\rm PNC}|\Psi_\alpha^{+(0)}\rangle}{E_\alpha - E_I} + D \Leftrightarrow H_{\rm PNC}, E_\alpha \Leftrightarrow E_\beta \tag{4.27}$$

Considering the ASF's to be single determinant and using the Slater Condon rules [3] we get

$$E1PNC^{(1)} = \sum_{i \notin \alpha} \frac{\langle\phi_\beta^{+(0)}|D|\phi_i^{(0)}\rangle\langle\phi_i^{(0)}|H_{\rm PNC}|\phi_\alpha^{+(0)}\rangle}{\epsilon_\alpha - \epsilon_i} + c.c., \tag{4.28}$$

where ϕ, ϵ are the single-particle orbitals and their energies respectively. Since dipole and PNC are one-body operators, they can be represented in the form of a single-particle operator which can have four forms given as in Fig. 4.1.

Using Wick's theorem [3] and considering diagrams only of the form given in Fig. 4.2, we get four diagrams corresponding to zeroth-order $E1PNC$. These are represented in Fig. 4.3. From now on we will be considering α and β states as i

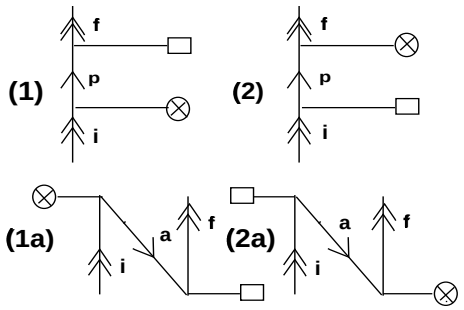

Figure 4.3: Diagrams representing zeroth-order $E1PNC$ terms.

and f which denote the initial and final states. The expressions for the zeroth-order diagrams are given by

$$
\begin{aligned}
(1) \sum_p & \frac{\langle f|D|p\rangle\langle p|H_{\rm PNC}|i\rangle}{\epsilon_i - \epsilon_p} \\
(1a) \sum_a & \frac{\langle f|D|a\rangle\langle a|H_{\rm PNC}|i\rangle}{\epsilon_a - \epsilon_i} \\
(2) \sum_p & \frac{\langle f|H_{\rm PNC}|p\rangle\langle p|D|i\rangle}{\epsilon_f - \epsilon_p} \\
(2a) \sum_a & \frac{\langle f|H_{\rm PNC}|a\rangle\langle a|D|i\rangle}{\epsilon_a - \epsilon_f}
\end{aligned}
\tag{4.29}
$$

where the terms (1) and (2) are the contributions from virtual orbital and (1a) and (2a) are the contributions from the core orbital when the initial and final states are perturbed.

4.4.1.2 Evaluation of $E1PNC^{(2)}$ Terms

Similarly, $E1PNC^{(2)}$ can be obtained by taking $D^{(2)}_{\rm eff}$ which depends on $\Omega^{(2)}_0$ and $\Omega^{(2)}_{\rm PNC}$. These in turn are related to $\Omega^{(1)}_0$ and $\Omega^{(1)}_{\rm PNC}$ through the Bloch equation as

$$\hat{Q}[\Omega^{(2)}, H_0]\hat{P} = \hat{Q}[V\Omega^{(1)} - \Omega^{(1)}\hat{P}V\Omega^{(0)}]\hat{P}. \tag{4.30}$$

This clearly shows that the wave operator in each order can be obtained by operating the perturbation on the wave operator of lower order. Substituting for Ω and considering only same parity states in the P space leading to $\hat{P}H_{\rm PNC}\hat{P} = 0$ and $\hat{P}D\hat{P} = 0$, we get eight terms given by

$$
\begin{aligned}
E1PNC^{(2)} &= \langle\Psi^{+(0)}_\beta|\hat{P}DR'V_{es}R'H_{\rm PNC}\hat{P} + \hat{P}DR'H_{\rm PNC}R'V_{es}\hat{P} \\
&- \hat{P}DR'^2H_{\rm PNC}\hat{P}V_{es}\hat{P} + \hat{P}V^\dagger_{es}R''DR'H_{\rm PNC}\hat{P}
\end{aligned}
$$

$$+ \quad \hat{P}V_{es}^{\dagger}R''H_{\rm PNC}^{\dagger}R''D\hat{P} - \hat{P}V_{es}^{\dagger}\hat{P}H_{\rm PNC}^{\dagger}R''^{2}D\hat{P}$$
$$+ \quad \hat{P}H_{\rm PNC}^{\dagger}R''DR'V_{es}\hat{P} + \hat{P}H_{\rm PNC}^{\dagger}R''V_{es}^{\dagger}R''D\hat{P}|\Psi_{\alpha}^{+(0)}\rangle. \qquad (4.31)$$

By applying Slater Condon rule, we get various diagrams for the above terms by contracting single, double, ... lines between the dipole, PNC and the Couloumb operators. All possible diagrams for the Couloumb operator are given in Appendix A. From now onwards, we show only the diagrammatic representation of the direct terms that are contributed from the virtual orbitals. However, in our calculations, we evaluate both direct and exchange diagrams contributed from the virtual as well as the core orbitals. The possible diagrams arising from $\hat{P}DR'V_{es}R'H_{\rm PNC}\hat{P}$ and $\hat{P}DR'H_{\rm PNC}R'V_{es}\hat{P}$ are given in Fig. 4.4(a). The set of diagrams given in Fig. 4.4(b) are got by interchanging $H_{\rm PNC}$ and V_{es} with respect to the diagrams given in Fig. 4.4(a). The expressions for each of them are given by

$$(3)\sum_{pqa}\frac{\langle f|D|p\rangle\langle pa|V_{es}|iq\rangle\langle q|H_{\rm PNC}|a\rangle}{(\epsilon_a-\epsilon_q)(\epsilon_i-\epsilon_p)}, \qquad (4.32)$$
$$(4)\sum_{pqa}\frac{\langle a|D|q\rangle\langle fq|V_{es}|pa\rangle\langle p|H_{\rm PNC}|i\rangle}{(\epsilon_i-\epsilon_p)(\epsilon_i+\epsilon_a-\epsilon_f-\epsilon_q)},$$
$$(5)\sum_{pqa}\frac{\langle a|D|p\rangle\langle fp|V_{es}|iq\rangle\langle q|H_{\rm PNC}|a\rangle}{(\epsilon_a-\epsilon_q)(\epsilon_i+\epsilon_q-\epsilon_p-\epsilon_f)},$$
$$(6)\sum_{pqa}\frac{\langle f|D|p\rangle\langle pq|V_{es}|ia\rangle\langle a|H_{\rm PNC}|q\rangle}{(\epsilon_i-\epsilon_p)(\epsilon_i+\epsilon_a-\epsilon_p-\epsilon_q)}, \qquad (4.33)$$
$$(7)\sum_{pqa}\frac{\langle a|D|q\rangle\langle pq|V_{es}|ia\rangle\langle f|H_{\rm PNC}|p\rangle}{(\epsilon_i+\epsilon_a-\epsilon_p-\epsilon_q)(\epsilon_i+\epsilon_a-\epsilon_q-\epsilon_f)},$$
$$(8)\sum_{pqa}\frac{\langle a|D|p\rangle\langle fq|V_{es}|ia\rangle\langle p|H_{\rm PNC}|q\rangle}{(\epsilon_i+\epsilon_a-\epsilon_f-\epsilon_q)(\epsilon_i+\epsilon_a-\epsilon_f-\epsilon_p)}.$$

The possible diagrams from the term $\hat{P}V_{es}^{\dagger}R''DR'H_{\rm PNC}\hat{P}$ and $\hat{P}V_{es}^{\dagger}R''H_{\rm PNC}^{\dagger}R'D\hat{P}$ are given in Fig. 4.5 with the expressions

$$(9)\sum_{pqa}\frac{\langle q|D|a\rangle\langle fa|V_{es}|pq\rangle\langle p|H_{\rm PNC}|i\rangle}{(\epsilon_i-\epsilon_p)(\epsilon_f+\epsilon_a-\epsilon_p-\epsilon_q)}, \qquad (4.34)$$
$$(10)\sum_{pqa}\frac{\langle p|D|i\rangle\langle fa|V_{es}|pq\rangle\langle q|H_{\rm PNC}|a\rangle}{(\epsilon_f+\epsilon_a-\epsilon_p-\epsilon_q)(\epsilon_a-\epsilon_q)},$$
$$(11)\sum_{pqa}\frac{\langle p|D|q\rangle\langle fa|V_{es}|ip\rangle\langle q|H_{\rm PNC}|a\rangle}{(\epsilon_a-\epsilon_q)(\epsilon_f+\epsilon_a-\epsilon_i-\epsilon_p)},$$
$$(12)\sum_{pqa}\frac{\langle fa|V_{es}|pq\rangle\langle q|H_{\rm PNC}|a\rangle\langle p|D|i\rangle}{(\epsilon_f-\epsilon_p)(\epsilon_f+\epsilon_a-\epsilon_p-\epsilon_q)}, \qquad (4.35)$$
$$(13)\sum_{pqa}\frac{\langle fa|V_{es}|pq\rangle\langle p|H_{\rm PNC}|i\rangle\langle q|D|a\rangle}{(\epsilon_f+\epsilon_a-\epsilon_p-\epsilon_q)(\epsilon_f+\epsilon_a-\epsilon_q-\epsilon_i)},$$

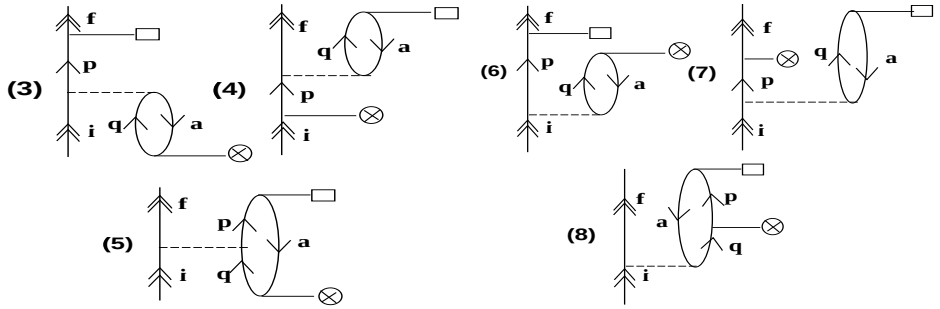

Figure 4.4: Diagrams representing first-order $E1PNC$ terms from $\hat{P}DR'V_{es}R'H_{\rm PNC}\hat{P}$ and $\hat{P}DR'H_{\rm PNC}R'V_{es}\hat{P}$.

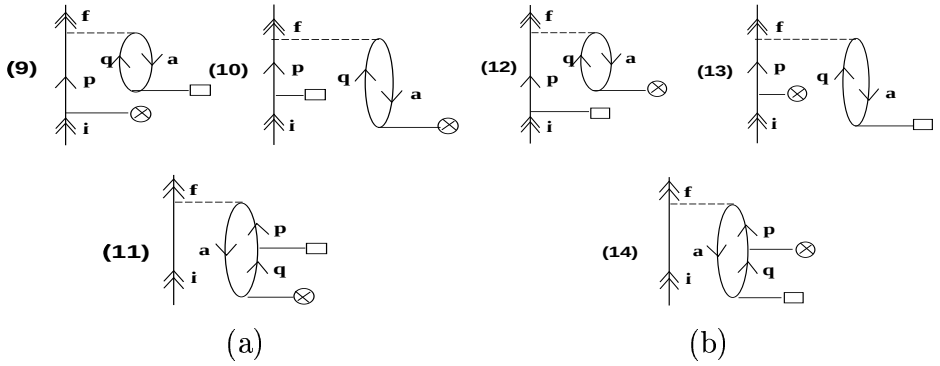

Figure 4.5: Diagrams representing first-order $E1PNC$ terms from $\hat{P}V_{es}^{\dagger}R''DR'H_{\rm PNC}\hat{P}$ and $\hat{P}V_{es}^{\dagger}R''H_{\rm PNC}^{\dagger}R'D\hat{P}$.

$$(14)\sum_{pqa}\frac{\langle fa|V_{es}|ip\rangle\langle p|H_{\rm PNC}|q\rangle\langle q|D|a\rangle}{(\epsilon_f+\epsilon_a-\epsilon_i-\epsilon_p)(\epsilon_f+\epsilon_a-\epsilon_i-\epsilon_q)}.$$

The diagrams in Fig. 4.5(b) are obtained by interchanging $H_{\rm PNC}$ and D with respect to the diagrams given in Fig. 4.5(a). The possible diagrams from the term $\hat{P}H_{\rm PNC}^{\dagger}R''DR'V_{es}\hat{P}$ and $\hat{P}H_{\rm PNC}^{\dagger}R''V_{es}^{\dagger}R''D\hat{P}$ are given in Fig. 4.6 with the expressions

$$(15)\sum_{pqa}\frac{\langle f|H_{\rm PNC}|p\rangle\langle a|D|q\rangle\langle pq|V_{es}|ia\rangle}{(\epsilon_f-\epsilon_p)(\epsilon_i+\epsilon_a-\epsilon_p-\epsilon_q)}, \tag{4.36}$$

$$(16)\sum_{pqa}\frac{\langle a|H_{\rm PNC}|q\rangle\langle f|D|p\rangle\langle pq|V_{es}|ia\rangle}{(\epsilon_a-\epsilon_q)(\epsilon_i+\epsilon_a-\epsilon_p-\epsilon_q)},$$

$$(17)\sum_{pqa}\frac{\langle a|H_{\rm PNC}|p\rangle\langle p|D|q\rangle\langle fq|V_{es}|ia\rangle}{(\epsilon_a-\epsilon_p)(\epsilon_i+\epsilon_a-\epsilon_f-\epsilon_q)},$$

$$(18)\sum_{pqa}\frac{\langle f|H_{\rm PNC}|p\rangle\langle q|D|a\rangle\langle pa|V_{es}|iq\rangle}{(\epsilon_f-\epsilon_p)(\epsilon_f+\epsilon_a-\epsilon_i-\epsilon_q)}, \tag{4.37}$$

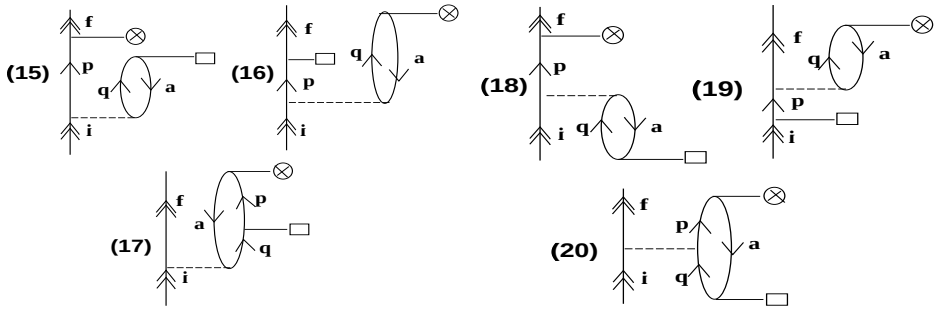

Figure 4.6: Diagrams representing first-order $E1PNC$ terms from $\hat{P}H^{\dagger}_{\rm PNC}R''DR'V_{es}\hat{P}$ and $\hat{P}H^{\dagger}_{\rm PNC}R''V^{\dagger}_{es}R''D\hat{P}$.

$$(19)\sum_{pqa}\frac{\langle a|H_{\rm PNC}|q\rangle\langle p|D|i\rangle\langle fq|V_{es}|pa\rangle}{(\epsilon_a-\epsilon_q)(\epsilon_f-\epsilon_p)},$$
$$(20)\sum_{pqa}\frac{\langle a|H_{\rm PNC}|p\rangle\langle q|D|a\rangle\langle fp|V_{es}|iq\rangle}{(\epsilon_a-\epsilon_p)(\epsilon_f+\epsilon_b-\epsilon_i-\epsilon_q)}.$$

The set of diagrams given in Fig. 4.6(b) are obtained by interchanging V_{es} and D with respect to the diagrams given in Fig. 4.6(a). There are two more terms which give rise to folded diagrams, but on contraction they do not yield diagrams of the form as given in Fig. 4.2. In the next section we look at various ways in which these first-order diagrams can be grouped together and effectively summed to all orders to yield the Coupled Perturbed Hartree Fock (CPHF), Random Phase Approximation (RPA) and CPHF-RPA terms. We first discuss the CPHF theory [13, 14] which has proved to be a very useful tool for the *ab initio* calculation of certain atomic and molecular properties which correspond to one-electron perturbation operators. In this case, the parity non-conserving interaction between the nucleus and the core electrons causes the core orbitals to have a PNC admixture in it, which perturbs all the other core orbitals through the DF potential. We also discuss about RPA [14, 15, 16] where due to the application of an oscillating electric field the core electrons get polarised. By taking these orbital modifications into account in DF potential, leads to coupled equations for the electric dipole perturbed functions. In the end we discuss the CPHF-RPA approach in which the core orbitals are perturbed due to the presence of the PNC operator and of an external electric field. It can be viewed as a particular double perturbation theory as discussed by Caves and Karplus [17].

4.5 Coupled Perturbed Hartree Fock

We consider a closed shell 2N electron system with the DF Hamiltonian. According to DF approximation, we write the exact wave function as a single determinantal state consisting of single-particle orbitals. We solve the Schrödinger equation by the variational principle by minimising the energy with respect to the single-particle orbitals and by imposing orthonormality condition on the single-particle orbitals. This leads to

$$(h^0 + g^0 - \epsilon_i)|\phi_i^0(r)\rangle = 0 \tag{4.38}$$

where h^0 and g^0 are the single and two-body operators which together are called the Fock operator denoted as f^0. g^0 can be explicitly written as

$$g^0|\phi_i^0(r)\rangle = \langle\phi_j^0(r_2)|g|\phi_j^0(r_2)\rangle|\phi_i^0(r_1)\rangle - \langle\phi_j^0(r_2)|g|\phi_i^0(r_1)\rangle|\phi_j^0(r_2)\rangle.$$

Here we consider $H_{\rm PNC}$ as the perturbation and the above equation for one order in $H_{\rm PNC}$ reduces to

$$(f^0 - \epsilon_i^0)|\phi_i^1(r)\rangle = (\epsilon_i^1 - H_{\rm PNC} - g^1)|\phi_i^0\rangle, \tag{4.39}$$

where $\epsilon_i^1 = 0$ due to the odd parity nature of the $H_{\rm PNC}$ operator. The perturbed g^1 can be written as

$$\begin{aligned} g^1|\phi_i^0(r)\rangle &= \langle\phi_j^0(r_2)|g|\phi_j^1(r_2)\rangle|\phi_i^0(r_1)\rangle - \langle\phi_j^0(r_2)|g|\phi_i^0(r_1)\rangle|\phi_j^1(r_2)\rangle \\ &+ \langle\phi_j^1(r_2)|g|\phi_j^0(r_2)\rangle|\phi_i^0(r_1)\rangle - \langle\phi_j^1(r_2)|g|\phi_i^0(r_1)\rangle|\phi_j^0(r_2)\rangle. \end{aligned} \tag{4.40}$$

Now we expand each of the perturbed orbitals $|\phi_i^1(r)\rangle$ as a linear combination of the unperturbed virtual orbitals given by

$$|\phi_i^1(r)\rangle = \sum_p C_{pi}|\phi_p^0(r)\rangle. \tag{4.41}$$

Substituting the above in Eq. 4.39, we get

$$\sum_p (f^0 - \epsilon_i^0)C_{pi}|\phi_p^0(r)\rangle = (-H_{\rm PNC} - g^1)|\phi_i^0(r)\rangle. \tag{4.42}$$

Acting by $\langle\phi_p^0(r)|$, we get

$$\begin{aligned} C_{pi}(\epsilon_p - \epsilon_i) &+ \sum_{aq}\{\langle pq|g|ia\rangle - \langle pq|g|ai\rangle\}C_{qa}^* \\ &+ \sum_{aq}\{\langle pa|g|iq\rangle - \langle pa|g|qi\rangle\}C_{qa} \\ &+ \langle p|H_{\rm PNC}|i\rangle = 0, \end{aligned} \tag{4.43}$$

where

$$C_{qa} = - \frac{\langle q|H_{\rm PNC}|a\rangle}{(\epsilon_q - \epsilon_a)} \tag{4.44}$$

and

$$C^*_{qa} = -C_{qa} \tag{4.45}$$

since $H_{\rm PNC}$ is an imaginary operator. Eq. 4.43 is named as PNC HF or as CPHF equation. Using the above relationship in Eq. 4.43, we get

$$\begin{aligned} C_{pi}(\epsilon_p - \epsilon_i) &- \sum_{aq}\{\langle pq|g|ia\rangle - \langle pq|g|ai\rangle\}C_{qa} \\ &+ \sum_{aq}\{\langle pa|g|iq\rangle - \langle pa|g|qi\rangle\}C_{qa} \\ &= -\langle p|H_{\rm PNC}|i\rangle. \end{aligned} \tag{4.46}$$

We define

$$A_{pi,qa} = -\tilde{V}_{pq,ia} + \tilde{V}_{pa,iq} + (\epsilon_p - \epsilon_i)\delta_{pq}\delta_{ia} \tag{4.47}$$

and

$$B_{pi} = \langle p|H_{\rm PNC}|i\rangle. \tag{4.48}$$

This leads to a linear equation of the form

$$AX = -B, \tag{4.49}$$

where the order of matrix A depends on the various combinations of p and i orbitals which have different parity. Alternatively the same equation can be solved by keeping the A part of the matrix as the energy difference and the left hand side (B) of the linear equation as the sum of the PNC and Couloumb matrix element. This can be represented as

$$\begin{aligned} (\epsilon_p - \epsilon_i)\delta_{pq}\delta_{ia}C_{pi} &= \sum_{aq}\{\langle pq|g|ia\rangle - \langle pq|g|ai\rangle\}C_{qa} \\ &- \sum_{aq}\{\langle pa|g|iq\rangle - \langle pa|g|qi\rangle\}C_{qa} - \langle p|H_{\rm PNC}|i\rangle. \end{aligned} \tag{4.50}$$

This kind of rearrangement is slower in convergence compared to the previous one due to the large energy difference in the denominator when one does order-by-order calculation. The above equation can be rewritten as

$$(\epsilon_q - \epsilon_j)\delta_{pq}\delta_{ia}C_{qa} = -\langle p|H_{\rm PNC}|i\rangle + \sum_{aq}\{\tilde{V}_{pq,ia} - \tilde{V}_{pa,iq}\}C_{qa} \tag{4.51}$$

or

$$\sum_{a,q}\{(\epsilon_q - \epsilon_j)\delta_{pq}\delta_{ia}C_{qa} + \tilde{V}_{pa,iq} - \tilde{V}_{pq,ia}\}C_{qa} + \langle p|H_{\rm PNC}|i\rangle = 0. \tag{4.52}$$

By solving the linear Eqs. 4.51 or 4.52 we obtain C_{qa} amplitudes for excitations from core-virtual as well as valence to virtual. The electric dipole transition amplitude is then computed using the following expression

$$E1PNC = \langle f|D|i^{\rm PNC}\rangle + \langle f^{\rm PNC}|D|i\rangle \tag{4.53}$$

or

$$E1PNC = \langle f|D|p\rangle C_{pi}^{\rm PNC} + C_{fp}^{\rm PNC\star}\langle p|D|i\rangle. \tag{4.54}$$

Thus, we need to evaluate $C_{pi}^{\rm PNC}$ and $C_{fp}^{\rm PNC}$ where i and f in this case are denoted as the initial and final states. This can be obtained directly using C_{qa} as

$$C_{pi}^{\rm PNC} = -\frac{\langle p|H_{\rm PNC}|i\rangle}{\epsilon_p - \epsilon_i} + \sum_{qa}\frac{C_{qa}}{(\epsilon_p - \epsilon_i)}\{V_{pq,ia} - V_{pq,ai}\} - \sum_{qa}\frac{C_{qa}}{(\epsilon_p - \epsilon_i)}\{V_{pa,iq} - V_{pa,qi}\} \tag{4.55}$$

and

$$C_{fp}^{\rm PNC} = -\frac{\langle p|H_{\rm PNC}|f\rangle}{\epsilon_p - \epsilon_f} + \sum_{qa}\frac{C_{qa}}{(\epsilon_p - \epsilon_f)}\{V_{pq,fa} - V_{pq,af}\} - \sum_{qa}\frac{C_{qa}}{(\epsilon_p - \epsilon_f)}\{V_{pa,fq} - V_{pa,qf}\}. \tag{4.56}$$

Below we discuss some aspects of CPHF formalism and its relation with MBPT.

First we consider that the residual Couloumb interaction is zero. Then Eq. 4.55 reduces to

$$C_{pi}^{(0,1)} = \frac{\langle p|H_{\rm PNC}|i\rangle}{(\epsilon_i - \epsilon_p)} \tag{4.57}$$

where $C_{pi}^{(x,y)}$ represents x orders of Couloumb and y orders of $H_{\rm PNC}$. Using one order in PNC, the electric dipole transition amplitude takes the form

$$E1PNC^{(1)} = \langle f^0|D|i^1\rangle + \langle f^1|D|i^0\rangle. \tag{4.58}$$

Writing the perturbed single-particle orbitals in terms of the $C's$ and the unperturbed amplitudes, we get

$$E1PNC^{(1)} = \sum_p \frac{\langle f|D|p\rangle\langle p|H_{\rm PNC}|i\rangle}{(\epsilon_p - \epsilon_i)} + D \Leftrightarrow H_{\rm PNC},\ \epsilon_i \Leftrightarrow \epsilon_f. \tag{4.59}$$

Similarly taking the Couloumb term to be non-zero, we get

$$\begin{aligned} C_{pi}^{(1,1)} &= \frac{\langle p|H_{\rm PNC}|i\rangle}{(\epsilon_i - \epsilon_p)} - \sum_{qa}\frac{\langle a|H_{\rm PNC}|q\rangle(\langle pq|g|ia\rangle - \langle pq|g|ai\rangle)}{(\epsilon_i - \epsilon_p)(\epsilon_q - \epsilon_a)} \\ &+ \sum_{qa}\frac{\langle q|H_{\rm PNC}|a\rangle(\langle pb|g|iq\rangle - \langle pb|g|qi\rangle)}{(\epsilon_i - \epsilon_p)(\epsilon_a - \epsilon_q)}. \end{aligned} \tag{4.60}$$

Using this, second-order electric dipole transition amplitude is given by

$$\begin{aligned} E1PNC^2 &= \sum_p \frac{\langle f|D|p\rangle\langle p|\mathrm{PNC}|i\rangle}{(\epsilon_i-\epsilon_p)} \\ &- \sum_{pqa} \frac{\langle f|D|p\rangle\langle pq|g|ia\rangle\langle a|\mathrm{PNC}|q\rangle}{(\epsilon_i-\epsilon_p)(\epsilon_q-\epsilon_a)} \\ &+ \sum_{pqa} \frac{\langle f|D|p\rangle\langle pa|g|iq\rangle\langle q|\mathrm{PNC}|a\rangle}{(\epsilon_i-\epsilon_p)(\epsilon_a-\epsilon_q)} + c.c., \end{aligned} \tag{4.61}$$

where *c.c.* refers to complex conjugate terms. The first, third and the corresponding complex conjugate terms in the above equation in comparison with the MBPT diagrams are equivalent to the diagrams designated as MBPT(1), MBPT(3) and its complex conjugates designated as MBPT(2) and MBPT(19). The second term of the above equation can be got by adding the MBPT diagrams designated as MBPT(6) and MBPT(16).

$$\begin{aligned} MBPT(6)+MBPT(16) &= \sum_{pqa} \frac{\langle f|D|p\rangle\langle a|H_{\mathrm{PNC}}|q\rangle\langle pq|g|ia\rangle}{(\epsilon_i+\epsilon_a-\epsilon_p-\epsilon_q)(\epsilon_i-\epsilon_p)} \\ &+ \sum_{pqa} \frac{\langle f|D|p\rangle\langle a|H_{\mathrm{PNC}}|q\rangle\langle pq|g|ia\rangle}{(\epsilon_i+\epsilon_a-\epsilon_p-\epsilon_q)(\epsilon_a-\epsilon_q)} \\ &= \sum_{pqa} \frac{\langle f|D|p\rangle\langle a|H_{\mathrm{PNC}}|q\rangle\langle pq|g|ia\rangle}{(\epsilon_i-\epsilon_p)(\epsilon_a-\epsilon_q)} \\ &= (-1)\sum_{pqa} \frac{\langle f|D|p\rangle\langle a|H_{\mathrm{PNC}}|q\rangle\langle pq|g|ia\rangle}{(\epsilon_i-\epsilon_p)(\epsilon_q-\epsilon_a)} \end{aligned} \tag{4.62}$$

This can be schematically represented like diagram (A) as in Fig. 4.7 wherein the sense of the core and virtual particle are different from the accepted convention for the PNC bubble. This can also be interpreted the following way. In the $E1PNC^{(2)}$ expression given by Eq. 4.61, take the $(-)$ sign inside for the second term and this gives

$$\sum_{pqa} \frac{\langle f|D|p\rangle\langle pq|g|ia\rangle\langle a|H_{\mathrm{PNC}}|q\rangle}{(\epsilon_i-\epsilon_p)(\epsilon_a-\epsilon_q)} \tag{4.63}$$

which is nothing but the diagram (B) given in Fig. 4.7 with the local energy denominator for both the perturbation vertex. Similarly, by adding MBPT(10) and MBPT(12) we get the conjugate term which can be interpreted the same way as before.

The diagram we get from the conjugate term is given in Fig. 4.8. Hence, by solving the CPHF linear equation, we take eight of the MBPT diagrams to all order out of which two are from zeroth-order and three each from initial and final state

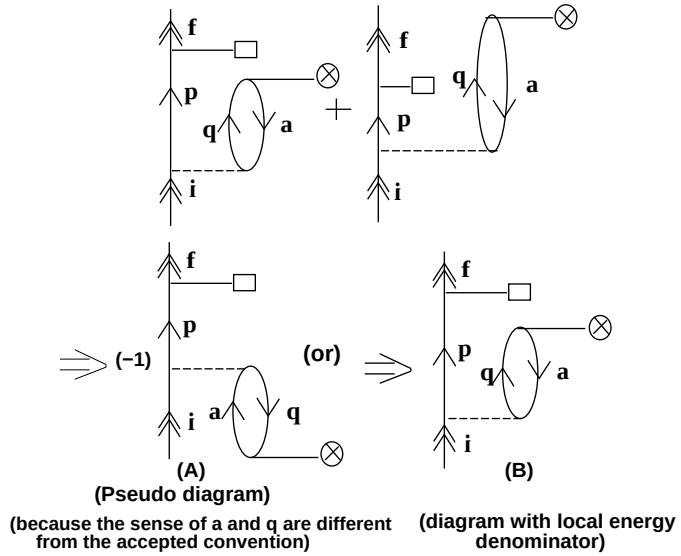

Figure 4.7: Pseudo diagram (or) diagram with local energy denominator got by adding the MBPT(6) and MBPT(16) diagrams.

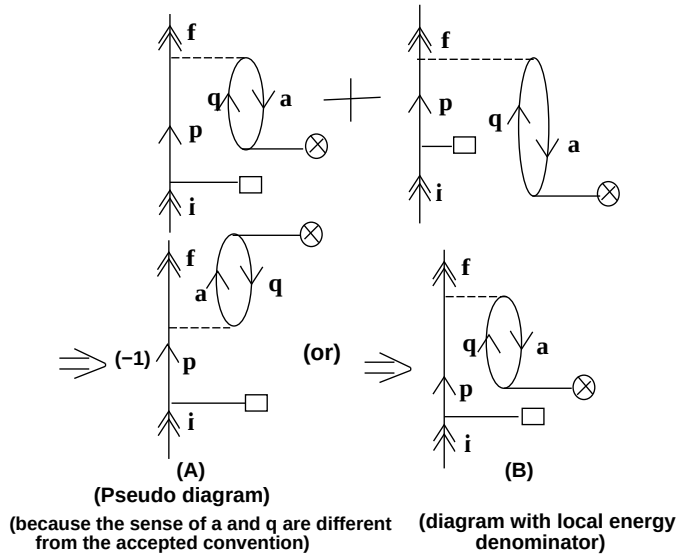

Figure 4.8: Pseudo diagram (or) diagram with local energy denominator got by adding the MBPT(10) and MBPT(12) diagrams.

first ordered perturbed terms. Mathematically, we can interpret CPHF to have got by considering PNC as the perturbation and Dipole as an operator connecting states of same parity. In the next section we consider RPA effect, where the application of an electric field on the system perturbs the single-particle orbitals.

4.6 Random Phase Approximation

The influence by an external oscillating electric field on the single-particle orbitals of an atom can be obtained by solving the DF equation in an external electric field. This leads to coupled equation for the electric dipole perturbed functions. By taking PNC as an operator between these perturbed states gives rise to the electric dipole transition amplitude which we are interested in. In the lowest order, $E1PNC^{(1)}$ is given by

$$\begin{aligned} E1PNC^{(1)} &= \sum_I \frac{\langle f|D|I\rangle\langle I|H_{\rm PNC}|i\rangle}{(\epsilon_i-\epsilon_I)} + \sum_I \frac{\langle f|H_{\rm PNC}|I\rangle\langle I|D|i\rangle}{(\epsilon_f-\epsilon_I)} \\ &= \langle f^D|H_{\rm PNC}|i\rangle + \langle f|H_{\rm PNC}|i^D\rangle, \end{aligned} \tag{4.64}$$

where we have defined

$$|f^D\rangle = \sum_I \frac{|I\rangle\langle I|D|f\rangle}{(\epsilon_i-\epsilon_I)} \tag{4.65}$$

and

$$|i^D\rangle = \sum_I \frac{|I\rangle\langle I|D|i\rangle}{(\epsilon_f-\epsilon_I)}. \tag{4.66}$$

To avoid the explicit summation in the above two equations over an infinite number of states, we use the inhomogeneous differential equation technique first introduced by Sternheimer for hyperfine structure calculations [18]. Multiply Eq. 4.65 and Eq. 4.66 by $(\epsilon_i - h^0)$ and $(\epsilon_f - h^0)$ on both sides, we get

$$\begin{aligned} (\epsilon_i-h^0)|f^D\rangle &= \sum_I \frac{(\epsilon_i-h^0)|I\rangle\langle I|D|f\rangle}{(\epsilon_i-\epsilon_I)} \\ &= \sum_I |I\rangle\langle I|D|f\rangle \end{aligned} \tag{4.67}$$

and

$$\begin{aligned} (\epsilon_f-h^0)|i^D\rangle &= \sum_I \frac{(\epsilon_f-h^0)|I\rangle\langle I|D|i\rangle}{(\epsilon_f-\epsilon_I)} \\ &= \sum_I |I\rangle\langle I|D|i\rangle, \end{aligned} \tag{4.68}$$

where h^0 is the unperturbed Hamiltonian which acts on any general state to give

$$h^0|I\rangle = \epsilon_I|I\rangle. \tag{4.69}$$

By making use of the closure relation and removing the infinite summation over I, both the equations take the form

$$\begin{aligned}(\epsilon_f - \omega - h^0)|f^-\rangle &= D|f\rangle \\ (\epsilon_i + \omega - h^0)|i^+\rangle &= D|i\rangle,\end{aligned} \tag{4.70}$$

where we have used $\omega = \epsilon_f - \epsilon_i$ which is the transition frequency between final and initial state. From now onwards we define the perturbed function with a superscript $+/-$ with respect to the sign of ω. Let us consider a general orbital denoted as i. Taking the orbital modifications into account in the DF potential denoted as $v^{\pm}$, we get the modified working equation as

$$(\epsilon_i \pm \omega - h^0)|i^{\pm}\rangle = D|i\rangle + v^{\pm}|i\rangle, \tag{4.71}$$

where

$$v^{\pm}|i\rangle = \sum_b \left[\langle b|v|b^{\pm}\rangle|i\rangle - \langle b|v|i\rangle|b^{\pm}\rangle + \langle b^{\mp}|v|b\rangle|i\rangle - \langle b^{\mp}|v|i\rangle|b\rangle\right]. \tag{4.72}$$

As we did for CPHF, we write the perturbed orbitals as the linear combination of unperturbed DF orbitals,

$$|i^{\pm}\rangle = \sum_p R^{\pm}_{pi}|p\rangle \tag{4.73}$$

and substituting this expression we get,

$$\begin{aligned}\sum_p(\epsilon_i \pm \omega - h^0)R^{\pm}_{pi}|p\rangle &= D|i\rangle + \sum_{bq}\{\langle b|v|q\rangle|i\rangle - \langle b|v|i\rangle q\rangle\}R^{\pm}_{qb} \\ &+ \sum_{bq} R^{-*}_{bq}\{\langle q|v|b\rangle|i\rangle - \langle q|v|i\rangle b\rangle\}.\end{aligned} \tag{4.74}$$

Let us take the $(+)$ index first and operate it by $\langle p|$ from the left side, we get

$$\begin{aligned}(\epsilon_i + \omega - \epsilon_p)R^{+}_{pi} &= \langle p|D|i\rangle + \sum_{bq}\{\langle pb|v|iq\rangle - \langle pb|v|qi\rangle\}R^{+}_{qb} \\ &+ \sum_{bq} R^{-*}_{qb}\{\langle pq|v|ib\rangle - \langle pq|v|bi\rangle\}.\end{aligned} \tag{4.75}$$

Using the result,

$$R^{\pm\star}_{qb} = R^{\pm}_{qb} \tag{4.76}$$

we can write the above equation with rearrangement as

$$(\epsilon_i+\omega-\epsilon_p)R^+_{pi}-\sum_{bq}\{\langle pb|v|iq\rangle-\langle pb|v|qi\rangle\}R^+_{qa}-\sum_{bq}R^-_{qb}\{\langle pq|v|ib\rangle-\langle pq|v|bi\rangle\}=\langle p|D|i\rangle. \tag{4.77}$$

The above linear equation can be solved in two steps. In the first step, we consider the general orbital i to be the core orbital designated as a. We get

$$(\epsilon_a+\omega-\epsilon_p)R^+_{pa}-\sum_{bq}\{\langle pb|v|aq\rangle-\langle pb|v|qa\rangle\}R^+_{qb}-\sum_{bq}R^-_{qb}\{\langle pq|v|ab\rangle-\langle pq|v|ba\rangle\}=\langle p|D|a\rangle. \tag{4.78}$$

We define

$$A_{pa,qb}=-\tilde{V}_{pb,aq}+\tilde{V}_{pq,ab}+(\epsilon_a+\omega-\epsilon_p)\delta_{pq}\delta_{ab} \tag{4.79}$$

and

$$B_{pa}=\langle p|D|a\rangle. \tag{4.80}$$

This leads to a linear equation of the form

$$AX=B, \tag{4.81}$$

which is solved to self-consistency. Similarly, one solves for R^-_{pa} using the linear equation

$$(\epsilon_a-\omega-\epsilon_p)R^-_{pa}-\sum_{bq}\{\langle pb|v|aq\rangle-\langle pb|v|qa\rangle\}R^-_{qb}-\sum_{bq}R^+_{qb}\{\langle pq|v|ab\rangle-\langle pq|v|ba\rangle\}=\langle p|D|a\rangle. \tag{4.82}$$

Once the amplitudes for the excitation from core to virtual orbitals designated as R^+_{qb} and R^-_{qb} are obtained, we can get the amplitudes for the excitation from valence to virtual orbital by their substitution on Eq. 4.64 which leads to

$$E1PNC=\langle f|H_{\rm PNC}|p\rangle R^+_{pi}+R^{-\star}_{pf}\langle p|H_{\rm PNC}|i\rangle, \tag{4.83}$$

where

$$\begin{aligned} R^+_{pi} &= \frac{\langle p|D|i\rangle}{(\epsilon_i+\omega-\epsilon_p)}+\sum_{bq}\frac{(\langle pb|v|iq\rangle-\langle pb|v|qi\rangle)R^+_{qb}}{(\epsilon_i+\omega-\epsilon_p)} \\ &+ \sum_{bq}\frac{(\langle pq|v|ib\rangle-\langle pq|v|bi\rangle)R^{-\star}_{qb}}{(\epsilon_i+\omega-\epsilon_p)}, \end{aligned} \tag{4.84}$$

$$\begin{aligned} R^-_{pf} &= \frac{\langle p|D|f\rangle}{(\epsilon_f-\omega-\epsilon_p)}+\sum_{bq}\frac{(\langle pb|v|fq\rangle-\langle pb|v|qf\rangle)R^-_{qb}}{(\epsilon_f-\omega-\epsilon_p)} \\ &+ \sum_{bq}\frac{(\langle pq|v|fb\rangle-\langle pq|v|bf\rangle)R^{-\star}_{qb}}{(\epsilon_f-\omega-\epsilon_p)}. \end{aligned} \tag{4.85}$$

Since R's are computed self-consistently, it means that we have taken the effects represented by the Couloumb interaction to all order. We can get order-by-order equivalence for RPA at each iteration which in turn can be checked with the first-order MBPT for RPA diagrams. From the all order equation, we show below such an equivalence. We first assume that the residual Couloumb interaction is zero. Then Eq. 4.84 reduces to

$$R_{pi}^{\pm(0,1)} = \frac{\langle p|D|i\rangle}{(\epsilon_i \pm \omega - \epsilon_p)}, \tag{4.86}$$

where $R_{pi}^{+(x,y)}$ represents x orders of Couloumb and y orders of D. Using one order in D, the electric dipole transition amplitude takes the form

$$E1PNC^{(1)} = \langle f|H_{\rm PNC}|i^+\rangle + \langle f^-|H_{\rm PNC}|i\rangle. \tag{4.87}$$

Substituting the R's we get

$$E1PNC^{(1)} = \sum_p \frac{\langle f|H_{\rm PNC}|p\rangle\langle p|D|i\rangle}{(\epsilon_i + \omega - \epsilon_p)} + c.c. \tag{4.88}$$

Similarly taking the Couloumb term to be non-zero, we get

$$\begin{aligned} R_{pi}^{+(1,1)} &= \frac{\langle p|D|i\rangle}{(\epsilon_i + \omega - \epsilon_p)} + \sum_{aq} \frac{\langle pa|v|iq\rangle\langle q|D|a\rangle}{(\epsilon_i + \omega - \epsilon_p)(\epsilon_a + \omega - \epsilon_q)} \\ &+ \sum_{bq} \frac{\langle pq|v|ib\rangle\langle a|D|q\rangle}{(\epsilon_i + \omega - \epsilon_p)(\epsilon_a - \omega - \epsilon_q)}. \end{aligned} \tag{4.89}$$

On taking out a negative sign from the third term, we get

$$\begin{aligned} R_{pi}^{+(1,1)} &= \frac{\langle p|D|i\rangle}{(\epsilon_i - \omega - \epsilon_p)} + \sum_{aq} \frac{\langle pa|v|iq\rangle\langle a|D|b\rangle}{(\epsilon_i + \omega - \epsilon_p)(\epsilon_a + \omega - \epsilon_q)} \\ &- \sum_{aq} \frac{\langle pq|v|ia\rangle\langle a|D|q\rangle}{(\epsilon_i + \omega - \epsilon_p)(\epsilon_q + \omega - \epsilon_a)}. \end{aligned} \tag{4.90}$$

Using this, second-order electric dipole transition amplitude can be obtained as

$$\begin{aligned} E1PNC^{(2)} &= \sum_p \frac{\langle f|H_{\rm PNC}|p\rangle\langle p|D|i\rangle}{(\epsilon_i + \omega - \epsilon_p)} \\ &+ \sum_{paq} \frac{\langle f|H_{\rm PNC}|p\rangle\langle pa|v|iq\rangle\langle q|D|a\rangle}{(\epsilon_i + \omega - \epsilon_p)(\epsilon_a + \omega - \epsilon_q)} \\ &- \sum_{paq} \frac{\langle f|H_{\rm PNC}|p\rangle\langle pq|v|ia\rangle\langle a|D|q\rangle}{(\epsilon_i + \omega - \epsilon_p)(\epsilon_q + \omega - \epsilon_a)}. \end{aligned} \tag{4.91}$$

The first, second and its complex conjugate terms in the above equation in comparison with the MBPT diagrams are equivalent to diagrams designated as MBPT(1),

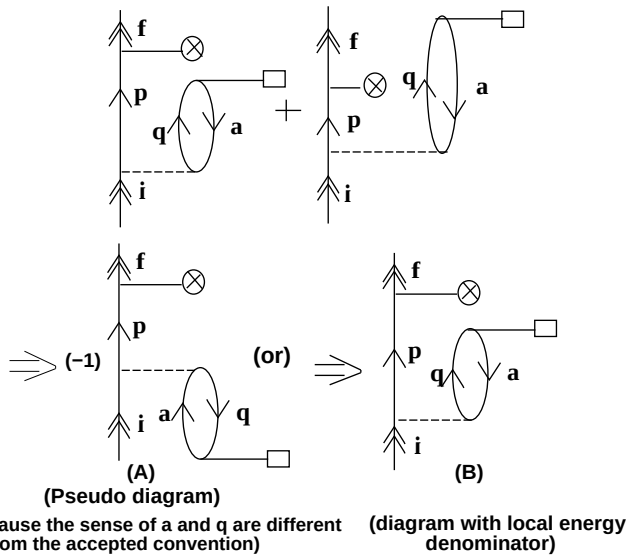

Figure 4.9: Pseudo diagram (or) diagram with local energy denominator got by adding the MBPT(7) and MBPT(15) diagrams.

MBPT(18) and its complex conjugate designated as MBPT(2) and MBPT(4). Third term in the above equation is obtained by adding MBPT diagrams designated as MBPT(7) and MBPT(15). The expression is given by

$$\begin{aligned} MBPT(7)+MBPT(15) &= \sum_{pqa}\frac{\langle f|H_{\rm PNC}p\rangle\langle pq|v|ia\rangle\langle a|D|q\rangle}{(\epsilon_i+\epsilon_a-\epsilon_p-\epsilon_q)(\epsilon_i+\epsilon_a-\epsilon_q-\epsilon_f)} \quad (4.92)\\ &+ \frac{\langle f|H_{\rm PNC}p\rangle\langle pq|v|ia\rangle\langle a|D|q\rangle}{(\epsilon_i+\epsilon_a-\epsilon_p-\epsilon_q)(\epsilon_f-\epsilon_p)}\\ &= \frac{\langle f|H_{\rm PNC}p\rangle\langle pq|v|ia\rangle\langle a|D|q\rangle}{(\epsilon_i+\epsilon_a-\epsilon_q-\epsilon_f)(\epsilon_f-\epsilon_p)}\\ &= (-)\frac{\langle f|H_{\rm PNC}p\rangle\langle pq|v|ia\rangle\langle a|D|q\rangle}{(\epsilon_i+\omega-\epsilon_p)(\epsilon_q+\omega-\epsilon_a)}, \end{aligned}$$

which is represented diagrammatically in Fig. 4.9. This can also be interpreted in the same way as we did for CPHF. In the case of pseudo diagrams the sense of the arrows are opposite to the Goldstone convention and in the case of local energy denominator again we deviate from the usual rules for energy expression. Similarly by adding MBPT(13) and MBPT(9) we get the conjugate terms which are illustrated in Fig. 4.10. Using this method, 4 RPA diagrams which totally adds up to 6 MBPT diagrams are taken to all order. In order to avoid double counting while computation the lowest order value is subtracted to get the RPA contribution. The rest correspond to CPHF-RPA diagrams which we explicitly do in the next section.

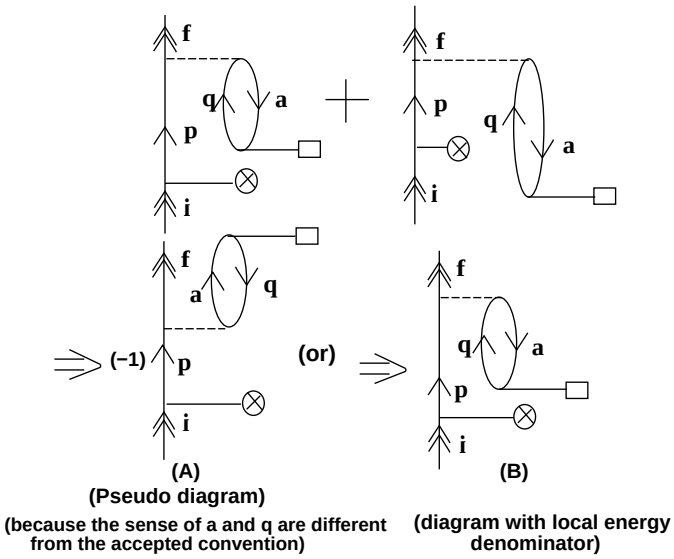

Figure 4.10: Pseudo diagram (or) diagram with local energy denominator got by adding the MBPT(13) and MBPT(9) diagrams.

4.7 CPHF-RPA: Double Perturbation

In this approach, we take dipole and PNC as the perturbation along with the Couloumb operator as compared to CPHF and RPA, where the PNC and dipole operators are considered as perturbation and operator and *vice versa*. The perturbations are denoted in terms of λ's and the total Hamiltonian is given by

$$H = h^0 + V_{es} + \lambda_1 D + \lambda_2 H_{\rm PNC}. \tag{4.93}$$

Due to these perturbations, the wave function and the DF potential gets perturbed and it takes the form

$$|i\rangle = \lambda_1 |i^{\pm}\rangle + \lambda_2 |i^{\rm PNC}\rangle + \lambda_1\lambda_2 |i^{\pm{\rm PNC}}\rangle, \tag{4.94}$$

$$v = V_{es} + \lambda_1 v^{\pm} + \lambda_2 v^{\rm PNC} + \lambda_1\lambda_2 v^{\pm{\rm PNC}}. \tag{4.95}$$

When we consider PNC and Couloumb operator as the perturbation, we get the coupled equation as

$$(\epsilon_i - h^0)|i^{\rm PNC}\rangle = (H_{\rm PNC} + v^{\rm PNC})|i^0\rangle, \tag{4.96}$$

which is nothing but the CPHF equation which we solved in the previous section. With D and Couloumb operator as perturbation, we get RPA equation given by

$$(\epsilon_i \pm -h^0)|i^{\pm}\rangle = (D + v^{\pm})|i^0\rangle. \tag{4.97}$$

Considering both D and PNC as perturbation along with Couloumb operator leads to an equation given by

$$(\epsilon_i \pm \omega - h^0)|i^{\pm}\rangle = (H_{\rm PNC} + v^{\rm PNC})|i^{\pm}\rangle + (D + v^{\pm})|i^{\rm PNC}\rangle + v^{\pm{\rm PNC}}|i\rangle, \tag{4.98}$$

where

$$\begin{aligned} v^{\pm{\rm PNC}}|i\rangle &= \sum_b \Big[\langle b^{\mp}|v|b^{\rm PNC}\rangle|i\rangle + \langle b^{\rm PNC}|v|b^{\pm}\rangle|i\rangle \\ &+ \langle b|v|b^{\pm{\rm PNC}}\rangle|i\rangle + \langle b^{\mp{\rm PNC}}|v|b\rangle|i\rangle \\ &- \langle b^{\mp}|v|i\rangle|b^{\rm PNC}\rangle - \langle b^{\rm PNC}v|i\rangle|b^{\pm}\rangle \\ &- \langle|b|v|i\rangle|b^{\pm{\rm PNC}}\rangle - \langle b^{\mp{\rm PNC}}|v|i\rangle|b\rangle\Big]. \end{aligned} \tag{4.99}$$

To solve Eq. 4.98 we need $|i^{\pm{\rm PNC}}\rangle$, $|i^{\pm}\rangle$ and $|i^{\rm PNC}\rangle$ which can be expanded as

$$\begin{aligned} |i^{\pm{\rm PNC}}\rangle &= \sum_p C_{pi}^{\pm{\rm PNC}}|p\rangle, \\ |i^{\pm}\rangle &= \sum_q C_{qi}^{\pm}|q\rangle, \\ |i^{\rm PNC}\rangle &= \sum_r C_{ri}^{\rm PNC}|r\rangle. \end{aligned}$$

Substituting them we get

$$\begin{aligned} \sum_p(\epsilon_i \pm \omega - h_0)C_{pi}^{\pm{\rm PNC}}|p\rangle &= (H^{\rm PNC} + v^{\rm PNC})\sum_q C_{qa}^{pm}|q\rangle \\ &+ (D + v^{\pm})\sum_r C_{ri}^{\rm PNC}|r\rangle + v^{\pm{\rm PNC}}|i\rangle. \end{aligned} \tag{4.100}$$

Scalar multiplication by $\langle p|$, we get

$$\begin{aligned} (\epsilon_i \pm \omega - \epsilon_p)C_{pi}^{\pm{\rm PNC}} &= \sum_q\langle p|(H^{\rm PNC} + v^{\rm PNC})|q\rangle C_{qi}^{\pm} \\ &+ \sum_r\langle p|(D + v^{\pm})|r\rangle C_{ri}^{\rm PNC} + \langle p|v^{\pm{\rm PNC}}|i\rangle. \end{aligned} \tag{4.101}$$

The above equation can be rewritten as

$$(\epsilon_i \pm \omega - \epsilon_p)C_{pi}^{\pm{\rm PNC}} = X^{\pm} + \langle p|v^{\pm{\rm PNC}}|i\rangle, \tag{4.102}$$

where

$$X^{\pm} = \sum_q\langle p|(H_{\rm PNC} + v^{\rm PNC})|q\rangle C_{qi}^{\pm} + \sum_r\langle p|(D + v^{\pm})|r\rangle C_{ri}^{\rm PNC}. \tag{4.103}$$

Using the expansions for the perturbed functions, Eq. 4.101 takes the form

$$\begin{aligned}(\epsilon_i \pm \omega - \epsilon_p)C_{pi}^{\pm\mathrm{PNC}} &= X^{\pm} + \sum_{bqs}\Big[\{\langle ps|v|iq\rangle - \langle ps|v|qi\rangle\}C_{sb}^{\mp\star}C_{qb}^{\mathrm{PNC}} \\ &+ \{\langle pq|v|is\rangle - \langle pq|v|si\rangle\}C_{qb}^{\star\mathrm{PNC}}C_{sb}^{\pm} \\ &+ \{\langle pb|v|ri\rangle - \langle pb|v|ir\rangle\}C_{rb}^{\pm\mathrm{PNC}} \\ &+ \{\langle pr|v|bi\rangle - \langle pr|v|ib\rangle\}C_{rb}^{\mp\mathrm{PNC}\star}\Big]. \end{aligned} \tag{4.104}$$

Since CPHF and RPA equations are solved, we know the solutions $|i^{\mathrm{PNC}}\rangle$ and $|i^{\pm}\rangle$. Using the properties of the solutions we can write the above equation as

$$\begin{aligned}(\epsilon_i \pm \omega - \epsilon_p)C_{pi}^{\pm\mathrm{PNC}} &= X^{\pm} + \sum_{bqs}\Big[\{\langle ps|v|iq\rangle - \langle ps|v|qi\rangle\}C_{sb}^{\mp}C_{qb}^{\mathrm{PNC}} \\ &- \{\langle pq|v|is\rangle - \langle pq|v|si\rangle\}C_{qb}^{\mathrm{PNC}}C_{sb}^{\pm} \\ &+ \{\langle pb|v|ri\rangle - \langle pb|v|ir\rangle\}C_{rb}^{\pm\mathrm{PNC}} \\ &- \{\langle pr|v|bi\rangle - \langle pr|v|ib\rangle\}C_{rb}^{\mp\mathrm{PNC}}, \end{aligned} \tag{4.105}$$

where we have used $C_{rb}^{\star\mathrm{PNC}} = -C_{rb}^{\mathrm{PNC}}$, $C_{rb}^{\pm\star} = C_{rb}^{\pm}$ and $C_{rb}^{\star\pm\mathrm{PNC}} = -C_{rb}^{\pm\mathrm{PNC}}$. The above equation can be written as a linear equation and can be solved for the C's which can be used in the determination of $E1PNC$. One can get the contribution for $E1PNC$ using the perturbed potential taken between the initial and final states as given by

$$E1PNC = \langle f|d + v^{+}|i^{\mathrm{PNC}}\rangle + \langle f|H_{\mathrm{PNC}} + v^{\mathrm{PNC}}|i^{+}\rangle + \langle f|v^{+\mathrm{PNC}}|i\rangle. \tag{4.106}$$

Here the first and second terms gives the RPA and the CPHF contribution with the third term contributing to double perturbation which relates to PNC shielding. Below we show that from the term $\langle f|v^{+\mathrm{PNC}}|i\rangle$ we get CPHF-RPA terms. Expanding the potential we get

$$\langle f|v^{\pm\mathrm{PNC}}|i\rangle = \sum_{b}\Big\{\langle fb^{\mp}|v|ib^{\mathrm{PNC}}\rangle + \langle fb^{\mathrm{PNC}}|v|ib^{\pm}\rangle + \langle fb|v|ib^{\pm\mathrm{PNC}}\rangle + \langle fb^{\mp\mathrm{PNC}}|v|ib\rangle\Big\}. \tag{4.107}$$

Substituting for $|b^{\mathrm{PNC}}\rangle$, $|b^{\pm}\rangle$ and $|b^{\pm\mathrm{PNC}}\rangle$ as

$$\begin{aligned}|b^{\mathrm{PNC}}\rangle &= \sum_{q} A_{qb}^{\mathrm{PNC}}|q\rangle \\ |b^{\pm}\rangle &= \sum_{s} A_{sb}^{\pm}|s\rangle \\ |b^{\pm\mathrm{PNC}}\rangle &= \sum_{r} A_{rb}^{\pm\mathrm{PNC}}|r\rangle, \end{aligned} \tag{4.108}$$

we get

$$\begin{aligned}\langle f|v^{\pm\mathrm{PNC}}|i\rangle &= \sum_{sbq}\Big[\langle fs|v|iq\rangle A_{sb}^{\star\mp}A_{qb}^{\mathrm{PNC}} + \langle fq|v|is\rangle A_{qb}^{\star\mathrm{PNC}}A_{sb}^{\pm} \\ &+ \langle fb|v|ir\rangle A_{rb}^{\pm\mathrm{PNC}} + \langle fr|v|ib\rangle A_{rb}^{\star\pm\mathrm{PNC}}\Big]. \end{aligned}$$

The zeroth-order coefficients can be got by taking appropriate approximations in the CPHF, RPA and CPHF-RPA equations. From the CPHF equation by neglecting the v terms we get

$$A_{qb}^{\mathrm{PNC}} = \frac{\langle q|H_{\mathrm{PNC}}|b\rangle}{\epsilon_b - \epsilon_q)}. \tag{4.109}$$

From the RPA equation, by neglecting the v terms we get

$$A_{sb}^{\pm} = \frac{\langle s|D|b\rangle}{(\epsilon_b \pm -\epsilon_s)}. \tag{4.110}$$

From the CPHF-RPA equation, by neglecting the v terms we get

$$A_{rb}^{\pm\mathrm{PNC}} = \sum_q \frac{\langle r|H_{\mathrm{PNC}}|q\rangle\langle q|D|b\rangle}{(\epsilon_b \pm \omega - \epsilon_r)(\epsilon_b \pm \omega - \epsilon_q)} + \sum_q \frac{\langle r|D|q\rangle\langle q|H_{\mathrm{PNC}}|b\rangle}{(\epsilon_b pm\omega - \epsilon_r)(\epsilon_b - \epsilon_q)}. \tag{4.111}$$

Expanding the coefficients for + we get

$$\begin{aligned}
\langle f|v^{+\mathrm{PNC}}|i\rangle &= \sum_{sbq} \frac{\langle fs|v|iq\rangle\langle b|d|s\rangle\langle q|\mathrm{PNC}|b\rangle}{(\epsilon_b - \omega - \epsilon_s)(\epsilon_b - \epsilon_q)} \\
&+ \sum_{sbq} \frac{\langle fq|v|is\rangle\langle s|d|b\rangle\langle b|\mathrm{PNC}|q\rangle}{(\epsilon_b + \omega - \epsilon_s)(\epsilon_b - \epsilon_q)} \\
&+ \sum_{sbq} \frac{\langle fb|v|is\rangle\langle s|H_{\mathrm{PNC}}|q\rangle\langle q|D|b\rangle}{(\epsilon_b \pm \omega - \epsilon_s)(\epsilon_b \pm \omega - \epsilon_q)} \\
&+ \sum_{sbq} \frac{\langle fb|v|is\rangle\langle s|D|q\rangle\langle q|H_{\mathrm{PNC}}|b\rangle}{(\epsilon_b \pm \omega - \epsilon_s)(\epsilon_b - \epsilon_q)} \\
&- \sum_{sbq} \frac{\langle fs|v|ib\rangle\langle s|H_{\mathrm{PNC}}|q\rangle\langle q|D|b\rangle}{(\epsilon_b \mp \omega - \epsilon_s)(\epsilon_b \mp \omega - \epsilon_q)} \\
&- \sum_{sbq} \frac{\langle fs|v|ib\rangle\langle s|D|q\rangle\langle q|H_{\mathrm{PNC}}|b\rangle}{(\epsilon_b \mp \omega - \epsilon_s)(\epsilon_b - \epsilon_q)}.
\end{aligned} \tag{4.112}$$

Taking the negative sign inside and rearranging the PNC matrix element and the dipole we get

$$\begin{aligned}
\langle f|v^{+\mathrm{PNC}}|i\rangle &= \sum_{sbq} \frac{\langle fs|v|iq\rangle\langle b|d|s\rangle\langle q|\mathrm{PNC}|b\rangle}{(\epsilon_b - \omega - \epsilon_s)(\epsilon_b - \epsilon_q)} \\
&+ \sum_{sbq} \frac{\langle fq|v|is\rangle\langle s|d|b\rangle\langle b|\mathrm{PNC}|q\rangle}{(\epsilon_b + \omega - \epsilon_s)(\epsilon_b - \epsilon_q)} \\
&+ \sum_{sbq} \frac{\langle fb|v|is\rangle\langle s|H_{\mathrm{PNC}}|q\rangle\langle q|D|b\rangle}{(\epsilon_b \pm \omega - \epsilon_s)(\epsilon_b \pm \omega - \epsilon_q)} \\
&+ \sum_{sbq} \frac{\langle fb|v|is\rangle\langle s|D|q\rangle\langle q|H_{\mathrm{PNC}}|b\rangle}{(\epsilon_b \pm \omega - \epsilon_s)(\epsilon_b - \epsilon_q)}
\end{aligned} \tag{4.113}$$

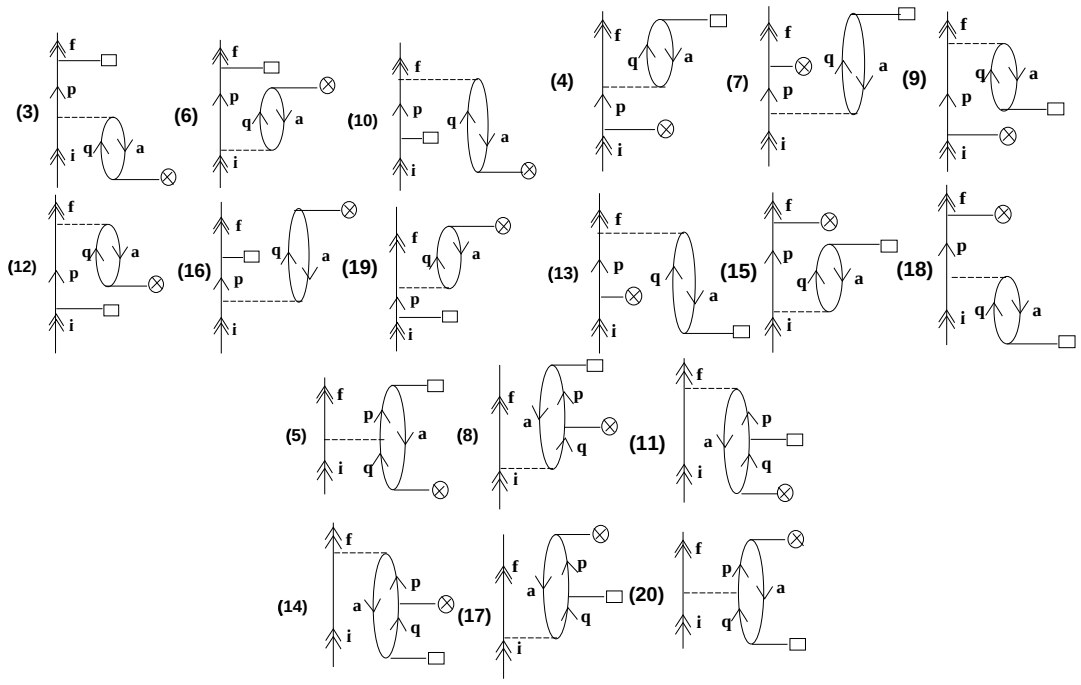

Figure 4.11: MBPT diagrams contributing to CPHF (a), RPA (b) and CPHF-RPA (c).

$$+ \sum_{sbq} \frac{\langle fs|v|ib\rangle\langle q|H_{\rm PNC}|s\rangle\langle b|D|q\rangle}{(\epsilon_b \mp \omega - \epsilon_s)(\epsilon_b \mp \omega - \epsilon_q)}$$
$$+ \sum_{sbq} \frac{\langle fs|v|ib\rangle\langle q|D|s\rangle\langle b|H_{\rm PNC}|q\rangle}{(\epsilon_b \mp \omega - \epsilon_s)(\epsilon_b - \epsilon_q)}.$$

Comparing the above terms with the first-order MBPT diagrams, it can be found out that in the order given above these terms are equivalent to MBPT(5), MBPT(20), MBPT(14), MBPT(11), MBPT(8) and MBPT(17).

From the above analysis of the zeroth and first-order MBPT diagrams it is clear that the diagrams can be classified according to different effects and they can be taken to all orders by summing each respective groups of diagrams. In Fig. 4.11, all the MBPT diagrams contributing to each effect are drawn separately. Zeroth-order contribution will be present in each group and hence only the respective diagram related to each approximation is given. During computation, zeroth-order contribution is taken once and subtracted from all other effects in order to avoid double counting.

In the next section we discuss few of the third-order MBPT diagrams which contribute to $E1PNC$.

4.8 Evaluation of $E1PNC^{(3)}$ Terms

Contributions to this order can be got in a similar way in which the second-order contributions were found. In the previous section the second-order diagrams considered can be regarded as a first-order modification of the core orbitals, and is therefore referred to as the first-order core polarisation diagrams. Generally, core polarisation is defined as the perturbations which in each order can be described by means of single excitations from the core. The remaining effects which involve at least one multiple excitation will be referred to as pure correlation effects. So we consider only the pure correlation diagrams which have one order in dipole, PNC and two orders of Couloumb which involve at least one double excitation.

Diagrams contributing to pair correlation effects are categorised in two classes and are drawn in Fig. 4.12 and Fig. 4.13. The exchange counterparts for the above categories are not drawn but for computation both direct and exchange terms are considered.

To reduce the time taken for computing each of the pair correlation diagrams we define a function called pair function which is computed first and stored in fast memory, which can then be used for the computation of both direct and the exchange matrix elements. Let us consider the diagram where the PNC and Couloumb operator are acting as perturbation to the initial state. The expression for the direct diagram can be written as

$$P_1^{dir} = \sum_{srapq} \frac{\langle f|D|s\rangle\langle s|H_{\rm PNC}|r\rangle\langle ra|v|pq\rangle\langle pq|v|ia\rangle}{(\epsilon_i-\epsilon_s)(\epsilon_i-\epsilon_r)(\epsilon_i+\epsilon_a-\epsilon_p-\epsilon_q)}. \tag{4.114}$$

Define

$$\rho^{dir}(i,a) = \sum_{pq} \frac{|pq\rangle\langle pq|v|ia\rangle}{((\epsilon_i+\epsilon_a-\epsilon_p-\epsilon_q)}. \tag{4.115}$$

Substituting the pair function $\rho(i,a)$ defined in Eq. 4.115 in the direct diagram, we get

$$P_1^{dir} = \sum_{asr} \frac{\langle f|D|s\rangle\langle s|H_{\rm PNC}|r\rangle \sum_{pq}\langle ra|v|pq\rangle C_{ia}^{pq}}{(\epsilon_i-\epsilon_s)(\epsilon_i-\epsilon_r)}. \tag{4.116}$$

The pair function $\rho(i,a)$ can also be used for the exchange counterpart of the above direct diagram which is illustrated below. The expression for the exchange diagram is

$$P_1^{exc} = \sum_{srqpq} \frac{\langle f|D|s\rangle\langle s|H_{\rm PNC}|r\rangle\langle ra|v|qp\rangle\langle qp|v|ai\rangle}{(\epsilon_i-\epsilon_s)(\epsilon_i-\epsilon_r)(\epsilon_i+\epsilon_a-\epsilon_p-\epsilon_q)}. \tag{4.117}$$

Define

$$\rho^{exc}(i,a) = \sum_{pq} \frac{|qp\rangle\langle qp|v|ai\rangle}{((\epsilon_i+\epsilon_a-\epsilon_p-\epsilon_q)}. \tag{4.118}$$

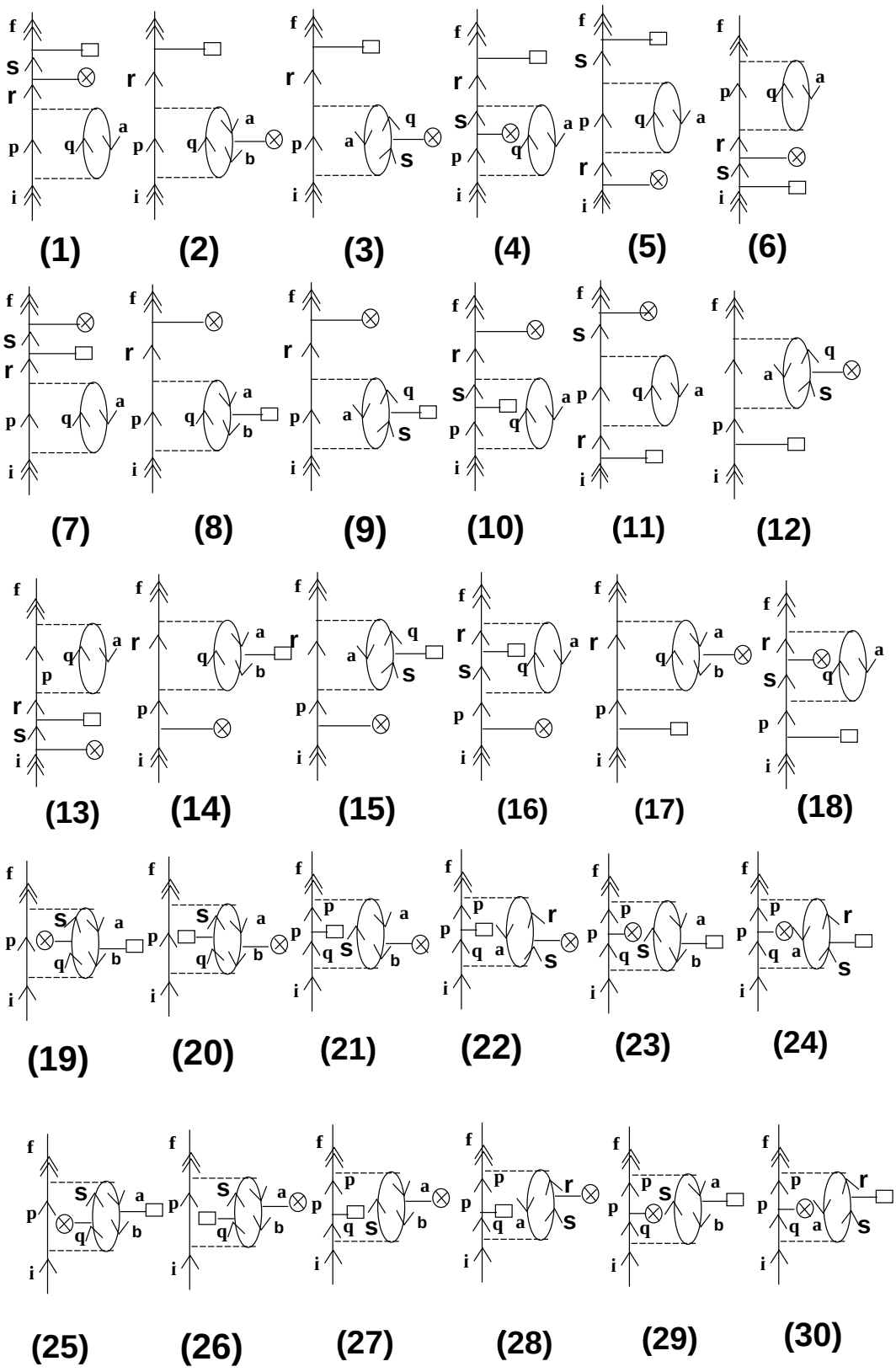

Figure 4.12: MBPT diagrams contributing to Pair Correlation effects (Class I).

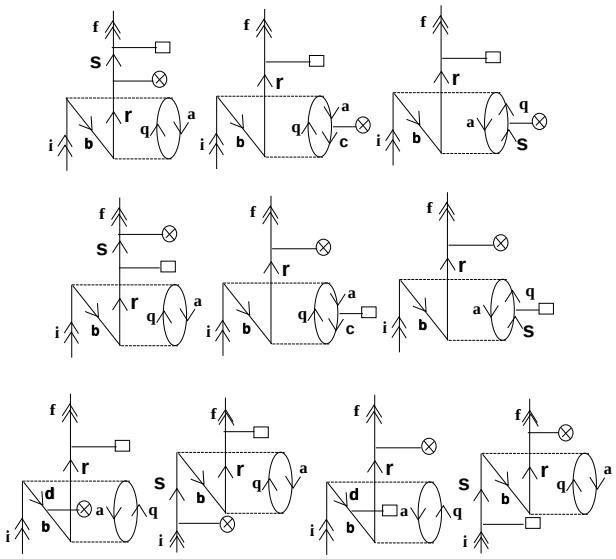

Figure 4.13: Typical MBPT diagrams contributing to Pair Correlation effects (Class II).

Substituting the pair function $\rho(i,a)$ in the exchange diagram and using the symmetry conditions for Couloumb operator given by

$$\langle qp|v|ai\rangle = \langle pq|v|ia\rangle,$$

we get

$$P_1^{exc} = \sum_{asr} \frac{\langle f|D|s\rangle\langle s|H_{\rm PNC}|r\rangle \sum_{pq}\langle ra|v|qp\rangle C_{ia}^{pq}}{(\epsilon_i-\epsilon_s)(\epsilon_i-\epsilon_r)}. \tag{4.119}$$

In our case the initial state i is fixed and the orbital a runs over all the core orbitals. So for the computation of the pair correlation diagram given in Fig. 4.12, we need to compute the pair function $\rho(i,a)$. By examining the diagrams given in Fig. 4.12, we can see that diagrams numbered (1), (2), (3), (4), (7), (8), (9), (10) can be got by computing $\rho(i,a)$ first and then using it to compute both the direct and exchange counterpart expressions. These pair functions for fixed i and a are first computed and stored in a file. This reduces the time taken for the calculation of complete pair correlation diagrams tremendously. The expressions for the diagrams which can be computed using $\rho(i,a)$ are

$$P_1 = \sum_{srapq} \frac{\langle f|D|s\rangle\langle s|H_{\rm PNC}|r\rangle[\langle ra|v|pq\rangle - \langle ra|v|qp\rangle]C_{ia}^{pq}}{(\epsilon_i-\epsilon_s)(\epsilon_i-\epsilon_r)}, \tag{4.120}$$

$$P_2 = \sum_{abspq} \frac{\langle f|D|s\rangle\langle a|H_{\rm PNC}|b\rangle[\langle sb|v|pq\rangle - \langle sb|v|qp\rangle]C_{ia}^{pq}}{(\epsilon_i-\epsilon_s)(\epsilon_i+\epsilon_b-\epsilon_p-\epsilon_q)},$$

$$P_3 = \sum_{arspq} \frac{\langle f|D|r\rangle\langle s|H_{\rm PNC}|q\rangle[\langle ra|v|ps\rangle - \langle ra|v|sp\rangle]C_{ia}^{pq}}{(\epsilon_i - \epsilon_r)(\epsilon_i + \epsilon_a - \epsilon_s - \epsilon_p)},$$

$$P_4 = \sum_{arspq} \frac{\langle f|D|s\rangle\langle r|H_{\rm PNC}|p\rangle[\langle sa|v|rq\rangle - \langle sa|v|qr\rangle]C_{ia}^{pq}}{(\epsilon_i - \epsilon_s)(\epsilon_i + \epsilon_a - \epsilon_r - \epsilon_q)},$$

$$P_7 = \sum_{arspq} \frac{\langle f|H_{\rm PNC}|s\rangle\langle s|D|r\rangle[\langle ra|v|pq\rangle - \langle ra|v|qp\rangle]C_{ia}^{pq}}{(\epsilon_i - \epsilon_r)(\epsilon_i - \epsilon_s)},$$

$$P_8 = \sum_{abrpq} \frac{\langle f|H_{\rm PNC}|r\rangle\langle a|D|b\rangle[\langle rb|v|pq\rangle - \langle rb|v|qp\rangle]C_{ia}^{pq}}{(\epsilon_f - \epsilon_r)(\epsilon_f + \epsilon_b - \epsilon_p - \epsilon_q)},$$

$$P_9 = \sum_{arspq} \frac{\langle f|H_{\rm PNC}|r\rangle\langle s|D|q\rangle[\langle ra|v|ps\rangle - \langle ra|v|sp\rangle]C_{ia}^{pq}}{(\epsilon_f - \epsilon_r)(\epsilon_f + \epsilon_a - \epsilon_p - \epsilon_s)},$$

$$P_{10} = \sum_{arspq} \frac{\langle f|H_{\rm PNC}|r\rangle\langle s|D|p\rangle[\langle ra|v|sq\rangle - \langle ra|v|qs\rangle]C_{ia}^{pq}}{(\epsilon_i - \epsilon_r)(\epsilon_f + \epsilon_b - \epsilon_s - \epsilon_q)},$$

where

$$C_{ia}^{pq} = \frac{\langle pq|v|ia\rangle}{(\epsilon_i + \epsilon_a - \epsilon_p - \epsilon_q)}. \tag{4.121}$$

Using similar arguments we can find that pair correlation diagrams (6), (12), (13), (14), (15), (16), (17) and (18) drawn in Fig. 4.12 can be computed by knowing $\rho(f,a)$ defined as

$$\rho(f,a) = \sum_{pq} \frac{|pq\rangle\langle pq|v|fa\rangle}{(\epsilon_f + \epsilon_a - \epsilon_p - \epsilon_q)}. \tag{4.122}$$

Examining Fig. 4.12 the diagram (5) in the similar way and writing down the direct matrix elements we get

$$P_5^{dir} = \sum_{srpqa} \frac{\langle f|D|s\rangle\langle r|H_{\rm PNC}|i\rangle\langle sa|v|pq\rangle\langle pq|v|ra\rangle}{(\epsilon_i - \epsilon_r)(\epsilon_i - \epsilon_s)(\epsilon_i + \epsilon_a - \epsilon_p - \epsilon_q)}. \tag{4.123}$$

Define

$$\rho^{dir}(\bar{i},a) = \sum_{pqr} \frac{|pq\rangle\langle pq|v|ra\rangle\langle r|H_{\rm PNC}|i\rangle}{((\epsilon_i + \epsilon_a - \epsilon_p - \epsilon_q)(\epsilon_i - \epsilon_r)}. \tag{4.124}$$

Substituting the pair function $\rho(\bar{i},a)$ in the exchange diagram and using the symmetry conditions for Couloumb operator given by

$$\langle qp|v|ar\rangle = \langle pq|v|ra\rangle,$$

we get

$$P_5^{exc} = \sum_{srpqa} \frac{\langle f|D|s\rangle\langle sa|v|qp\rangle C_{\bar{i}a}^{pq}}{(\epsilon_i - \epsilon_s)}. \tag{4.125}$$

Adding the direct and exchange counterparts we get

$$P_5 = \sum_{srpqa} \frac{\langle f|D|s\rangle[\langle sa|v|pq\rangle - \langle sa|v|qp\rangle]C_{\bar{i}a}^{pq}}{(\epsilon_i - \epsilon_s)}. \tag{4.126}$$

Similar to $\rho(\bar{i}, a)$ one can compute $\rho(\bar{f}, a)$ which can be stored in memory for the computation of diagram (11) (Fig. 4.12). Rest of the diagrams drawn in Fig. 4.12 require both the pair functions $\rho(i, a)$ and $\rho(f, a)$. The other class of diagrams in Fig. 4.13 can also be computed the same way by defining a particular kind of pair functions which are not taken for study in this thesis.

4.9 Computation of $E1PNC$

In this section, we give the results of the computation of electric dipole transition amplitude in Ba^+ ion using MBPT. In the previous chapter we used numerical bound orbitals as the single-particle basis for the computation of $E1PNC$ and for MBPT we use analytical bound and continuum orbitals got by solving DF equation using Finite Basis Set Expansion (FBSE) method [19]. Before going into the results and discussion related to Ba^+ $E1PNC$ we first discuss about the generation of the basis using FBSE method developed by our group. At the end of this section, we discuss about a new method of generation of the basis in which we combine the analytical orbitals with the numerical orbitals.

4.9.1 Relativistic Basis Generation for Atoms

Since we are dealing with large Z atoms, we consider Dirac Hamiltonian

$$H_D = \sum_i [c\alpha_i.p_i + (\beta_i - 1)c^2 - V_{nuc}(r_i)] + \sum_{i>j} \frac{e^2}{r_{ij}} \tag{4.127}$$

as the starting point for the self-consistent procedure where α_i and β_i are Dirac matrices, r_i and p_i are respectively, the position with respect to the nucleus and momentum vectors of the i^{th} electron. r_{ij} represents the distance between electrons i and j. Since wave function and energy cannot be solved exactly, we take the perturbation procedure in which one starts with the eigenfunction Φ_0 of an approximate Hamiltonian H_0 satisfying the equation

$$H_0\Phi_0 = E_0\Phi_0. \tag{4.128}$$

For the zeroth-order Hamiltonian H_0, V^{N-1} approximation has been found to be most convenient for the study of atomic properties. The relativistic form of H_0 in this approximation is given by

$$H_0 = \sum_i [c\alpha_i.p_i + (\beta_i - 1)c^2 - V_{nuc}(r_i) + V_i^{(N-1)}]. \tag{4.129}$$

The matrix element of the V^{N-1} potential over single-particle states is given by

$$\langle i|V^{N-1}|j\rangle = \sum_{a=1}^{N-1}\{\langle ia|\frac{1}{r_{12}}|ja\rangle - \langle ia|\frac{1}{r_{12}}|aj\rangle\}, \tag{4.130}$$

where the summation over a being taken over all the occupied states of the atom except the valence orbital. In the case of singly ionised barium $6s$ is the valence orbital and all other orbitals below it are considered core orbitals. This is equivalent to considering Ba^{++} as the starting potential of our calculation. For the construction of unperturbed and perturbed many electron states for the evaluation of MBPT matrix elements, one needs to obtain the complete set of one-electron states which are the solutions of the one-electron Dirac equation. The form of the single-particle orbitals ϕ_n and the related details are explained in the previous chapter.

4.9.1.1 Numerical Basis Functions

The DF equation is solved numerically using the GRASP DF code [20]. The single-particle wave functions and the respective energies of the core and the virtual orbitals can be generated by doing a step by step procedure as given below with reference to singly ionised barium. The core orbitals are first generated by considering a potential from $|1s^22s^2.....5p^6\rangle$. This is then kept fixed and the valence orbital $6s$ is obtained by considering a configuration $|1s^22s^2.....5p^66s\rangle$, and virtual orbitals nr's are obtained by replacing the valence orbital by the i^{th} orbital resulting in a configuration $|1s^22s^2.....5p^6nr\rangle$ where n is the principal quantum number and r is the azimuthal quantum number. Hence the core, valence and the virtual orbitals see a potential from all the core electrons uniformly. Since the boundary conditions allows one to get only bound orbitals from GRASP [20], we get a very good description of core and virtual numerical bound orbitals defined on a grid. But for some atoms it has been found out that there is a convergence problem when we solve the above equation for high lying orbitals. Since any basis is not complete without the continuum, the above method of generation of the basis should be supplemented by another method where one can solve for both bound and continuum orbitals. For getting both bound and continuum orbitals we have used the FBSE method [19] which is described below.

4.9.1.2 Analytical Basis Functions

The DF equation in this case is solved through a pseudo eigenvalue [19] approach where basis functions are defined on grid and one- and two-electron radial integrals are evaluated numerically. Like the traditional analytical basis set expansion approach,

the large and small components of the radial wave functions are expressed as linear combinations of basis functions, *i.e.*,

$$P_{n\kappa}(r) = \sum_p C^L_{\kappa p} g^L_{\kappa p}(r) \tag{4.131}$$

and

$$Q_{n\kappa}(r) = \sum_p C^S_{\kappa p} g^S_{\kappa p}(r), \tag{4.132}$$

where the summation index p runs over the number of basis function N, $g^L_{\kappa p}(r)$ and $g^S_{\kappa p}(r)$ are basis functions belonging to the large and small components, respectively, and $C^L_{\kappa p}$ and $C^S_{\kappa p}$ are the corresponding expansion coefficients. Though any basis functions can be used, here Gaussian-Type Orbitals (GTOs) that have the following form for the large component is used:

$$g_{\kappa p^L(r)} = N^L_p r^{n_\kappa} e^{-\alpha_p r^2} \tag{4.133}$$

with

$$\alpha_p = \alpha_0 \beta^{p-1}, \tag{4.134}$$

where α_0, β are user defined constants, n_κ specifies the orbital symmetry (1 for s, 2 for p, etc.,) and N^L_p is the normalisation factor for the large component. The small component part of the basis function is obtained by imposing the kinetic balance and has the form

$$g^S_{\kappa p}(r) = N^S_p (\frac{d}{dr} + \frac{\kappa}{r}) g^L_{\kappa p}(r), \tag{4.135}$$

where

$$N^S_p = \sqrt{\frac{\alpha_p}{2n_\kappa - 1}\,[4(\kappa^2 + \kappa + n_\kappa) - 1]}. \tag{4.136}$$

The kinetic balance condition allows us to use the same exponents for the large and small components which reduces the computational costs. To obtain a basis which is accurate at small and large radial distances one adjusts the parameters N, α_0 and β to get the bound orbitals as close to the numerical orbitals obtained previously. As a first-order check the convergence of analytical DF energy with the numerical DF energy for varying N, α and β is performed. But in order to check the validity of the wave functions one needs to check the accuracy of the radial distribution of the small and large components for each orbitals using these exponents. It should be noted that Mark [21] reported relativistic basis sets for H through Ne obtained by least-squares fitting to numerical DF wave functions. We have tried these checks to find out the accuracy of the wave functions at each of the grid points for singly ionised barium and calcium. This kind of exponent wherein we have the same α and

β for all symmetries is referred to be the Universal Basis (UB) generation as tried by various groups [22, 23]. We can consider two other categories, one in which we have same α and β for all the symmetries but with more parameters like γ and δ as given by

$$\alpha_p \;=\; \alpha_0\beta^{p-1}[1+\gamma(\frac{p}{N})^{\delta}]. \tag{4.137}$$

This leads to well tempered (WT) condition [24, 25]. In another approach one makes use of only two parameters just as in UB but different for different symmetry which is referred to as Even Tempered (ET) condition.Large basis sets can be efficiently generated by utilising the concept of an ET Gaussian basis set [26]. For the present calculation, we have made use of UB condition. By using numerical bound core orbitals [20] in this approach for the computation of the one and two electron integrals, the $N(N+1)/2$ operations are reduced to N_c operations where N is the number of basis and N_c is the number of core orbitals.

The numerical DF energy obtained from the GRASP code for Ca^+ is -679.5206070 Hartrees. The analytical DF energy got for $\alpha = 0.00725$ and $\beta = 2.73$ for a basis $30s25p25d20f$ is given by -679.1363561 Hartrees. The numerical and analytical bound single-particle energies for the particular basis set for which better convergence was obtained is tabulated in Table 4.1. The analytical continuum orbital energies are tabulated in Table 4.2. As a check for the wave functions at each grid point we have plotted the absolute difference between the numerical and analytical wave function for the large and small components for few of the orbitals from each symmetry. Examining the plots, one can come to a conclusion that for the particular parameter, the analytical wave functions near the nuclear region (small radial distances) shows better agreement with the numerical wave functions compared to the agreement at large radial distances for both large and small components of the wave function. Also the parameters for each symmetry is found to be giving different fits. Hence an even tempered condition with α and β different for each symmetry will be most appropriate for getting very good single-particle wave functions.

In this case, we adjusted the parameters like N, α and β for generating the basis. It is then checked with the single-particle orbital energies, radial matrix elements and also the overlap of the analytical and numerical wave functions.

Same checks were performed on the single-particle wave function for Ba^+ ion taking $\alpha = 0.00725$ and $\beta = 2.73$. With a basis $32s28p25d20f15g10h$ the analytical DF energy is found to be -8135.8883754 Hartrees as compared to the numerical DF energy obtained from GRASP as -8135.1429542 Hartrees. The bound and continuum single-particle energies of Ba^+ are given in Tables 4.3 and 4.4.

The comparisons of the wave functions at each grid points as shown in Figs. 4.14 and 4.15 shows very clearly that we need ET exponents to get basis matching at each

Table 4.1: Comparison of analytical and numerical single-particle orbital energies for Ca^+.

orbital	analytical	numerical	orbital	analytical	numerical
1s	−150.74645	−150.71745	3d⋆	−0.33109	−0.33087
2s	−17.52251	−17.51578	4d⋆	−0.16853	−0.16874
3s	−2.79829	−2.79675	...	...	...
4s	−0.41666	−0.41663	3d	−0.33098	−0.307596
...	...	...	4d	−0.16846	−0.168664
2p⋆	−14.28327	−14.28280	...	...	...
3p⋆	−1.88758	−1.87185	4f⋆	−0.125055	−0.12517
4p⋆	−0.30991	−0.30909	5f⋆	−0.07958	−0.08014
...	...	...	...	...	...
2p	−14.14477	−14.14362	4f	−0.1250552	−0.12518
3p	−1.87219	−1.87185	5f	−0.079580	−0.08014
4p	−0.30901	−0.30909	...	...	...

point for different symmetry. This is a laborious process, which mainly relies on the accuracy of the numerical orbitals. This resulted in a new idea of completely replacing all the bound orbitals which can be solved using the GRASP code and then using the continuum from the analytical approach. But it was found out that the bound numerical orbitals were not orthogonal to the analytical continuum orbitals, which in principle can be orthogonalised using some known orthogonalisation procedure. This new method of generation of basis wherein we have part numerical orbitals and part analytical orbitals is described in the next section.

4.9.1.3 Partly Analytical and Partly Numerical Basis Functions

For a system with n_c closed shell occupied orbitals, we generate Gaussian basis using DF equations for closed shell core by expanding the single-particle basis in terms of Gaussian as

$$|\phi_i\rangle = \sum_k c_{ik}|G_k\rangle$$

and this satisfy the equation

$$t|\phi_i\rangle + \sum_c \langle\phi_c|v|\phi_c\rangle|\phi_i\rangle - \langle\phi_c|v|\phi_i\rangle|\phi_c\rangle = \epsilon_i|\phi_i\rangle. \tag{4.138}$$

This produces occupied and unoccupied orbitals as given below

$$\{\phi_1, \phi_2, ..., \phi_{n_c}, \phi_{n_c+1}, ..., \phi_{NB}\},$$

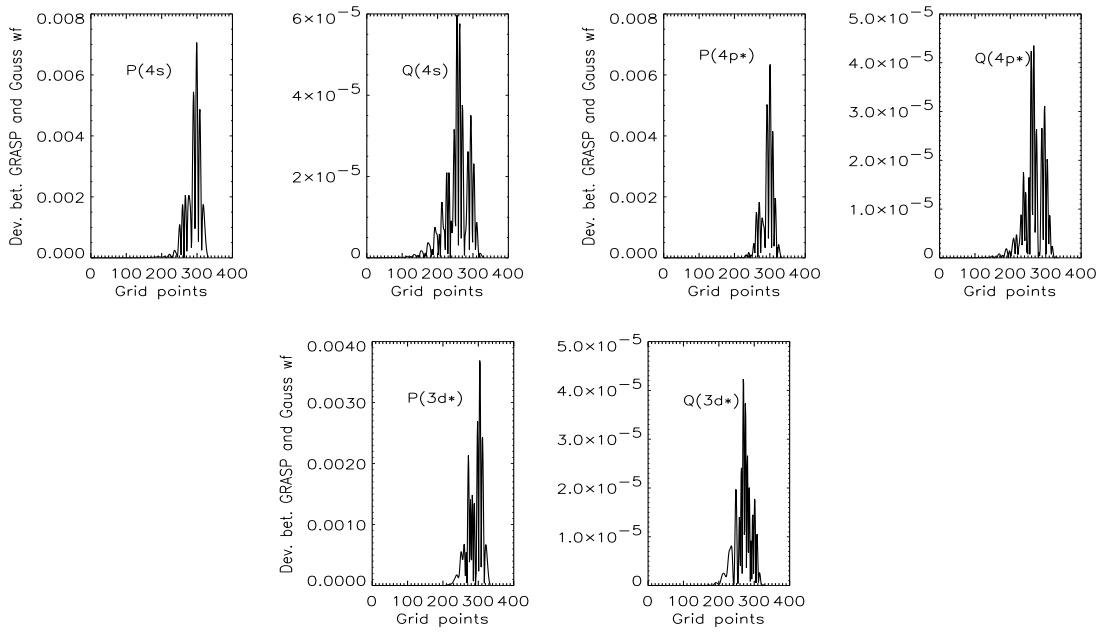

Figure 4.14: Deviation of the GRASP and Gaussian single-particle wave function (large (P) and small (Q) components)for Ca^+.

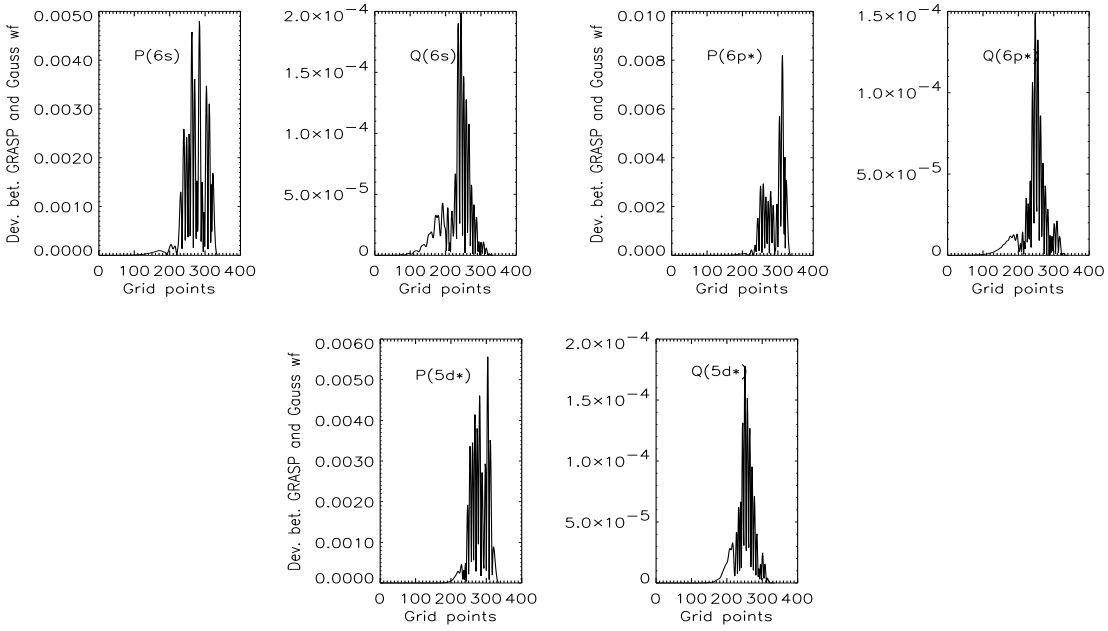

Figure 4.15: Deviation of the GRASP and Gaussian single-particle wave function (large (P) and small (Q) components)for Ba^+.

Table 4.2: Analytical continuum single-particle orbital energies for Ca^+.

orbital	orbital energy	orbital	orbital energy	orbital	orbital energy
7s	0.10574	7p	0.11249	7f⋆	0.24128
8s	1.81710	8p	1.50596	8f⋆	1.12414
9s	11.31845	9p	7.92705	9f⋆	3.51412
...	...	...	...	...	...
7p⋆	0.11046	7d⋆	0.29286	7f	0.24125
8p⋆	1.49416	8d⋆	1.59409	8f	1.12398
9p⋆	7.87450	9d⋆	5.73838	9f	3.51451

where NB is the total number of basis as combined for all symmetry. In this present method we obtain the occupied and the low lying unoccupied orbitals of each symmetry as numerical orbitals generated from multi configuration Dirac Fock GRASP [20] code. The numerical orbitals are denoted as

$$\{\psi_1, \psi_2, ..., \psi_{n_c}, ..., \psi_n\},$$

where n is the number of numerical (GRASP) orbitals used. Since part of the orbitals are numerical and part are analytical obtained using two different methods the orbitals will not be orthogonal. So one obtains new unoccupied orbitals $\{\psi_{n+1}, ..., \psi_{NB}\}$ by the Schmidt orthogonalisation procedure defined as

$$|\psi_{n+k}\rangle = |\phi_{n+k}\rangle - \sum_{m=1}^{n+k-1} |\psi_m\rangle\langle\psi_m|\phi_{n+k}\rangle, \tag{4.139}$$

where k goes from 1 to $NB - n$. By this procedure the new virtual orbitals are made orthogonal to the numerical orbitals and among each other. It is not possible to use this basis as such since the new virtual orbitals are not got by diagonalisation of DF Hamiltonian and hence not Hartree-Fock (HF) orbitals. One can use non-HF orbitals for further calculations by proper use of the potential seen by them. But HF orbitals are more preferred due to the reduction of Fock potential to single-particle energies on acting on same symmetry orbitals.

Hence, in order to generate HF orbitals from the non-HF but Schmidt orthogonalised orbitals the Hamiltonian given in Eq. 4.129 is diagonalised only in the unoccupied space $\{\psi_{n+1}, ..., \psi_{NB}\}$. Here, the unoccupied orbitals $\{\psi'_{n+1}, ..., \psi'_{NB}\}$ are expressed as a linear combination of the Schmidt orthogonalised unoccupied orbitals as given below.

$$|\psi'_k\rangle = \sum_{l=n+1}^{NB} b_{kl}|\psi_l\rangle$$

Table 4.3: Comparison of analytical and numerical single-particle orbital energies for Ba^+.

orbital	analytical	numerical	orbital	analytical	numerical
1s	−1385.03575	−1384.27674	3d⋆	−30.77503	−30.73944
2s	−223.26693	−223.01882	4d⋆	−4.35773	−4.35308
3s	−49.19932	−49.09236	5d⋆	−0.31052	−0.31046
4s	−10.72994	−10.69610	6d⋆	−0.15137	−0.15157
5s	−2.03962	−2.03365	...	...	...
6s	−0.34383	−0.34327	3d	−30.19184	−30.15348
..	...	...	4d	−4.25719	−4.25210
2p⋆	−209.58638	−209.52994	5d	−0.30837	−0.30830
3p⋆	−43.43683	−43.39804	6d	−0.15059	−0.15078
4p⋆	−8.54028	−8.53916	...	...	...
5p⋆	−1.38712	−1.38773	4f	−0.12853	−0.12859
6p⋆	−0.26077	−0.26092	5f	−0.08308	−0.06612
..	...	...	...	...	...
2p	−195.52599	−195.45214	5g⋆	−0.07974	−0.08001
3p	−40.65130	−40.60875	6g⋆	−0.05192	−0.0556
4p	−7.95588	−7.95320	..	...	...
5p	−1.30294	−1.30310	5g	−0.07974	−0.08001
6p	−0.25444	−0.25458	6g	−0.05192	−0.05557

Table 4.4: Analytical continuum single-particle orbital energies for Ba^+.

orbital	orbital energy	orbital	orbital energy	orbital	orbital energy
9s	0.30213	11p	25.41013	7f⋆	0.05494
10s	3.73696	...	...	8f⋆	0.34993
11s	37.36571	9d⋆	0.58096	...	...
...	...	10d⋆	0.05655	7f	0.05655
9p⋆	0.29468	11d⋆	18.12937	8f	0.35221
10p⋆	2.98004	...	...	...	...
11p⋆	23.34434	9d	0.59368	7g⋆	0.04180
...	...	10d	3.50602	8g⋆	0.41192
9p	0.32929	11d	18.43325	7g	0.041787
10p	3.23349	...	...	8g	0.41169

The coefficients b_{kl} got using diagonalisation is used for the generation of the new unoccupied HF single-particle orbitals which are orthogonal to the numerical orbitals and to themselves. This method has been extended to the open shell atoms by starting with an open shell Gaussian code developed by our group and then using a potential which has a closed part and and an open shell part. An elaborate checking of the wave functions by computing Excitation Energy (EE) and Ionisation Potential (IP) for Ba^+ and lifetimes for Ca^+ and Ba^+ using CCM are explained in the next chapter.

4.9.2 Zeroth-Order Contribution to NSI $E1PNC$

We have used the new basis approach to generate basis for Ba^+. The numerical bound orbitals are generated using GRASP [20] and the analytical basis using the FBSE [19] method. For the generation of the analytical basis we have used $\alpha_0 = 0.00725$ and $\beta = 2.73$ and the single-particle orbital energies are tabulated in Table 4.3. The number of Gaussian type orbitals used in our calculation for orbitals of different symmetry is given in Table 4.5. We take the core and some of the low lying virtual orbitals as numerical orbitals and these are tabulated in Table 4.6. As discussed in

Table 4.5: Number of Gaussian basis functions used for the computation of orbitals of each symmetry for Ba^+.

$s_{1/2}$	$p_{1/2}$	$p_{3/2}$	$d_{3/2}$	$d_{5/2}$	$f_{5/2}$	$f_{7/2}$	$g_{7/2}$	$g_{9/2}$	$h_{9/2}$	$h_{11/2}$
32	28	28	25	25	20	20	15	15	10	10

second chapter, due to the presence of the nuclear density, the PNC matrix element is non-zero only when they are connected between single-particle orbitals s and $p_{1/2}$. If the bound orbital lie deep in the core it will have larger overlap inside the nucleus and hence an enhancement of the PNC matrix elements. In the case of continuum orbitals due to their high kinetic energy, the matrix element between a continuum and a bound orbital will also get enhanced due to its overlap inside the nucleus. But the large energy denominator suppresses the contribution to the $E1PNC$. In the case of singly ionised barium, we look for electric dipole transition amplitude between $|5p^6 6s\rangle_{1/2}$ and $|5p^6 5d\rangle_{3/2}$ connected through NSI PNC Hamiltonian. The CSFs which connect the above two states will have to be opposite in parity and also on reduction from CSFs to single-particle level will have to have the matrix element for PNC to be between s and $p_{1/2}$. The expression for the lowest order $E1PNC$ in terms of

Table 4.6: Orbital generation.

Symmetry -	No.of orbitals in each symmetry	Numerical orbitals used in the calculation	Gaussian orbitals used in the calculation
s	32	1s,2s,...8s	9s,....32s
p(1/2)	28	2p,3p,...8p	9p,....29p
p(3/2)	28	2p,3p,...8p	9p,....29p
d(3/2)	25	3d,4d,...7d	8d,....27d
d(5/2)	25	3d,4d,...7d	8d,....27d
f(5/2)	20	4f,5f	6f,....23f
f(7/2)	20	4f,5f	6f,....23f
g(7/2)	15	-	5g,....19g
g(9/2)	15	-	5g,....19g
h(9/2)	10	-	6h,....15f
h(11/2)	10	-	6h,....15f

single-particle orbitals and energies will be

$$\sum_n \frac{\langle 5d_{3/2}|D|np_{1/2}\rangle\langle np_{1/2}|H^{\rm NSI}_{\rm PNC}|6s_{1/2}\rangle}{(\epsilon_{6s_{1/2}}-\epsilon_{np_{1/2}})}+\sum_n \frac{\langle 5d_{3/2}|H^{\rm NSI}_{\rm PNC}|np_{1/2}\rangle\langle np_{1/2}|D|6s_{1/2}\rangle}{(\epsilon_{5d_{3/2}}-\epsilon_{np_{1/2}})}, \tag{4.140}$$

where the first term represents PNC admixtures into the initial state and the second term admixtures into the final state. Dipole operator is a rank 1 tensor which scales linearly on r and the selection rule for the z component is $\Delta J = 0, \pm 1$ and $\Delta M = 0$. The zeroth-order contribution from the bound virtual $p_{1/2}$ orbitals are tabulated in Table 4.7. From the Table 4.7 it is clear that the core $5p\star$ and the lowest virtual $6p\star$ orbital contributes the maximum to the lowest order $E1PNC$ calculation. Even though the PNC matrix elements between the core $p\star$ and $6s$ are larger the small dipole matrix element and the large energy denominator makes the contribution smaller. There is a sign change in the total $E1PNC$ due to the change in the sign of dipole matrix element where we have the intermediate state as $5p\star$ For the $6p\star$ the sign again changes but due to the denominator becoming negative and hence the contribution becomes additive. For the other bound virtual orbitals the dipole as well as the PNC matrix elements shows a fall and this with the increasing energy difference makes the whole contribution smaller. From the total contribution, one can deduce that the contribution to $E1PNC$ from core orbitals is $\sim 13\%$ out of which maximum contribution comes from $5p\star$ orbital. The bound virtuals contribute

Table 4.7: Lowest order contribution to $E1PNC$ from bound core and virtual orbitals. The PNC matrix elements are multiplied by the factor $\frac{G_F}{2\sqrt{2}}(-N)$. $E1PNC$ is given in the units $iea_0(-Q_W/N) \times 10^{-11}$.

$np\star$	$\langle 5d\|D\|np\star\rangle$	$\langle np\star\|H_{\rm PNC}\|6s\rangle$	$\epsilon_i - \epsilon_{np\star}$	$E1PNC_i$	Total
2p⋆	0.002192	4.824848	209.186672	−0.000051	−0.00005
3p⋆	0.007098	2.284567	43.054771	−0.000377	−0.00043
4p⋆	0.003044	1.038440	8.195888	−0.000386	−0.00081
5p⋆	−0.792167	0.377718	1.044456	0.286478	0.28566
6p⋆	1.529071	0.100839	−0.082351	1.872333	2.15800
7p⋆	0.143415	0.063114	−0.205488	0.044049	2.20205
8p⋆	0.079867	0.044501	−0.257395	0.013808	2.21586

to the rest with the $6p\star$ contributing to $\sim 97\%$ compared to the contribution from all the bound virtual orbitals. The contribution of the bound virtual orbitals to $E1PNC$ with respect to the intermediate $p\star$ orbitals is represented in Fig. 4.16.

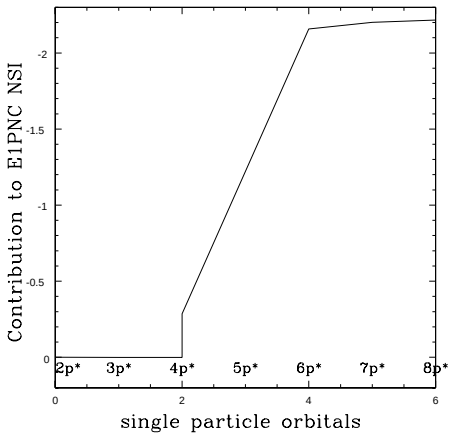

Figure 4.16: Contribution of $E1PNC$ with respect to the intermediate bound single-particle orbitals designated as $np\star$.

The zeroth-order contribution from the continuum $p\star$ orbitals are tabulated in Table 4.8. Examining the Table 4.8 and comparing with the Table 4.7, we find that the contribution from continuum $9p\star$ is larger than the contribution from bound $7p\star$ orbital. This very well clarifies the importance of the continuum orbitals in the $E1PNC$ calculation. Comparing with the total contribution coming from continuum

Table 4.8: Lowest order contribution to $E1PNC$ from continuum virtual orbitals. The PNC matrix elements are multiplied by the factor $\frac{G_F}{2\sqrt{2}}(-N)$. $E1PNC$ is given in the units $iea_0(-Q_W/N) \times 10^{-11}$. Notation: (-x)=$10^{-x}$.

$np\star$	$\langle 5d\|D\|np\star\rangle$	$\langle np\star\|H_{\rm PNC}\|6s\rangle$	$\epsilon_i - \epsilon_{np\star}$	$E1PNC_i$	Total
9p$\star$	−0.192071	−0.241880	−0.642638	0.722930(−1)	0.722930(−1)
10p$\star$	−0.545593(−1)	−0.658162	−0.333825(1)	0.107568(−1)	0.830498(−1)
11p$\star$	0.911818(−2)	0.195205(1)	−0.238369(2)	0.746706(−3)	0.837965(−1)
12p$\star$	0.329675(−3)	−0.493804(1)	−0.158680(3)	−0.102593(−4)	0.837862(−1)
13p$\star$	−0.364446(−3)	−0.113059(2)	−0.721973(3)	0.570714(−5)	0.837920(−1)
14p$\star$	0.143602(−3)	−0.258440(2)	−0.245373(4)	−0.151249(−5)	0.837904(−1)
15p$\star$	0.709504(−4)	0.647487(2)	−0.681122(4)	0.674467(−6)	0.837911(−1)
16p$\star$	−0.352165(−4)	0.146320(3)	−0.160907(5)	−0.320240(−6)	0.837908(−1)
17p$\star$	−0.180975(−4)	−0.343266(3)	−0.335240(5)	0.185308(−6)	0.837910(−1)
18p$\star$	0.949640(−5)	−0.707185(3)	−0.639890(5)	−0.104951(−6)	0.837909(−1)
19p$\star$	0.507861(−5)	0.153835(4)	−0.115480(6)	0.676538(−7)	0.837910(−1)
20p$\star$	−0.275052(−5)	0.299262(4)	−0.201385(6)	−0.408732(−7)	0.837909(−1)
21p$\star$	−0.150204(−5)	−0.616310(4)	−0.344191(6)	0.268957(−7)	0.837909(−1)
22p$\star$	0.823969(−6)	−0.112476(5)	−0.581989(6)	−0.159241(−7)	0.837910(−1)
23p$\star$	−0.452519(−6)	−0.211546(5)	−0.980470(6)	0.976354(−8)	0.837910(−1)
24p$\star$	−0.247704(−6)	0.319629(5)	−0.165608(7)	−0.478075(−8)	0.837909(−1)
25p$\star$	−0.134317(−6)	−0.392945(5)	−0.281494(7)	0.187497(−8)	0.837909(−1)
26p$\star$	0.717006(−7)	−0.157073(4)	−0.482253(7)	−0.233533(−10)	0.837909(−1)
27p$\star$	−0.382509(−7)	0.650709(4)	−0.827590(7)	−0.300755(−10)	0.837909(−1)
28p$\star$	0.205134(−7)	−0.233139(4)	−0.141729(8)	−0.337438(−11)	0.837909(−1)
29p$\star$	0.108042(−7)	−0.762522(3)	−0.246153(8)	−0.334691(−12)	0.837909(−1)

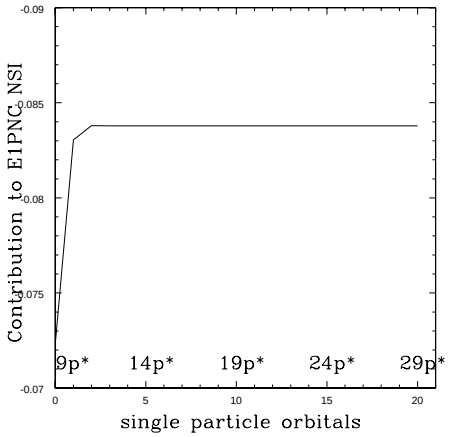

Figure 4.17: Contribution of $E1PNC$ with respect to the intermediate continuum single-particle orbitals designated as $np\star$.

orbitals starting from $9p\star$ to $29p\star$, 99% of contribution to $E1PNC$ comes from $9p\star$ and $10p\star$ and the rest contributing to minimum. Hence the total contribution from lowest order to $E1PNC$ is $2.299646 \times 10^{-11} iea_0 Q_W/(-N)$ with 96.36% coming from bound orbitals and the rest from the continuum orbitals. The complex conjugate term connecting the initial state $6s$ through dipole to the intermediate $p\star$ and then through the PNC to the final state is zero due to PNC matrix element becoming zero due to the final state being j=3/2. The contribution to $E1PNC$ from continuum $p\star$ orbitals are represented in Fig. 4.17.

4.9.3 CPHF/PNCHF Contribution to NSI $E1PNC$

Due to $H_{\rm PNC}^{\rm NSI}$ operator being a tensor of rank 0 and odd under parity, angular momentum considerations puts the individual direct terms and the lowest order energy $\epsilon^{(1)}$ to be zero in the PNCHF Eq. 4.43. This is discussed elaborately by Sandar [27]. The feature of the PNCHF equations is the presence of potential due to the admixture in the core orbitals which can be called the PNC core polarisation. The PNCHF potential is also equivalent to including RPA corrections to $H_{\rm PNC}$ [28]. This approach has been used by several groups and for a historical perspective one is referred to Blundell et al. [29]. The first complete calculations were done by members of the Novosibirsk group [30, 31]. This method applied to caesium atom by different groups has been checked extensively and it shows that PNCHF leads to 25% correlation correction. This method is applied to singly ionised barium and the results of first-order and all

order effects due to CPHF are tabulated in Table 4.9.

Table 4.9: Contributions from zeroth-order, first-order and all order CPHF.

		$\langle 5d\|D\|6s^{\rm PNC}\rangle$	$\langle 5d^{\rm PNC}\|D\|6s\rangle$		Total
Zeroth-order	core	0.285665	0.00	0.285665	
	virtual	2.013981	0.00	2.013981	
Total		2.299646	0.00		2.299646
CPHF/PNCHF					
First-order	core	0.105404	0.005555	0.110958	
in Couloumb	virtual	0.332454	−0.305494	0.026959	
Total		0.437858	−0.299939		0.137919
All order	core	0.149187	0.009892	0.159079	
in Couloumb	virtual	0.419800	−0.492354	−0.072554	
Total		0.568987	−0.482462		0.086525
Total CPHF					
(all orders)		2.868633	−0.482462		2.386172

4.9.4 RPA Contribution to NSI $E1PNC$

A detailed description of the RPA with the classical discussion is given by Sandars [32]. When an atom is placed in a static electric field, interaction between the electrons and the potential due to the field polarises the atom. This leads to an induced potential which tends to cancel the potential due to an external field. Hence this effect is often called the shielding of the electric field. This in other words is also called the RPA correction to the dipole operator. In comparison with CPHF where we had PNC as the perturbation and Dipole as an operator, here we consider Dipole as a kind of perturbation and PNC is taken as an operator which connects the perturbed wave functions. The PNC transition element can be evaluated as

$$E1PNC = \langle f|H^{\rm NSI}_{\rm PNC}|\rho^+_i\rangle + \langle \rho^-_f|H^{\rm NSI}_{\rm PNC}|i\rangle. \tag{4.141}$$

The same effect can be calculated using Time Dependent Hartree-Fock (TDHF) method [33, 34] with PNC added and one can show that it is equivalent to the former method with additional approximations [32]. The zeroth-order will be the same as described above and to avoid double counting should be omitted. The first-order and all order effects due to RPA are tabulated in Table 4.10.

Table 4.10: Contributions from first-order and all order RPA.

		$\langle 5d\|H^{\rm NSI}_{\rm PNC}\|6s^+\rangle$	$\langle 5d^-\|H^{\rm NSI}_{\rm PNC}\|6s\rangle$		Total
RPA/TDHF					
First-order	core	0.00	−0.093587	−0.093587	
in Couloumb	virtual	0.00	−0.003835	−0.003835	
Total		0.00	−0.097421		−0.097421
All order	core	0.00	−0.115389	−0.115389	
in Couloumb	virtual	0.00	0.104712	0.104712	
Total		0.00	−0.010676		−0.010676
Total RPA					
(all orders)		0.00	−0.010676		−0.010676

4.9.5 CPHF-RPA Contribution to NSI $E1PNC$

One can consider parity admixtures also in the electric dipole excitations which leads to double perturbation analysis wherein we consider both the dipole and PNC as perturbations. Since the contribution due to such terms are very less as shown for Cs by Martensson-Pendril [14], we have done only a first-order calculation for CPHF-RPA term. Here the potential is perturbed due to the simultaneous action of PNC and the electric field of the photon. Hence $E1PNC$ can be evaluated either as the overlap between $\langle 5d|$ and the right-hand side of the equation for $|6s^{+\rm PNC}\rangle$ *i.e.*

$$E1PNC = \langle 5d|D + v^+|i^{\rm PNC}\rangle + \langle 5d|H^{\rm NSI}_{\rm PNC} + v^{\rm PNC}|i^+\rangle + \langle 5d|v^{+\rm PNC}|6s\rangle \qquad (4.142)$$

or as an overlap between $|6s\rangle$ and the right hand side of the equation for $\langle f^{-\rm PNC}|$. Only the exchange terms contribute due to angular-momentum restrictions when summing over closed shells. The first-order contribution to the above expression is tabulated in Table 4.11.

Table 4.11: Contributions from first-order CPHF-RPA.

	core contribution	virtual contribution	Total
First-order in Couloumb	−0.001847	−0.009533	−0.011380

Table 4.12: Contribution to NSI $E1PNC$ from pair correlation effects.

Pair	Pair correlation effects	Contribution	Total
$\rho(i,a)$	Bruckner effect	0.145382	
	Structural Radiation	0.049088	
	others	−0.010496	0.18397
$\rho(f,a)$	Bruckner effect	−0.297338	
	Structural Radiation	−0.046477	
	others	0.078664	−0.26515
Total			−0.08118

4.9.6 Pair Correlation Contribution to NSI $E1PNC$

As discussed in the formulation for the evaluation of $E1PNC^{(3)}$ terms, we have taken only diagrams designated as class I for the computation. These diagrams are given in Fig. 4.12. As a first step the pairs $\rho(i,a)$, $\rho(f,a)$ and $\rho(\bar{i},a)$ are computed and stored in a file. In the case of singly ionised barium, $\rho(\bar{f},a)$ is zero due to the restriction of PNC matrix element becoming zero for $j = 3/2$. Examining the diagrams in Fig. 4.12 we can find out that, using $\rho(i,a)$ (8 direct + 8 exchange), $\rho(f,a)$ (8 direct + 8 exchange) and $\rho(\bar{i},a)$ (1 direct + 1 exchange) can be computed. Using both $\rho(i,a)$ and $\rho(f,a)$ one can compute the rest of the diagrams which are designated by numbers from 19-30. These diagrams are also not included in the present calculation. Contribution from pair correlation diagrams got using $\rho(i,a)$, $\rho(f,a)$ and using a restricted basis given by $11s10p9d9f$ are tabulated in Table 4.12. For the above calculation we have taken core correlation from all the core orbitals which in this case is till $5p^6$.

The contribution from $\rho(\bar{i},a)$ is found to diverge due to the denominator becoming small and at the same time the numerator which has the two Couloumb matrix elements becoming large. The expression for the diagram (5) in Fig. 4.12 is given by

$$\sum_{spqar} \frac{\langle f|D|s\rangle\langle sa|v|pq\rangle\langle pq|v|ra\rangle\langle r|\mathrm{PNC}|i\rangle}{(\epsilon_i-\epsilon_r)(\epsilon_i-\epsilon_s)(\epsilon_i+\epsilon_a-\epsilon_p-\epsilon_q)}. \tag{4.143}$$

Here i and f are fixed to be $6s_{1/2}$ and $5d_{3/2}$. Since PNC can connect only $s_{1/2}$ and $p_{1/2}$ symmetries, r will be $p_{1/2}$. The Couloumb vertex preserves symmetry, hence s will again be $p_{1/2}$. So in the denominator we get $(\epsilon_{6s_{1/2}}-\epsilon_{6p_{1/2}})^2$ which is $\sim$ 0.006 a.u. This on multiplication with $(\epsilon_{6s}+\epsilon_a-\epsilon_p-\epsilon_q)$ is of the order 10^{-3}. The Couloumb matrix elements $\langle 6s_{1/2}5d_{5/2}|v|6p_{1/2}5p_{3/2}\rangle$ in the numerator is of the order

10^{-1} due to the close lying nature of the orbitals considered. Hence the above term diverges leading to the total contribution larger than the zeroth-order. For such atomic systems with very close lying levels one needs to avail different theories like multi-reference perturbation theory or a theory combined with CI and MBPT wherein one takes the close lying ones using CI and the others through MBPT. In this case, contribution from core-valence correlation involving $5p$ and $6s$ which is responsible for the divergence is taken out from MBPT(5) diagram, and the effect is computed to all order using Coupled Electron Pair Approximation CEPA. The contribution from all the other core states till $5s$ are obtained using first-order MBPT and is found to be 0.295 $iea_0(-Q_W/N) \times 10^{-11}$. A very detailed study of CEPA is given in the thesis by Angom [36]. The contribution from $\rho(\bar{f}, a)$ will be zero due to the property of PNC operator.

4.10 Coupled Electron Pair Approximation

Here for computation Epstein-Nesbet(EN) partitioning [6] is used. Defining

$$H = H_0 + V_{es} + \lambda H_{\rm PNC} \tag{4.144}$$

the unperturbed Hamiltonian and the residual interaction takes the form

$$\begin{aligned} H_0 &= \sum_i \langle\Phi_i H|\Phi_i\rangle|\Phi_i\rangle\langle\Phi_i| \\ V_{es} &= \sum_{ij,i\neq j} \langle\Phi_i|H|\Phi_j\rangle|\Phi_i\rangle\langle\Phi_j|. \end{aligned}$$

In the similar manner $H_{\rm PNC}$ can be written as

$$H_{\rm PNC} = \sum_{ij} \langle\bar{\Phi}_i|H_{\rm PNC}|\Phi_j\rangle|\bar{\Phi}_i\rangle\langle\Phi_j|, \tag{4.145}$$

where $i \in P, j \in Q$ and $\bar{\Phi}_i$ denotes the opposite parity to Φ_j. From RSPT we know $\Omega|\Phi_0\rangle = |\Psi_0\rangle$. This is equal to

$$|\Psi_0\rangle = |\Phi_0\rangle + |\Phi_0^{(1)}\rangle + ..., \tag{4.146}$$

which in terms of unperturbed CSFs can be written as

$$|\Psi_0\rangle = |\Phi_0\rangle + \sum_{n\neq 0} C_n^{(1)}|\Phi_n\rangle + \sum_{n\neq 0} C_n^{(2)}|\Phi_n\rangle. \tag{4.147}$$

Combining in terms of the order of perturbation the above equation reduces to

$$|\Psi_0\rangle = \sum_{n,i\neq 0} C_{i0}^{(n)}|\Phi_i\rangle\langle\Phi_0|\Phi_0\rangle, \tag{4.148}$$

where n refers to the order of perturbation and i refers to the index of the CSF.

Below we analyse the MBPT(5) diagram. PNC perturbation acting on the initial state can be mathematically represented as $\Omega^{(1,0)}|5p^6 6s\rangle$ where the first and second index in the superscript defines the order of PNC and Couloumb perturbation. The wave operator can be obtained from Bloch equation as

$$\Omega^{(1,0)}\hat{P} = RH_{\rm PNC}\hat{P} = \sum_k C_k^{(1,0)}|\bar{\Phi}_k\rangle. \tag{4.149}$$

Since PNC is odd under parity and the initial CSF is $|5p^6 6s\rangle$ the resulting CSF will be of different parity and this case it is $|5p^6 kp\rangle$. Hence

$$C_k|5p^6 6s\rangle = RH_{\rm PNC}\hat{P} = \frac{\langle 5p^6 kp|H_{\rm PNC}|5p^6 6s\rangle}{(E_{5p^6 6s} - E_{5p^6 kp})}. \tag{4.150}$$

The next perturbation is Couloumb which is restricted to have double excitation with one electron from $6s$ and the other from $5p$. Physically it can be written as

$$\Omega^{(1,1)}|5p^6 kp\rangle \rightarrow |5p^5 kpk's\rangle k' \neq 6. \tag{4.151}$$

Using Bloch equation we can write

$$\Omega^{(1,1)} = RV\Omega^{(1,0)} + RH_{\rm PNC}\Omega^{(0,1)}. \tag{4.152}$$

Here the second term will be neglected since at present we consider only pair correlation diagrams of the kind like MBPT(5). We define the Q space to be

$$Q = \sum_{pq} |5p^5 pq\rangle\langle 5p^5 pq| \tag{4.153}$$

and hence the resolvent operator

$$R = \sum_{pq} \frac{|5p^5 pq\rangle\langle 5p^5 pq|}{(E_{5p^6 6s} - E_{5p^5 pq})}. \tag{4.154}$$

Since Q space is restricted to the type give above and only the specific diagram is taken into account, the unlinked terms will not arise in the first term. Hence renormalisation terms which cancels these terms are not needed for the above calculation. Also it can be shown that due to EN partitioning scheme the renormalisation terms goes to zero by itself. Hence,

$$\begin{aligned} \Omega^{(1,1)}\hat{P} &= RV\Omega^{(1,0)}|5p^6 6s\rangle \\ &= \sum_{kpq} \frac{|5p^5 pq\rangle\langle 5p^5 pq|v|5p^6 kp\rangle C_k}{(5p^6 6s - 5p^5 pq)}. \end{aligned}$$

The above vertex is iterated to all order using the Bloch equation given by

$$\Omega^{(1,n)}\hat{P} = RV\Omega^{(1,n-1)}\hat{P}. \tag{4.155}$$

The next step is to define a particular Couloumb vertex and resolvent operator given by

$$V' = \sum_{ij} |i\rangle\langle i|v|j\rangle\langle j| = |5p^6r\rangle\langle 5p^5pq|\langle 5p^6r|v|5p^5pq\rangle \tag{4.156}$$

and

$$R' = \sum_{r} \frac{|5p^6r\rangle\langle 5p^6r|}{(E_{5p^66s} - E_{5p^6r})}. \tag{4.157}$$

The Bloch equation to be solved is

$$\Omega^{(1,n+1)}\hat{P} = R'V'\Omega^{(1,n)}. \tag{4.158}$$

Once $\Omega^{(1,n+1)}\hat{P}$ is found out, we can get

$$E1PNC = \frac{\langle\Phi_f|D\Omega^{(1,n+1)}|\Phi_i\rangle}{\sqrt{\langle\Psi_i|\Psi_i\rangle\langle\Psi_f|\Psi_f\rangle}}. \tag{4.159}$$

In this case, we have taken a basis consisting of seven symmetries *viz.*, s, $p\star$, p, $d\star$, d, $f\star$ and f by restricting the virtual single-particle orbitals below 100 a.u., The basis which we have considered is given by $11s10p9d9f$. Using the above basis the possible singley and doubley excited CSFs are $|5p^66s\rangle_e$, $|5p^65d\rangle_e$, $|5p^6kp\rangle_o$ (where k = 6, 7, ..., 11) and $|5p^5kpk'f\rangle_o$ (where k =6, 7, ..., 11 and k' = 4, 5, ..., 12), $|5p^5ksk'd\rangle_o$ (where k = 6, 7, ..., 11 and k' = 5, 6, ..., 11), $|5p^5kpk'p\rangle_o$ (where k and k' = 6, 7, ..., 11), $|5p^5ksk's\rangle_o$ (where k and k' = 6, 7, ..., 11), $|5p^5kdk'd\rangle_o$ (where k and k' = 5, 6, ..., 11) and $|5p^5kfk'f\rangle_o$ (where k and k' = 4, 5, ..., 12). Comparing the coefficients of the singly excited determinants with $H_{\rm PNC}$, we find that the CSF $|5p^66p\rangle$ contributes the most. Similarly, for doubly excited CSFs with Couloumb interaction to all order the coefficient is larger for the CSF given by $|5p^55d^1_{3/2}5d^1_{5/2}\rangle$. The application of one order in Couloumb interaction leads to singly excited CSFs of the kind given by $|5p^6kp\rangle$, where $k = 6$ has the maximum contribution which is connected to the final state CSF through dipole. The all order contribution to NSI $E1PNC$ taking double excitations from $5p$ and $6s$ is found to be $-0.39899\ iea_0(-Q_W/N)\ \times\ 10^{-11}$. Hence adding the contribution from the other core orbitals $1s, 2s, 2p...5s$ with the above we get the NSI $E1PNC$ to be $-0.10399\ iea_0(-Q_W/N)\ \times\ 10^{-11}$.

Table 4.13: Total contribution to NSI $E1PNC$ from various effects in units of $10^{-11}iea_0(-Q_W/N)$.

Different effects	Contribution	Total
Zeroth-order	2.29965	2.29965
CPHF(all order)	0.08653	2.38617
RPA (all order)	−0.01068	2.37550
CPHF-RPA(first-order)	−0.01138	2.36412
Pair correlation(first-order)($\rho(i,a)$ $\rho(f,a)$)	−0.08118	2.28294
Pair correlation($\rho(\bar{i}$,a)(upto $5s$ core first order and $5p$ all order using CEPA)	−0.10399	2.17894

4.11 Total Contribution to NSI $E1PNC$ through MBPT

The total contribution to $E1PNC$ from different effects are given in Table 4.13. All the numbers are given in the units $10^{-11}iea_0(-Q_W/N)$. By comparing the contributions from various effects it is clear that CPHF contributes $\sim 3.8\%$ with RPA and CPHF-RPA effect $< 1\%$. The contribution from few of the pair correlation diagrams is $\sim 3\%$. In case of CPHF, the PNC perturbed initial state and final state contributions are 0.568987 $10^{-11}iea_0(-Q_W/N)$ and -0.482462 $10^{-11}iea_0(-Q_W/N)$ respectively leading to the total contribution to all order CPHF to be 0.086525 $10^{-11}iea_0(-Q_W/N)$. Whereas in the case of RPA, the Dipole perturbed initial state is zero for the lowest and all order due to the presence of PNC in the final vertex. The contribution from the Dipole perturbed final state to RPA is $\sim 0.5\%$. For Cs CPHF results contributes to the 25% whereas for Ba^+ it is $\sim 4\%$. Since the contribution from CPHF-RPA in the case of Cs is small we did only a first-order calculation of the above mentioned effect and it contributes $\sim 0.5\%$ to the total $E1PNC$. The total contribution to NSI $E1PNC$ through pair correlation effects from $\rho(i,a)$ and $\rho(f,a)$ are given by 0.081 $10^{-11}iea_0(-Q_W/N)$ which in comparison with the other effects is $\sim 3\%$. Dzuba et al. [35] have computed the NSI $E1PNC$ using the mixed parity approach in which fitted Bruckner orbitals are used as the starting point of the calculation. In this approach, the CPHF, RPA and CPHF-RPA effects are done to all orders and the total contribution to NSI $E1PNC$ is found to be $2.17 \times 10^{-11}iea_0(-Q_W/N)$. The contribution from $\rho(\bar{i},a)$ by considering the contribution from the core except $5p$

using lowest order is found to be $0.295 \times 10^{-11} iea_0(-Q_W/N)$. The contribution from $5p$ using CEPA is $\sim -0.399 \times 10^{-11} iea_0(-Q_W/N)$. Hence the total contribution from $\rho(\bar{i}, a)$ is $\sim -0.104 \times 10^{-11} iea_0(-Q_W/N)$. The contribution to our all order CPHF, RPA, first-order CPHF-RPA and pair correlation diagrams are found to be $2.18 \times 10^{-11} iea_0(-Q_W/N)$. The results of our calculations on $E1PNC$ NSI agrees with the calculation by Dzuba et al. [35].

Bibliography

[1] N.M. Hugenholtz, *Physica (Utrecht)* **23**, 481 (1957).

[2] J. Goldstone, *Proc. R. Soc. London A* **239**, 267 (1957).

[3] I. Lindgren, J. Morrison, *Atomic Many-Body Theory*, Springer-Verlag, New York (1981).

[4] A. Szabo and N.S. Ostlund, *Modern Quantum Chemistry*, Dover Publications, Mineola, New York.

[5] R.J. Bartlett, *Ann. Rev. Phys. Chem.* **32**, 359 (1981).

[6] P.S. Epstein, *Phys. Rev.* **28**, 695 (1926).

[7] R.K. Chaudhuri and K.F. Freed, *J. Chem. Phys.* **107**, 6699 (1997).

[8] R.K. Chaudhuri, J.P. Finley and K.F. Freed, *J. Chem. Phys.* **106**, 4067 (1997).

[9] J.P. Finley, R.K. Chaudhuri, and K.F. Freed, *Phys. Rev. A* **54**, 343 (1996).

[10] R.K. Chaudhuri, J.P. Finley and K.F. Freed, *J. Chem. Phys.* **103**, 4990 (1995).

[11] J.J. Sakurai, *Modern Quantum Mechanics*, Addison-Wesley Publishing Company, New York (1994).

[12] I. Lindgren, *J. Phys. B. Atom. Molec. Phys* **7**, 2441 (1974).

[13] P.G.H. Sander, *J. Phys. B* **10**, 2983 (1977).

[14] A.M. Martensson-Pendril, *J. Physique* **46**, 1949 (1985).

[15] P.G.H. Sanders, *Physica Scripta* **21**, 293 (1980).

[16] V.A. Dzuba, V.V. Flambaum, Silvestrov and O.P. Sushkov, *J. Phys. B* **18**, 597 (1985).

[17] T.C. Caves and M. Karplus, *J. Chem. Phys.* **50**, 3649 (1969).

[18] R.M. Sternheimer, *Phys. Rev.* **80**, 102 (1950); **84**, 244 (1951); **86**, 315 (1952).

[19] R.K. Chaudhuri, P.K. Panda and B.P. Das, *Phys. Rev. A*, **59**, 1187 (1999).

[20] F.A. Parpia, C.F. Fisher, and I.P. Grant (unpublished).

[21] F. Mark, *Theoret. Chim. Acta* **70**, 165 (1986).

[22] O. Matsuoka, M. Klobukowski and S. Huzinaga, *Chem. Phys. Lett.* **113**, 395 (1985).

[23] O. Matsuoka and S. Okada, *Chem. Phys. Lett.* **155**, 547 (1989).

[24] O. Matsuoka and S. Huzinaga, *Chem. Phys. Lett.* **140**, 567 (1987).

[25] S. Okada and O. Matsuoka, *J. Chem. Phys.* **91**, 4193 (1989).

[26] R.C. Raffenetti, *J. Chem. Phys.* **59**, 5936 (1972).

[27] P.G.H. Sandars, *J. Phys.* **B10**, 2983 (1977); C. E. Loving, Ph.D. Thesis Oxford.

[28] S.A. Blundell, *Applied Many-Body Methods in Spectroscopy and Electronic Structure*, ed. D. Mukherjee, Plenum Press, New York, (1992).

[29] S.A. Blundell, A.C. Hartley, Z.W. Liu, A.M. Martensson-Pendrill and J. Sapirstein, *Proceedings from the Workshop on Coupled Cluster Theory at the Interface of Atomic Physics and Quantum Chemistry*, Harvard, 6-11 August 1990, ed. R.J. Bartlett, Springer (1991).

[30] V.A. Dzuba, V.V. Flambaum and O.P. Sushkov, *Phys. Lett. A*, **141**, 147 (1989).

[31] V.A. Dzuba, V.V. Flambaum, P.G. Silvestrov and O.P. Sushkov, *Physica Scripta* **35**, 69 (1987); *J. Phys. B* **20**, 3297:311 (1987).

[32] P.G.H. Sandars, *Physica Scripta* **21**, 284 (1980).

[33] A. Dalgarno and G.A. Victor, *Proc. Roy. Soc.* **A291**, 291 (1966).

[34] W.R. Johnson and C.D. Lin, *Phys. Rev. A* **A14**, 565 (1976).

[35] V.A. Dzuba, V.V. Flambaum and J.S.M. Ginges, *Phys. Rev. A* **63** 62101 (2001).

[36] A.D. Singh, A study of the Electric Dipole Moment of Atoms, Ph.D. Thesis,,Bangalore University (1998).

Chapter 5

Coupled Cluster Method (CCM) applied to Parity Non-Conservation in Atoms

---

5.1 Coupled Cluster Method: An Introduction

5.1.1 General Considerations

We examined and applied Configuration Interaction (CI) [1] and Many-Body Perturbation Theory (MBPT) [2] to compute atomic properties like electric dipole and PNC matrix elements in previous chapters. These approaches are rather different in terms of the assumptions underlying their practical use, and we have identified their drawbacks for the computation of various properties. The CI method focuses on configurations of modest degree of excitations relative to a reference state. Such configurations enable a correlated description of the particles involved with the remaining particles being restricted to their distributions in the reference configuration. For example, a double excitation CI contains sets of configurations that provide a correlated wave function for the corresponding particle pair. Thus a CI with all possible double excitation yields a wave function containing effects that arise from the correlation of one pair of particle at a time. In other words, a double excitation CI contains no terms describing the simultaneous correlations of two independent pairs. The lack of size-extensivity in a truncated CI can be traced to the omission of configurations describing the simultaneous correlations of two independent pairs [1]. Also the num-

ber of pairs of particles proliferate rapidly as one considers systems of larger size. However, for systems of smaller size, taking all possible excitations into account is realisable in state of the art computers, which leads to an exact solution.

The MBPT approach avoids the size-inextensivity problem of the CI method, but at the cost of an overwhelming proliferation of terms. There are different methods by which some of these terms can be grouped together and evaluated to all orders. Individual terms in perturbation theory correspond to fragmented contributions to the correlation phenomenon, and even to describe the correlation of a single pair of particles higher order perturbation terms may be necessary. An important positive feature of MBPT is that it is size-extensive *via* the Linked Cluster Theorem (LCT). The disconnected diagrams representing disjoint excitations are cancelled in the MBPT formulation through LCT.

The CCM is based on an expansion scheme that satisfies the twin criteria of physical appropriateness or validity and practical realisability. It is well known that in many-electronic structure calculations the dominant correlation effects are from the interactions of individual pairs of electrons, and that other electrons influence this interaction mainly in an average sense. This pairwise interaction is not small. Moreover in a many-electron problem, terms involving the simultaneous description of two or more such pairs occur, and their combined effect is not small relative to terms describing single electron pairs. This clearly points to the need for an expansion scheme which depends on a physically relevant parameter of the system which in this case is the degree of excitation of particles whose detailed correlation we are interested in. Once the size of the "cluster" of such particles has been specified, the wave function must be permitted to include arbitrary numbers of such correlated clusters. Expansions of this type may be called cluster expansions. In this chapter we will be discussing in detail the properties of the cluster operator and the application of CCM to closed and open-shell atoms with the aim of finding the Electric Dipole Transition amplitude induced by PNC for singly ionised barium.

5.1.2 Form of Coupled Cluster Wave Function

Consider the problem of obtaining the ground-state wave function $|\Psi\rangle$ and energy E of a system of N interacting electrons described by the Hamiltonian operator H. In other words, we wish to solve the time-independent Schrödinger equation

$$H|\Psi\rangle = E|\Psi\rangle. \tag{5.1}$$

If the electrons in a many-body system do not interact with one another, the only constraint on the many-particle wave function is the Pauli's exclusion principle, which

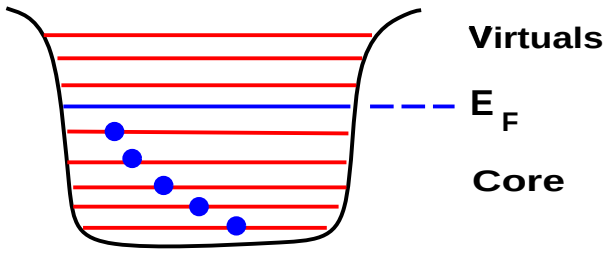

Figure 5.1: Schematic representation of the filled Fermi sea state $|\Phi\rangle$.

requires each electron to be in a different single-particle eigenstate. The N-body ground state in this simple case is obtained by filling the N lowest single-particle states as shown in Fig. 5.1. This wave function is a sum of products of the one-body wave functions of the "occupied states". This is most compactly expressed in the determinantal form and is called the "Slater determinant". The set of occupied levels is often referred to as the "filled Fermi sea". In the Dirac-Fock (DF) approximation, the interacting many-particle system is replaced by an effective non-interacting one, in which each particle moves independently in a potential well that is determined self-consistently by the average motion of all the particles. Once the single-particle basis functions are obtained as mentioned in the Chapter 3 of this thesis, the ground state wave function and energy can be obtained as outlined above. Now consider how the correlations induced by interactions modify this picture of the ground state. The first thing one can consider is that two-particles interact and lift themselves out of the Fermi sea, so that after interaction both particles are in orbitals which were unoccupied previously. This process can be described by a quantum mechanical operator T_2, which acts on the Fermi sea wave function or the DF wave function to produce the wave function $T_2|\Phi\rangle$, which describes two-particles outside the Fermi sea and remaining $N-2$ particles in their previous orbitals. The same phenomena can happen independently and the operator representation for that can be obtained by applying the operator T_2 twice, with the provision to include statistical weighting factor of $1/2$ to avoid counting the pairs twice. Hence, the contribution to the resulting wave function is $1/2T_2^2|\Phi\rangle$. This kind of independent excitation of pairs out of the Fermi sea may be continued to obtain a contribution $(1/m!)T_2^m|\Phi\rangle$ for the amplitude describing the excitation of m independent pairs. By the principle of linear superposition, the total amplitude for the excitation of an arbitrary number (including zero) of independent pairs is

$$\sum_{m=0}^{\infty} \frac{1}{m!} T_2^m |\Phi\rangle = e^{T_2}|\Phi\rangle. \tag{5.2}$$

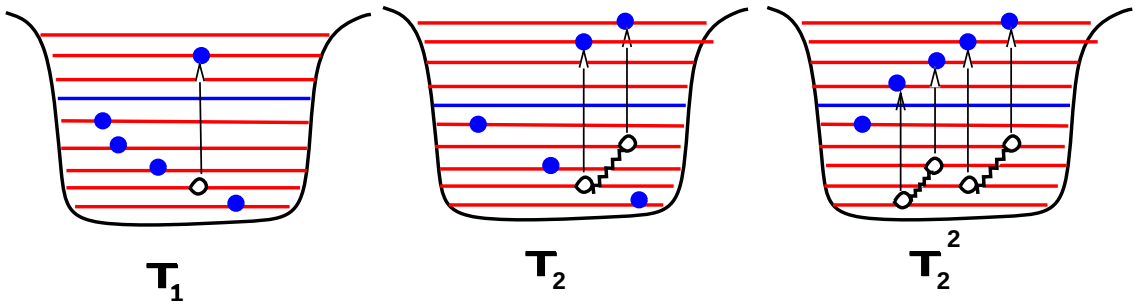

Figure 5.2: Coupled Cluster (CC) wave function for singles, doubles and higher order excitations.

Similarly, we can consider processes involving excitation of one and three-particles and simultaneous excitation of one and two-particles and so on with respect to the Fermi sea. Wave function representing independent singles, doubles and simultaneous singles & doubles can be represented as

$$\sum_{n=0}^{\infty}\frac{1}{n!}T_1^n|\Phi_0\rangle+\sum_{m=0}^{\infty}\frac{1}{m!}T_2^m|\Phi_0\rangle+\sum_{n=0}^{\infty}\sum_{m=0}^{\infty}\frac{1}{n!m!}T_1^nT_2^m|\Phi_0\rangle=e^{T_1+T_2}|\Phi_0\rangle. \tag{5.3}$$

Schematically such excitations can be represented as given in Fig. 5.2. Proceeding in this way with the excitation of clusters of 4, 5, $\cdots$, N particles we arrive at the exact wave function

$$|\Psi\rangle=e^{T_1+T_2+\cdots}|\Phi_0\rangle=e^T|\Phi_0\rangle. \tag{5.4}$$

The exponential representation of the wave function of a quantum many-body system can be regarded as the cluster decomposition of quantum mechanical amplitudes for exciting finite number of particles. This form of the many-particle wave function is a direct consequence of the law of probability theory that states that the probability of the statistically independent processes is a product of the probabilities of the individual processes. We now briefly discuss about the origin of CCM from the famous LCT.

Historically, the papers which led to the CCM appear to be those of Hugenholtz [4] and Hubbard [5] in 1957. It was Goldstone [6] and Hubbard who proved the existence of the now-famous LCT for interacting electron systems. The theorem, in effect, states that the perturbation corrections to the wave function and total energy beyond the independent-particle approximation can be represented by linked Feynman graphs. Earlier to that Bruckner [7] had pointed out that this holds for a few orders of interaction by explicitly demonstrating the cancellation of unlinked terms in the first few orders of the Rayleigh- Schrödinger perturbation theory. Goldstone together with

Hubbard and Hugenholtz introduced the mathematical techniques of quantum field theory to all orders. The main significance of the LCT is the direct proportionality of the energy corrections for a system like crystal or electrons at a given density with the number of particles. But the proofs used an interaction representation, thereby introducing time dependence in an intrinsically time-independent physical problem. The importance of the LCT from a wave function point of view is its recognition of the fast convergence of the linked-cluster type terms beyond the independent-particle approximation. However, the overall emphasis remained on the connection with the quantum-electrodynamical methods of Feynman, leading to the order-by-order view of many-body effects and scattering pictures. In other words the LCT was based on a perturbative argument. In 1960's Kelly [8] used diagrammatic Goldstone perturbation theory to study the correlation effects in closed-shell atoms and proposed several very successful approximation schemes.

The idea of cluster ansatz originated in statistical mechanics [9]. It's usefulness for the expansion of the exact many-electron wave function, in contrast to the linear expansions characteristic of variational approaches, was first inferred from the structure of the many-body perturbation theory by Hubbard. The use of such expansions in quantum many-body theory was first introduced by Coester and Kummel [10] in the context of nuclear physics as early as 1957, but it remained obscure for a considerable period. This had much to do with the fact that the sort of high-precision calculations that the CCM allows one to perform were neither fashionable nor considered necessary at that time, because our understanding of nuclear forces was then rather rudimentary. The development of the many-electron correlation problem in the early sixties was very much influenced by a series of papers by Sinanoglu [11], who proposed a theory based on the cluster expansion and an approximate treatment of pair clusters. Similar ideas were later pursued by Nesbet [12]. The need of precise determination of molecular structures and binding energies from a microscopic quantum mechanical calculation has been a problem of utmost importance for many quantum chemists since the development of quantum theory of the chemical bond. The first application of CCM to electronic structure problems were by the quantum chemists, Cizek and Paldus [13]. Later, this led to the development of a general technique enabling a simple and systematic generation of the explicit CC equations for the components of the cluster operator. Further development of the theory to the present form can be obtained from the review paper by Bartlett [14].

5.1.3 Properties of Cluster Operator

5.1.3.1 Size-Extensivity

This term is borrowed from thermodynamics, where an extensive property is one that is proportional to the size of a homogeneous system. Pople et al. [15] proposed the term "size-consistency" for a closely related property. A method is considered size-consistent if the energy of a system made up of two subsystems A and B far apart is equal to the sum of the energies A and B computed separately by the same method. The maintenance of size-consistency is more rigorous than size-extensivity. The method is automatically size-extensive if it is size-consistent. However a size-extensive method may not be size-consistent. The idea of size-extension is implicit in the work of Brueckner, Goldstone, and co-workers, although Primas was one of the first to emphasize the concept [16]. Size-extensivity is guaranteed by the evaluation of terms that the many-body development identifies as linked diagrams, hence theorem based on this, like MBPT/CCM are size-extensive. In simpler words, size-extensivity means that the wave function and energy scale properly with molecular size.

This is usually illustrated by the N non-interacting H_2 molecules. Assuming localised orbitals, the correct wave function for the super molecule is

$$\Psi(NH_2) = [\Psi(H_2)]^N \tag{5.5}$$

with energy

$$E(NH_2) = NE(H_2). \tag{5.6}$$

Describing each H_2 molecule with localised orbitals and using CCM, we can write the exact wave function as

$$\Psi_{CC}(NH_2) = e^{T(1)+T(2)+....+T(N)}\Psi_o(NH_2) \tag{5.7}$$

where

$$\Psi_o(NH_2) = \Phi_o(1)\Phi_o(2)....\Phi_o(N).$$

On further simplification and using multiplicative separability, we get

$$\begin{aligned}\Psi_{CC}(NH_2) &= e^{T(1)}\Phi_o(1)e^{T(2)}\Phi_o(2)....e^{T(N)}\Phi_o(N)\\ &= \Psi_o(1)(H_2)\Psi_o(2)(H_2)....\Psi_o(N)(H_2).\end{aligned}$$

Since $[T(1), T(2)] = 0$, the total energy using additive separability becomes

$$E(NH_2) = E(1)(H_2) + E(2)(H_2)..... + E(N)(H_2) \tag{5.8}$$

Even though the above property is explained with respect to a non-interacting system, size-extensivity of any method imposes the absence of unlinked diagrams too. Hence non-interacting limit is a necessary but not a sufficient condition that a method be extensive. The exponential wave function guarantees extensivity even in the interacting case, provided that T itself is separable. Multiplicative separability of the wave function is guaranteed in CCM, even if the T operator is truncated. Thus CCM obeys size-extensivity at each level of approximation.

5.1.3.2 Equivalence with CI

The CI form of the perturbed wave function $|\Psi_o\rangle$ constructed with respect to the unperturbed wave function $|\Phi_o\rangle$ written using intermediate normalisation ($\langle\Phi_o|\Psi_o\rangle = \langle\Phi_o|\Phi_o\rangle = 1$) is as follows.

$$|\Phi_o\rangle = (1 + \sum_{l\geq 1} C_l)|\Phi_o\rangle \tag{5.9}$$

where C_l is an operator creating a fixed linear combination of the l-excited configurations or states. In CCM, the perturbed wave function is written using the exponential operator acting on the unperturbed wave function, as

$$|\Phi_o\rangle = e^T|\Phi_o\rangle \tag{5.10}$$

Expanding T operator as $T_1 + T_2 + T_3 + ...$, we get

$$|\Phi_o\rangle = |\Phi_o\rangle + T_1|\Phi_o\rangle + (T_2 + \frac{1}{2!}T_1^2)|\Phi_o\rangle + (T_3 + T_1T_2 + \frac{1}{3!}T_1^3)|\Phi_o\rangle + ... \tag{5.11}$$

Comparing the right hand sides of equation we get

$$\begin{aligned} C_1 &= T_1, \\ C_2 &= T_2 + \frac{1}{2!}T_1^2, \\ C_3 &= T_3 + T_1T_2 + \frac{1}{3!}T_1^3. \end{aligned} \tag{5.12}$$

Paldus [17] suggested that single terms can be called connected and the terms expressed as the product of the connected terms can be called disconnected. One can solve the system of equations for the cluster operator from the Eq. 5.12. The relative importance of exponential to CI for the correlation energy calculations can be well understood by looking at the full CI calculations [18] and intuition [19], tells clearly that the largest part of the correlation effects is accounted for by the first few cluster operators T_1, T_2, T_3, T_2T_2 etc., and the remaining ones may be omitted. Also in CI, there is an inbuilt arbitrariness about the configurations which are added, whereas in CCM we solve directly for the cluster operators in a given basis. Considering the same

example of two non-interacting H_2 molecule the exact wave function is described by the product of single H_2 wave functions. But the product of the simultaneous double excitations on each H_2 molecule corresponds to quadruple excitations, if the two molecules are treated as a super molecule in CI. Since the number of configurations is proportional to $(n)^l$, where n is the number of basis functions and l is the level of excitation, a prohibitive $\approx 10^8$ configurations would be necessary for $n = 100$ to include just the quadruple excitations [20]. But in CCM, from the beginning we can include only the dominant terms that are responsible for the main part of the correlations. The relative importance of each of the individual cluster operators depends in particular, upon
(i) whether the system studied is closed-shell or open-shell type,
(ii) the size of the system (Z),
(iii) the type of the single-particle basis used (numerical/analytical) and
(iv) the type of correlation effects which are to be accounted for (this decides the number of orbitals (core and virtuals) in the calculation.
The rest of the sections will be devoted to studying about the application of CCM to closed and open-shell type atoms.

5.2 Application of CCM to Closed-Shell Atoms

5.2.1 Form of the Cluster Operator (T)

The fundamental idea of CCM is the exponential wave function ansatz,

$$|\Psi_{CC}\rangle = e^T |\Phi_o\rangle \tag{5.13}$$

where, $|\Phi_o\rangle$ is considered to be the independent-particle reference state such as the DF and T operator takes excitations from it. One can choose non-DF reference state instead of the usual approximations and for a multi-reference method it is replaced by a linear combinations of determinants. In the single reference case, the operator is given by

$$T = \sum_i T_i, \tag{5.14}$$

where

$$T_1 = \sum_{a,p} t_a^p a_p^\dagger a_a, \tag{5.15}$$

$$T_2 = \frac{1}{(2!)^2} \sum_{a,b,p,q} t_{ab}^{pq} a_p^\dagger a_q^\dagger a_b a_a \tag{5.16}$$

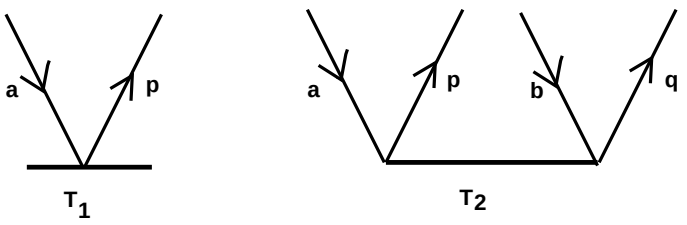

Figure 5.3: Diagrammatic representation of T operator.

and so on. The creation-annihilation operators for orbitals occupied in $|\Phi_o\rangle$ (core) are denoted as $a^\dagger,\ b^\dagger,\ c^\dagger$ ... and $a,\ b,\ c,$ ... and for unoccupied orbitals (virtuals) as $p^\dagger,\ q^\dagger,\ r^\dagger$ ... and $p,\ q,\ r$ .... The labels $i,\ j,\ k,\ l$ ... represents either core or virtual orbitals. These operators act on the reference state functions to give

$$T_1|\Phi_o\rangle = \sum_{p,a} t_a^p|\Phi_a^p\rangle, \tag{5.17}$$

$$T_2|\Phi_o\rangle = \sum_{p,q,a,b} \frac{1}{(2!)^2} t_{a,b}^{p,q}|\Phi_{a,b}^{p,q}\rangle = \sum_{p\geq q,a\geq b} t_{a,b}^{p,q}|\Phi_{a,b}^{p,q}\rangle \tag{5.18}$$

and so on, where $|\Phi_a^p\rangle$, $|\Phi_{a,b}^{p,q}\rangle$ are single and double excitations from $|\Phi_o\rangle$. Schematically the T operator can be represented as given in Fig. 5.3. Restricting T to just CC Doubles (CCD) [13, 21, 22] originally termed Coupled-Pair Many-Electron Theory (CPMET), [13] we get the CCD wave function as

$$|\Psi_{CCD}\rangle = e^{T_2}|\Phi_o\rangle = (1 + T_2 + T_2^2/2 + ...)|\Phi_o\rangle \tag{5.19}$$

where it includes disconnected quadruples given by T_2^2 and other higher excitations like hextuple. Considering T_1 and T_2 clusters, the CCSD [23] wave function takes the form

$$|\Psi_{CCSD}\rangle = e^{(T_1+T_2)}|\Phi_o\rangle. \tag{5.20}$$

Expanding the exponential part, we get

$$\begin{aligned} |\Psi_{CCSD}\rangle &= (1 + T_1 + T_2 + T_2^2/2 + T_1T_2 + T_1^2T_2 + ...)|\Phi_o\rangle \\ &= |\Psi_{CCD}\rangle + (T_1 + T_1^2/2 + T_1T_2 + T_1^2T_2/2 + ...)|\Phi_o\rangle. \end{aligned}$$

Here the wave function now includes the disconnected triple excitations T_1T_2 and also disconnected quadruple excitations $T_1^2T_2$ and many other excitations. To include connected triples we will have to consider CCSDT [24, 25, 26] wave function. If one

continues till T_N, where N is the number of electrons, we reach the exact or full CI limit, where

$$|\Psi_{FCI}\rangle = (1+C)|\Phi_o\rangle = (1+C_1+C_2+C_3+...C_N)|\Phi_o\rangle. \tag{5.21}$$

It is clear that at a given truncation of the respective operators defining CCM and CI, we expect the former to converge more rapidly than the latter due to its much greater inclusion of higher excitations.

5.2.2 Theoretical Details

5.2.2.1 Evaluation of Working Equations

The objective of a CC calculation is to formulate and compute various properties using the CC amplitudes t_a^p, $t_{a,b}^{p,q}$, etc. Let us consider the atomic Hamiltonian H_a which is an exact no-virtual pair Dirac-Couloumb Hamiltonian of the system as discussed by [27, 28], with the usual one- and two-particle electronic parts. Effects due to Breit, negative-energy states and radiation corrections are omitted in the present calculation which will have to be added later. The T amplitude with a superscript '0' is considered to be PNC unperturbed amplitudes. The equation we have to solve is the Schrödinger equation given by

$$H_a|\Psi_0\rangle = E_0|\Psi_0\rangle, \tag{5.22}$$

where

$$H_a = \sum_i T_i + \sum_{i<j} v_{ij}. \tag{5.23}$$

The matrix elements of T and v are given by

$$\langle i|T|j\rangle = \int \phi_i^\star(1) T_1 \phi_j(1) d\tau_1, \tag{5.24}$$

$$\langle ij|v|kl\rangle = \int\int \phi_i^\star(2)\phi_j^\star(2) v_{12} \phi_k(1)\phi_l(1) d\tau_1 d\tau_2, \tag{5.25}$$

where

$$T_i = c\alpha_i.p_i + c^2(\beta_i - 1) + V_{nuc}(i), \tag{5.26}$$

$$v_{ij} = \frac{1}{r_{ij}}. \tag{5.27}$$

Subtracting $\langle\Phi_0|H|\Phi_0\rangle$ from both sides, we get

$$(H_a - \langle\Phi_0|H|\Phi_0\rangle)|\Psi_0\rangle = (E - \langle\Phi_0|H|\Phi_0\rangle)|\Psi_0\rangle. \tag{5.28}$$

We know for any operator O the normal ordered operator O_N is defined as

$$O_N = O - \langle\Phi_0|O|\Phi_0\rangle. \tag{5.29}$$

Hence the above equation reduces down to

$$H_N|\Psi_0\rangle = \Delta E|\Psi_0\rangle, \tag{5.30}$$

where $\Delta E = E - E_0$ is the correlation energy. Substituting the exponential form of wave function for $|\Psi_0\rangle$ and multiplication by $e^{-T^{(0)}}$ to the left we get

$$e^{-T^{(0)}} H_N e^{T^{(0)}}|\Phi_0\rangle = \Delta E|\Phi_0\rangle. \tag{5.31}$$

Now the left hand side of the above equation can be written as a finite commutation series as,

$$e^{-T^{(0)}} H_N e^{T^{(0)}} = \bar{H}_N = \sum_{n=0}^{\infty} \frac{1}{n!}[H_N, T^{(0)}]^{(n)}, \tag{5.32}$$

where

$$[H_N, T^{(0)}]^{(n)} = [[H_N, T^{(0)}]^{(n-1)}, T^{(0)}]. \tag{5.33}$$

For n=0 the above reduces to

$$[H_N, T^{(0)}]^{(0)} = H_N$$

and for n=1

$$[H_N, T^{(0)}]^{(1)} = [H_N, T^{(0)}]$$

and so on. Using the above results Eq. 5.32 reduces to

$$\bar{H_N} = H_N + [H_N, T^{(0)}] + \frac{1}{2}[[H_N, T^{(0)}], T^{(0)}] + ... + \frac{1}{4}[[[[H_N, T^{(0)}], T^{(0)}], T^{(0)}], T^{(0)}]. \tag{5.34}$$

The series terminates after five fold terms since H_N contains at most two-particle operators. Since at least one operator in each T has to be contracted with one of the four creation-annihilation operators in the two-particle part of H_N, there can be only four T's. Also from the generalised Wicks theorem [2] and LCT [2] one can very well show that any commutator of two objects [29] (an arbitrary operator containing the same number of creation and annihilation operators standing inside a normal product) contains only contracted terms. Applying this idea to $[H_N, T^{(0)}]^{(1)}$, we get

$$[H_N, T^{(0)}]^{(1)} = [H_N, T^{(0)}] = \{\overbrace{H_N T^{(0)}}\} - \{\overbrace{T^{(0)} H_N}\}. \tag{5.35}$$

Here $\overbrace{\ \ }$ means that only connected terms are taken into account. Using the form of $T^{(0)}$ operator, it can be shown that $\{\overbrace{T^{(0)} H_N}\}$=0, since it contains $\overbrace{a_p^\dagger M}$ and/or $\overbrace{a_h M}$

where M is an arbitrary creation and annihilation operator for $p, h \in$ of reference state. More clearly,

$$\{\overbrace{a_p^\dagger M}\} = \langle\Phi_o|a_p^\dagger M|\Phi_o\rangle = 0, \tag{5.36}$$

since $a_p|\Phi_o\rangle = 0 \rightarrow \langle\Phi_o|a_p^{dagger} = 0$ and

$$\{\overbrace{a_h M}\} = \langle\Phi_o|a_h M|\Phi_o\rangle = 0 \tag{5.37}$$

since $a_h^\dagger|\Phi_o\rangle = 0 \rightarrow \langle\Phi_o|a_h = 0$. Using the above results one can write

$$[H_N, T^{(0)}]^{(1)} = [H_N, T^{(0)}] = \{\overbrace{H_N T^{(0)}}\} \tag{5.38}$$

and for

$$[H_N, T^{(0)}]^{(2)} = [[H_N, T^{(0)}], T^{(0)}] = \{\overbrace{\overbrace{H_N T^{(0)}} T^{(0)}}\} \tag{5.39}$$

and so on. In general we can write

$$[H_N, T]^{(n)} = \{\overbrace{\overbrace{H_N T^{(0)}} ... T^{(0)}}\}. \tag{5.40}$$

Generalising these considerations, the expression $e^{-T^{(0)}} H_N e^{T^{(0)}}$ may be formally written in the form of the so-called LCT as

$$e^{-T^{(0)}} H_N e^{T^{(0)}} = (H_N e^{T^{(0)}})_C. \tag{5.41}$$

Here the subscript C means that only connected diagrams are taken into account. Scalar multiplication from the left hand side by $\langle\Phi_0|$ in Eq. 5.31 gives correlation energy, given by

$$\langle\Phi_0|(H_N e^{T^{(0)}})_C|\Phi_0\rangle = \Delta E. \tag{5.42}$$

Projecting on the left by singly and doubly excited determinants with $T^{(0)}$ approximated to be only singles and doubles gives the corresponding one and two-particle CC equations as given by

$$\begin{aligned} \langle\Phi_a^p|(H_N e^{T^{(0)}})_C|\Phi_0\rangle &= 0, \\ \langle\Phi_{a,b}^{p,q}|(H_N e^{T^{(0)}})_C|\Phi_0\rangle &= 0, \end{aligned}$$

where the reference, singly and doubly excited determinants are defined as

$$\begin{aligned} |\Phi_o\rangle &= \frac{1}{\sqrt{N!}} det\{a, b, c ... N_c\}, \\ |\Phi_a^p\rangle &= \frac{1}{\sqrt{N!}} det\{0, b, c, ... N_c, p\}, \\ |\Phi_{a,b}^{p,q}\rangle &= \frac{1}{\sqrt{N!}} det\{0, 0, c, ... N_c, p, q\}. \end{aligned} \tag{5.43}$$

Here, N_c is the number of core orbitals or doubly occupied orbitals in the DF reference state.

5.2.2.2 Linear Approximation

Taking $T^{(0)} = T_1^{(0)} + T_2^{(0)}$ and the linear approximation

$$(H_N e^{T^{(0)}})_C = H_N + \widehat{H_N T^{(0)}}, \tag{5.44}$$

the singles and doubles equation reduces to

$$\begin{aligned} \langle \Phi_a^p | H_N + \widehat{H_N T_1^{(0)}} + \widehat{H_N T_2^{(0)}} | \Phi_0 \rangle &= 0, \\ \langle \Phi_{a,b}^{p,q} | H_N + \widehat{H_N T_1^{(0)}} + \widehat{H_N T_2^{(0)}} | \Phi_0 \rangle &= 0. \end{aligned}$$

On application of T_1 and T_2 operators on $|\Phi_o\rangle$ we get

$$\begin{aligned} \langle \Phi_a^p | H_N | \Phi_o \rangle + \langle \Phi_a^p | H_N | \Phi_b^s \rangle t_1 + \langle \Phi_a^p | H_N | \Phi_{b,c}^{s,t} \rangle t_2 &= 0, \\ \langle \Phi_{a,b}^{p,q} | H_N | \Phi_o \rangle + \langle \Phi_{a,b}^{p,q} | H_N | \Phi_c^t \rangle t_1 + \langle \Phi_{a,b}^{p,q} | H_N | \Phi_{cd}^{tu} \rangle t_2 &= 0. \end{aligned}$$

The above two equations reduces to CC equations of the form

$$\begin{aligned} H_{11} t_1 + H_{12} t_2 &= -H_{10}, \\ H_{21} t_1 + H_{22} t_2 &= -H_{20}, \end{aligned}$$

and they can be written as linear equation of the form $AT^{(0)} = -B$ as

$$\begin{pmatrix} H_{11} & H_{12} \\ H_{21} & H_{22} \end{pmatrix} \begin{pmatrix} t_1 \\ t_2 \end{pmatrix} = - \begin{pmatrix} H_{10} \\ H_{20} \end{pmatrix}. \tag{5.45}$$

5.2.2.3 Determination of Matrix Elements

In second quantised form, the Hamiltonian H can be written as

$$H = \sum_{i,j} T_{ij}^{(0)} a_i^\dagger a_j + \frac{1}{4} \sum_{ijkl} \langle ij||v||kl\rangle a_i^\dagger a_j^\dagger a_k a_l. \tag{5.46}$$

Using Wick's theorem, we can write the above Eq. 5.46 as

$$\begin{aligned} H &= \sum_{i,j} T_{ij}^{(0)} \{a_i^\dagger a_j\} + \sum_{i,j} T_{ij}^{(0)} \{\widehat{a_i^\dagger a_j}\} + \frac{1}{4} \sum_{ijkl} \langle ij||v||kl\rangle \{a_i^\dagger a_j^\dagger a_k a_l\} \\ &+ \frac{1}{4} \sum_{ijkl} \langle ij||v||kl\rangle [\{a_i^\dagger \overbrace{a_j^\dagger a_k} a_l\} + \{\overbrace{a_i^\dagger a_j^\dagger a_k} a_l\} + \{a_i^\dagger \overbrace{a_j^\dagger a_k a_l}\} \\ &+ \{\overbrace{a_i^\dagger a_j^\dagger a_k a_l}\} + \{\overbrace{a_i^\dagger \overbrace{a_j^\dagger a_k} a_l}\} + \{\overbrace{a_i^\dagger \overbrace{a_j^\dagger a_k} a_l}\}]. \end{aligned}$$

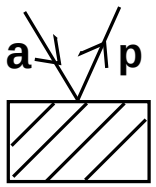

Figure 5.4: Form of the effective diagram which contributes to singles equation.

Using the contraction rules and Eq. 5.29, we get the normal ordered Hamiltonian as

$$\{H\} = H_N = \sum_{ij} T_{ij}^{(0)} \{a_i^\dagger a_j\} + \frac{1}{4}\langle ij|v|kl\rangle \{a_i^\dagger a_j^\dagger a_k a_l\}. \tag{5.47}$$

Similarly, any one electron operator can be written as

$$\{O\} = O_N = \sum_{ij} O_{ij} \{a_i^\dagger a_j\} \tag{5.48}$$

where i, j, k and l are all general orbitals. Similarly, the cluster operators $T_1^{(0)}$ and $T_2^{(0)}$ can also be written in normal ordered form as

$$T_1^{(0)} = \sum_{a,p} t_a^p \{a_p^\dagger a_a\}, \tag{5.49}$$

$$T_2^{(0)} = \sum_{a,b,p,q} \frac{1}{4} t_{a,b}^{p,q} \{a_p^\dagger a_q^\dagger a_b a_a\},, \tag{5.50}$$

where $a,\ b$ are core and $p,\ q$ are virtual orbitals. The normal ordered atomic Hamiltonian H_N can be graphically represented using the Goldstone diagrammatic rules [2]. The diagrammatic representation of single and two-particle part of H_N is given in Appendix A. Using Wick's theorem, all possible connected diagrams which are of our interest are considered. Here let us denote the one-particle operator part of H_N as H_o and the two-particle operator part as V_{es}.

(i) Evaluation of effective single-particle diagrams arising from H_{11}, H_{12}

We consider connected diagrams of the form as given in Fig. 5.4 which gives contribution to the singles equation. H_{11} term of the matrix equation is

$$H_{11} = \langle \Phi_a^p | H_N | \Phi_b^s \rangle. \tag{5.51}$$

This connects the reference state to the singly excited determinant by single and double contraction of $T_1^{(0)}$ and H_N which can be written as

$$H_{11} = \langle \Phi_o | a_a^\dagger a_p (H_o + V_{es}) a_s^\dagger a_b | \Phi_o \rangle, \tag{5.52}$$

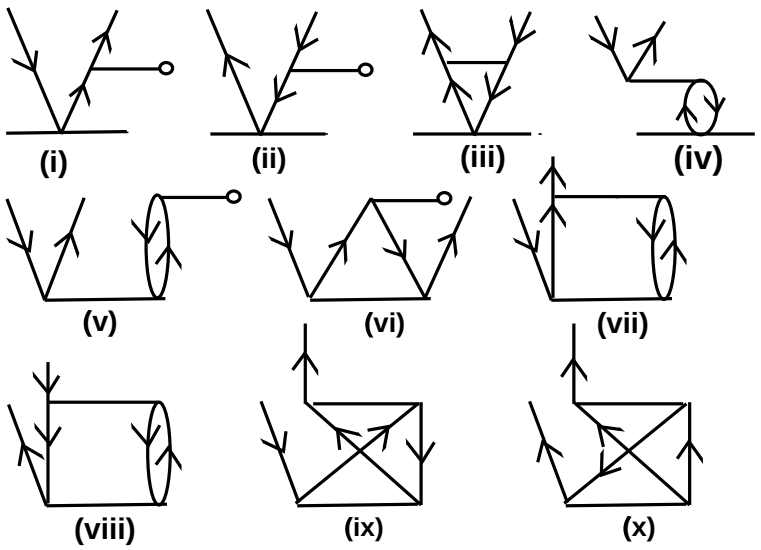

Figure 5.5: Diagrams which contribute to singles equation.

H_{12} term of the matrix equation is

$$H_{12} = \langle \Phi_a^p | H_N | \Phi_{bc}^{st} \rangle, \tag{5.53}$$

which can be written as

$$H_{12} = \langle \Phi_o | a_a^\dagger a_p (H_o + V_{es}) a_s^\dagger a_t^\dagger a_c a_b | \Phi_o \rangle. \tag{5.54}$$

This connects $T_2^{(0)}$ operator with H_N through double and triple contractions. H_{10} term in the right hand side of the matrix equation can connect the reference state with the singly excited state only through the one electron operator H_0. The two electron operator V_{es} can give only double excitation when it acts on the reference state. If the one-body operator of the Hamiltonian is DF operator then H_{10} is equal to zero due to the orthogonal nature of DF orbitals. Considering all possible contractions and keeping in mind to consider diagrams of the form given above we get 10 diagrams as drawn in Fig. 5.5. Here diagrams (i), (ii), (v) and (vi) are obtained by the contraction of the one-body operator H_0 with the $T_1^{(0)}$ and $T_2^{(0)}$ and the rest by the contraction with the two-body part given by V_{es}. If we use DF Hamiltonian then the diagrams (v) and (vi) will be zero due to the orthogonal nature of the DF orbitals.

(ii) Evaluation of effective two-particle diagrams arising from H_{21}, H_{22}

We consider diagrams of the form as given in Fig. 5.6 which contributes to the

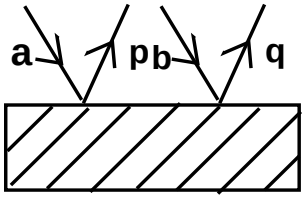

Figure 5.6: Form of the effective diagram which contributes to doubles equation.

doubles equation. H_{21} term is given by

$$H_{21} = \langle \Phi_{ab}^{pq} | H_N | \Phi_c^t \rangle. \tag{5.55}$$

Expanding them, we get

$$H_{21} = \langle \Phi_o | a_a^\dagger a_b^\dagger a_p a_q (H_o + V_{es}) a_t^\dagger a_c | \Phi_o \rangle, \tag{5.56}$$

which connects the reference state to the doubly excited state through single contraction of V_{es} with $T_1^{(0)}$. The one-body part of H_N does not contribute since it cannot connect the reference state with the doubly excited state. H_{22} term of the matrix equation is given by

$$H_{22} = \langle \Phi_{ab}^{pq} | H_N | \Phi_{cd}^{st} \rangle \tag{5.57}$$

and can be further simplified as

$$H_{22} = \langle \Phi_o | a_a^\dagger a_b^\dagger a_p a_q (H_o + V_{es}) a_s^\dagger a_t^\dagger a_c a_d | \Phi_o \rangle, \tag{5.58}$$

which connects the reference state with the doubly excited state through double contractions between $T_2^{(0)}$ and the one and two-body parts of the Hamiltonian. The diagrams which contribute to doubles equation through H_{21} and H_{22} terms are given in Fig. 5.7. H_{20} can connect the reference state with the doubly excited state only with V_{es} since H_0 cannot connect the reference state with the doubly excited state.

5.2.2.4 Non-Linear Approximation

Considering only singles and doubles, the non-linear CC amplitude equations take the form

$$\langle \Phi_a^p | \bar{H}_N | \Phi_0 \rangle = 0 \tag{5.59}$$

$$\langle \Phi_{ab}^{pq} | \bar{H}_N | \Phi_0 \rangle = 0, \tag{5.60}$$

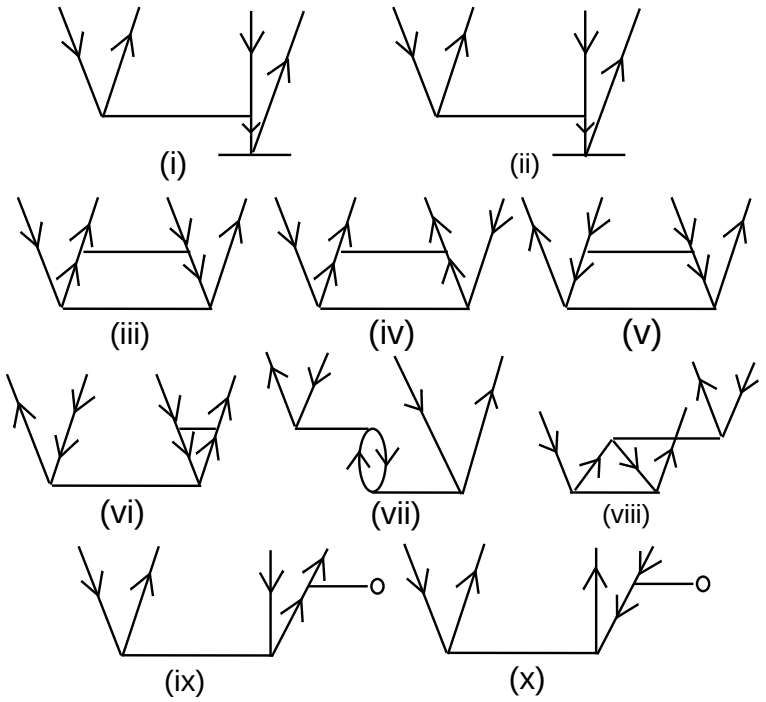

Figure 5.7: Diagrams which contribute to doubles equation.

where $\bar{H}_N$ is given by the Eq. 5.34. The possible terms from the expansion of $\bar{H}_N$, for each of the terms are

$$\begin{aligned} TT &= \mathbf{T_1^2 + 2T_1T_2 + T_2^2} \\ TTT &= \mathbf{T_1^3 + 3T_1^2T_2} + 3T_{11}T_2^2 + T_2^3 \\ TTTT &= \mathbf{T_1^4} + 4T_1^3T_2 + 6T_{11}^2T_2^2 + 4T_{11}T_2^3 + T_2^4. \end{aligned}$$

From the following terms only the terms in boldface give contribution. Rest of the terms will not give connected diagrams of the type given in Fig. 5.4 and Fig. 5.6. Contraction of above terms in boldface give rise to 54 diagrams which contribute to non-linear part of CC calculations. The typical diagrams are given in Fig. 5.8. After the contraction of the operators is carried out, the cluster equation can be written as a matrix equation of the kind

$$A + B(T).T = 0, \tag{5.61}$$

where A is a constant vector which consists of the elements $\langle\Phi^*|\bar{H}|\Phi\rangle$ and T is a vector of the excitation amplitudes. The matrix $B(T)$ itself depends on the cluster amplitude so that the above equation has to be solved in an iterative procedure.

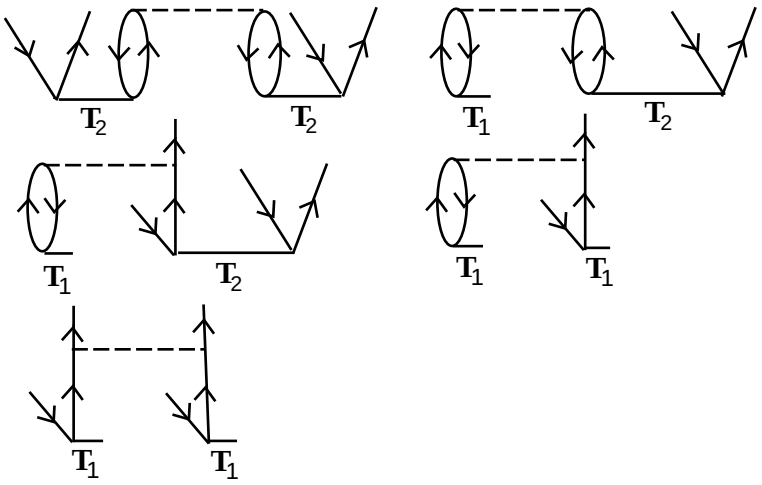

Figure 5.8: Typical diagrams representing the non-linear terms.

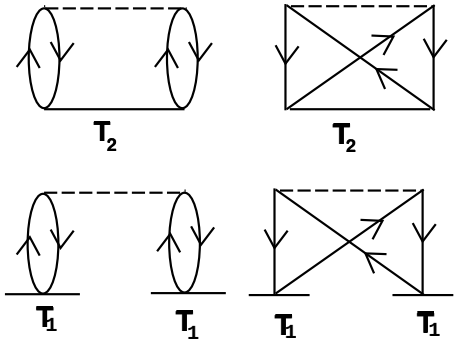

Figure 5.9: Diagrams contributing to correlation energy.

Using the linear and non-linear T amplitudes, the correlation energy can be obtained and the diagrams contributing to this property are given in Fig. 5.9.

5.3 Application of CCM to Open-Shell Atoms

In this case we consider excitations from core and valence to virtual orbitals where valence orbital is designated as 'v'. In the single reference case, the operator which brings in the excitation from core and valence to virtual is given by

$$S = \sum_i S_i, \tag{5.62}$$

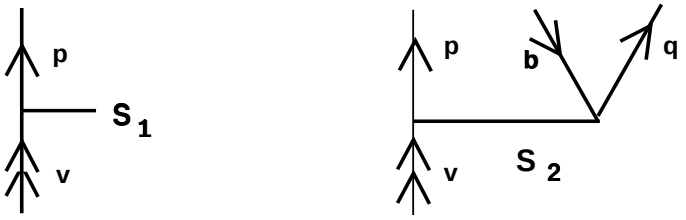

Figure 5.10: Diagrammatic representation of S operator.

where

$$\begin{aligned} S_1 &= \sum_p s_v^p a_p^\dagger a_v, \\ S_2 &= \frac{1}{(2!)^2} \sum_{a,p,q} s_{va}^{pq} a_p^\dagger a_q^\dagger a_a a_v. \end{aligned}$$

Schematically the S operator can be represented as given in Fig. 5.10.

5.3.1 Solving $S_1^{(0)}$ and $S_2^{(0)}$ Coupled Equations

In our CC calculations, we use the DF reference state corresponding to N−1 electron closed-shell configuration, then add one electron to the k^{th} virtual orbital and obtain the N electron system on which calculations are carried out. The addition of valence electron to the k^{th} virtual orbital of the reference state can therefore be written as

$$|\Phi_k^N\rangle = a_k^\dagger |\Phi_0\rangle. \tag{5.63}$$

Any general state can be written in open-shell CCM [2]as

$$|\Psi_k^N\rangle = \{e^{S_k^{(0)}}\} e^{T^{(0)}} |\Phi_k^N\rangle. \tag{5.64}$$

Due to normal ordering and the presence of particle annihilation operator

$$\{e^{S_k^{(0)}}\} = 1 + S_k^{(0)}.$$

Hence

$$|\Psi_k^N\rangle = (1 + S_k^{(0)}) e^{T^{(0)}} |\Phi_k^N\rangle.$$

Carrying out mathematical operations similar to the one used earlier on $T^{(0)}$ operators, we obtain an equation for the Ionisation Potential (IP) and another one for the CC amplitudes. The equation for the evaluation of IP is

$$\langle \Phi_k^N | \bar{H}_N (1 + S_k^{(0)}) | \Phi_k^N \rangle = \Delta E_k \tag{5.65}$$

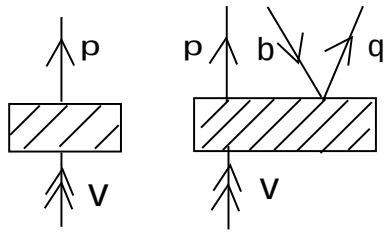

Figure 5.11: Form of the effective diagram contributing to singles and doubles equation.

and the equation for CC amplitudes is obtained by projecting on the singly and doubly excited determinants which leads to

$$\langle \Phi_k^{\star,N} | \bar{H}_N (1 + S_k^{(0)}) | \Phi_k^N \rangle = \Delta E_k^N \langle \Phi_k^{\star,N} | S_k^{(0)} | \Phi_k^N \rangle, \tag{5.66}$$

where ΔE_k^N is the difference between the energy of the closed-shell state $|\Psi_{N-1}\rangle$ and the single valence state $|\Psi_k^N\rangle$ and in comparison with the Eq. 5.65 IP is the negative of ΔE_k^N. In other words it is the energy which must be given to an electron to promote it to the k^{th} virtual orbital. Once the IPs are computed, the Excitation Energies (EE) are obtained by finding the difference between the IPs of the valence (6s) and appropriate virtual orbitals. The equation for CC amplitudes Eq. 5.66 is non-linear, since ΔE_k itself depends on the $S^{(0)}$ amplitudes and so an iterative procedure is needed for its solution. Rearranging the terms in Eq. 5.66 we get

$$\begin{aligned} \langle \Phi_k^{\star,N+1} | \bar{H}_N S_k^{(0)} | \Phi_k^{N+1} \rangle = -\langle \Phi_k^{\star,N+1} | \bar{H}_N | \Phi_k^{N+1} \rangle + \\ \langle \Phi_k^{\star,N+1} | S_k^{(0)} | \Phi_k^{N+1} \rangle \langle \Phi_k^{N+1} | \bar{H}_N (1 + S_k^{(0)}) | \Phi_k^{N+1} \rangle, \end{aligned} \tag{5.67}$$

where $\bar{H}_N = H_N + \overbrace{H_N T^{(0)} + ...}$. The diagrams arising from $\bar{H}$ can be categorised according to the number and type of open lines. Let us denote H to be the core type and P to be the virtual type. Then the possible terms which can give rise to effective single or double dressed Hamiltonian are PP, PH, HP, HH, HH-HH, PP-PP, PH-PP, HH-HP, PH-PH, PH-HP, PP-HP and PH-HH. The effective diagrams which contribute to the singles and doubles equation are given in Fig. 5.11. The effective diagrams of the form given in Fig. 5.11 which contribute to the left hand side of the Eq. 5.67 are given in Fig. 5.12. We consider the initial guess the same way as it was done for the closed-shell part by taking $S_1^{(0)}$ to be zero and $S_2^{(0)}$ to be the two electron matrix elements divided by the energy denominator. Then one constructs a matrix equation of the form

$$BS^{(0)} = -A, \tag{5.68}$$

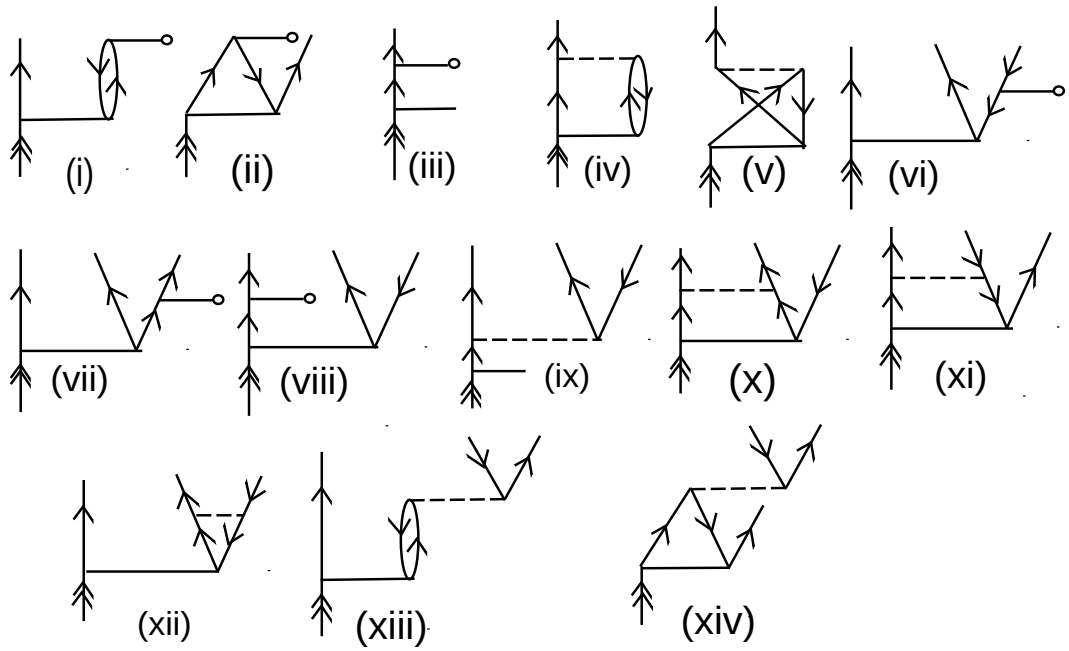

Figure 5.12: Diagrams contributing to singles and doubles equation (left hand side of Eq. 5.67).

where $BS^{(0)} = \langle \Phi_k^{\star,N+1} | \bar{H}_N S_k^{(0)} | \Phi_k^{N+1} \rangle$ and $A = \langle \Phi_k^{\star,N+1} | \bar{H}_N | \Phi_k^{N+1} \rangle$. This is done by taking the second term in the right hand side as zero. We solve for $S^{(0)}$ from the above matrix equation and then construct a new A which is the sum of the two terms in the right hand side of Eq. 5.67. This procedure is repeated untill self consistency is achieved. Once it is obtained we find the approximate triples got using T_2 and $S_2^{(0)}$ defined as

$$S_{abk}^{pqr} = \frac{\widehat{VT}_2 + \widehat{VS}_2}{\epsilon_a + \epsilon_b + \epsilon_k - \epsilon_p - \epsilon_q - \epsilon_r}\,, \tag{5.69}$$

where S_{abk}^{pqr} represents the amplitudes for the simultaneous excitation of one electron from orbital a, b, k to p, q, r, $\widehat{VS^{(0)}}$ is the contraction of all creation/annihilation operators and ϵ_i orbital energy of the i^{th} orbital. This contribution is then added to the energy obtained using singles and doubles. Typical diagrams which contribute to such an effect are given in Fig. 5.13. The application on singly ionised barium and the comparison with experimental numbers for IPs and EEs are described at the end of this chapter.

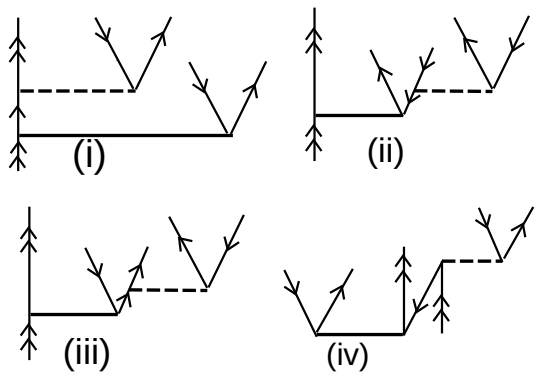

Figure 5.13: Typical diagrams representing the approximate triples diagrams: (i), (ii), (iii) gives the $VS_2^{(0)}$ contributions and (iv) gives the VT_2 contributions.

5.4 Application of CCM to PNC in Atoms

We propose two different approaches to PNC using CCM. They are as follows:

1. Sum over intermediate states approach in which we consider all order contributions from bound states as well as the lowest order contributions from bound core and continuum virtual orbitals.

2. Mixed parity approach in which we compute all order CC amplitudes for closed and open-shell systems with and without PNC as the perturbation and construct $E1PNC$ with one order in PNC.

In this thesis, we present results using only the first approach. The theoretical details related to the second approach is also described below. Electric dipole transition amplitude induced by the NSI and NSD weak interactions can be expressed as

$$E1PNC = \frac{\langle \tilde{\Psi}_f \mid D \mid \tilde{\Psi}_i \rangle}{\sqrt{\langle \tilde{\Psi}_i \mid \tilde{\Psi}_i \rangle}\sqrt{\langle \tilde{\Psi}_f \mid \tilde{\Psi}_f \rangle}}, \tag{5.70}$$

where $\mid \tilde{\Psi}_i \rangle$ and $\mid \tilde{\Psi}_f \rangle$ are the initial and final atomic states of mixed parity given by

$$|\tilde{\Psi}_i\rangle = |\Psi_i^{(0)}\rangle + |\Psi_i^{(1)}\rangle,$$
$$|\tilde{\Psi}_f\rangle = |\Psi_f^{(0)}\rangle + |\Psi_f^{(1)}\rangle.$$

Here $|\Psi^{(0)}\rangle$ are the eigenfunctions of the atomic Hamiltonian and $|\Psi^{(1)}\rangle$ is the first order perturbed functions due to NSI/NSD PNC.

5.4.1 Evaluation of $E1PNC$ using the Sum over Intermediate States

Taking only one order in perturbation and using first order perturbation theory the expression for $E1PNC$ reduces to

$$E1PNC = \frac{1}{\left(\sqrt{\langle\Psi_i^{(0)}|\Psi_i^{(0)}\rangle}\sqrt{\langle\Psi_f^{(0)}|\Psi_f^{(0)}\rangle}\right)}\sum_I \left(\frac{\langle\Psi_f^{(0)}|D|\Psi_I^{(0)}\rangle\langle\Psi_I^{(0)}|\mathrm{PNC}|\Psi_i^{(0)}\rangle}{(E_i - E_I)} + \frac{\langle\Psi_f^{(0)}|H_{\mathrm{PNC}}|\Psi_I^{(0)}\rangle\langle\Psi_I^{(0)}|D|\Psi_i^{(0)}\rangle}{(E_f - E_I)}\right).$$

Using CCM one can write these states as

$$|\ \Psi_i\rangle = e^T\{e^{S_i}\}\ |\ \Phi_i\rangle,$$

$$|\ \Psi_f\rangle = e^T\{e^{S_f}\}\ |\ \Phi_f\rangle,$$

$$|\ \Psi_I\rangle = e^T\{e^{S_f}\}\ |\ \Phi_I\rangle.$$

In the first approach using $T^{(0)}$ and $S^{(0)}$ cluster amplitudes, one constructs all order dipole and PNC matrix elements for various intermediate bound $p_{1/2,3/2}$ orbitals. In this case, we have 3 bound p virtual orbitals starting from $6p$ for the basis that we have choosen. The ASFs are

$$\begin{aligned} |\Psi_i\rangle &= |5p^6 6s_{1/2}\rangle, \\ |\Psi_f\rangle &= |5p^6 5d_{3/2}\rangle, \\ |\Psi_i\rangle &= |5p^6 np_{1/2,3/2}\rangle, n = 6,7,8. \end{aligned}$$

5.4.2 Evaluation of $E1PNC$ using the Mixed Parity Approach

In the second approach, using $T^{(0)}, S^{(0)}, T^{(1)}$ and $S^{(1)}$ amplitudes one constructs $E1PNC$ with the constraint that only one order in PNC is allowed. Here we denote the T and S amplitudes with a superscript '1' to consider them as PNC perturbed. We present below the details regarding the computation of the PNC CC amplitudes.

5.4.2.1 Solving $T_1^{(1)}$ and $T_2^{(1)}$ Coupled Equations

We consider H_{PNC} as the perturbation to the closed-shell atomic Hamiltonian and hence the total Hamiltonian is

$$H = H_a^0 + \lambda H_{\mathrm{PNC}}, \tag{5.71}$$

where the ground state satisfies the equation

$$H_a^0|\Psi_0\rangle = E_0|\Psi_0\rangle, \tag{5.72}$$

where E_0 is the reference state energy. Using CCM one can write the ground state wave function as

$$|\Psi_0\rangle = e^T|\Phi_0\rangle, \tag{5.73}$$

where $|\Phi_0\rangle$ is the reference state. Due to the presence of $H_{\rm PNC}$ operator, the wave function will have perturbed and unperturbed PNC parts given by

$$|\,\tilde{\Psi}\rangle = e^{\tilde{T}}\,|\,\Phi_0\rangle, \tag{5.74}$$

where $\tilde{T} = T^{(0)} + \lambda T^{(1)}$. Since PNC scales as G_F, we consider terms that are linear in λ. Projection with excited state determinants in the Schrödinger equation with the above substitutions gives the perturbed cluster amplitudes as

$$\langle\Phi^\star\,|\,(\bar{H}_a - E_0)T^{(1)}\,|\,\Phi_o\rangle = -\langle\Phi^\star\,|\,\bar{H}_{\rm PNC}\,|\,\Phi_0\rangle, \tag{5.75}$$

where $\bar{H}_a^0 = e^{-T^{(0)}}H_a^0 e^{T^{(0)}}$ and $\bar{H}_{\rm PNC} = e^{-T^{(0)}}H_{\rm PNC}e^{T^{(0)}}$. The diagrams which contribute to the left hand side of the above equation are given in Fig. 5.14.

5.4.2.2 Solving $S_1^{(1)}$ and $S_2^{(1)}$ Coupled Equations

We consider again $H_{\rm PNC}$ to be the perturbation to the open-shell atomic Hamiltonian and the procedure is followed as done for the PNC unperturbed part by taking one order of PNC in the equations. The total Hamiltonian is

$$H = H_a + \lambda H_{\rm PNC}, \tag{5.76}$$

where the PNC unperturbed part satisfies the equation given by

$$H_a|\Psi_k\rangle = E_k|\Psi_k\rangle, \tag{5.77}$$

where E_k is the energy of the k^{th} excited state. Considering the perturbation in wave function we get

$$|\,\tilde{\Psi}\rangle = e^{\tilde{T}}\{e^{\tilde{S}}\}\,|\,\Phi_k\rangle \tag{5.78}$$

where $\tilde{T} = T^{(0)} + \lambda T^{(1)}$ and $\tilde{S} = S^{(0)} + \lambda S^{(1)}$. Here $|\Phi_k\rangle$ is the k^{th} excited reference state. Applying these on the Schrödinger equation, we get

$$(H_a+\lambda H_{\rm PNC})e^{T^{(0)}}(1+\lambda T^{(1)})(1+S^{(0)}+\lambda S^{(1)})\,|\,\Phi_k\rangle = E_k e^{T^{(0)}}(1+\lambda T^{(1)})(1+S^{(0)}+\lambda S^{(1)})\,|\,\Phi_k\rangle. \tag{5.79}$$

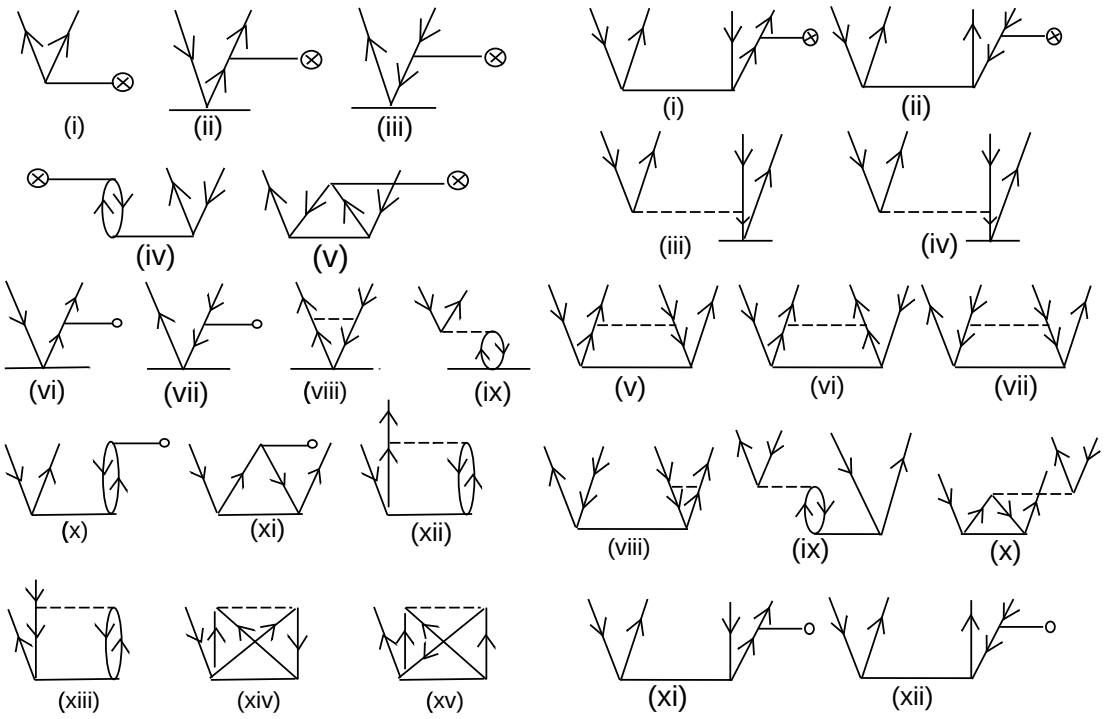

Figure 5.14: Diagrams contributing to the evaluation of $T^{(1)}$ for singles and doubles equation.

Taking only one order in PNC we get the equation of the form

$$\begin{aligned}(\bar{H}_a - E_k^{(0)})S^{(1)} \mid \Phi_k\rangle &= -(\bar{H}_{\rm PNC} + \bar{H}_{\rm PNC}S^{(0)}) - (\bar{H}_a - E_k^{(0)})T^{(1)} \\ &- (\bar{H}_a - E_k^{(0)})T^{(1)}S^{(0)} \mid \Phi_k\rangle,\end{aligned} \tag{5.80}$$

where

$$\begin{aligned}\bar{H}_a &= e^{-T^{(0)}} H_a e^{T^{(0)}}, \\ \bar{H}_{\rm PNC} &= e^{-T^{(0)}} H_{\rm PNC} e^{T^{(0)}}.\end{aligned}$$

Projection by the single and double excited determinants gives the perturbed amplitudes as

$$\begin{aligned}\langle\Phi_k^\star \mid (\bar{H}_a - E_k^{(0)})S^{(1)} \mid \Phi_k\rangle &= -\langle\Phi_k^\star \mid (\bar{H}_{\rm PNC} + \bar{H}_{\rm PNC}S^{(0)}) \\ &- (\bar{H}_a - E_k^{(0))}T^{(1)} \mid \Phi_k\rangle - (\bar{H}_a - E_k^{(0)})T^{(1)}S^{(0)} \mid \Phi_k\rangle.\end{aligned} \tag{5.81}$$

The effective diagrams contributing to the right hand side of the above equation is similar to the diagrams contributing to the PNC unperturbed open-shell part but with an additional one order in PNC in any of the vertex. The left hand side of

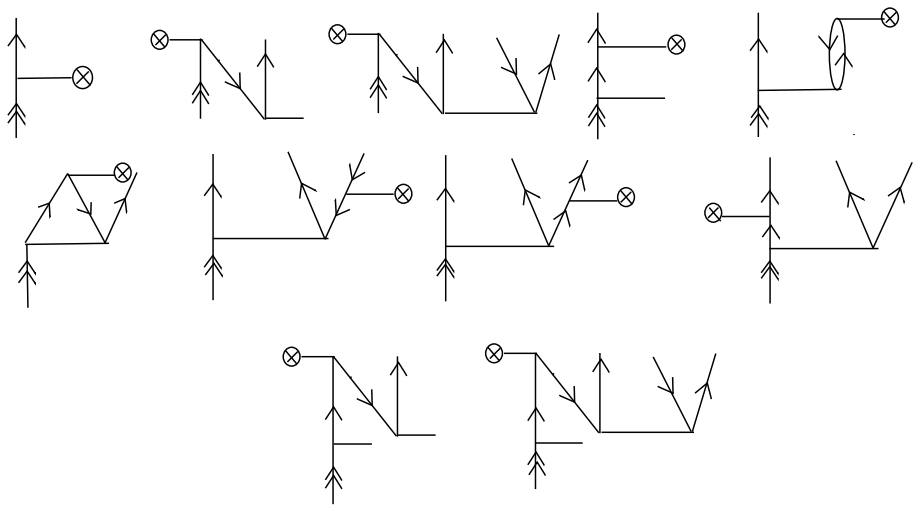

Figure 5.15: Diagrams contributing to the evaluation of right hand side of the $S^{(1)}$ determining equations.

the above equation gives rise to 14 diagrams as shown in Fig. 5.12. The diagrams contributing to the right hand side of the Eq. 5.82 consisting of $\bar{H}_{\rm PNC}$ and $\bar{H}_{\rm PNC}S^{(0)}$ are given in Fig. 5.15.

5.4.2.3 Evaluation of $E1PNC$ using $T^{(0)}, T^{(1)}, S^{(0)}$ and $S^{(1)}$ CC amplitudes

Substituting the form of the CC wave function constructed using both PNC perturbed and unperturbed T and S CC amplitudes, $E1PNC$ given in Eq. 5.70 takes the form

$$E1PNC = \frac{\langle\Phi_f^{(0)}|e^{\{\tilde{S}_f^\dagger\}}e^{\tilde{T}^\dagger}De^{\tilde{T}}e^{\{\tilde{S}_i\}}|\Phi_i^{(0)}\rangle}{\sqrt{\langle\Psi_i^{(0)}|\Psi_i^{(0)}\rangle}\sqrt{\langle\Psi_f^{(0)}|\Psi_f^{(0)}\rangle}}, \tag{5.82}$$

where out of 4 amplitudes (2 pertaining to the initial and 2 to the final state) at least one of the amplitudes should have one order of PNC, in order to have non-zero electric dipole transition between the states $|\Psi_i\rangle$ and $|\Psi_f\rangle$. In the case of Ba^+,

$$|\Psi_i\rangle = |5p^6 6s_{1/2}\rangle \text{ and } |\Psi_f\rangle = |5p^6 5d_{3/2}\rangle. \tag{5.83}$$

The T operator produces excitations from the core orbitals which are filled upto $5p^6$ and the S operator produces excitations from the valence and core orbitals. In the above case $6s$ and $5d$ are considered as valence orbitals. Hence for $E1PNC$, diagrams of the form given by Fig. 4.2 in Chapter 4 are considered. Some of the typical diagrams of the form given in Fig. 4.2 are given in Fig. 5.16.

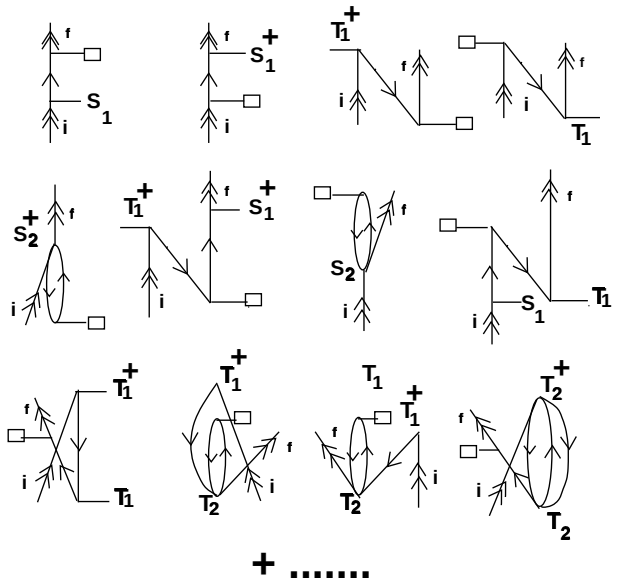

Figure 5.16: Typical diagrams contributing to $E1PNC$.

5.5 Computation of all Order Matrix Elements for Various Properties

In a PNC experiment, measurement of the electric dipole transition between states of same nominal parity induced by weak interaction is sought after. These amplitudes are products of two factors: a scale factor and an atomic electric dipole matrix element. To determine the weak-interaction scale factor in atomic physics experiments, one must first have reliable values for the associated electric dipole matrix elements. Accurate calculations of these matrix elements are difficult for several reasons. The electric dipole operator samples the atomic wave function at large distances from the nucleus. Whereas the weak interactions responsible for the non-zero values of the matrix elements are predominant near the nucleus. Therefore wave functions accurate at both large and small radii are required [30] for an accurate calculation. Hence, we need to check the accuracy of these all order wave functions at large and small radii by evaluating properties which mimic such a situation. For example, calculation of all order electric dipole matrix elements for various bound to bound transitions using all order CC amplitudes is a good check of these wave functions at large radii due to it's 'r' dependence. One can also evaluate electric dipole transition amplitude and lifetime of the states which puts stringent checks on the wave functions at large radii. Similarly hyperfine matrix elements are very sensitive to small radii and hence

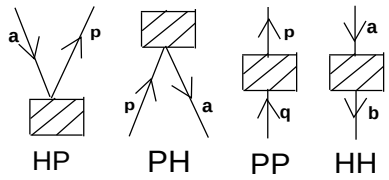

Figure 5.17: Form of effective $\bar{O}$ one-body diagrams.

evaluation of magnetic hyperfine constant (A) is a check of the all order wave functions near the nuclear region. Here in this section, we discuss the formulation for evaluating electric dipole, lifetime and magnetic hyperfine constant matrix elements. CC formulation has been used to compute some of the properties mentioned above by various authors and groups [31, 32, 33, 34, 35]. Blundell et al. have computed all order dipole and PNC matrix elements for caesium using linearised CCSD and approximate triples which has been used in the computation of $E1PNC$ using sum over intermediate states [36]. For Ba^+ we have used such an approach for the calculation of $E1PNC$. Solving the perturbed T and S amplitudes will be done as the next step of our work and only formulation is given in this thesis. Any general state can be written in CCM as given in Eq. 5.64 using T and S CC amplitudes. Here our aim is to compute various matrix elements pertaining to different properties sandwiched between the CC wave functions. If we consider O to be a general single-particle operator, then the all order matrix element of the operator O between an initial and final state is given by [37]

$$\langle O\rangle = \frac{\langle\Phi_f^{(0)}|e^{\{S_f^\dagger\}}e^{T^\dagger}\hat{O}e^{T}e^{\{S_i\}}|\Phi_i^{(0)}\rangle}{\sqrt{\langle\Psi_f^{(0)}|\Psi_f^{(0)}\rangle}\sqrt{\langle\Psi_f^{(0)}|\Psi_f^{(0)}\rangle}}. \tag{5.84}$$

Here we first evaluate the quantity $e^{T^\dagger}Oe^{T} = \bar{O}$ which can be expanded using Hausdorff expansion [38]. We consider only effective one-body diagrams of the kind given in Fig. 5.17, where P refers to virtuals and H refers to core orbitals. Typical one-body PP diagrams are given in Fig. 5.18. Same kind of diagrams can be drawn for other types designated as HH, PH and HP. Effective two-body diagrams are not taken into consideration for the present computation. These effective one-body operators are stored in a file and later read when they are sandwiched between the S operators. Depending on the quantity which we are interested in, the initial and final states can be different like in the case of electric dipole transition amplitude or same as in the case of the hyperfine constant. In the Eq. 5.84, the numerator consists of terms $\langle f|\bar{O}|i\rangle$, $\langle f|[S^\dagger\bar{O}]_c|i\rangle$, $\langle f|[\bar{O}S]_c|i\rangle$ and $\langle f|[S^\dagger\bar{O}S]_c|i\rangle$. The possible diagrams from the

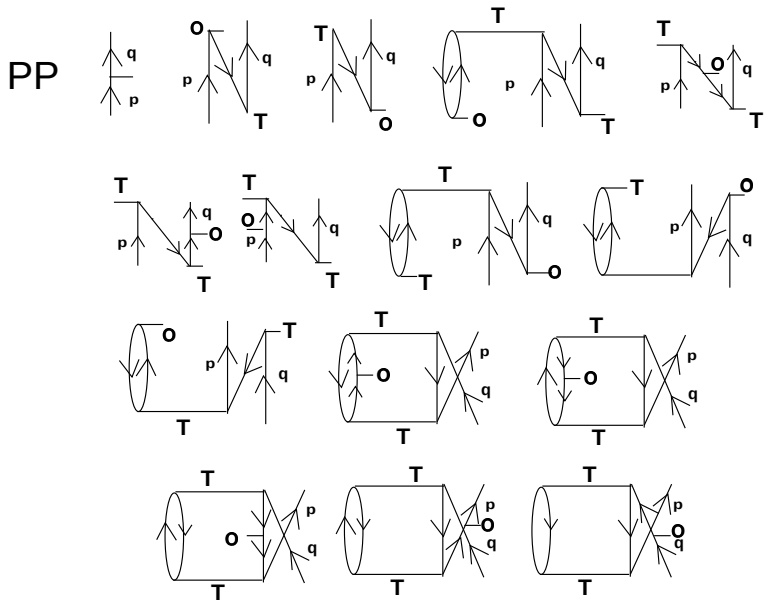

Figure 5.18: Typical effective one-body diagrams ($\bar{O}$)for a one-body operator.

above terms are given in Fig. 5.19. The denominator in the Eq. 5.84 takes the form

$$N^2 = \langle\Phi_0|a_k\{1+S_k^\dagger\}^\dagger(1+T^\dagger+[T^\dagger T]_c+...)\{1+S_k\}a_k^\dagger|\Phi_o\rangle, \tag{5.85}$$

where 'c' denotes completely connected diagrams. The effect of this denominator is to cancel disconnected terms from the numerator. This cancellation is complete for closed-shells and it has been shown by Blundell et al. [39] that for the single valence states there is a residual normalisation factor given by

$$\left[\frac{1}{(1+\sqrt{\langle\Psi_f|\Psi_f\rangle})(1+\sqrt{\langle\Psi_i|\Psi_i\rangle})}-1\right]. \tag{5.86}$$

Hence, we multiply the above factor by the contribution from various other terms which will be described when we discuss the application on various different properties. The possible diagrams given in Fig. 5.19 can be classified according to their effects as lowest order, RPA correction, Bruckner correction, structural radiation correction and the correction due to the normalisation in the denominator. A very elaborate description of the above types of corrections with the associated diagrams are given in the paper by Blundell et al. [40].

The T part of Eq. 5.85 gives rise to possible diagrams of the type PP, HP, PH and HP as shown in Fig. 5.17. This on further connecting with the S operator leads to the same kind of diagrams shown in Fig. 5.19 with the open lines denoted by v

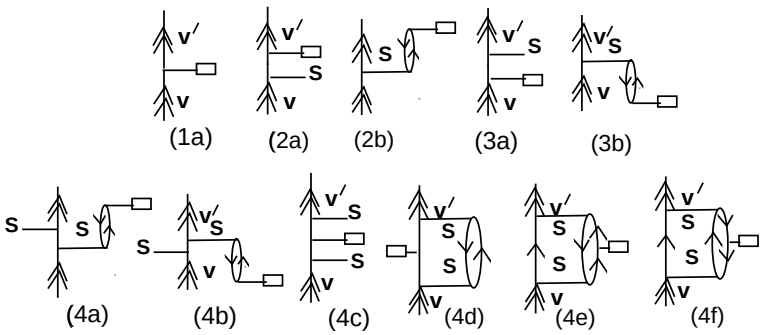

Figure 5.19: Diagrams contributing to the numerator of Eq. 5.84 where $\bar{O}$ is sandwiched between the S operators.

and v' being same and with the $\bar{0}$ interchanged by the connected effective one-body T part.

5.5.1 Electric Dipole/Quadrapole Matrix Elements

The single-particle matrix elements in length form is calculated in atomic units as

$$u_{mn} = C^L(m,n) \int dr r^L [P_m(r)P_n(r) + Q_m(r)Q_n(r)], \tag{5.87}$$

where

$$C^L(m,n) = (-1)^{j_m+1/2}\sqrt{2j_m+1}\sqrt{2j_n+1}\begin{pmatrix} j_m & L & j_n \\ \frac{1}{2} & 0 & -\frac{1}{2} \end{pmatrix}. \tag{5.88}$$

Here $L = 1$ for dipole and $L = 2$ for quadrapole transitions.

5.5.2 Lifetime of the States

The following formulae [41] are used for calculation of the transition probabilities:

$$A_{E1} = \frac{(2.0261 \times 10^{18})S_{E1}}{g_k \lambda^3} \tag{5.89}$$

and

$$A_{E2} = \frac{(1.1199 \times 10^{18})S_{E2}}{g_k \lambda^5}, \tag{5.90}$$

where λ is the transition wavelength in AA, g_k is the $(2J+1)$ degeneracy of the upper level, S_{E1} and S_{E2} are the E1 and E2 line strength in atomic units ea_o and ea_o^2. This

gives the transition probability in the units of $\sec^{-1}$. Hence, lifetime of the upper level is the sum of the inverse of the transition probabilities to all possible lower levels in seconds.

5.5.3 Hyperfine Constant (A)

Hyperfine interaction is located in the vicinity of the nucleus, just as the weak interaction. Therefore hyperfine constant calculations could give an indication of the accuracy of the parity-violating effects. The relativistic hyperfine Hamiltonian is given by

$$H_{hfs} = \sum_k M^{(k)}.T^{(k)}, \tag{5.91}$$

where $M^{(k)}$ and $T^{(k)}$ are spherical tensor operators of rank k, representing the nuclear and electronic parts, respectively. The hyperfine matrix element in the single-particle level is given by

$$\langle \kappa m|t_q^{(1)}|\kappa' m'\rangle = -\langle -\kappa m|C_q^{(1)}|\kappa' m'\rangle(\kappa+\kappa')\int r^{-2}(P_\kappa Q_{\kappa'} + Q_\kappa P_{\kappa'})dr, \tag{5.92}$$

where

$$\langle \kappa m|C_q^{(1)}|\kappa' m'\rangle = (-1)^{j-m}\begin{pmatrix} j & k & j' \\ -m & q & m' \end{pmatrix}\langle \kappa||C(1)||\kappa'\rangle \tag{5.93}$$

and the reduced matrix element is given in Eq. 5.88 with rank equal to 1.

5.5.4 $E1PNC$: Dipole and PNC NSI Matrix Elements

For the determination of $E1PNC$ using sum over intermediate states, we need to have all order dipole and PNCNSI matrix elements to be computed to very high accuracy. The single-particle matrix element for Dipole and PNCNSI are described previously in Chapter 2 of the thesis. Even though PNC matrix elements in single-particle level are non-zero only between $s_{1/2}$ and $p_{1/2}$ orbitals due to correlation one can have non-zero P$\bar{\text{N}}$C between any orbital other than j=1/2. For the determination of $\bar{D}$ and P$\bar{\text{N}}$C matrix elements we give appropriate parity considerations and the values are stored in a file and later read to compute the diagrams given in Fig. 5.19. Here we compute all order dipole and PNC matrix elements separately and multiply them with the appropriate energy denominator and normalisation to get $E1PNC$ using sum over the intermediate states method. The contribution from core states and the continuum states are considered at the DF level. Blundell et.al., [36] have done an all order calculation for caesium for the intermediate bound virtual orbitals. The details of our calculation will be described in Section 5.7.5.

5.6 Computational Details

5.6.1 Angular Reduction and Selection Rules for CC Matrix Elements

While computing the matrix elements the relativistic notation of the two component orbitals will be used. The expressions are given in Chapter 2. The presence of spherical symmetry in the atomic many-particle Hamiltonian facilitates the reduction of the DF and the CC matrix elements solely to radial integrals multiplied by some constant factors. The reduction of the angular part greatly simplifies the computational complexity of both the DF and post-DF calculations. Here we make use of a graphical method of the angular momentum adaptation scheme, popularly known as the JLV scheme [42]. The angular reduction scheme of the DF equation can be obtained elsewhere [43].

In the 'jm' basis, two-particle Couloumb operator $\frac{1}{r_{12}}$ is expressed as

$$\begin{aligned}\langle ab|\frac{1}{r_{12}}|cd\rangle &= \sum_{q,k,j_a,j_b,j_c,j_d,m_a,m_b,m_c,m_d} X^k_q(j_a,j_b,j_c,j_d)(-1)^{(j_a-m_a+j_d-m_d)} \\ &\begin{pmatrix} j_a & k & j_c \\ -m_a & q & m_c \end{pmatrix}\begin{pmatrix} j_d & k & j_b \\ -m_d & -q & m_b \end{pmatrix},\end{aligned} \tag{5.94}$$

where

$$\begin{aligned}X^k_q(j_a,j_b,j_c,j_d) &= (-1)^{(k-q)}(-1)^{(j_a-\frac{1}{2}+j_b+\frac{1}{2})} \\ &\begin{pmatrix} j_a & k & j_c \\ \frac{1}{2} & 0 & -\frac{1}{2} \end{pmatrix}\begin{pmatrix} j_d & k & j_b \\ \frac{1}{2} & 0 & -\frac{1}{2} \end{pmatrix}[j_a,j_b,j_c,j_d]^{\frac{1}{2}}R^k(a,b,c,d)\end{aligned} \tag{5.95}$$

and $[L] = 2L + 1$. The quantity $R^k(a,b,c,d)$ denotes the two-electron radial integral given by

$$\begin{aligned}R^k(a,b,c,d) &= \int_0^\infty\int_0^\infty [P_a(r_1)P_c(r_1)+Q_a(r_1)Q_c(r_1)]\times\frac{r^k_<}{r^{k+1}_>} \\ &[P_b(r_2)P_d(r_2)+Q_b(r_2)Q_d(r_2)]dr_1dr_2.\end{aligned} \tag{5.96}$$

The product of $3j$ terms appearing in Eq. 5.94 represents the angular momentum diagram for the Couloumb operator [44, 45, 2].

Similarly, the one and the two-body cluster operators T_1 and T_2 can be expressed as

$$\langle p|T_1|a\rangle = \sum_{j_a m_a} T^0_1(p,a)\delta(j_a,j_p)\delta(m_a,m_p) \tag{5.97}$$

and

$$\langle pq|T_2|ab\rangle = \sum_{k,j_a,m_a,j_p,m_p,j_b,m_b,j_q,m_q} T_2^k(p,q,a,b)(-1)^{(j_p-m_p+j_q-m_q)} \begin{pmatrix} j_p & k & j_a \\ -m_p & q & m_a \end{pmatrix} \begin{pmatrix} j_q & k & j_b \\ -m_q & q & m_b \end{pmatrix}. \quad (5.98)$$

Here, $T_2^k(p,q,a,b)$ denotes the radial cluster operator, which is multiplied by a phase factor and the appropriate Wigner 3j-symbols. In the multi-pole expansion of the Couloumb matrix element $\langle ab|1/r_{12}|cd\rangle$, only a subset of the multi-poles k leads to non-vanishing contributions. Triangular conditions for the angular momenta is given by

$$|j_a - j_c| \leq k \leq j_a + j_c \text{ and } |j_b - j_d| \leq k \leq j_b + j_d \quad (5.99)$$

set the upper and lower limit for the multi-pole moment k. Additionally, the overall parity selection rule demands that the orbital angular momenta satisfy the relation

$$(-1)^{l_a+l_b+l_c+l_d} = 1. \quad (5.100)$$

From the angular part of the Couloumb matrix element we can derive additional constraints

$$(-1)^{l_a+l_c+k} = 1 \text{ and } (-1)^{l_b+l_d+k} = 1. \quad (5.101)$$

The selection rules given by Eq. 5.100 and Eq. 5.101 imply that for a given set of orbitals a, b, c, d, for either even or odd values of k, lead to non-vanishing contributions. For the T operator, the selection rules given by Eq. 5.99 and Eq. 5.100 are valid but the selection rule given by Eq. 5.101 leads to the Even Parity Channel (EPC) [46, 47, 48] approximation. In [46] it has been argued that the EPC approximation provides the dominant contribution to the CC equations and therefore it might be a valid approximation to discard the odd-parity pair channels and in this way reduce the number of cluster amplitudes and the computational effort by a factor of half. Hence the above approximation in CC is further referred as CCSD-EPC approximation.

5.7 Results and Discussion

5.7.1 Computation of Correlation Energy for Ba^+

Using the closed-shell CC one can determine correlation energy from the Eq. 5.30, which is the difference between the exact energy and the DF energy. Since weak interactions are limited to the nuclear region, the effect of correlation between core

and virtual $s_{1/2}$ and $p_{1/2}$ orbitals with other orbitals must be taken into account as accurately as possible for a high precision calculation of the $E1PNC$ transition amplitude. A study on the core correlations for heavy atom like Tl^+ have been performed by Merlitz et al. [48] and the results show that the third sub-shell (n=3) contributes almost 20% to the correlation energy of Tl^+.

Such a study was carried out on singly ionised barium to determine the effect of core electrons on the correlation energy. The DF ground state for Ba^+ was evaluated using the FBSE [49] with a large basis set of $(32s28p25d20f15g10h)$ Gaussian functions described in Chapter 4. The single-particle bound and continuum energies are tabulated in Table 4.3 and Table 4.4. Since the study was focussed on the effect of core orbitals we have truncated the virtual orbital space to orbitals less than 5 a.u. This implies that orbitals up to $n = 10$ sub-shell for s, p, d and f symmetry were taken for the above mentioned calculation. It has been shown by Merlitz et al.

Table 5.1: Correlation energy for Ba^+ using linear CCSD and second order MBPT with the number of cluster amplitudes for each calculation with the total memory and the CPU time used. Here we study about the dependence of ΔE with core orbitals.

System	Core orbitals	Cluster amp.	ΔE (CCSD) (a.u.)	ΔE (MBPT) (a.u.)	RAM (MB)	time (hours)
Ba(1)	5s5p	2811	-0.171496	-0.154739	65	0.15
Ba(2)	4s5s4p5p4d	23627	-0.703348	-0.746042	98	1.67
Ba(3)	3s4s5s3p4p 5p3d4d	64959	-0.771019	-0.827036	149	3.59
Ba(4)	2s3s4s5s2p 3p4p5p3d4d	93952	-0.771975	-0.827993	190	7.07
Ba(5)	1s2s3s4s5s 2p3p4p5p3d4d	102986	-0.771979	-0.827996	206	7.49

[48], that EPC approximation leads to correlation energies which differ from the full linear CCSD results only by $0.2-0.3\%$ for a heavy atom like thallium. Hence for a singly ionised barium we have done a CCSD-EPC approximation calculation and it is tabulated in Table 5.1. We have also done a second order MBPT calculation and is tabulated in the same table. The CCSD-EPC approximation reduces the number of cluster amplitudes by a factor of 1/2, which leads to a very considerable reduction of the computational effort. Further calculations and the discussions in this thesis both linear and non-linear CCSD are performed with the EPC approximation only.

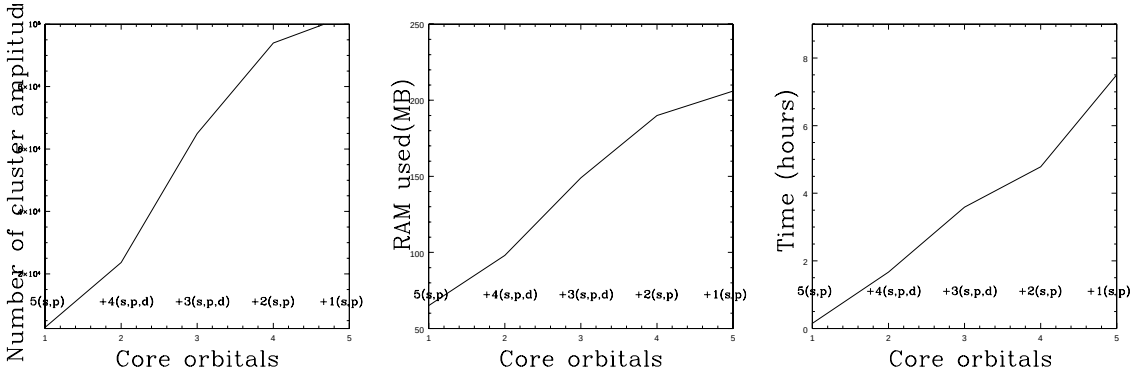

Figure 5.20: Comparison of the effect on correlation energy with the increase in the number of core orbitals with respect to the number of cluster amplitudes, memory and execution time. The core orbitals are denoted by principal quantum number and symmetry.

The increase in the number of cluster amplitudes with respect to the increase in the core orbitals (or with respect to the sub-shells) denoted by their principal quantum number n is shown in Fig. 5.20(a). This graph clearly shows that a d shell in the core leads to more number of cluster amplitudes due to the possible angular momenta. In Fig. 5.20(b), the amount of total memory needed for storing the Couloumb matrix elements and the index for the cluster amplitudes is also compared with the increase in the core electrons. This also shows a similar trend as before. As shown in Fig. 5.20(c), the comparison of the time taken for the linear CCSD with the increase in the number of core orbitals shows large change with the increase in the core orbitals irrespective of the symmetry of the core orbital.

A study to carry out the effect of the virtual orbitals on correlation energy was also performed on Ba^+. Since the previous study showed that the effect of the inner core orbitals from the sub-shell $n = 2$ and $n = 1$ is $\sim 0.1\%$, we have taken only excitations from $n = 3$ sub-shell onwards for further calculations. Hence the $n = 1$ and $n = 2$ sub-shells are frozen and no electrons are excited from them to higher virtual orbitals. With the addition of more virtual orbitals in the calculation for correlation energy we compare the number of cluster amplitudes, total RAM (Random Access Memmory) used and the time taken for the execution as in the case of core orbitals we studied previously. The behaviour is shown in Fig. 5.21. Comparing the contribution to correlation energy from core with the virtual orbitals, the core contribution from $n = 4,\ 5$ sub-shells makes comparable contribution to that of the virtual orbitals. By comparing the percentage contribution from virtual orbitals to correlation energy,

Table 5.2: Correlation energy for Ba^+ using linear CCSD and second order MBPT with the number of cluster amplitudes for each calculation with the total fast memory and the CPU time used. Here we study the dependence of ΔE with virtual orbitals.

System	Basis	Cluster amp.	ΔE (CCSD) (a.u.)	ΔE (MBPT) (a.u.)	RAM (MB)	time (hours)
Ba(6)	$8s8p9d7f$	64959	-0.771019	-0.827036	121	3.59
Ba(7)	$9s9p10d9f$	114384	-1.479034	-1.593130	227	5.15
Ba(8)	$11s11p10d$ $9f$	126653	-1.533174	-1.651054	263	6.96
Ba(9)	$11s11p10d$ $9f4g$	155333	-1.534222	-1.651955	390	12.47
Ba(10)	$11s11p10d$ $9f4g3h$	171833	-1.534389	-1.651956	596	14.54

one can infer that the low lying virtual orbitals contribute more than the high lying ones like g and h symmetries. Hence the above study gives an idea that high lying core and low lying virtuals gives the maximum contribution to the correlation energy of a system. Even though the above computation shows convergence of correlation energy with more basis, one cannot generalise it as a complete basis since different properties show completely different dependence on the basis. This will be more clear when we discuss computation of the properties which are very much dependent on wave functions.

For the non-linear calculation, we have taken only terms T_2T_2, T_1T_1 and T_2T_1 to reduce the computation time for the evaluation of the T amplitudes. This approximation is justified since T_1 cluster amplitudes are small. Using non-linear T amplitudes one can compute the contribution of non-linear terms to correlation energy. Comparing the contribution of linear and non-linear T amplitudes for a basis given by $11s11p10d9f4g$, it is inferred that non-linear terms contributes to $\sim 0.3\%$ with respect to the linear terms. The time taken for linear and non-linear computation of T amplitudes is shown in Fig. 5.22 and the values are tabulated in Table 5.3.

5.7.2 Computation of IP and EE for Ba^+

The Ionisation Potential (IP) of the valence electron is given by

$$\langle \Psi^{N-1}|H|\Psi^{N-1}\rangle - \langle \Psi^{N}|H|\Psi^{N}\rangle, \tag{5.102}$$

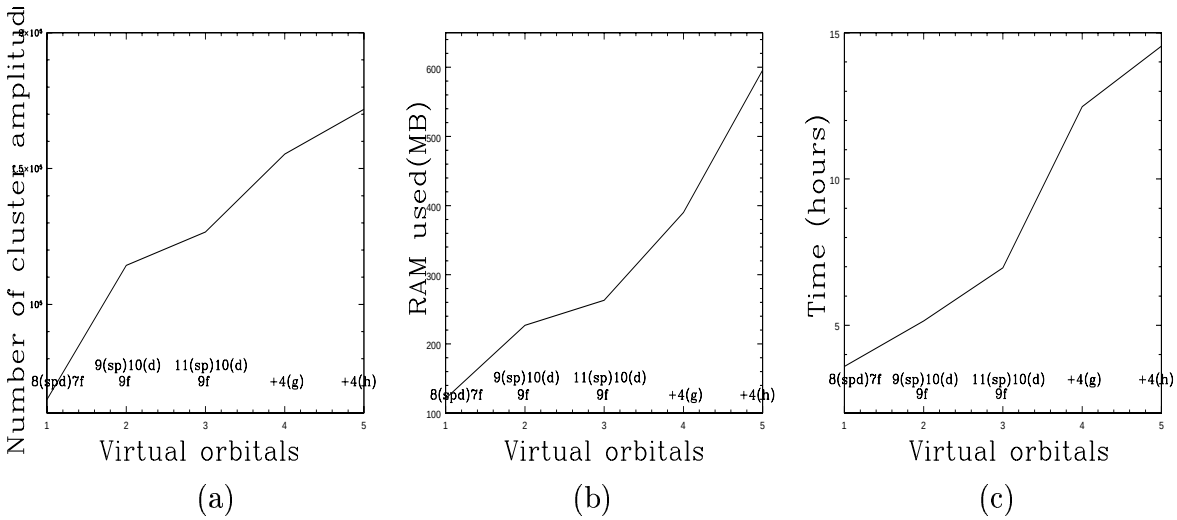

Figure 5.21: Comparison of the effect on correlation energy with the increase in the number of virtual orbitals with respect to the number of cluster amplitudes, memory and execution time. The core orbitals are denoted by the principal quantum number and symmetry.

Table 5.3: Comparison of time taken for the linear with the non-linear computation of T amplitudes.

No.	CC amp.	Time (linear) hours	Time (non-linear) hours	ΔE (linear) (a.u.)	ΔE(non-linear) (a.u.)
1	126653	6.96	20.9	-1.533340	-1.527953
2	155333	12.47	37.4	-1.534389	-1.528926
3	171833	14.54	116.8	-1.534389	-1.528925
4	233988	36.9	193	-1.829326	-1.818049

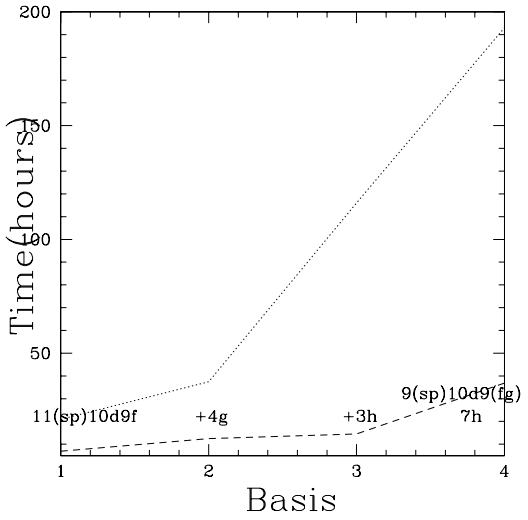

Figure 5.22: Time taken for the non-linear part of the code in comparison with that of the linear case.

where $|\Psi^{N-1}\rangle$ and $|\Psi^{N}\rangle$ represent states of the N−1 and N electron systems respectively. In other words it is $E(N-1)-E(N)$ which, using Koopman's theorem, reduces to negative of the single-particle orbital energy of the N^{th} electron. With correlations added, IP of the valence electron becomes

$$E_{DF}^{(N-1)} + E_{corre}^{(N-1)} - E_{DF}^{N} - E_{corre}^{N} = -(\epsilon_N^{DF} + \epsilon_N^{corre}). \tag{5.103}$$

Excitation energy (EE) for the excited state can be obtained from IP's as

$$EE(exc) = IP_{ground} - IP_{exci} \tag{5.104}$$

Accurate theoretical prediction of transition energies in heavy atoms requires high-order inclusion of both relativistic and correlation terms in the Hamiltonian. An *ab initio* relativistic CC method incorporating these effects has been applied to series of heavy atoms, like gold [50], mercury [51], several lanthanides and actinides [52, 53], and elements 104 [54], 111 [55] and 112 [51]. Several calculations of IPs and EEs of the barium atom have been reported [56, 57, 58]. For singly ionised barium, a few literatures are available, with the first being the application of relativistic many-body perturbation theory by Guet and Johnson [59]. We will be comparing our calculations in Ba^+ mostly with the work by Eliav et al. [60], where IP's and EE's are computed using relativistic CCM.

We have done a series of calculations wherein different basis were used and the dependency of them to EE's and IP's with respect to core and virtual orbitals were

studied in detail. For all the calculations presented here the analytical basis was generated with $32s28p25d20f15g10h$. Using the above analytical basis as the starting point, we show an improvement using the new basis over the analytical basis. As a first step in order to find out the dependency on the core orbitals on IP and EE we performed two different calculations which are tabulated in Table 5.4. For the CC

Table 5.4: IP and EE for the low lying levels of Ba^+ using linear CCSD with respect to the core orbitals included in the calculation.

Basis	Core orbitals	Cluster amp.	IP of $6s_{1/2}$	IP of $5d_{3/2}$	EE ($6s_{1/2}$-$5d_{3/2}$)
Expt:			0.36764	0.34543	0.02221
$8s, 8p, 9d, 9f$	$5(sp)4(spd)3d$	61667	0.368374	0.338812	0.029563
$9s, 9p, 10d, 9f$	$5(sp)4(spd)3(spd)$	114384	0.368523	0.339311	0.029212

calculations, we have restricted the basis by imposing lower and upper bounds in energy for the all single-particle orbitals. This was done to reduce the huge memory requirement which is needed to store the matrix elements of the dressed operator $\bar{H}$ and the two electron Couloumb interaction in the memory. Since the change in IP and EE is less than 0.1% by the addition of $n = 3$ shell with respect to $n = 4$ shell, for further calculations we have taken the core orbitals only above $n = 3$ sub-shell and all the other shells below $n = 3$ are frozen. Considering $n = 1$ and above with a 7 symmetry calculation the IP value obtained for $6s$ is ~ -0.36861599 which in comparison with $n = 2$ and above is -0.3686409. This also very well establishes that the contribution due to omitted shells less than 3 is 0.01% to IPs. To this we added more virtual orbitals of different symmetry and the study of the dependence of IP and EE on the basis is described below. It is clear from calculations by Kaldor [60] that high lying virtual orbitals contribute very little to the excitation energies. This also supports the approximation for taking orbitals below a particular cut off in energy. In Table 5.5, we give the DF values for IP and EE for the low lying levels along with the experimental values from the Moors catalogue [61, 62] [1 a.u. = 27.21139634 ev, 1 ev = 8065.6 cm^{-1}].

The percentage error in IPs for the low lying bound states due to the addition of more virtual orbitals is shown in Fig. 5.23. With no g and h symmetry in the calculation, the IPs for d orbitals are $\sim 1.3\%$. Due to the addition of g and h orbitals one can find change in the accuracy in the positive direction. The accuracy of s and

Table 5.5: DF values and experimental values for IPs and EEs for the low lying levels of Ba^+.

Property	state	DF value (a.u.)	experiment cm^{-1} (a.u.)
IP	$6s_{1/2}$	0.343827	80686(0.367634)
	$5d_{3/2}$	0.310522	75813(0.345427)
	$5d_{5/2}$	0.308371	75012(0.341777)
	$6p_{1/2}$	0.260767	60425(0.275314)
	$6p_{3/2}$	0.254443	58735(0.267614)
EE	$6s_{1/2}$-$5d_{3/2}$	0.033305	4874(0.022207)
	$6s_{1/2}$-$5d_{5/2}$	0.035456	5675(0.025857)
	$6s_{1/2}$-$6p_{1/2}$	0.083060	20262(0.092320)
	$6s_{1/2}$-$6p_{3/2}$	0.089384	21952(0.100020)

p orbitals are very good compared to d orbitals even for the first calculation with the basis $9s9p10d9f$ and this can very well be understood. For an orbital to be described correctly one needs to have the basis made of a complete set of orbitals. For example, for any property related to d orbitals one needs to have a basis with a complete set of s, p, d, f and g orbitals. In this case by the addition of h orbitals in the fourth run we find that the change in accuracy for all the orbitals considered here are minimum. Whereas the addition of more g orbitals (5th run) compared to the earlier ones, we find that the change in the accuracy for d orbitals to be drastic which points to the importance of the g symmetry in the basis for IP of the particular orbital. At the same time the reduction in the accuracy of s and p orbitals with the addition of more g, h orbitals and with less s, p orbitals very well explains the importance of the completeness of the basis. It is clear that in order to get accurate IPs for different symmetries one needs to have different single-particle basis. Hence with a very large basis with 11 symmetries the average percentage error in IPs for the low lying bound orbitals for singly ionised barium is found to be $\sim 0.4\%$. Comparing the IPs, with and without non-linear terms in T computation, we find that non-linearity in T amplitudes leads to very small change of the order 0.4% for $6s_{1/2}$, 0.16% for $5d$ and 0.03% for $6p$ orbitals. Whereas the percentage contribution from approximate triples to IPs is found to be varying between 3-4% for the low lying bound orbitals. The trend is shown in Fig. 5.24. This very well highlights the importance of triples effect which is mainly responsible for achieving this accuracy in the present CC calculations.

Similar kind of study is done for EE and the values are tabulated in Table 5.8

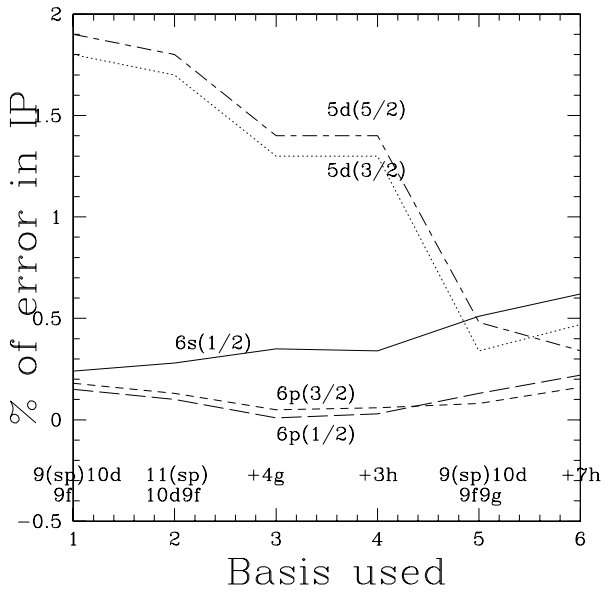

Figure 5.23: Percentage error in IPs for Ba^+ with the addition of more virtual orbitals in the basis.

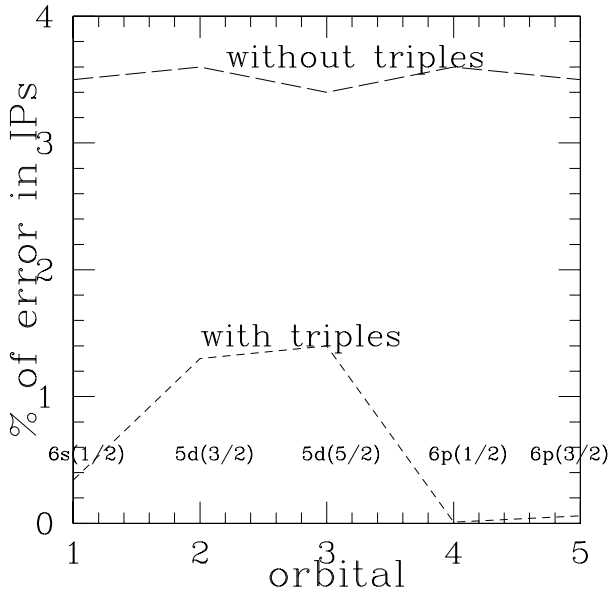

Figure 5.24: Percentage error in IPs for Ba^+ with and without approximate triples added.

Table 5.6: IP for the low lying levels of Ba^+ using linear and non-linear CCSD (with approximate triples) with respect to the virtual orbitals included in the calculation. (in parentheses: contribution from triples)

Basis	State	Theory IP (a.u.) (linear)	Theory IP (a.u.) (non-linear)	% error (non-linear)
$11s, 11p, 10d, 9f$				
	$6s_{1/2}$	0.368538	0.368682(0.011789)	0.28
	$5d_{3/2}$	0.339167	0.339667(0.017070)	1.7
	$5d_{5/2}$	0.335188	0.335727(0.016456)	1.8
	$6p_{1/2}$	0.274985	0.275064(0.009950)	0.1
	$6p_{3/2}$	0.267196	0.267270(0.009624)	0.13
$11s, 11p, 10d, 9f, 4g$				
	$6s_{1/2}$	0.368923	0.368923(0.011754)	0.35
	$5d_{3/2}$	0.341042	0.341042(0.017041)	1.3
	$5d_{5/2}$	0.337111	0.337111(0.016430)	1.4
	$6p_{1/2}$	0.275319	0.275319(0.010025)	0.01
	$6p_{3/2}$	0.267488	0.267488(0.009697)	0.05
$11s, 11p, 10d, 9f, 4g, 3h$				
	$6s_{1/2}$	0.368729	0.368872(0.011746)	0.34
	$5d_{3/2}$	0.340432	0.340941(0.017032)	1.3
	$5d_{5/2}$	0.336464	0.337011(0.016421)	1.4
	$6p_{1/2}$	0.275195	0.275273(0.010018)	0.03
	$6p_{3/2}$	0.267374	0.267448(0.009691)	0.06

and Table 5.9. Similar kind of explanation for IPs holds good for EEs. The trend is shown in Fig. 5.25. Comparing the values of IPs and EEs using different basis, the average error in IP and EE for the largest basis considered (9s9p10d9f 9g7h) is $\sim$ 0.4% and 2.7%. Hence using the new basis approach with partly analytical and partly numerical orbitals, we computed the IPs and EEs and the results showed very good improvement over the calculations using the analytical basis. Numerical orbitals used in the above calculation with respect to each symmetry are given in Table 5.10. The average error in IP and EE for Ba^+ using the new basis $9s9p10d9f9g7h$ (partly numerical and partly analytical) is $\sim$ 0.1% and 0.6% as against the analytical basis with 0.4% and 2.7%. The results of the calculations of our IPs and EEs are given

Table 5.7: IP for the low lying levels of Ba^+ using linear and non-linear CCSD (with approximate triples) with respect to the virtual orbitals included in the calculation.(in parentheses: contribution from triples)

Basis	State	Theory IP (a.u.) (non-linear)	% error (non-linear)
$9s, 9p, 10d, 9f, 9g$			
	$6s_{1/2}$	0.369495(0.012820)	0.51
	$5d_{3/2}$	0.344240(0.018856)	0.34
	$5d_{5/2}$	0.340143(0.018144)	0.48
	$6p_{1/2}$	0.275663(0.011294)	0.13
	$6p_{3/2}$	0.267817(0.010930)	0.08
$9s, 9p, 10d, 9f, 9g, 7h$			
	$6s_{1/2}$	0.369905(0.012931)	0.62
	$5d_{3/2}$	0.347064(0.019016)	0.47
	$5d_{5/2}$	0.342935(0.018290)	0.34
	$6p_{1/2}$	0.275911(0.010418)	0.22
	$6p_{3/2}$	0.268052(0.010071)	0.16

in Table 5.11 and Table 5.12 and compared with the previous calculations by Guet and Johnson [59] and Eliav et al. [60]. It is clear that our CCSD with partial triples results are more accurate than the other two calculations. The contribution from partial triples to IPs is about 4−5% and it is the major reason for the high accuracy of our calculations. Comparisons with Eliav et al with no triples and our calculations with triples suggest that the omitted triples will have $\leq 0.1\%$ error in the computation of IPs and EEs. The choice of our orbital basis has also contributed to the accuracy of our calculations. By representing the core, valence and the appropriate virtual single-particle states by numerical DF/V^{N-1} orbitals, we have been able to obtain the best physical description for them. The average error in our IPs is about 0.1% except $5d_{3/2}$ which is 0.23%. The EEs also show the same trend, the average error is about 0.6%; most of them being below 0.7% except $6s - 5d_{3/2}$ which is 1.4%. Eliav et al. have used the uncontracted well-tempered basis set of Huzinaga and Klobukowski [63] with l up to 5. Only virtual orbitals below 100 a.u. and core orbitals with n=4 and above were considered for this calculation.

In the calculation by Guet and Johnson using the relativistic MBPT to second order, the IPs were computed to an accuracy of $\leq 2\%$ and EEs $\sim 4\%$. The accuracy

Table 5.8: EE for the low lying levels of Ba^+ using linear and non-linear CCSD (with approximate triples) with respect to the virtual orbitals included in the calculation.

Basis	State	Theory EE (a.u.) (linear)	Theory EE (a.u.) (non-linear)	% error (non-linear)
$11s, 11p, 10d, 9f$				
	$6s_{1/2}$-$5d_{3/2}$	0.029371	0.029015	30.7
	$6s_{1/2}$-$5d_{5/2}$	0.033350	0.032955	27.5
	$6s_{1/2}$-$6p_{1/2}$	0.093553	0.093618	1.4
	$6s_{1/2}$-$6p_{3/2}$	0.101342	0.101412	1.4
$11s, 11p, 10d, 9f, 4g$				
	$6s_{1/2}$-$5d_{3/2}$	0.027881	0.027881	25.6
	$6s_{1/2}$-$5d_{5/2}$	0.031812	0.031812	23.0
	$6s_{1/2}$-$6p_{1/2}$	0.093604	0.093604	1.4
	$6s_{1/2}$-$6p_{3/2}$	0.101435	0.101435	1.4
$11s, 11p, 10d, 9f, 4g, 3h$				
	$6s_{1/2}$-$5d_{3/2}$	0.028297	0.027931	25.8
	$6s_{1/2}$-$5d_{5/2}$	0.032265	0.031861	23.2
	$6s_{1/2}$-$6p_{1/2}$	0.093534	0.093599	1.4
	$6s_{1/2}$-$6p_{3/2}$	0.101355	0.101424	1.4

of their $6s - 5d_{3/2}$ excitation energy calculation is somewhat misleading, as it is a consequence of the cancellation of the errors of their $6s$ and $5d_{3/2}$ IPs. The accuracies of their $6s$ and $5d_{3/2}$ IPs are 1.5% and 1.8%. The corresponding values for Eliav et al. are 0.23% and 0.28% and our calculations are 0.14% and 0.23% [64]. The accuracies of IPs of $6s$ and $5d_{3/2}$ obtained by Dzuba et al. [65] using the relativistic correlation potential method including three series of higher order diagram to all orders is 0.16% and 0.78%. Comparing the accuracy of IPs and EEs for d states, it is very clear that the above calculations by different groups show a large error which can be attributed to the huge correlations in these states. Using the CC method with approximate triples and a fairly big basis the correlations were taken care and this led to high accuracy in d states. In order to show the completeness of higher symmetries in the basis to the accuracy of the states we performed two different calculations. The results are tabulated in Table 5.13. With the basis $12s13p13d11f7g$ the accuracy of s and p orbitals are very good compared to the accuracy in d orbitals which points to

Table 5.9: EEs for the low lying levels of Ba^+ using linear and non-linear CCSD (with approximate triples) with respect to the virtual orbitals included in the calculation. (in parentheses: contribution from triples)

Basis	State	Theory EE (a.u.) (non-linear)	% error (non-linear)
9s,9p,10d,9f,9g			
	$6s_{1/2}$-$5d_{3/2}$	0.025255	13.7
	$6s_{1/2}$-$5d_{5/2}$	0.029352	13.5
	$6s_{1/2}$-$6p_{1/2}$	0.093832	1.6
	$6s_{1/2}$-$6p_{3/2}$	0.101678	1.6
9s,9p,10d,9f,9g,7h			
	$6s_{1/2}$-$5d_{3/2}$	0.022841	2.9
	$6s_{1/2}$-$5d_{5/2}$	0.026970	4.3
	$6s_{1/2}$-$6p_{1/2}$	0.093994	1.8
	$6s_{1/2}$-$6p_{3/2}$	0.101853	1.8

the importance of the completeness of f and g orbitals. The other calculation with $9s9p10d9f9g7h$ shows that the correlation for s and p were not very good leading to reduction in accuracy whereas the presence of more g and h orbitals increased the accuracy of d orbitals. This is schematically represented in Fig. 5.26. The accuracy of the IPs of bound orbitals with the new and old basis are given in Fig. 5.27 and the comparison with the calculations by Kaldor [60], Guet [59] and Dzuba [65]. are given in Fig. 5.28.

5.7.3 Computation of E1/E2 Transition Probability and Lifetime

Accurate absolute transition probabilities for transitions between eigenstates in atoms, ions and molecules are important in many applications. They are mainly used as a sensitive test for calculated wave functions [66], because the transition probability is related to the matrix element of the electric dipole operator between them. This operator is proportional to r which is very sensitive to the large radial distances. Experimentally more accurate data are usually obtained by measuring the lifetime of the upper level and the branching ratio [67]. Hence a measurement of the transition probability and thereby the lifetimes of upper levels can be considered as a check of

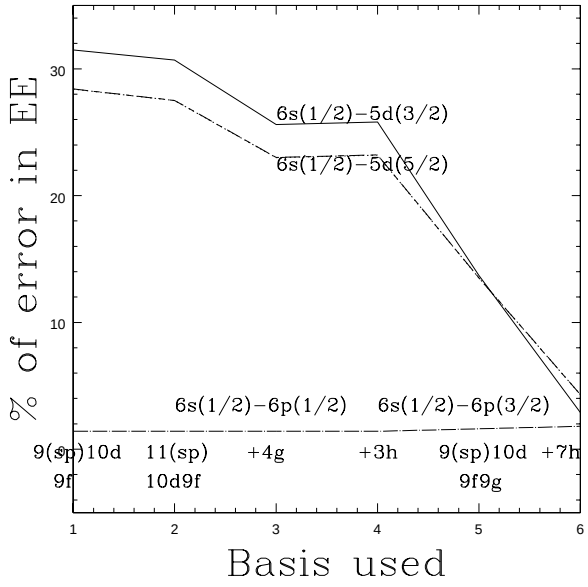

Figure 5.25: Percentage error in EEs for Ba^+ with the addition of more virtual orbitals in the basis.

Table 5.10: Orbital generation.

Symmetry	No of orbitals in each symmetry	numerical orbitals used in the calculation	Gaussian orbitals used in calculation
s	9	3,4...8s	9s,..11s
p(1/2)	9	3p,...8p	9p,...11p
p(3/2)	9	3p,...8p	9p,...11p
d(3/2)	10	3d,...7d	8d,...12d
d(5/2)	10	3d,...7d	8d,...12d
f(5/2)	9	4f,5f	6f,...12f
f(7/2)	9	4f,5f	6f,...12f
g(7/2)	9	-	5g,...13g
g(9/2)	9	-	5g,...,13g
h(9/2)	7	-	6h,...12h
h(11/2)	7	-	6h,...12h

Table 5.11: IP got using non-linear CCSD in units of (a.u.) (in parentheses: contribution from approximate triples.)

orbital	Experiment	CCSD (T)	Kaldor [60] (CCSD)	Guet [59] (MBPT)	Error (%)
6s(1/2)	0.36764	0.36814(−0.0130784)	0.36848	0.37308	0.14
5d(3/2)	0.34543	0.34623(−0.019412)	0.34448	0.35172	0.23
5d(5/2)	0.34178	0.34211(−0.018676)	0.34072	0.34748	0.10
6p(1/2)	0.27534	0.27568(−0.010146)	0.27555	0.27742	0.12
6p(3/2)	0.26762	0.26781(−0.009801)	0.26777	0.26946	0.07

Table 5.12: EE got using non-linear CCSD in units of (a.u.).

orbital	Experiment	CCSD	Kaldor [60] (CCSD)	Guet [59] (MBPT)	Error (%)
6s(1/2)-5d(3/2)	0.02221	0.02191	0.02400	0.02136	1.4
6s(1/2)-5d(5/2)	0.02586	0.02603	0.02776	0.02561	0.66
6s(1/2)-6p(1/2)	0.09230	0.09246	0.09293	0.09566	0.17
6s(1/2)-6p(3/2)	0.10002	0.10033	0.10071	0.10033	0.31

Table 5.13: Comparison of the IPs and EEs using two different basis which shows the importance of the completeness of the higher symmetries in the basis.
[h]

Basis	State	Theory IP (a.u.) (non-linear)	% error (non-linear)	% error ($9s9p10d9f9g7h$)
$12s, 13p, 13d, 11f, 7g$				
	$6s_{1/2}$	0.367648	0.002	0.14
	$5d_{3/2}$	0.344080	0.38	0.23
	$5d_{5/2}$	0.340031	0.51	0.1
	$6p_{1/2}$	0.275503	0.06	0.12
	$6p_{3/2}$	0.267656	0.01	0.07
Basis	State	Theory EE (a.u.) (non-linear)	% error (non-linear)	% error ($9s9p10d9f9g7h$)
$12s, 13p, 13d, 11f, 7g$				
	$6s_{1/2}$-$5d_{3/2}$	0.023568	6.1	1.4
	$6s_{1/2}$-$5d_{5/2}$	0.027617	6.8	0.66
	$6s_{1/2}$-$6p_{1/2}$	0.092145	0.19	0.17
	$6s_{1/2}$-$6p_{3/2}$	0.099992	0.03	0.31

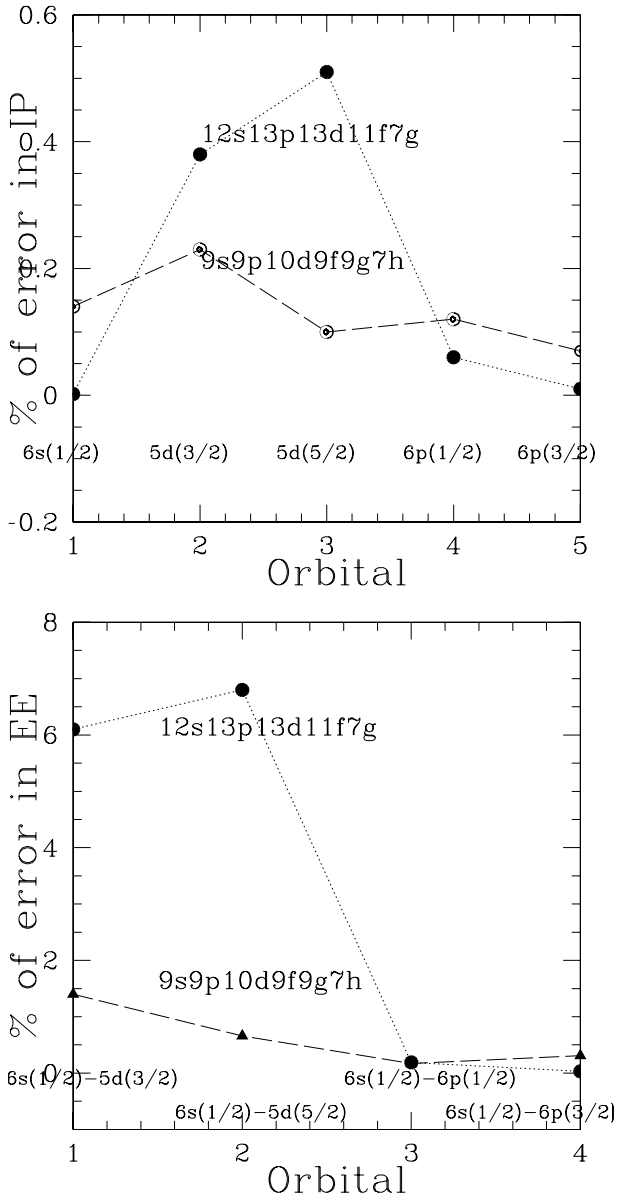

Figure 5.26: Percentage error in IPs and EEs for Ba^+ for two different basis explicitly showing the dependence of higher symmetries in the basis.

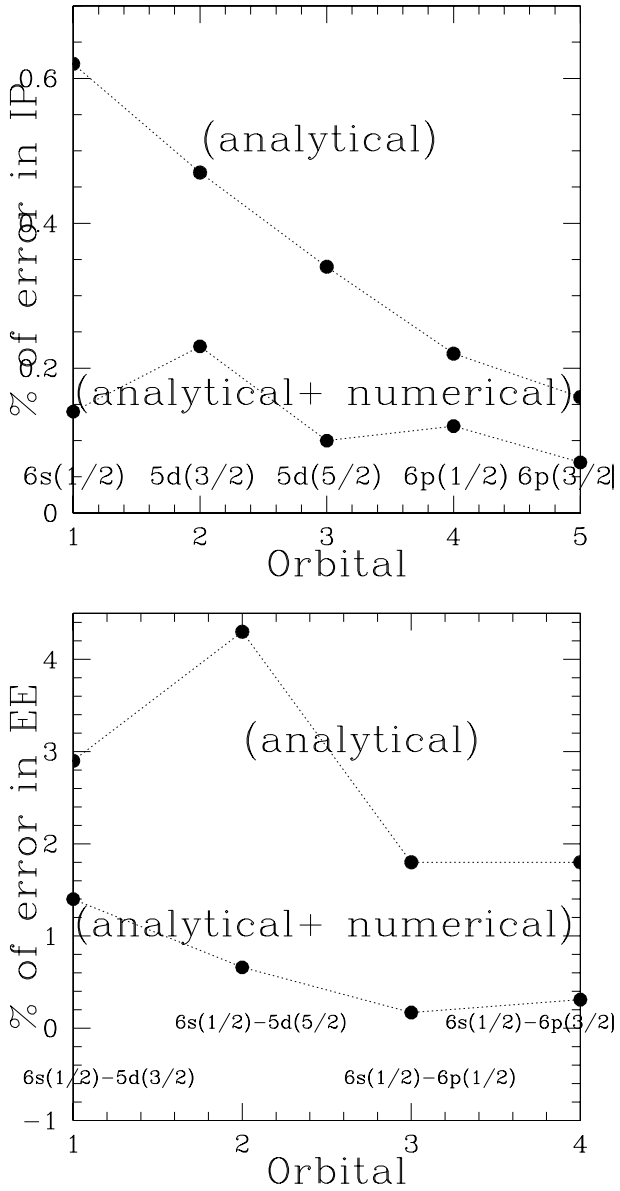

Figure 5.27: Percentage of error in IPs and EEs for Ba^+ with analytical and partly analytical and partly numerical orbital basis.

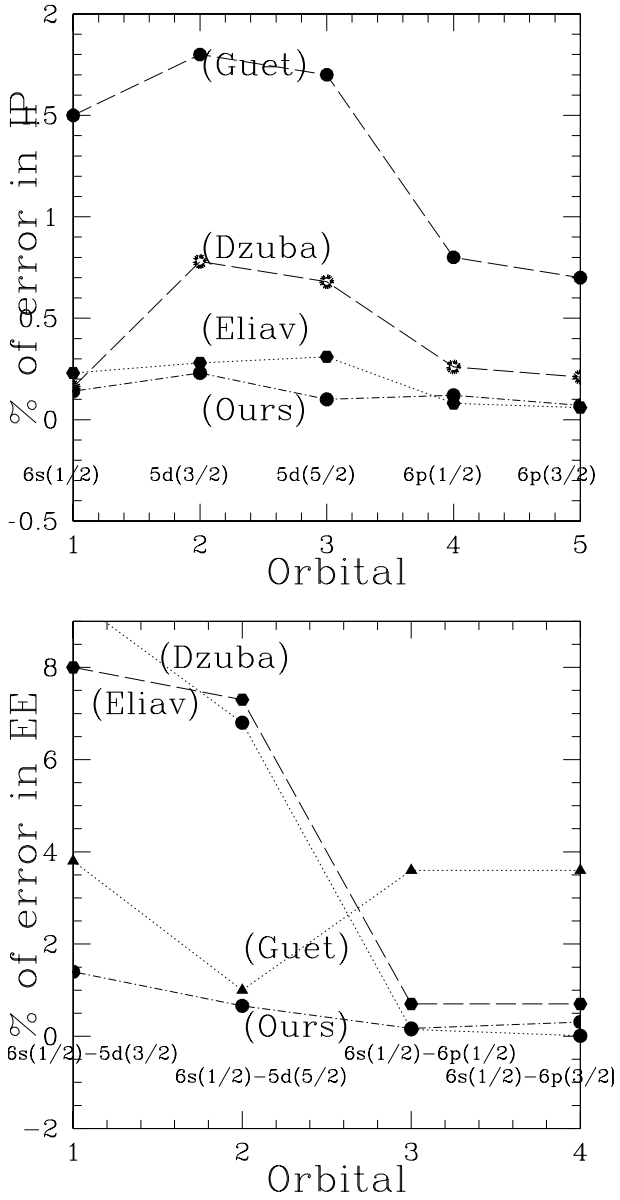

Figure 5.28: Percentage error in IPs and EEs for Ba^+ with the calculations by Eliav et al. [60], Guet [59] and Dzuba [65].

the wave functions at the large r regions. Here in this thesis, we have done a preliminary study on the dependence of the basis on the accuracy of the dipole matrix elements. Comparing the calculations done for Ba^+ for electric dipole and quadrapole transitions and thereby the lifetimes, we have tried to evaluate the accuracy of the wave functions chosen for further calculations. For the calculations presented below, we have used the new basis with partly analytical and part numerical orbitals. We have also done a lifetime calculation for Ca^+ as a check for the feasibility of the code and the results are presented below.

The electric dipole/quadrapole matrix elements using different basis are tabulated in Table 5.14. Comparing the dipole and quadrapole matrix elements got using the three different basis, it is clear that to obtain the correlation required to compute different transitions involving different symmetries one needs to consider different basis which are to be selected by physical considerations. For example, for a transition involving $p-s$ one needs to have a very good description of d orbitals and at the same time a transition involving $p-d$ needs s, p, d and f in the basis. Comparing with Guet et al. [59] it is clear that using a basis $14s14p15d14f$ the transitions of the kind $p-d$ are closer due to the better description of s, p, d and f states in the basis whereas it is poorer in the other cases. But for the $s-p$ transition we find that the error is more for the particular basis compared to the previous ones where we have less s orbitals in the basis. For the quadrapole matrix elements we compared the accuracy by comparing the lifetimes of $5d_{3/2}$ and $5d_{5/2}$ states. Using the allowed E1 and E2 transitions we have computed the lifetimes of $6p$ and $5d$ states and the values are compared with the experiment and other literature tabulated in Table 5.16.

In the Table 5.14, the contribution from different matrix elements pertaining to different physical effects are given separately. By comparing the classification done by Blundell et al. [40], one finds that the lowest order correction given by $\langle f|\bar{D}|i\rangle$, gives the maximum contribution. The effective one-body corrections namely RPA contributes to $\sim 15\%$ and Bruckner and structural radiation together gives $\sim 5\%$ with the normalisation correction $\sim 0.5\%$. Using the transition probabilities tabulated in Table 5.15, we have computed the lifetimes of the upper levels using allowed E1 and E2 transitions. These results are tabulated in Table 5.16. The calculations are in good agreement with experiment and other literature. Dzuba et al. [65] used M1 and E2 transition for the computation of the lifetime of d states which effectively decreased it leading to a better result. In our calculation we have taken only E2 transition for the determination of $5d$ lifetimes. The lifetimes of $6p$ is also in good agreement with the other literatures. We have also performed a CC calculation for Ca^+ and the lifetime of the levels $4p$ and $3d$ were also computed. The results of it

Table 5.14: Comparison of electric dipole/quadrapole matrix elements for Ba^+ using different basis.

Basis	Trans.	DF	DF+MBPT(1)	$\langle f\|D\|i\rangle$	$\langle f\|[S^+D]_c\|i\rangle$	$\langle f\|[DS]_c\|i\rangle$	$\langle f\|[S^+DS]_c\|i\rangle$	Norm. corr.	D/Q matrix element
9s9p									
10d9f	$6s_{1/2}$-$6p_{1/2}$	3.8909	3.4729	3.8922	-0.3586	-0.1667	0.0529 3	-0.0165	3.3686
9g7h	$6s_{1/2}$-$6p_{3/2}$	-5.4776	-4.9108	-5.4795	0.5248	0.2046	-0.0719 1	0.0208	4.7551
	$5d_{3/2}$-$6p_{3/2}$	-1.6354	-1.4917	-1.6370	0.3892	0.0234	-0.0303	0.0065	1.2360
	$5d_{5/2}$-$6p_{1/2}$	-5.0011	-4.5697	-5.0057	1.1455	0.0696	-0.0913	-0.0021	3.8483
	$5d_{3/2}$-$6p_{1/2}$	-3.7454	-3.3883	-3.7498	0.8547	0.0721	-0.0723	0.0164	2.8479
	$6s_{1/2}$-$5d_{3/2}$	14.7633	14.5566	14.7656	-0.3840	-2.6075	0.3226	-0.0872	11.9821
	$6s_{1/2}$-$5d_{5/2}$	-18.3840	-18.1559		-18.3835	0.4735	3.0174	-0.3539	-15.1521
12s13p									
13d11f	$6s_{1/2}$-$6p_{1/2}$	3.8909	3.4729	3.8918	-0.3550	-0.1666	0.0524	-0.0161	3.3717
7g	$6s_{1/2}$-$6p_{3/2}$	-5.4776	-4.9108	-5.4790	0.5194	0.2052	-0.0712	0.0205	-4.7586
	$5d_{3/2}$-$6p_{3/2}$	-1.6354	-1.4917	-1.6363	0.3656	0.0236	-0.0288	0.0053	-1.2583
	$5d_{5/2}$-$6p_{1/2}$	-5.0011	-4.5697	-5.0043	1.0729	0.0705	-0.0870	-0.0051	-3.9171
	$5d_{3/2}$-$6p_{1/2}$	-3.7454	-3.3882	-3.7488	0.8031	0.0728	-0.0682	0.0135	-2.8965
	$6s_{1/2}$-$5d_{3/2}$	14.7633	14.5565	14.7643	-0.3753	-2.3354	0.2628	-0.0593	12.2769
	$6s_{1/2}$-$5d_{5/2}$	18.1560	18.3840	-18.3820	0.4622	2.9172	-0.3307	0.0684	-15.2857
14s14p									
15d14f	$6s_{1/2}$-$6p_{1/2}$	3.8909	3.4729	3.8922	-0.3417	-0.1664	0.0490	-0.0171	3.3815
	$6s_{1/2}$-$6p_{3/2}$	-5.4776	-4.9108	-5.4783	0.4990	0.2057	-0.0668	0.0227	-4.7718
	$5d_{3/2}$-$6p_{3/2}$	-1.6354	-1.4917	-1.6358	0.3137	0.0257	-0.0250	0.0060	-1.3032
	$5d_{5/2}$-$6p_{1/2}$	-5.0011	-4.5697	-5.0021	0.9153	0.0772	-0.0756	-0.0008	-4.0503
	$5d_{3/2}$-$6p_{1/2}$	-3.7454	-3.3882	-3.7475	0.6912	0.0772	-0.0589	0.0146	-2.9926
	$6s_{1/2}$-$5d_{3/2}$	14.7633	14.5582	14.7619	-0.3387	-1.9384	0.1532	-0.0799	12.6261
	$6s_{1/2}$-$5d_{5/2}$	18.3840	18.1581	-18.3794	0.4151	2.3787	-0.2221	0.0703	-15.7848

Table 5.15: Electric dipole matrix elements in different transitions for Ba^+ and the comparison of transition probabilities with experimental values.

Trans.	ours D (a.u.)	ours A_{fi} $\times 10^{-9} sec^{-1}$	[59] D (a.u.)	A_{fi} [59] $\times 10^{-9} sec^{-1}$	A_{fi} [65] $\times 10^{-9} sec^{-1}$	Expt. A_{fi} $\times 10^{-9} sec^{-1}$
$6s_{1/2}$ -$6p_{1/2}$	3.3686	0.095137	3.300	0.09178	0.092327	0.095±0.009,[a] 0.0955±0.0010,[b] 0.095±0.007[c]
$6s_{1/2}$ -$6p_{3/2}$	4.75508	0.121148	4.658	0.11625	0.117066	0.106± 0.009,[a] 0.117±0.004,[b] 0.118±0.008[c]
$5d_{3/2}$ -$6p_{3/2}$	1.30317	0.004284	1.312	0.00435	0.004492	0.00469± 0.00029,[a] 0.0048±0.0005,[b] 0.0048±0.0006 [c]
$5d_{5/2}$ -$6p_{3/2}$	4.0503	0.033053	4.057	0.03595	0.034453	0.0377±0.0024,[a] 0.037±0.004,[b] 0.037±0.004 [c]
$5d_{3/2}$ -$6p_{1/2}$	2.9926	0.035830	3.009	0.03342	0.037033	0.0338±0.00019 [a] 0.0333±0.008 [b] 0.033±0.004 [c]

[a] A. Kastberg, P. Villemoes, et al. *J. Opt. Soc. Am. B* **10**, 1330 (1993).

[b] J. Reader, et al. *Wavelengths and Transition Probabilities for Atoms and Atomic Ions*, Nat. Bur. Stand. Ref. Data Ser., Natl. Bur. Stand.(US) Circ. No. 68. Vol. 10.

[c] A. Gallagher, *Phys. Rev.* **157**,24 (1967).

Table 5.16: Lifetimes of states of Ba^+ and Ca^+ computed using E1 and E2 transition amplitudes.

Ion	State	Ours (nsec)	Guet [59] (nsec)	Dzuba [65] (nsec)	Expt. (nsec)
Ba^+	6p(1/2)	7.8	7.99	7.89	7.90(10) $^\bullet$
	6p(3/2)	6.20	6.39	6.30	6.32(10)$^\bullet$
Ca^+	4p(1/2)	7.02	6.94	7.047	7.098(0.020)*
	4p(3/2)	6.8233	6.75	6.833	6.924(0.019)*
Ion	State	Ours (sec)	Guet [59] (sec)	Dzuba [65] (sec)	Expt. (sec)
Ba^+	5d(3/2)	81.4	83.7	81.5	79.8(4.6)$^\square$
	5d(5/2)	36.5	37.2	30.3	34.5(3.5)$^\triangle$
Ca^+	3d(3/2)	1.397	1.080	1.271	1.108$\pm$0.160*
	3d(5/2)	1.335	1.045	1.236	1.023$\pm$0.104*

$\bullet$ E.H. Pinnington, R.W. Berends and M. Lumsden, *J. Phys. B* **28** 2095 (1995),
$*$ J. Jin and D.A. Church, *Phys. Rev. Lett.* **70**, 3213 (1993),
$\star$ M. Knoop, D. Lunney,J. Rocher, M. Vedel and F. Vedel (unpublished),
$\square$ N. Yu, W. Nagourney and H. Dehmelt, *Phys. Rev. Lett.* **78**, 4893(1997) and
$\triangle$ A.A. Madej and J.D. Sankey, *Phys. Rev. A* **41**, 2621 (1990).

are quiet encouraging and it is tabulated in the Table 5.16.

The difference in the accuracy of the lifetimes of the levels computed using E1 and E2 can be understood like this. As pointed out earlier, we have taken only effective one-body dressed single-particle operator in the present calculation. The effective two-body operators of the kind shown in Fig. 5.29 are not considered at this moment for the computation. For the E1 transition with dipole as the operator which is odd under parity, the two-body diagrams will have very less effect compared to the E2 operator which is even under parity. Hence the addition of two-body effective operator will lead to a better accuracy in the lifetime of $3d$ levels as comparable to the accuracy obtained for $4p$ levels.

5.7.4 Computation of Hyperfine Constant (A) for Ba^+

Calculations of hyperfine constant A follow the same procedure as the calculations of the electric dipole matrix elements described above. Since the matrix element

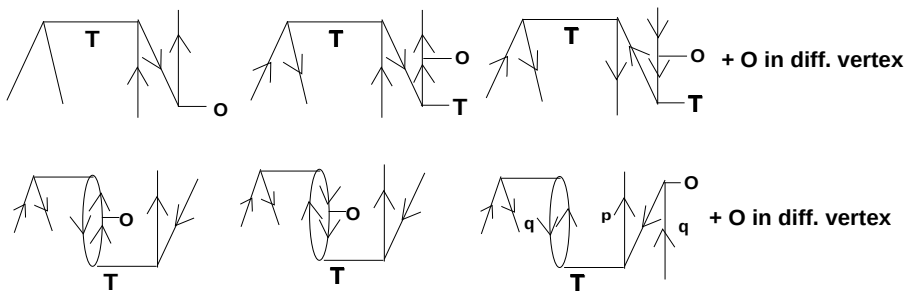

Figure 5.29: Typical effective two-body $\bar{O}$ diagrams which have not been considered in the present computation.

for A is proportional to $1/r^2$ it can be used as a sensitive test of the wave function at small distances from the nucleus and hence a check of the PNC matrix element. Here the dependence of hyperfine constant on basis is done at a very preliminary level and the results are tabulated in Table 5.17. The physical effects contributing to hyperfine constant are classified in the usual terminology as direct, exchange core polarisation and correlation terms. The direct or zeroth order approximation arises from the unpaired spin valence electron. The exchange core polarisation (ECP) effect represents the influence of the preferential exchange interaction between valence electron and the core electrons with spin parallel to the former, leading to a net density at the nucleus due to the core electrons. Any effect in which two electrons are simultaneously excited belongs to correlation terms. In the terminology used by Blundell et al. [39], the first term in the table contributes to the zeroth order and correlations from T, the second term refers to RPA correction which is same as the ECP contribution, and the third and fourth term leads to pair correlation types. Here Bruckner correction with the perturbation on the valence contributes the maximum compared to Structural corrections. Looking at the dependence on the basis in the computation of hyperfine constant, it is very clear that one needs to have a better description of core symmetries like s, p, d in this case. We observe that for a basis with a relatively small number of orbitals for the symmetries s, p, d compared to when compared to a larger basis shows a remarkable difference and this points to the need for a good description of the occupied orbitals. In Table 5.18, we tabulate the values of the hyperfine constant A for a basis $14s14p15d14f$ obtained by a partly analytical and partly numerical single-particle orbitals. The experimentally available values and other theoretical calculations are also given in the Table 5.18. Comparing with the experimental values for $6s$, $6p(1/2, 3/2)$ and $5d(3/2)$ orbitals we find that the accuracy is $\sim 5\%$. The effective two-body hyperfine matrix elements will have to

Table 5.17: Comparison of magnetic hyperfine constant (MHz) for Ba^+, I=3/2, $g_I = 0.6238$, for different basis.

Basis	orbital	DF	DF+MBPT(1)	$\langle f\|\bar{Hy}\|i\rangle$	$\langle f\|[S^+\bar{Hy}]_c\|i\rangle$	$\langle f\|[\bar{Hy}S]_c\|i\rangle$	$\langle f\|[S^+\bar{Hy}S]_c\|i\rangle$	Norm. corr.	Hyperfine constant (A) (MHz)
9s9p									
10d9f	$6s_{1/2}$	2925.6534	3307.0788	2824.7677	673.1045	673.1045	181.8034	-19.3300	4278.7392
9g7h	$5d_{3/2}$	128.0069	136.4669	131.8147	34.5556	34.5556	17.9377	−1.4133	209.4129
	$5d_{5/2}$	51.355086	-6.4810	53.2569	-25.8019	-25.8019	6.8080	0.0431	3.3985
	$6p_{1/2}$	492.1156	529.41175	477.9508	147.7189	147.7189	38.8680	-4.7233	801.3116
	$6p_{3/2}$	71.7522	99.7029	70.4693	31.0006	31.0006	10.5459	-0.4414	138.9594
12s13p									
13d11f	$6s_{1/2}$	2925.6534	3317.3965	2831.6968	670.5637	670.5637	180.3921	-18.9517	4279.1033
7g	$5d_{3/2}$	128.0069	136.8109	131.5908	32.4137	32.4137	14.3811	-0.9463	201.8285
	$5d_{5/2}$	51.3556	-6.2273	53.1622	-26.4497	-26.4497	6.2562	0.0187	1.3614
	$6p_{1/2}$	492.1156	562.8623	480.5664	145.6671	145.6671	32.1605	-4.5414	799.1300
	$6p_{3/2}$	71.7522	100.2874	71.0890	31.0429	31.0429	9.9951	-0.4226	139.6035
14s14p									
15d14f	$6s_{1/2}$	2925.6534	3317.4560	2859.9781	622.0414	622.04139	159.9298	-18.6979	4193.0212
	$5d_{3/2}$	128.0069	136.8168	131.0997	30.1643	30.1643	16.0891	-1.0597	198.7597
	$5d_{5/2}$	51.3551	-6.2318	52.3147	-28.0433	-28.0434	6.2446	-0.0244	-2.5783
	$6p_{1/2}$	492.1156	562.8682	487.4478	136.1278	136.1278	33.9000	-4.3325	783.3350
	$6p_{3/2}$	71.7521	100.2858	71.8614	28.4628	28.4628	9.4595	-0.5516	134.0795

Table 5.18: Hyperfine Constant (A) in MHz for Ba^+ as compared with the experimental values.

State	Ours (MHz)	Expt.(MHz)	Other theory (MHz)
$6s_{1/2}$	4193.02	4018.02[a]	4203±200 *
$5d_{3/2}$	198.759	191.2(6)[b]	-
$6p_{1/2}$	783.335	742.04[a]	-
$6p_{3/2}$	134.079	125.9[a]	-

[a] W. Becker, W. Fischer and H. Huhnermann, *Z. Physik* **299**, 93 (1981).
[b] R.E. Silverans, G. Borghs, G. Dumont, and J.M. Van den Cruyce, *Z. Physik A*, **295** 311 (1980),
* S. Ahmad, J. Andriessen, K. Raghunathan and T.P. Das, *Phys. Rev. A* **25**, 2923 (1982).

be included for better accuracy.

5.7.5 Computation of $E1PNC$ using Sum over Approach for Ba^+

With a knowledge of the error in the dipole and hyperfine matrix elements from the earlier study using the CC method, we computed $E1PNC$ by sum over intermediate states by taking only $(6-8)p(1/2)$ states for the direct term and $(6-8)p(3/2)$ for the conjugate term. This approach is similar to the work done by Blundell et al. [36] for caesium, for which the largest contribution to $E1PNC$ is from $6p_{1/2}$ and $7p_{1/2}$ intermediate states. Similar calculation performed on singly ionised barium by Dzuba et al. [65] clearly points that the dominant contribution comes from the intermediate $6p_{1/2}$ state. We have performed all order CCSD calculations for the determination of dipole and PNC matrix elements.

The results of such calculations with the theoretical energy difference is tabulated in Table 5.19. We obtain good agreement with the values obtained by Dzuba et al. [65].

The DF contributions to $E1PNC$ from the bound core $(2p-5p)$ and continuum $(9p-29p)$ virtual $p_{1/2}$ orbitals are found to be 0.28566 $iea_0(-Q_W/N)\times 10^{-11}$ and 0.083791 $iea_0(-Q_W/N)\times 10^{-11}$ respectively. The all order contribution from $6p-8p(1/2,3/2)$ intermediate states to $E1PNC$ is found to be
1.9844 $iea_0(-Q_W/N)\times 10^{-11}$. In the paper by Dzuba et al. [65] the contribution

Table 5.19: Contribution to $E1PNC$ in Ba^+ from the intermediate states $X = 6 - 8p_{1/2}$. PNC and the final matrix elements are in units of $10^{-11} iea_o(-Q_W/N)$. Dipole matrix elements and energy are in a.u. Normalisation = 1.005494.

n	$\langle 5d_{3/2}\|D\|np_{1/2}\rangle$ (a.u.)	$\langle np_{1/2}\|\mathrm{PNC}\|6s_{1/2}\rangle$	$E_{6s} - E_{np_{1/2}}$ (a.u.)	Contribution	Dzuba
6	3.0010	−2.510	−0.0925	2.102	2.036
7	0.3065	−1.4551	−0.2257	0.051	0.045
8	0.1110	−0.9372	−0.2803	0.0096	0.012
n	$\langle 5d_{3/2}\|\mathrm{PNC}\|np_{3/2}\rangle$ (a.u.)	$\langle np_{3/2}\|D\|6s_{1/2}\rangle$	$E_{5d_{3/2}} - E_{np_{3/2}}$ (a.u.)	Contribution	Dzuba
6	−0.1437	−4.7964	−0.10033	−0.1773	−0.264
7	−0.0988	−0.3441	−0.2286	−0.0038	−0.001
8	−0.0611	0.5289	−0.2817	0.0029	0.0

Table 5.20: Contribution to $E1PNC$ in Ba^+ in the units $10^{-11} iea_o(-Q_W/N)$.

Method	intermediate states	Contribution	Dzuba [65]
DF	2p-5p and 9p-29p	0.3695	-
CC (all order)	6p-8p	1.9844	-
Total		2.35	2.34

from the intermediate states consisting of bound core and bound and continuum virtuals is given as 2.34 $iea_0(-Q_W/N) \times 10^{-11}$. The total contribution to NSI $E1PNC$ by considering contributions from $2p - 5p$ and $9p - 29p$ at the DF level and $6p - 8p$ to all order is found to be 2.35 $iea_0(-Q_W/N) \times 10^{-11}$. The contribution to $E1PNC$ using sum over approach is tabulated in Table 5.20.

The error in the computation of dipole matrix element in comparison with the experimentally available transition probabilities and lifetimes is $\sim 2\%$. This limits the accuracy of the wave functions at large r regions to be be around this range. Similarly the average percentage error in the determination of hyperfine constant A for the low lying levels limits the accuracies of the wavefunctions near the nuclear regions to be $\sim 5\%$. Excitation energies which depend on the electron-electron interaction which in turn is dependent on the electron density which is larger at the mid r region is found to be accurate to less than 1%. In order to determine the percentage error in

the computed $E1PNC$ using sum over intermediate states one needs to have more analysis. But the interpolation of accurcies of wave functions at various grid points puts a limit on the accuracy of the $E1PNC$ computed using sum over intermediate states.

In the Section 5.8 we compare Unitary Coupled Cluster (UCC) Method with Many-Body Perturbation Theory (MBPT) described in Chapter 4. It is well known that CC can be reduced to a particular order in MBPT by suitable deductions. In the previous chapter we classified the first order MBPT diagrams as CPHF, RPA and CPHF-RPA. Using the CC method described in this chapter, we find that there is no one to one correspondence between CC diagrams and the various classes of MBPT diagrams mentioned above. For example, the CPHF has 2 pseudo and 2 direct diagrams which cannot be directly got from the CC formalism given above. For the pseudo diagrams one needs to add two of the MBPT diagrams for which the CC counterparts are available. Here we show that with the new Unitary CC, there is a one to one correspondence between the CC and these classes of diagrams specified in Chapter 4. The formulation of UCC is given below and at the end we show how the CPHF diagrams can be obtained from the CC diagrams generated using UCC method.

5.8 UCC method in Comparison with MBPT

The many-electron wave function in UCC Method is given by

$$|\Psi_0\rangle = e^{(T-T^\dagger)}\{e^S\}|\Phi_0\rangle, \tag{5.105}$$

where $|\Phi_0\rangle$ is the reference state and T and S are the cluster operators which considers excitations from core orbitals and valence orbitals. We write

$$|\Psi_i\rangle = e^{(T-T^\dagger)}\{e^{S_i}\}|\Phi_i\rangle, \tag{5.106}$$

$$|\Psi_f\rangle = e^{(T-T^\dagger)}\{e^{S_f}\}|\Phi_f\rangle. \tag{5.107}$$

The Hamiltonian for the above problem is given by

$$H = H_a + \lambda H_{\rm PNC} \tag{5.108}$$

hence

$$T = T^{(0)} + \lambda T^{(1)}, \tag{5.109}$$

$$S = S^{(0)} + \lambda S^{(1)}. \tag{5.110}$$

5.8.1 Solving $T_1^{(0)}$ and $T_2^{(0)}$ Coupled Equations

The equation we have to solve is the Schrödinger equation given by

$$H_a|\Psi_0\rangle = E_0|\Psi_0\rangle, \tag{5.111}$$

where

$$H_a = H_0 + V. \tag{5.112}$$

We define

$$E_{HF} = \langle\Phi_0|H_a|\Phi_0\rangle. \tag{5.113}$$

Subtract E_{HF} from both the sides, we get

$$(H_a - E_{HF})|\Psi_0\rangle = (E_0 - E_{HF})|\Psi_0\rangle. \tag{5.114}$$

We know for any operator O the normal ordered operator O_N is

$$O_N = O - \langle\Phi_0|O|\Phi_0\rangle. \tag{5.115}$$

Hence the above equation reduces down to

$$H_N|\Psi_0\rangle = \Delta E|\Psi_0\rangle, \tag{5.116}$$

where $\Delta E = E_0 - E_{HF}$ which is the Correlation Energy. Here the many-body wave function is written as

$$|\Psi_0\rangle = e^{T^{(0)} - T^{\dagger(0)}}|\Phi_0\rangle = e^{\sigma}\Phi_0. \tag{5.117}$$

Substituting for $|\Psi_0\rangle$ and multiplying by $e^{-\sigma}$ to the left, we get

$$e^{-\sigma}H_N e^{\sigma}|\Phi_0\rangle = \Delta E|\Phi_0\rangle. \tag{5.118}$$

Baker-Campbell-Hauxdorf expansion is given by

$$e^{-\sigma}H_N e^{\sigma} = \sum_n 1/n![H_N, \sigma]^{(n)} = \bar{H}_N. \tag{5.119}$$

Projection by the reference state and single and double excited determinants leads to the correlation energy, singles and doubles cluster amplitudes given by

$$\langle\Phi_o \mid \bar{H}_N \mid \Phi_o\rangle = \Delta E, \tag{5.120}$$

$$\langle\Phi^{\star} \mid \bar{H}_N \mid \Phi_o\rangle = 0. \tag{5.121}$$

5.8.2 Solving $T_1^{(1)}$ and $T_2^{(1)}$ Coupled Equations

We consider $H_{\rm PNC}$ as the perturbation to the atomic Hamiltonian and hence the total Hamiltonian is

$$H = H_a + \lambda H_{\rm PNC}. \tag{5.122}$$

Due to the addition of $H_{\rm PNC}$, the wave function will have a PNC perturbed and PNC unperturbed part given by

$$\mid \tilde{\Psi}\rangle = e^{\tilde{T}} \mid \Phi_0\rangle, \tag{5.123}$$

where $\tilde{T} = T^{(0)} + \lambda T^{(1)}$. $T^{(0)}$ and $T^{(1)}$ are further defined as

$$T^{(0)} \rightarrow T^{(0)} - T^{(0)\dagger} = \sigma^{(0)}$$

and

$$T^{(1)} \rightarrow T^{(1)} - T^{(1)\dagger} = \sigma^{(1)}$$

respectively. Since PNC scales as G_F, we consider terms that are linear in λ. Writing $e^{\sigma^{(1)}} = 1 + \sigma^{(1)}$ we get

$$(\bar{H}_a - E_0)(1 + \sigma^{(1)}) \mid \Phi_0\rangle = -\bar{H}_{\rm PNC}(1 + \sigma^{(1)}) \mid \Phi_0\rangle. \tag{5.124}$$

Projection with excited state determinants in the Schrödinger equation with the above substitutions gives the perturbed cluster amplitudes

$$\langle \Phi^\star \mid (\bar{H}_a - E_0)\sigma^{(1)} \mid \Phi_o\rangle = -\langle \Phi^\star \mid \bar{H}_{\rm PNC} \mid \Phi_o\rangle, \tag{5.125}$$

where $\bar{H}_a = e^{-\sigma^{(0)}} H_a e^{\sigma^{(0)}}$ and $\bar{H}_{\rm PNC} = e^{-\sigma^{(0)}} H_{\rm PNC} e^{\sigma^{(0)}}$.

5.8.3 Solving $S_1^{(0)}$ and $S_2^{(0)}$ Coupled Equations

In this case we consider excitations from both core and valence to virtual orbitals. The addition of valence electron to the kth virtual orbital of the DF reference state is given by

$$|\Phi_k^{N+1}\rangle = a_k^\dagger |\Phi_0\rangle \tag{5.126}$$

and it satisfies the equation

$$H_a |\Phi_k^{N+1}\rangle = E_k |\Phi_k^{N+1}\rangle. \tag{5.127}$$

The exact state using excitation operators for core and valance orbitals can be represented as

$$|\Psi_k^{N+1}\rangle = e^{T^{(0)}}\{e^{S_k^{(0)}}\}|\Phi_k^{N+1}\rangle. \tag{5.128}$$

Due to normal ordering and the presence of particle annihilation operator the above equation reduces to

$$|\Psi_k^{N+1}\rangle = e^{T^{(0)}}(1 + S_k^{(0)})|\Phi_k^{N+1}\rangle. \tag{5.129}$$

Applying the same procedure as in the closed-shell case, and using the substitutions above the Schrödinger equation reduces to

$$\begin{aligned}\langle\Phi_k^{\star,N+1}|(\bar{H}_a - E_k)S_k^{(0)}|\Phi_k^{N+1}\rangle = -\langle\Phi_k^{\star,N+1}|\bar{H}_a|\Phi_k^{N+1}\rangle + \\ \langle\Phi_k^{\star,N+1}|S_k^{(0)}|\Phi_k^{N+1}\rangle\langle\Phi_k^{N+1}|\bar{H}_a(1 + S_k^{(0)})|\Phi_k^{N+1}\rangle,\end{aligned} \tag{5.130}$$

where $\bar{H}_a = e^{-\sigma}H_a e^{\sigma}$.

5.8.4 Solving $S_1^{(1)}$ and $S_2^{(1)}$ Coupled Equations

We consider again $H_{\rm PNC}$ to be the perturbation and the procedure is followed as derived for the PNC unperturbed part but by taking one order of PNC in the equations. Considering the perturbation in wave function we get

$$|\,\tilde{\Psi}\rangle = e^{\tilde{\sigma}}\{e^{\tilde{S}}\}\,|\,\Phi_k\rangle, \tag{5.131}$$

where $\tilde{\sigma} = \sigma^{(0)} + \lambda\sigma^{(1)}$ and $\tilde{S} = S^{(0)} + \lambda S^{(1)}$. Applying these on the Schrödinger equation, we get

$$(H_a + \lambda H_{\rm PNC})e^{\tilde{\sigma}}(1 + S^{(0)} + \lambda S^{(1)})\,|\,\Phi_k\rangle = E_k e^{\tilde{\sigma}}(1 + S^{(0)} + \lambda S^{(1)})\,|\,\Phi_k\rangle. \tag{5.132}$$

Considering linear terms in PNC, we write $e^{\tilde{\sigma}} = (1 + \lambda\sigma^{(1)})$, hence

$$(H_a+\lambda H_{\rm PNC})e^{\sigma^{(0)}}(1+\lambda\sigma^{(1)})(1+S^{(0)}+\lambda S^{(1)})\,|\,\Phi_k\rangle = E_k e^{\sigma^{(0)}}(1+\lambda\sigma^{(1)})(1+S^{(0)}+\lambda S^{(1)})\,|\,\Phi_k\rangle. \tag{5.133}$$

Taking only one order in PNC and projecting by single and double excited determinants we get the equation of the form

$$\langle\Phi_k^{\star}\,|\,(\bar{H}_a-E_k)S^{(1)}\,|\,\Phi_k\rangle = -\langle\Phi_k^{\star}|\left(\bar{H}_{\rm PNC}(1 + S^{(0)}) - (\bar{H}_a - E_k)\sigma^{(1)}S^{(0)} - (\bar{H}_a - E_k)\sigma^{(1)}\right)\,|\,\Phi_k\rangle, \tag{5.134}$$

where $\bar{H}_a = e^{-\sigma^{(0)}}H_a e^{\sigma^{(0)}}$ and $\bar{H}_{\rm PNC} = e^{-\sigma^{(0)}}H_{\rm PNC}e^{\sigma^{(0)}}$.

After the evaluation of the four CC amplitudes $T^{(0)}$, $T^{(1)}$, $S^{(0)}$ and $S^{(1)}$ the wave functions can be determined and they can be used to calculate the electric dipole transition amplitudes.

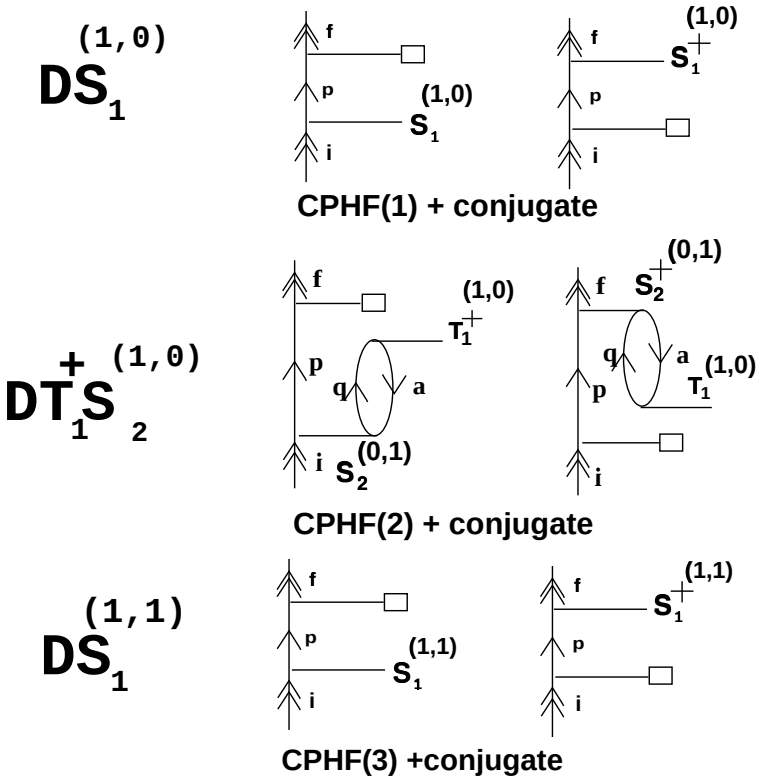

Figure 5.30: CC diagrams corresponding to CPHF term. CPHF(1) corresponds to zeroth order diagrams and CPHF(2) corresponds to pseudo diagrams and CPHF(3) corresponds to real diagrams. Here the superscript on S and T operators (x,y) refers to x orders of PNC and y orders of Couloumb.

5.9 Evaluation of Electric Dipole Transition Amplitude

Substituting the form of the CC wave function $E1PNC$ becomes

$$E1PNC = \langle \Phi_f^{(0)} | e^{\{\tilde{S}_f^\dagger\}} e^{\tilde{\sigma}^\dagger} D e^{\tilde{\sigma}} e^{\{\tilde{S}_i\}} | \Phi_i^{(0)} \rangle. \tag{5.135}$$

The terms that give rise to diagrams of the form given in Fig. 4.2 in Chapter 4 are given by DS_i, $S_f^\dagger D$, DTS_i, $-DT^\dagger S_i$, $S_f^\dagger TD$, $-S_f^\dagger T^\dagger D$ and so on. The diagrams which give rise to equivalent CPHF diagrams having one order in PNC and one order in Couloumb operator are given in Fig. 5.30. Similarly one can get equivalent diagrams for all the diagrams in first order MBPT, which corresponds to different physical effects like CPHF, RPA and CPHF-RPA.

Bibliography

[1] F.E. Harris, H.J. Monkhorst, D.L. Freeman, *Algebraic and Diagrammatic methods in many-fermion theory*, New York, Oxford Univ. Press, (1992).

[2] I. Lindgren, J. Morrison, *Atomic Many-Body Theory*, Springer-Verlag, New York (1981).

[3] N. Fortson, *Phys. Rev. Lett.* **70**, 2383 (1993).

[4] N.M. Hugenholtz, *Physica (Utrecht)* **23**, 481 (1957).

[5] J. Hubbard, *Proc. Roy. Soc.(London)* **A240**, 539 (1957).

[6] J. Goldstone, *Proc. Roy. Soc. (London)* **A239**, 267 (1957).

[7] K.A. Bruckner, *Phys. Rev.* **100**, 36 (1955).

[8] H.P. Kelly, *Phys. Rev.* **131**, 684 (1963); *Advan. Theoret. Physics* **2**, 75 (1968); *Advan. Chem. Phys.* **14**, 129 (1969) and references therein.

[9] For original literature, please see J.E. Mayer, and M.G. Mayer, *Statistical Mechanics*, Wily, New York, 1940. For quantum statistical version of cluster expansion, please see B. Khan and G.E. Uhlenbeck, *Physica (Utrecht)* **5**, 399 (1938).

[10] F. Coester, *Nucl. Phys.* **7**, 421 (1958); F. Coester, H. Kummel, *Nucl. Phys.* **17**, 477 (1960); H. Kummel, *Lectures on the Many-body problem (ed. E.R. Caianiello)*, **265**, Academic Press, New York (1962).

[11] O. Sinanoglu, *J. Chem. Phys.* **36**, 706 (1962); *Advan. Chem. Phys.* **6**, 315 (1964); **14**, 237 (1969) and references therein; Sinanoglu and J. Cizek, *Chem. Phys. Lett.* **1**, 337 (1967).

[12] R.K. Nesbet, *Advan. Chem. Phys.* **14**, 1 (1969).

[13] J. Cizek, *J. Chem, Phys.* **45**, 4256 (1966); *Adv. Chem. Phys.* **14**, 35 (1969).

[14] Coupled Cluster Theory: An overview of recent developments, R.J. Bartlett, *Advanced Series in Physical Chemistry Vol.2*, ed. D.R. Yarkony, World Scientific (1995).

[15] J.A. Pople, J.S. Binkley and R. Seeger, *Int. J. Quantum Chem.* Symp. 10:1 (1976).

[16] H. Primas, *Modern Quantum Chemistry,* ed. O. Sinanoglu, New York (1965).

[17] J. Paldus, *J. Chem. Phys.* **67**, 303 (1977).

[18] R.E. Watson, *Phys. Rev.* **119**, 170 (1960); D.D. Ebbing, *Ph.D.thesis*, Department of Chemistry, Indiana University, Bloomington (1960).

[19] W. Kutzelnigg, *Methods of Electronic Structure Theory*, ed. H.F. Schaefer III, Plenum Press, New York (1977).

[20] R.J. Bartlett, *Annu. Rev. Phys. Chem.,* **32**, 359 (1981).

[21] R.J. Bartlett and G.D. Purvis III, *Int. J. Quantum Chem. Symp.* **14**, 561 (1978); *Physica Scripta* **21**, 255 (1980).

[22] J.A. Pople, R. Krishnan, H.B. Schlegel and J.S. Binkley, *Int. J. Quantum Chem.*, Quantum Chem. Symp. **14**, 545 (1978).

[23] G.D. Purvis III and R.J. Bartlett, *J. Chem. Phys.* **76**, 1910 (1982).

[24] J. Noga and R.J. Bartlett, *J. Chem. Phys.* **86**, 7041 (1987); ibid. **89**, 3401 (1988).

[25] G.E. Scuseria and H.F. Schaefer III, *Chem. Phys. Lett.* **152**, 382 (1988).

[26] J.D. Watts and R.J. Bartlett, *J. Chem. Phys.* **93**, 6104 (1990).

[27] G.E. Brown and D.G. Ravenhall, *Proc. Roy. Soc. (London)* **A208**, 552 (1951).

[28] J. Sucher, *Phys. Rev. A* **22**, 348 (1980).

[29] N.M. Mukherjee, R.K. Moitra and A. Mukhopadhyay, *Mol. Phys.* **30**, 1861 (1975).

[30] W.R. Johnson, *Physica Scripta* **36**, 765 (1987).

[31] S.A. Blundell, W.R. Johnson, and J. Sapirstein, *Phys. Rev. A* **43**, 3407 (1991).

[32] E. Eliav and U. Kaldor, *Phys. Rev. A* **49**, 3 (1994).

[33] M.S. Safronova, A. Derevianko and W.R. Johnson, *Phys. Rev. A* **58**, 2 (1998).

[34] Z.W. Liu, *Ph.D.thesis*, Notre Dame University (1989).

[35] E. Eliav, U. Kaldor, and Y. Ishikawa, *Phys. Rev A.* **53**, 3050 (1998).

[36] S.A. Blundell, *Applied Many-Body Methods in Spectroscopy and Electronic Structure*, ed. D. Mukherjee, Plenum Press, New York (1992).

[37] S.A. Blundell, W.R. Johnson, Z.W. Liu, and J. Sapirstein, *Phys. Rev. A* **40**, 2233 (1989).

[38] J.J. Sakurai, *Modern Quantum Mechanics*, Addison-Wesley Company Inc., Revised Edition (1994).

[39] S.A. Blundell, W.R. Johnson and J. Sapirstein, *Phys. Rev. A*, **40**, 2233 (1989).

[40] S.A. Blundell, W.R. Johnson and J. Sapirstein, *Phys. Rev. A* **43**, 3407 (1991).

[41] L.I. Sobelman, *Introduction to the Theory of Atomic Spectra*, Pergamon, Oxford (1972).

[42] A.P. Jucys (Yutsis), I.B. Levinson and V.V. Vanagas, *Mathematical Apparatus of the Theory of Angular Momentum*, Jerusalem: Israel Program for Scientific Translation (1962).

[43] I.P. Grant, *J. Phys. B: At. Mol. Phys.* **19**, 3187 (1986); H.M. Quiney, I.P. Grant and S. Wilson, *J. Phys. B: At. Mol. Phys.* **20**, 1413 (1987); I.P. Grant and H.M. Quiney, *Adv. At. Mol. Phys.* **23**, 11413 (1987).

[44] E. Baz and E.B. Castel, *Graphical Methods for Spin Algebras in Atomic, Nuclear and Particle Physics*, New York: Dekker (1972).

[45] P.G.H. Sandars, *Atomic Physics and Astrophysics* eds. M. Chrestien and E. Lipworth, London: Gordon and Breach (1971).

[46] Z.W. Liu and H.P. Kelly, *Phys. Rev. A* **43**, 3305 (1991).

[47] H. Merlitz, G. Gopakumar, R.K. Chaudhuri, B.P. Das, U.S. Mahapatra, D. Mukherjee, *Phys. Rev. A* (2000).

[48] H. Merlitz, G. Gopakumar, R.K. Chaudhuri, B.P. Das, U.S. Mahapatra and D. Mukherjee, *Phys. Rev. A* (in press).

[49] R.K. Chaudhuri, P.K. Panda and B.P. Das, *Phys. Rev. A* **59**, 1187 (1999).

[50] E. Eliav, U. Kaldor and Y. Ishikawa, *Phys. Rev. A* **49**, 1724 (1994).

[51] E. Eliav, U. Kaldor and Y. Ishikawa, *Phys. Rev. A* **52**, 2765 (1995).

[52] E. Eliav, U. Kaldor and Y. Ishikawa, *Phys. Rev. A* **51**, 225 (1995).

[53] E. Eliav, U. Kaldor and Y. Ishikawa, *Phys. Rev. A* **52**, 291 (1995).

[54] E. Eliav, U. Kaldor and Y. Ishikawa, *Phys. Rev. Lett.* **74**, 1079 (1995).

[55] E. Eliav, U. Kaldor, P. Schwerdtfeger, B.A. Hess and Y. Ishikawa, *Phys. Rev. Lett.* **73**, 3203 (1994).

[56] S.J. Rose, N.C. Pyper, and I.P. Grant, *J. Phys. B* **11**, 755 (1978).

[57] J. Migdalek and W.E. Baylis, *Phys. Rev. A* **35**, 3227 (1987).

[58] S.A. Kotochigova and I.I. Tupizin, *J. Phys. B* **20**, 4759 (1987).

[59] C. Guet and W.R. Johnson, *Phys. Rev. A* **49**, 1531 (1991).

[60] E. Eliav, U. Kaldor and Y. Ishikawa, *Phys. Rev. A* **53**, 3050 (1996).

[61] C.E. Moore, *Atomic Energy Levels*, Natl. Bul. Stand. (U.S.), Circ. No. 467, U.S. GPO, Washington, DC, Vol. III (1958).

[62] S.G. Schmelling and G.O. Brink, *Phys. Rev. A* **12**, 2498 (1975); H.P. Palenius, *Phys. Lett.* **56A**, 451 (1976).

[63] S. Huzinaga and M. Klobukowski, *Chem. Phys. Lett.* **212**, 260 (1993).

[64] G. Gopakumar, H. Merlitz, R.K. Chaudhuri, S. Majumder, B.P. Das, U.S. Mahapatra and D. Mukherjee *Phys. Rev. A* (in press).

[65] V.A. Dzuba, V.V. Flambaum and J.S.M. Ginges, *Phys. Rev. A* **63** 62101 (2001).

[66] R. Crossley, *Physica Scriptica* **T8**, 117 (1984).

[67] S.E. Bisson, E.F. Worden, J.G. Conway, B. Comaskey, J.A.D. Stockdale and F. Nehring, *J. Opt. Soc. Am.* **B8**, 883 (1981).

Chapter 6

Conclusion and Future Directions

6.1 Conclusion

Parity non-conservation in atoms and ions has emerged as an active area of research embracing both elementary particle and atomic physics. Over the past years atomic physics has given rise to many elegant and powerful experimental and theoretical techniques. This has opened new vistas of looking for physics beyond the Standard Model. The atom that is currently best suited for this purpose is caesium for which the combined accuracy of PNC experiment and theory is below 1% [1]. However, there are other promising proposals to observe PNC in atomic systems. One of these involves applying the techniques of ion trapping and laser cooling to Ba^+ [2]. It has been pointed out that certain transitions in Ba^+ and Ra^+ could yield unambiguous information about NSD PNC [4]. Unlike the $S \rightarrow S$ transition for caesium, the transitions involved here are $S \rightarrow D$. The PNC calculations of Ba^+ are more demanding than those of caesium, as a many-body description of the D states unlike the S states requires configurations that are relatively complex.

In this thesis we have made an attempt to compute electric dipole transition amplitude induced by PNC ($E1PNC$) for singly ionised barium between the states $|5p^6 6s\rangle_{1/2}$ and $|5p^6 5d\rangle_{3/2}$.

To accomplish the above task we have used three different Many-body methods *viz.*, Configuration Interaction (CI) Method , Many-Body Perturbation Theory (MBPT) and Coupled Cluster Method (CCM).

We have computed $E1PNC$ induced by both Nuclear Spin Independent (NSI) and Nuclear Spin Dependent (NSD) interactions for different transitions using the CI

method. We have verified the findings of Malhotra et al. [3] that the contributions from low-lying configurations are important. This was performed by taking a larger number of CSFs which were generated by exciting inner core orbitals like $5s$ and also exciting it into higher virtual orbitals which were not considered in the previous work [3]. Such a calculation using a large basis with high-lying virtual orbitals leading to about 2000 relativistic configurations shows that the correlation contribution changes by about 1.6% with respect to the calculation of Malhotra et al. [3]. The total NSI $E1PNC$ reduced matrix element for the above transition is found to be 0.5264 $iea_0Q_W \times 10^{-12}$.

Computation of $E1PNC$ for the NSD effect for Ba^+ and Ra^+ for the transitions $|5p^6 6s\rangle_{1/2} \rightarrow |5p^6 5d\rangle_{5/2}$ and $|6p^6 7s\rangle_{1/2} \rightarrow |6p^6 6d\rangle_{5/2}$ was also performed using the CI method. The above transitions has an important advantage; it is sensitive to the NSD effect and is therefore a direct way of measuring the nuclear anapole moment [4]. We have done a fairly big calculation for the above mentioned transitions in both Ba^+ and Ra^+ by considering configurations arising from single and double excitations from $5s, 5p$ and $6s$ to $7s, 8s, 5d, 6d, 6p, 7p$ and $8p$ for Ba^+ and $6s, 6p$ and $7s$ to $8s, 9s, 6d, 7d, 8d, 7p, 8p$ and $9p$ for Ra^+. The NSD contribution to PNC for the above transitions in Ba^+ and Ra^+ was compared with the NSD contribution for Ba^+ for the transition $|5p^6 6s_{1/2}\rangle \rightarrow |5p^6 5d_{3/2}\rangle$ for the case $F_f = 3$ to $F_i = 2$. This shows that the NSD contribution for the $^2S_{1/2} \rightarrow {}^2D_{5/2}$ transition in Ba^+ is eight times smaller than that of the $^2S_{1/2} \rightarrow {}^2D_{3/2}$ transition, but it is worth pursuing since there is no masking by the NSI contribution. For Ra^+, the NSD contribution from the $^2S_{1/2} \rightarrow {}^2D_{5/2}$ transition is larger than the corresponding transition in Ba^+ making it an attractive choice for a clean measurement of the nuclear anapole moment. It is indeed worthwhile to carry out detailed feasibility studies to measure the nuclear anapole moments in these two ions. Since the CI method is not suitable due to the requirement of large memory and it's size-inextensive property for limited excitations, we have performed NSI calculations on Ba^+ using other size extensive theories like MBPT and CCM.

Using MBPT, the $E1PNC$ was calculated using a part numerical and part analytical basis consisting of bound and continuum orbitals. From the lowest order MBPT calculation, one can infer that,the bound orbitals contribute 96.36Terms containing one order in Couloumb interaction are categorised in three groups and done separately to all orders by expressing them as linear equations. The results show that, the CPHF largest contribution is the largest ; which is 3.8%. The contributions from RPA and CPHF-RPA are less than 1%. The CPHF effect has the same sign as the lowest order making it additive, whereas for RPA it is opposite in sign which in the physical sense is due to the shielding effect. We have also considered

lowest order pair correlation effects arising from two orders of Couloumb interaction. The contributions from core-core correlation diagrams were found to be less than 2% and hence only core-valence diagrams were considered in our calculation. The Bruckner type diagrams contributed the most followed by the structural radiation type diagrams. The MBPT(5) diagram with the initial state perturbed by PNC and then the Couloumb interaction is found to diverge due to the strong correlation between the valence and the outermost core orbital ($5p$). Hence the pair correlation contribution from $5p$ and $6s$ alone was computed to all orders using the Coupled Pair Electron Approximation (CEPA) [5]. The total contribution to $E1PNC$ using MBPT is 2.18 $iea_0(-Q_W/N) \times 10^{-11}$. Dzuba et al. [6] using a mixed parity approach obtained 2.17 $iea_0(-Q_W/N) \times 10^{-11}$.

Relativistic coupled cluster singles and doubles with and without PNC as the perturbation for closed and open-shell systems is elaborated in the beginning of the Chapter 5 on CCM applied to PNC. Using this approach, we obtain four cluster amplitudes designated as $T^{(0)}, S^{(0)}, T^{(1)}$ and $S^{(1)}$ where T and S refers to close and open-shell coupled cluster amplitudes. The theoretical method for computing $E1PNC$ using the sum over intermediate states and mixed parity approaches using the above four cluster amplitudes are described. It is necessary to compute as many atomic properties as possible before embarking on an ambitious PNC calculation. With this in mind, we have carried out non-linear CC calculations of Ionisation Potential (IP) and Excitation Energy (EE) by considering the terms T_1^2, T_1T_2 and T_2^2 for the non-linear contribution. We have also included triple excitations partially which were found to be crucial in achieving the accuracies around 0.2 and 1% for IPs and EEs [7]. On comparison with other calculations [8, 9] it is clear that the inclusion of triples partially and the choice of the orbital basis in which core, valence and the appropriate virtual single-particle states generated numerically [10] has led to these high precision results. As a check of the wave functions far away from the nucleus, properties like electric dipole, electric quadrapole transition matrix elements were calculated using various basis and compared with the available experimental data. Similarly for the wave functions near the nucleus, the hyperfine constant A, which depends on the region close to the nucleus like the PNC matrix elements was calculated for different states and compared with experimental data. Computation of the above mentioned properties using various single-particle basis has led to useful insights about the completeness of a basis with respect to a particular property. An atomic property like dipole and quadrapole transition matrix elements between various symmetries require a complete set of orbitals of a particular symmetry with a very good description of the polarising orbitals which are diffuse. For the case of the hyperfine interaction which is

Table 6.1: Comparison of $E1PNC$ for Ba^+ obtained using three different methods

Method	Contribution to $E1PNC$ $iea_0(-Q_W/N) \times 10^{-11}$	Contribution to E1PNC [6] $iea_0(-Q_W/N) \times 10^{-11}$
CI	1.74	
MBPT		
CC, MBPT	2.35 (zeroth order core + continuum virtual)	2.34
mixed parity	2.18	2.17

similar in form to PNC, the occupied orbitals should be very well described. For the electric dipole matrix elements, the effective single-particle excitations namely RPA, Bruckner and structural radiation and normalisation correction contributes approximately $\sim 15\%$, 5% and 0.5% respectively. The lifetimes of the $E1$ and $E2$ transitions of Ba^+ and Ca^+ are comparable with the published literature [9] and experimental data [11, 12]. The accuracy of the hyperfine constant A is found to be around 5% for the low lying levels. For all the property calculations, we have used only effective one-body diagrams derived from the $e^{T^\dagger}Oe^T$ term and as a next step of our calculation we are planning to include the effective two-body terms. Using the same technique we have calculated the all order PNC and dipole matrix elements which are used in the calculation of $E1PNC$ using the sum over states approach. We have performed a CCSD calculation for the intermediate states from $(6-8p)_{1/2,3/2}$ states. The contribution from the bound core states $2p-5p$ and the tail part consisting of continuum virtual states $9p-29p$ are considered approximately through the DF calculation. The total contribution to $E1PNC$ using the sum over intermediate states approach is found to be 2.35 $iea_0(-Q_W/N) \times 10^{-11}$ which is in good agreement with the value obtained by Dzuba et al. [6] tabulated in Table 6.1. Comparisons of the results obtained using three different approaches for the computation of $E1PNC$ is also given in Table 6.1.

Comparing the above results obtained using three different methods, it is clear that the contribution to Ba^+ PNC using the CI method has been underestimated due to the absence of the f symmetry and continuum orbitals in the basis.

6.2 Future Directions

The IP and EE values for the low lying bound states of Ba^+ obtained using the CC method shows that the inclusion of approximate triples to the energy term were responsible for the high degree of precision [7]. Hence the first logical step in our future Ba^+ PNC work is to include triples at least in an approximate way in the coupled cluster amplitude calculations. In this thesis we have given only the formulation to calculate CC PNC using the four cluster amplitudes $T^{(0)}, S^{(0)}, T^{(1)}$ and $S^{(1)}$. This method includes the contributions from all the opposite parity intermediate states. Hence the next step will be to implement it and compute $E1PNC$ using the PNC perturbed and unperturbed amplitudes. As a next step, we would like to implement, an all order CC which is capable of considering any arbitrary excitation in the cluster operator as done by Kallay and Surjan et al. [13]. Considering the Breit interaction in PNC calculations at all stages for caesium, Kozlov et al. [14] have shown the accuracy of the calculations to be around 1%. Since the Briet interaction could play an important role at the level of 1% accuracy, one must consider this effect for high precision PNC calculations.

A high accuracy calculation of Ba^+ PNC in the not too distant future may be possible by exploiting the power of all-order many-body methods and the remarkable advances that have been made in the area of parallel computation in the past few years. Relativistic many-body calculations of PNC in Ra^+ have only recently got off the ground, and there is certainly room for improving the present result. Indeed the stage is now set for important advances in the relativistic many-body theory of PNC in heavy ions.

Bibliography

[1] S.C. Bennett and C.E. Wieman, *Phys. Rev. Lett.* **82**, 2484 (1999).

[2] N. Fortson, *Phys. Rev. Lett.* **70**, 2383 (1993).

[3] S. Malhotra, A.D. Singh and B.P. Das, *Phys. Rev. A* **51**, R2665 (1995).

[4] K.P. Geetha, A.D. Singh, B.P. Das and C.S. Unnikrishnan, *Phys. Rev. A.* **58**, R2665 (1998).

[5] A. Szabo and N.S. Ostlund, *Modern Quantum Chemistry*, Dover Publications, Mineola, New York.

[6] V.A. Dzuba, V.V. Flambaum and J.S.M. Ginges, *Phys. Rev. A* **63** 62101 (2001), *Phys. Rev. A.* **63**, 062101 (2001).

[7] G. Gopakumar, H. Merlitz, R.K. Chaudhuri et al. *Phys. Rev. A* (in press).

[8] E. Eliav, U. Kaldor and Y. Ishikawa, *Phys. Rev. A* **53**, 3050 (1996).

[9] C. Guet and W.R. Johnson, *Phys. Rev. A* **49**, 1531 (1991).

[10] F.A. Parpia, C.F. Fischer and I.P. Grant (unpublished).

[11] M. Knoop, D. Lunney, J. Rocher, M. Vedel and F. Vedel (unpublished); J. Jin and D.A. Church,*Phys. Rev. Lett.* **70**, 3213 (1993).

[12] N. Yu, W. Nagourney and H. Dehmelt,*Phys. Rev. Lett.* **78**, 4893 (1997), E.H. Pinnington, R.W. Berends and M. Lumsden,*J. Phys. B* **28** 2095 (1995).

[13] Mihaly Kallay and Peter R. Surjan, *J. Chem. Phys.* **113**, 1359 (2000).

[14] M. G. Kozlov and S. G. Porsev, *Phys. Rev. Lett.* **86**, 3260 (2001).

Appendix:A

Diagrammatic Representaion of Couloumb Operator

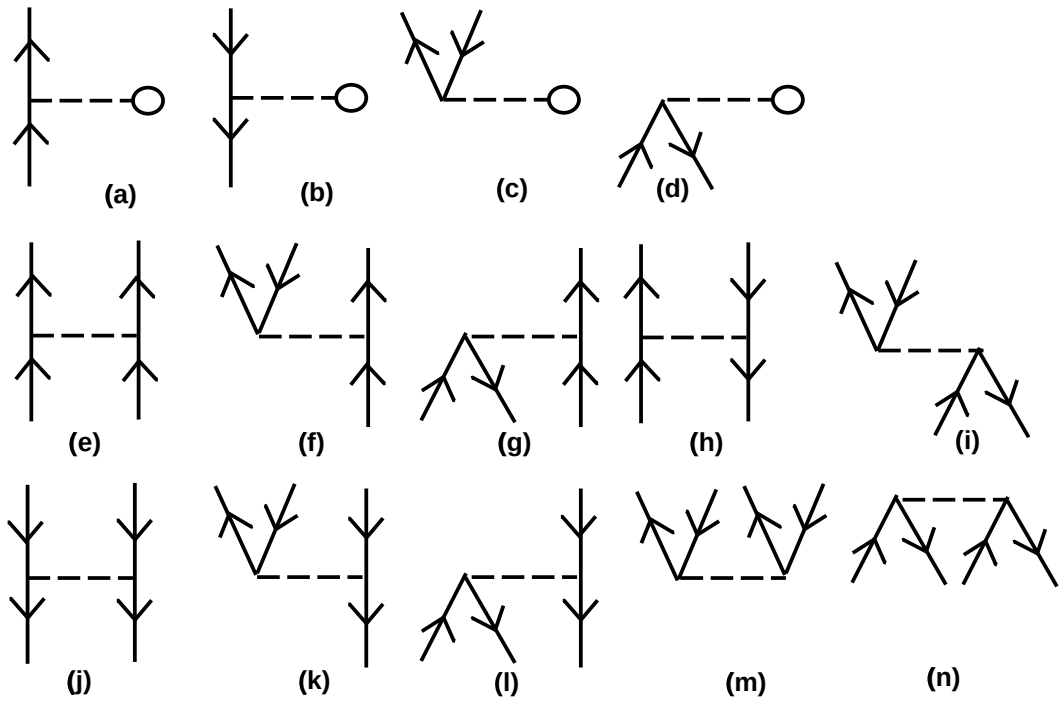

Figure A.1: Diagrammatic representation of normal ordered Hamiltonian (H_N)